FUNCTIONAL CHARACTERIZATION OF MEMBERS OF THE MICRORNA-17-92 CLUSTER IN THE VASCULAR SYSTEM

Dissertation

zur Erlangung des Doktorgrades der Naturwissenschaften

vorgelegt beim Fachbereich Biochemie, Chemie und Pharmazie (FB 14)

der Goethe-Universität in Frankfurt am Main

von Carmen Döbele

aus Waldshut

Frankfurt am Main 2011

(D30)

vom Fachbereich Biochemie, Chemie und Pharmazie (FB 14)
der Johann Wolfgang Goethe - Universität als Dissertation angenommen.

Dekan: Prof. Dr. Dieter Steinhilber

Gutachter: Prof. Dr. Volker Dötsch
Prof. Dr. Stefanie Dimmeler

Datum der Disputation: 01.09.2011

genau wissen tun wir nichts.
(SOKRATES)

janosch

Abbreviations

2D	2-dimensional
3D	3-dimensional
3p	3 prime
5-HT	5-hydroxytryptamine
5-HTT	5-hydroxytryptamine transporter
5p	5 prime
7-AAD	7-Amino-Actinomycin D
A-Co	control Antagomir
A-(17)	Antagomir-(17)
ACTA2	α-actin 2
ACVRL1	activin A receptor type II-like 1
ADAR	adenosine deaminase, RNA-specific
Ago	Argonaute
Ang	angiopoietin
ANOVA	analysis of variance
APAH	associated PAH
APS	ammonium persulfate
aqua dest	aqua destillata
ATP	adenosine triphosphate
AVD	apoptotic volume decrease
BM	basement membrane
BMP	bone morphogenetic protein
BMPR2	bone morphogenetic protein receptor 2
bp	base pairs
BrdU	bromodeoxyuridine
BSA	bovine serum albumine
bw	body weight
C. elegans	*Caenorhabditis elegans*
C13orf25	chromosome 13 open reading frame 25
Ca^{2+}	calcium
CaM	calmodulin
CDKN	cyclin-dependent kinase
cDNA	copy DNA
CHCl3	chloroform
CNN1	calponin 1
Co	control
CO	cardiac output
CO_2	carbon dioxide
COUP-TFII	chicken ovalbumin upstream promoter-transcription factor II
C_T	threshold cycle
CTGF	connective tissue growth factor
DAG	diacylglycerol
DAPI	4',6-diamidino-2-phenylindole
DGCR8	DiGeorge critical region 8
DMEM	Dulbecco's Modified Eagle Medium

DNA	deoxyribonucleic acid
Dnd1	dead end homolog 1
dNTP	deoxynucleotide Triphosphate
dsRNA	double-stranded RNA
DTT	dithiothreitol
E7.5	embronic day 7.5
EC	endothelial cell
ECCPS	Excellence Cluster Cardio-Pulmonary System
ECM	extracellular matrix
EEL	external elastic lamina
EFNB1	ephrin B1
e.g	exempli gratia, for example
EGF	epidermal growth factor
Egfl7	EGF-like domain 7
EGM	Endothelial Cell Growth Medium
EHS	Engelbreth-Holm-Swarm
ELISA	enzyme-linked immunosorbent assay
E_m	membrane potential
eNOS	endothelial nitric oxide synthase
EphB4	ephrin receptor B4
et al.	et alia, and others
ET-1	endothelin-1
EtOH	ethanol
FACS	fluorescence-activated cell sorting
FCS	fetal calf serum
FGF	fibroblast growth factor
FITC	fluorescein isothiocyanate
FNDC3A	fibronectin type-III domain containing 3A
FPAH	familial PAH
G-CSF	granulocyte colony-stimulating factor
GF	growth factor
GM-CSF	granulocyte macrophage colony-stimulating factor
GPCR	G protein-coupled receptor
GTP	guanosine triphosphate
h	hour(s)
H_2O	water
H_2O_2	hydrogen peroxide
hsa	*homo sapiens*
HC	healthy control
HEK	human embryonic kidney
HHV	human herpes virus
HIF	hypoxia-inducible factor
HIV	human immunodeficiency virus
HMVEC	human microvascular endothelial cell
hnRNPA1	heterogeneous nuclear ribonucleoprotein A1
HPASMC	Human pulmonary artery smooth muscle cell
HRP	horseradish peroxidase
HuR	human antigen R
HUVEC	human umbilical vein endothelial cell

i.e.	id est, that is
i.v.	intravenous
ICAM	intramolecular cell adhesion molecules
ID1	inhibitor of DNA binding 1
IEL	internal elastic lamina
IFN	interferone
IGF1	insulin-like growth factor 1
IGFBP2	insulin-like growth factor binding protein 2
IL	interleukin
IP3	inositol 1,4,5-trisphosphate
IPAH	idiopathic PAH
JAK	Janus kinase
kD	kilodalton
KSRP	K-homology-type splicing regulatory protein
Kv	voltage-dependent potassium channels
LB	Luria-Bertani
LLC	Lewis Lung Carcinoma
MAPC	multipotent adult progenitor cells
MCT	monocrotaline
MeOH	methanol
MEM	Minimum Essential Medium
MHz	Megahertz
min	minute(s)
miR, miRNA	microRNA
miRISC	microRNA induced silencing complex
MLC	myosin light chain
MLCK	myosin light chain kinase
MLCP	myosin light chain phosphatase
M-MLV	Moloney murine leukemia virus
MMP	matrix metalloproteinase
MRE	microRNA recognition element
mRNAs	messenger RNA
MZ	maternal-zygotic
ncRNA	non-coding RNA
n.d.	not determined
NO	nitric oxide
NOX	normoxia
NRP	neuropilin
nt	nucleotides
O_2	oxygen
ORF	open reading frame
P bodies	processing bodies
PAAT	pulmonary artery acceleration time
PABP	poly(A)-binding protein
PACT	protein activator of protein kinase R (PKR)
PAF	platelet activating factor
PAH	pulmonary arterial hypertension
PAP	pulmonary arterial pressure
PASMC	pulmonary artery smooth muscle cell

PBS	phosphate buffered saline
PC	pericytes
PCR	polymerase chain reaction
PDGF	platelet-derived growth factor
PEG	polyethylene glycol
PGI2	prostacyclin
PIK3R2	phosphoinositol-3 kinase regulatory subunit 2
PIP2	phosphatidylinositol biphosphate
piRNA	Piwi-interacting RNA
Piwi	P-element-induced wimpy testis
PKC	protein kinase C
PKD	polycystic kidney disease
PLC	phospholipase C
POD	peroxidase
poly(A)	polyadenosine
Pre-Co	control precursor
Pre-(17)	(miR-17) precursor
pre-miR	precursor microRNA
pri-miR	primary microRNA
PTGS	posttranscriptional gene silencing
qPCR	quantitative PCR
RER	rough endoplasmic reticulum
RIPA	radio immunoprecipitation assay
RISC	RNA-induced silencing complex
RLC	RISC loading complex
rlu	relative light units
RNA	ribonucleic acid
RNAi	RNA interference
ROC	receptor-operated calcium channels
ROK	Rho-associated kinase
ROS	reactive oxygen species
RPLP0	ribosomal protein, large, P0
rpm	rounds per minute
rRNA	ribosomal RNA
R-Smad	receptor-activated Smad
RT	room temperature
RTK	receptor tyrosine kinase
RV/LV+S	right ventricle/left ventricle+septum
RVSP	right ventricular systolic pressure
60S	60 Svedberg
s.c.	subcutaneous(ly)
S1P	sphingosine-1-phosphate
S1PR1	sphingosin-1-phosphate-receptor 1
SAP	systemic arterial pressure
scaRNA	small Cajal body-specific RNA
SCF	stem cell factor
SEM	standard error of the mean
siRNA	small interfering RNA
SM22a	smooth muscle protein 22-α

SMA	smooth muscle α-actin
SMC	smooth muscle cell
SM-MHC	smooth muscle myosin heavy chain
SMTN	smoothelin
snoRNA	small nucleolar RNA
snRNA	small nuclear RNA
SOC	store-operated calcium channels
SPRED1	sprouty-related protein
SR	sarcoplasmic reticulum
STAT	signal transducer and activator of transcription
SVEC	SV40 transformed lymphatic endothelial cells
TBS	Tris buffered saline
TBS-T	TBS with 0.1% Tween-20
TEMED	tetramethylethylenediamine
TGF-β	transforming growth factor beta
TGFBR2	transforming growth factor, beta receptor II
TNF	tumour necrosis factor
TNFAIP1	tumour necrosis factor alpha-induced protein 1
TNRC	trinucleotide repeat containing
TP53	tumour protein p53
t-PA	tissue-type plasminogen activator
TRBP	Tar RNA binding protein
tRNA	transfer RNA
TSP-1	thrombospondin-1
TUT4	terminal uridylyltransferase 4
TYK	tyrosine kinase
uPA	urokinase-type plasminogen activator
UTR	untranslated region
VCAM	vascular cell adhesion molecule
VDCC	voltage-dependent calcium channels
VE	vascular endothelial
VEGF	vascular endothelial growth factor
v/v	volume per volume
vol	volume(s)
vs	versus
VSMC	vascular smooth muscle cells
vWF	von Willebrand factor
w/v	weight per volume
XRN	exoribonuclease

Contents

I. Introduction

A. The circulatory system

In mammals, the circulatory system is composed of two vascular networks: the first filled with blood and belonging to the cardiovascular system, the second containing lymph and associated with the lymphatic system. In contrast to the closed cardiovascular system, where the blood permanently circulates through the vasculature, the lymphatic system is an open system in which the lymph flows unidirectionally from peripheral body tissue towards the heart, where it connects to the cardiovascular system via the subclavian veins.

Blood comprises of three types of blood cells: erythrocytes, leukocytes and platelets. These are distributed within the blood plasma, an aqueous solution containing dissolved proteins, electrolytes, nutrients, hormones and waste products. The distribution of blood and its cargo throughout the body is facilitated by blood vessels. Capillaries of the cardiovascular system extract components of the blood plasma to form the interstitial fluid that encloses all cells of the body. The lymphatic system helps maintain fluid balance by draining excess fluid from the interstitial space into the blood and returns leaked plasma proteins to the cardiovascular system.

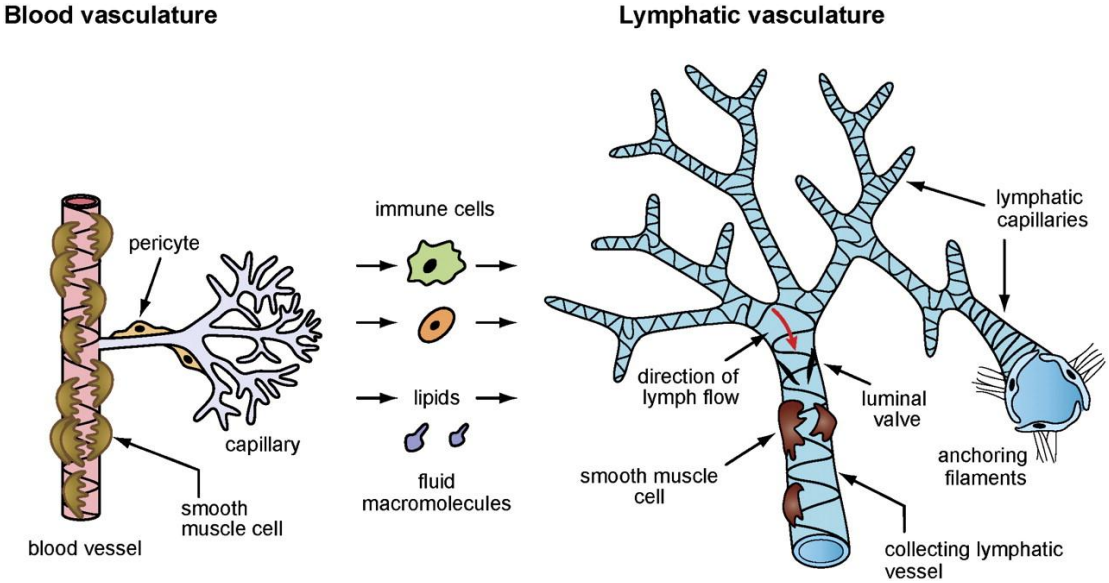

Figure I.1: **Schematic illustration of the blood and the lymphatic vasculature.** The blind-ended lymphatic capillaries consist of a single layer of overlapping endothelial cells which do not possess a continuous basement membrane providing them with the ability to absorb interstitial fluid, immune cells, lipids and macromolecules from the tissue. These substances are returned to the circulating blood via larger collecting lymphatic vessels. The latter are EC tubes with a basement membrane covered with smooth muscle cells. Lymph backflow is prevented by luminal valves. The organization and structure of the blood vasculature will be described in more detail in the following chapters. Y. Wang & G. Oliver Genes Dev. 2010 [2]

Moreover, due to their association with lymphatic tissue, the lymphatic vessels are an important transport route for immune cells during immune response. Additionally, they are involved in the

uptake of dietary lipids and lipid-soluble vitamins from the gastrointestinal tract into the blood. Since the lymphatic vessels arise from embryonic veins during development, both networks consist of interconnected tubes that are lined by endothelial cells and may be covered with smooth muscle cells (Fig. I.1) [3].

1. Circulatory routes in the cardiovascular system

The cardiovascular system can be subdivided into two main circulatory routes: the systemic circulation and the pulmonary circulation.

The heart is the central component of the cardiovascular system, acting as a double pump to drive blood through both the systemic and the pulmonary circulation. In order to fulfil this function, the human heart possesses four chambers. The two atria located at the upper part of the heart constitute the blood receiving units, whereas the two ventricles situated at the bottom of the heart are responsible for discharging the blood into the systemic and the pulmonary circulation. Both atria are separated by the interatrial septum, and the interventricular septum is located between both ventricles. To assure unidirectional flow, blood backflow is prevented by valves between each atrium and ventricle and at the exit of both ventricles. The right atrium accommodates oxygen-poor blood arriving through the superior and inferior vena cava, the coronary sinus from peripheral body tissues above and below the heart as well as the heart itself. After passage to the right ventricle, the blood is pumped through the pulmonary trunk into the left and right pulmonary arteries, directing the deoxygenated blood to the corresponding lung.

Within the lung, the pulmonary artery branches into arteries and arterioles, which finally form meshworks of pulmonary capillaries surrounding the alveolar sacs at the end of the bronchial tree, where gas exchange takes place. The oxygenated blood returns to the heart by travelling from the pulmonary capillaries via venules and veins through the two major pulmonary veins connecting each lung with the left atrium. After entering the left ventricle, the following heart contraction sends the oxygen-rich blood through the aorta and the systemic arteries to peripheral sites of the body.

In systemic capillaries, the blood releases oxygen, absorbs carbon dioxide and returns to the right side of the heart. During systole the heart contracts, and during diastole it relaxes [3].

Figure I.2 shows a schematic representation of the circulatory routes constituting the cardiovascular system.

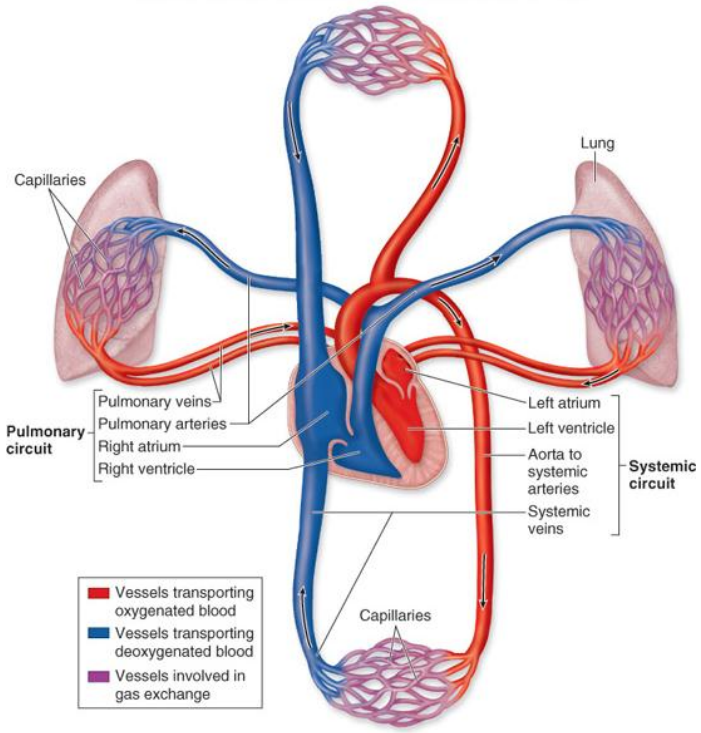

Figure I.2: **Schematic illustration of the pulmonary and the systemic circulation.** The heart represents the interface between the pulmonary and systemic circulation. The left ventricle receives oxygen-rich blood from the lung and supplies it to the systemic circulation which distributes oxygen and nutrients to peripheral tissues. Capillaries mediate the exchange of O_2 and CO_2 as well as nutrients within the periphery. The oxygen-depleted blood is accommodated by the right side of the heart to send it to the lung, where capillaries exchange CO_2 against O_2. [4]

2. Structure of blood vessels

Capillaries possess the simplest structure and are the smallest of all blood vessels. They consist of a layer of endothelial cells that is stabilized by vascular pericytes and enclosed by a basement membrane. Capillaries are responsible for the active and passive exchange of a variety of substances, such as oxygen, carbon dioxide, water, nutrients and waste between the blood and adjacent tissue.

Arteries are blood vessels that direct blood from the heart to peripheral tissue. Generally, they transport oxygenated blood with the exception of the pulmonary and the umbilical arteries. With regard to their diameters, they can be subdivided into large arteries (d = 1 - 2.5 cm, e.g. the aorta), medium-sized arteries (d = 0.3 mm - 1 cm) and arterioles (d = 10 µm - 0.3 mm) [5].

Veins mediate the transport of blood towards the heart. Apart from the pulmonary veins and the umbilical vein, all of them carry deoxygenated blood. Both arteries and veins consist of three different layers: intima, media and adventitia. The intima, that is located towards the lumen of the vessel, consists of basement membrane-anchored endothelium surrounded by connective tissue and the internal elastic lamina. The media contains smooth muscle cells as well as elastic tissue, which in arteries but not in veins, is separated from the adventitia by the external elastic lamina.

The adventitia is formed by fibroblasts, connective tissue and elastic fibres. Most arteries that are in close proximity to the heart, except for the coronary artery, are elastic arteries characterized by high elastin content within the media. Muscular arteries are connected to the elastic arteries and are responsible for further blood transport to organs and tissues. The structural feature of their media is 10-60 layers of helically arranged smooth muscle cells [6]. Since blood pressure is lower in veins than in arteries, the vascular wall of veins is much thinner than that of arteries. Additionally, veins are equipped with valves that prevent the backflow of blood [7]. Arterioles, capillaries and venules form the microcirculation. Blood supply to the vessel walls of large arteries and veins is accomplished by a network of small blood vessels known as the vasa vasorum. Nerve endings from the autonomic nervous system innervate muscular arteries and arterioles to control the contraction of smooth muscle cells [8]. Figure I.3 schematically represents the structure of the different types of blood vessels.

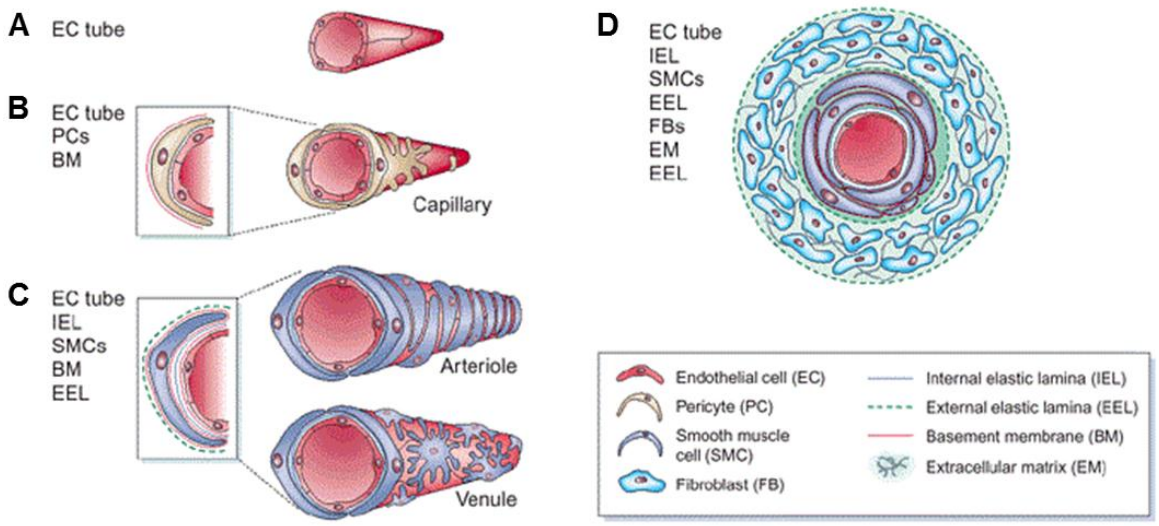

Figure I.3: **Structure of blood vessels and lymphatics. (A)** Initially, vessels consist of a simple endothelial cell (EC) tube which matures into capillaries, arteries or veins. **(B)** Capillaries are EC tubes that are regionally covered with pericytes (PCs) and surrounded by a basement membrane (BM). **(C)** Arterioles and venules link arteries and veins to the capillaries and are therefore increasingly covered with mural cells, i.e. pericytes or smooth muscle cells (SMCs). Precapillary arterioles are characterized by circumferentially arranged and closely packed mural cells (i.e. pericytes or SMCs), whereas the different arrangement of mural cells on postcapillary venules allows extravasation of cells and macromolecules. The endothelial cells rest on the internal elastic lamina (IEL) which may be incomplete or very thin. The SMCs synthesize their own basement membrane. An incomplete or very thin external elastic lamina (EEL) forms the outer boundary of the vessels. **(D)** Three speciliazed layers constitute the wall of larger vessels: intima, media and adventitia. The intima consists of endothelial cells, the media of smooth muscle cells and the adventitia of fibroblasts. Each layer is embedded in extracellular matrix material and is surrounded by an elastic lamina. Modified from Jain, Nat Med 2003 [9]

a) The endothelium

In an adult, the endothelium is made up by 1-6x10^{13} individual cells that are spread over an area of 4000-7000 square meters [10], representing the largest organ of the human body.

The endothelial cells form a continuous monolayer linked to each other by tight junctions, adherens junctions and/or gap junctions. Luminally, the endothelial cells are covered by a network of membrane-bound and plasma-derived glycoproteins and proteoglycans, the glycocalyx. Since the endothelium forms the direct border between the blood and tissue, it occupies multiple tasks to guarantee vascular homeostasis and proper functionality of the body. On the one hand, endothelial cells interact with a variety of circulating cells within the blood; on the other hand, they are in contact with the smooth muscle cells of the vascular wall. Thus, the endothelium coordinates signals arriving through the circulation with those in the vessel wall. Not surprisingly, endothelial dysfunction causes a variety of cardiovascular diseases, such as atherosclerosis, sepsis, coronary artery disease as well as systemic and pulmonary arterial hypertension [11].

The endothelium represents a semi-permeable barrier controlling the passage of small and large molecules from the blood into the surrounding tissue. Vascular endothelial growth factor (VEGF) was originally identified due its capability to promote vascular permeability [12]. A variety of substances from the blood are further converted or metabolized by endothelial enzymes into vasoactive compounds illustrating the important metabolic role of the endothelium in regulating blood flow and organ perfusion. Nitric oxide (NO) and prostacyclin (PGI_2) are examples of endothelial-derived vasodilators, whereas endothelin-1 is a potent vasoconstrictor [10]. Vasoactive compounds cause the de- or hyperpolarization of smooth muscle cells triggering their contraction or relaxation and thus determine vascular tone. The healthy endothelium prevents thrombus formation by constitutively synthesizing molecules that counteract platelet aggregation and blood coagulation, such as PGI_2, NO and thrombomodulin. Fibrinolysis is supported by secretion of tissue-type plasminogen activator (t-PA) under healthy conditions and additionally by urokinase upon endothelial cell activation. Both convert plasminogen into plasmin which degrades fibrin and therefore contributes to thrombus decay [13].

Vascular injury, inflammation and cytokines, like thrombin or histamine, are able to induce endothelial cell activation leading to an increased expression of cell adhesion molecules on the endothelial cell surface. Platelet activating factor (PAF), members of the selectin family, intramolecular cell adhesion molecules 1 and 2 (ICAM-1, ICAM-2) as well as vascular cell adhesion molecule (VCAM) enable adhesion of platelets, neutrophils, lymphocytes and leukocytes to the endothelium. Paracellular transmigration of leukocytes necessitates a transient dissolution of endothelial cell junctions and involves homophilic interactions of endothelial and leukocyte surface proteins that navigate the leukocyte through the endothelium [14].

b) Vascular smooth muscle cells (VSMCs)

During development, smooth muscle cells and pericytes, which belong to the same cell lineage, prevent the regression of blood vessels and stabilize them by secreting increased amounts of ECM components like collagen, elastin and proteoglycans.

In the adult, differentiated vascular smooth muscle cells are largely quiescent, non-migratory, synthesize few ECM components and are mainly committed to fulfilling their contractile function [15]. To accomplish this task, SMCs possess a repertoire of suitable receptors, ion channels, signal transducer molecules, calcium sensitive proteins and contractile proteins. The latter include smooth muscle α-actin (SMA), smooth muscle myosin heavy chain (SM-MHC), smooth muscle protein 22-alpha (SM22a), calponin, desmin and smoothelin. The name smooth muscle was chosen since it is not striated like the cardiac and skeletal muscle. The coordinated contraction and relaxation of VSMCs adapts luminal diameter to ensure adequate blood pressure within the vessels. Contraction of VSMCs is elicited by SMC-intrinsic (myogenic), electrical or chemical stimuli. Each stimulus promotes a rise in intracellular calcium concentration leading to the Calmodulin-Ca^{2+}-mediated activation of myosin light chain (MLC) kinase which phosphorylates the light chain of myosin and enables its interaction with actin. The cycling of the myosin-actin cross-bridges consumes energy from ATP generated by the myosin ATPase activity and causes cellular contraction. During relaxation the intracellular Ca^{2+} concentration drops, MLC phosphatase becomes activated, dephosphorylates myosin light chain and thus prevents actin binding [8]. Arterial SMCs in vivo are present in a partially constricted state since average intracellular Ca^{2+} concentration is held at a lower level than in the extracellular fluid [15].

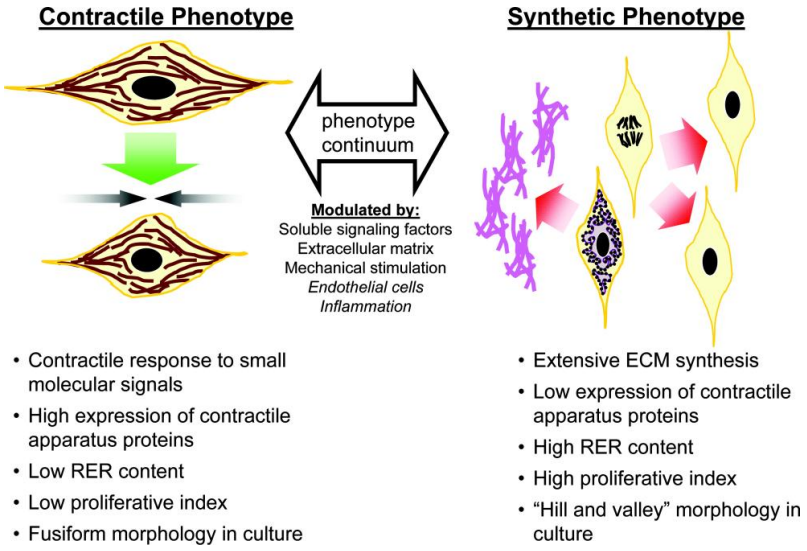

Figure I.4: **Characteristics of smooth muscle cell phenotypes**. The contractile and the synthetic phenotype of smooth muscle cells confine a continuum in which the cells assume different phenotypes in response to external stimuli. The properties of both phenotypes are given in the picture. ECM: extracellular matrix, RER: rough endoplasmic reticulum. Adopted from Beamish et al., Tissue Eng Part B Rev 2010 [16]

During vascular remodelling, e.g. after vascular injury, the contractile SMCs undergo a phenotypic switch into a synthetic phenotype which synthesizes plenty of ECM components and is characterized by the loss of contractility markers as well as increased proliferation and migration. The contractile and the synthetic phenotype define a spectrum of intermediate phenotypes clearly differing in cellular characteristics (Fig. I.4) [17]. In mature SMCs, platelet-derived growth factor (PDGF) isoforms assist the synthetic phenotype, whereas bone morphogenetic protein (BMP) and transforming growth factor-β (TGF-β) signalling induce the contractile phenotype [16].

3. Formation of blood vessels

During embryonic development, the *de novo* formation of the vascular system is initiated by the process of vasculogenesis, in which mesoderm-derived angiogenic progenitor cells (angioblasts) assemble at sites of neovascularization, differentiate into primitive endothelial tubes that subsequently fuse to form a primitive vascular plexus. In vivo studies in mice provide strong evidence that the vessel lumen forms between adjacent cells involving electrostatic cell-surface repulsion [18, 19]. After establishment, the primary vascular network is subjected to rapid expansion and remodelling by the process of angiogenesis which refers to the establishment of new capillaries from existing blood vessels by sprouting, branching or splitting. Stabilization of the nascent vasculature is achieved by recruitment of pericytes and smooth muscle cells (Fig. I.5).

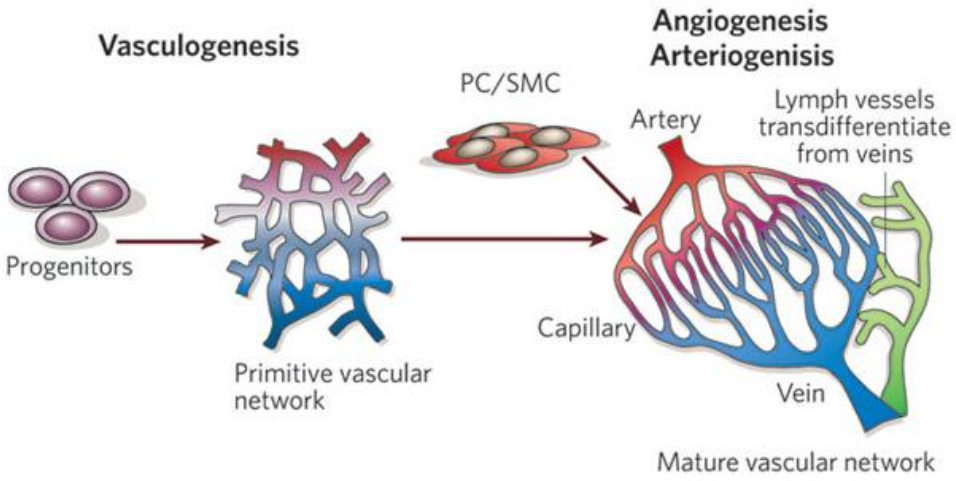

Figure I.5: **Mechanisms of vascular development**. During vasculogenesis, angiogenic progenitors form a primitive vascular network. Expansion of the primitive vascular plexus, stabilization of the vessels by recruitment of pericytes (PC) and smooth muscle cells (SMC) and maturation into a fully functional vascular network occurs by angiogenesis. The lymphatic vessels emerge from veins by transdifferentiation. Arteriogenesis is an adaptive remodelling process in response to physical forces (e.g. shear stress) involving the enlargement of the luminal diameter of pre-existing arterioles to form arteries. Carmeliet, Nature 2005 [20].

Although hemodynamics of blood flow play a role in the specification of arteries and veins [21], recent studies have shown that the arterial and venous identity is also genetically defined since

there are differences in expression of certain molecules before the initiation of blood flow [7]. Arteries are characterized by the expression of the receptor molecules ephrin B2 and neuropilin-1, as well as active Notch signalling in zebrafish, chicks and mice [21]. In veins, the transcription factor COUP-TFII crucially determines venous cell fate by repressing Notch signalling [22]. Moreover, the receptor of ephrin B2, EphB4, is predominantly found in veins (Fig. I.6) [7].

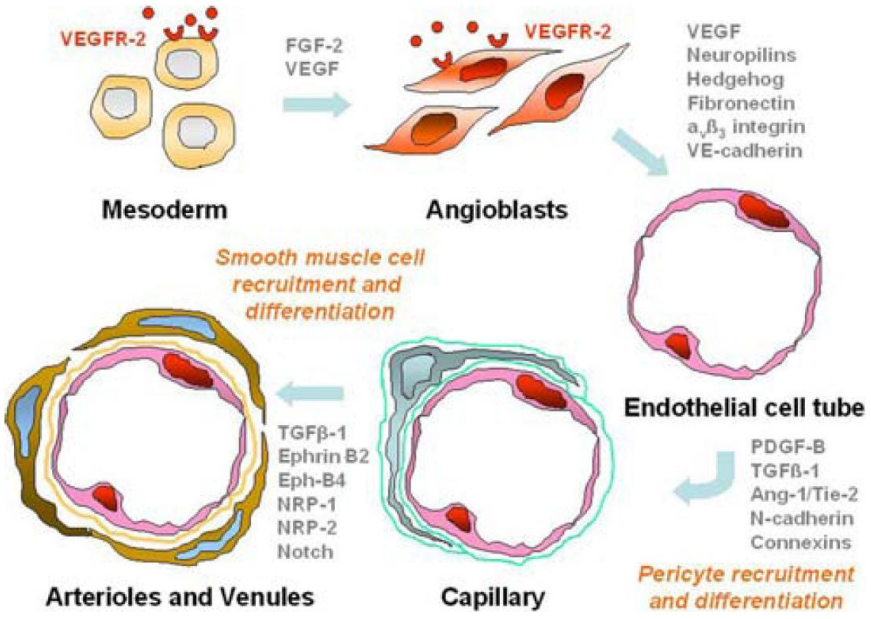

Figure I.6: **Factors regulating vasculogenesis and angiogenesis**. Specification of mesodermal cells into angionenic progenitors (angioblasts) and their migration to sites of neovascularization occurs in response to vascular endothelial growth factor (VEGF) and fibroblast growth factor-2 (FGF-2). VEGF further promotes differentiation of angioblasts into endothelial cells and EC tube formation by binding to the VEGF receptor-2 (VEGFR-2). Signalling via the VEGFR-2 is modulated by neuropilin (NRP) co-receptors, i.e. NRP-1 and NRP-2. Endoderm-derived Hedgehog promotes EC differentiation and tube formation. Vasculogenesis occurs in a fibronectin-rich extracellular matrix and interaction of the cells with the surrounding requires the expression of cell-matrix adhesion molecules (e.g. a_vb_3 integrin). Tube formation depends on the presence of cell-cell adhesion molecules (e.g. vascular endothelial (VE) cadherin). TGF-β induces differentiation of mural cells which proliferate, migrate and are recruited to nascent vessels in response to PDGF-B. Angiopoietin-1 and its receptor Tie-2 are also involved in recruitment of mural cells. N-cadherin and connexins are involved in EC-mural cell junction formation. TGF-β, Ephrin B2 and its receptor EphB4, the neuropilins and Notch signalling determine arterial or venous specification. Modified from Ribatti et al., Angiogenesis 2009 [23]

Although angiogenesis still supports organ growth after birth, the vasculature in the healthy adult is largely quiescent and angiogenesis only occurs in the female reproductive tract and in the placenta during pregnancy. Nevertheless, endothelial cells remain responsive to angiogenic stimuli and can be reactivated to undergo angiogenesis during wound healing and tissue repair. In addition, multipotent adult progenitor cells (MAPCs) are mobilized from the bone marrow in response to injury and are recruited to the affected sites, where they differentiate into endothelial cells to contribute to neovascularization by vasculogenesis [24]. In contrast to embryonic vasculogenesis, postnatal vasculogenesis occurs in response to insufficient supply with oxygen (hypoxia) and involves recruitment of inflammatory cells which do not contribute to vessel formation.

Physiological angiogenesis, as it occurs during development and in healthy adults, is well regulated: the angiogenic response is selectively initiated, sustained for a limited time and turned off upon established perfusion of the new vessel (Fig. I.7A). Hence, a tight control of endothelial cell proliferation is required. Aberrant activation of the vasculature to form new blood vessels due to an excess of growth promoting signals and the absence of cues necessary to coordinate vessel growth leads to pathological angiogenesis if resolution of the angiogenic cascade fails [25]. Uncontrolled vessel growth is associated with various diseases, including diabetic retinopathy, rheumatoid arthritis, atherosclerosis and cancer [26].

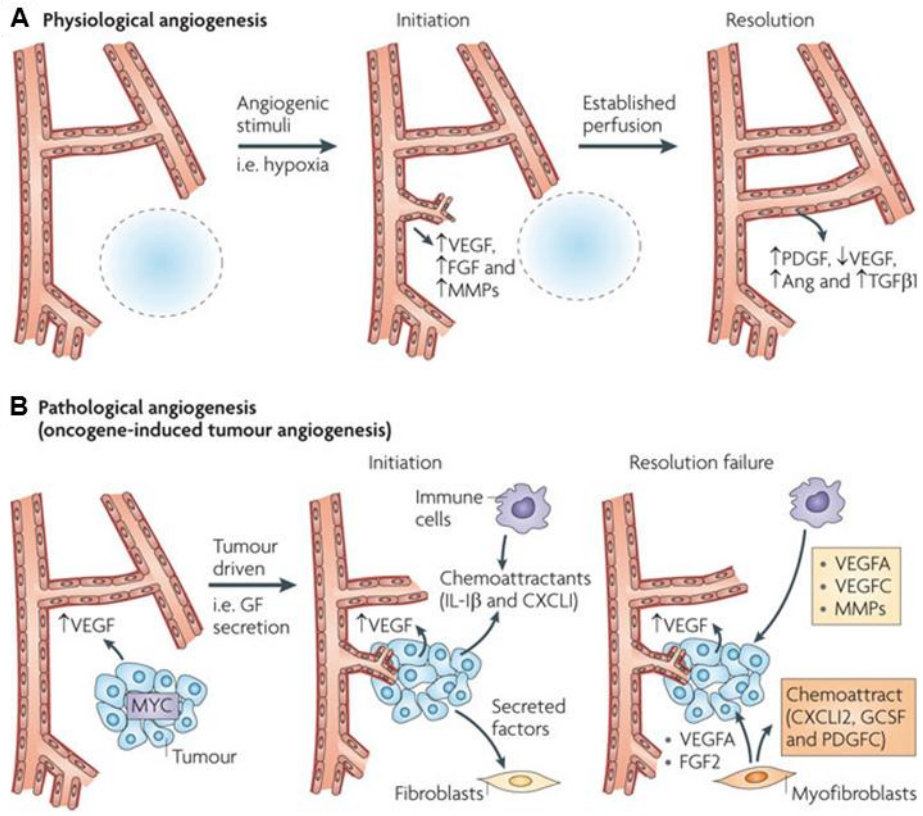

Figure I.7: **Comparison of physiological and pathological angiogenesis**. **(A)** During physiological angiogenesis, endothelial cells respond to an angiogenic stimulus (i.e. hypoxia) by increased secretion of growth factors like VEGF and FGF. These factors lead to vessel destabilization and promote vessel sprouting and endothelial proliferation. Endothelial cell-derived matrix metalloproteinases enable remodelling of the extracellular matrix and liberate ECM sequestered growth factors. Established perfusion of the newly formed vessels causes a decline in VEGF levels. The resolution phase is characterized by an increased expression of platelet derived growth factor (PDGF), Angiopoietin (Ang) and transforming growth factor (TGF) β resulting in the recruitment of mural cells to stabilize the new vessel. **(B)** Pathological angiogenesis during oncogenesis is initiated by tumour-derived VEGF. Other factors secreted by the tumour cause the activation of resident fibroblasts and the recruitment of immune cells which maintain an angiogenic environment by secretion of angiogenesis- and inflammation-promoting factors, thus preventing the resolution of the angiogenic response. GCSF: granulocyte stimulating factor, IL-1β: Interleukin-1β. Adopted from Chung et al., Nat Rev Cancer 2010 [25]

Of these angiogenic diseases, cancer has been investigated most extensively. Tumourigenesis is initiated by an avascular agglomeration of cells which have lost growth control and therefore proliferate in an atypical manner. Initially, the cell mass obtains nutrients and oxygen from the

existing vasculature of the host in the closer environment. Further growth of the tumour increases the distance to blood vessels beyond the effusion range (~200 µm) leading to insufficient oxygen supply of the tumour cells. To overcome the lack of oxygen and to enable tumour growth beyond 2-3 mm^3, tumour cells promote the formation of new blood vessels in a process referred to as tumour angiogenesis (Fig. I.7B). The angiogenic switch is activated by hypoxia within tumour cells leading to the stabilization of hypoxia-inducible factor 1α (HIF-1α) which associates with the constitutively expressed HIF-1β to activate the transcription of target genes. VEGF is a prime example of hypoxia inducible genes and a potent regulator of vasculogenesis and angiogenesis by stimulating EC migration, proliferation and survival. Nevertheless, various other factors and events are required for tumour angiogenesis to proceed. Although tumour angiogenesis is mechanistically similar to physiological angiogenesis, tumours display an abnormal vasculature since vessels are often formed by endothelial and tumour cells and lack pericytes causing vessel dilation and leakiness [24].

4. Pulmonary arterial hypertension

Pulmonary arterial hypertension (PAH) is a disorder of the lung characterized by extensive remodelling of the pulmonary vasculature. This involves vasoconstriction, increased muscularization of pulmonary arteries and occasional in situ thrombus formation. Together, these events lead to the obliteration of small peripheral arteries resulting in sustained elevation of pulmonary vascular resistance and increased pulmonary arterial pressure (PAP). As a consequence of the altered pulmonary vascular resistance, the workload of the heart rises leading to right ventricular hypertrophy and finally death due to right heart failure. Clinically, pulmonary arterial hypertension is diagnosed on the basis of the mean PAP, which is elevated in diseased individuals above 25 mmHg at rest or 30 mmHg during exercise [27].

The incidence of PAH is rather low, annually affecting two to three people in one million [28]. PAH is a disease of multifactorial nature involving all three cell layers of the vessel wall (i.e. endothelial cells, smooth muscle cells and fibroblasts) as well as circulating cells in the blood (e.g. platelets and inflammatory cells). The low incidence and the complexity of this disease might contribute to its largely unknown etiology.

In PAH, endothelial cells are frequently dysfunctional producing and secreting increased amounts of substances which promote vasoconstriction, smooth muscle cell proliferation and migration as well as thrombus formation and inflammation [29]. Under these conditions, distal arteries, which are normally not muscularized, are populated by smooth muscle cells. The media of more proxi-

mal muscular arteries is expanded due to the enhanced mitotic activity of SMCs and accumulation of intercellular connective tissue. Adventitial fibroblasts become activated to transdifferentiate into myofibroblasts and contribute to neointima formation together with medial SMCs [30]. Endothelial cell apoptosis might result either in the loss of pre-capillary arterioles or the selection of hyperproliferative, apoptosis-resistant ECs, which in advanced stages of the disease form abnormal channels within the obliterated lumen as part of plexiform lesions [27, 31]. Figure I.8 summarizes the pathobiological changes observed in the lung during PAH.

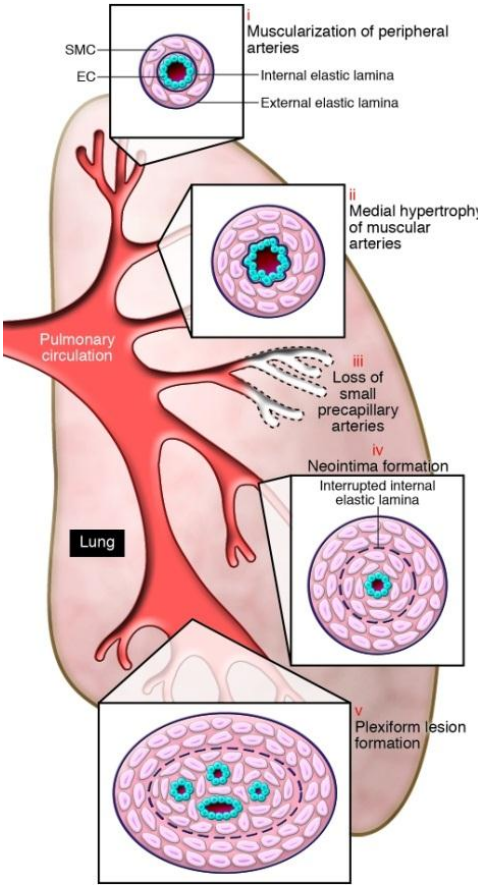

Figure I.8: **Pathological changes of the lung vasculature in pulmonary arterial hypertension.** Vasoconstriction and increased muscularization of pulmonary arteries due to endothelial dysfunction occur which lead to a rise in vascular resistance and impaired blood flow. Rabinovitch, JCI 2008 [27]

Based on its causes, pulmonary arterial hypertension can be classified in three forms: idiopathic PAH (IPAH), familial PAH (FPAH) and associated PAH (APAH). In IPAH, the cause is not apparent, meaning that no familial predisposition or other risk factors exist. In FPAH the disease is based on an inherited genetic defect. Finally, the associated form can occur either as a consequence of other diseases (e.g. HIV infection) or due to intake of drugs or toxins. Interestingly, ~75% of familial and ~25% idiopathic cases can be attributed to germline mutations in a single gene, namely the bone morphogenetic protein receptor 2 (BMPR2) [32].

The discovery that germline mutations of the BMPR2 frequently exist in individuals suffering from PAH, represents a milestone in the field. BMPR2 is, like TGFBR2, a type II transmembrane receptor for the TGF-β superfamily of growth factors with intrinsic serine/threonine kinase activity.

Signalling via BMPR2 and TGFBR2 necessitates the association with a representative of the type I transmembrane receptors in a heterotetrameric complex, leading to the phosphorylation of receptor-activated Smads. Upon phosphorylation, the receptor-activated Smads associate with the common Smad4 and translocate into the nucleus to modulate gene expression (Fig. I.9). BMPR2 is generally associated with BMPR1a or BMPR1b, promoting the phosphorylation of Smad1, Smad5 and Smad8. In contrast, TGFBR2 phosphorylates Smad2 and Smad3 when in a complex with TGFBR1, but is also capable of phosphorylating Smad1/5/8 upon association with activin A receptor type II-like 1 (ACVRL1).

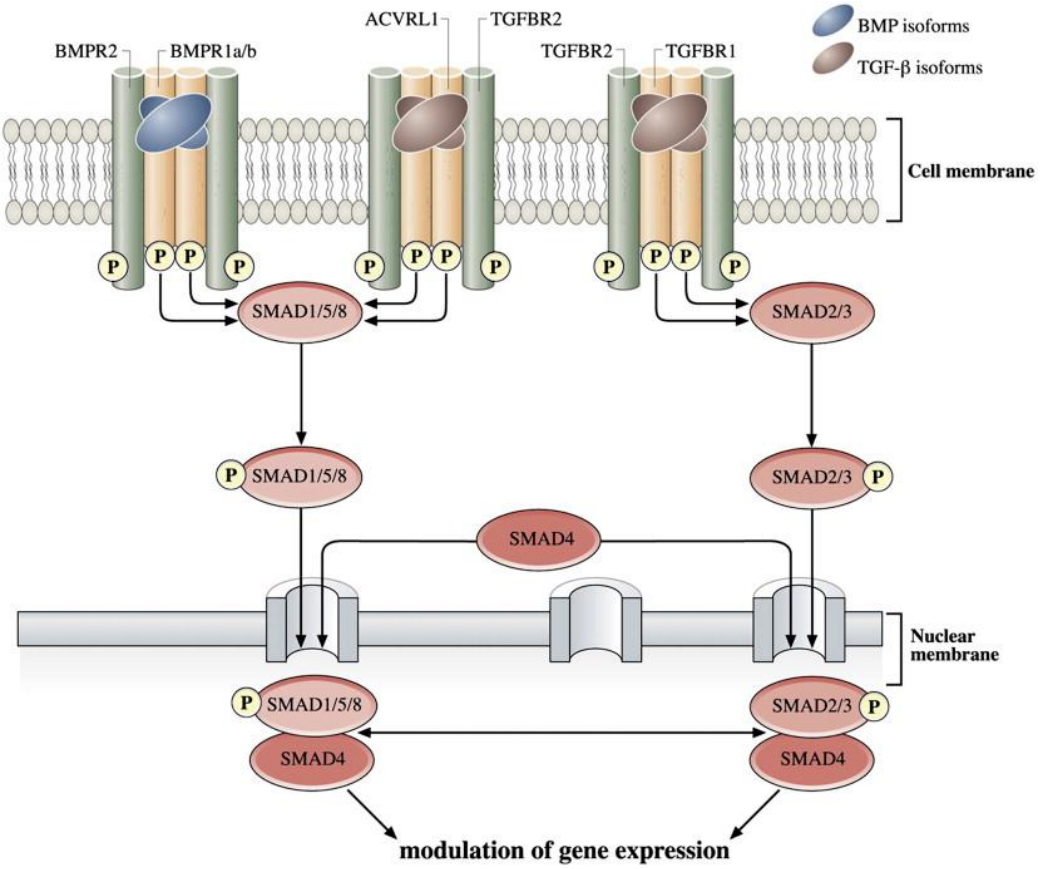

Figure I.9: **BMP and TGF-β signalling**. Ligand binding to a heterotetrameric complex of a type I receptor and a type II receptor for BMP or TGF-β in a 2:2 ratio induces the selective phosphorylation of receptor-activated Smad transcription factors. The latter associate with the common Smad4 upon phosphorylation and translocate into the nucleus to modulate gene expression. BMPR2 forms a complex with BMP type I receptors, and signal transduction occurs via Smad1/5/8. Depending on the type I receptor, TGFBR2 is capable of signalling via Smad1/5/8 or Smad2/3. Adopted from Eickelberg & Morty, Trends Cardiovasc Med. 2007 [32]

Nevertheless, the mechanisms by which the loss-of-function mutations of BMPR2 cause PAH are not yet fully understood. Additionally, BMPR2 levels were also shown to be reduced in PAH patients without having any genetic predisposition regarding BMPR2 [33].

Other signalling pathways contributing to PAH pathology are summarized in Figure I.10.

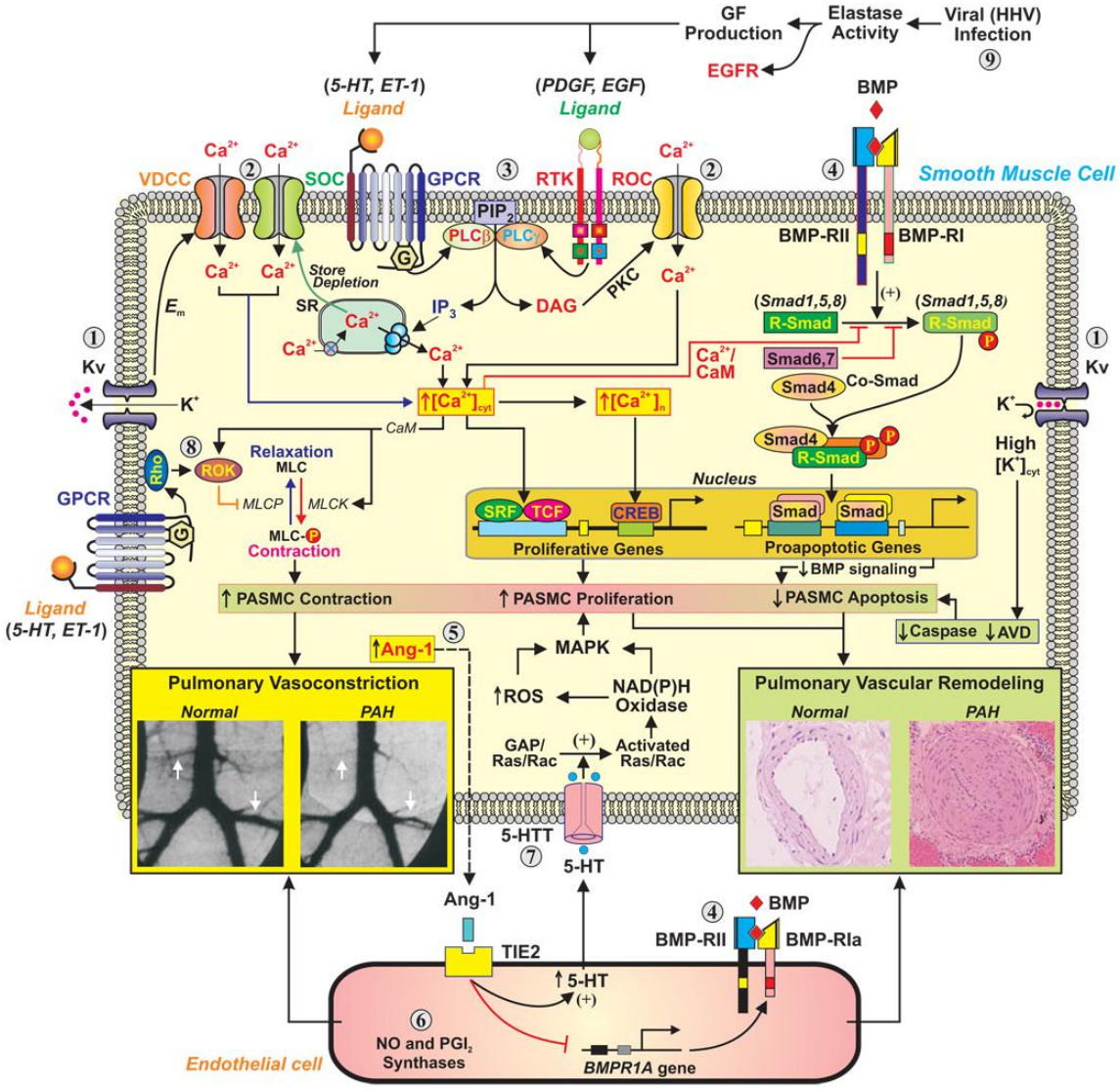

Figure I.10: **Signalling pathways involved in PAH development and pathology**. A variety of signalling pathways have been implicated in PAH leading to chronic vasoconstriction and increased muscularization of pulmonary arteries by governing pulmonary artery smooth muscle cell (PASMC) contraction, proliferation and apoptosis. Endothelial dysfunction causes alterations in the mitogenic and vasoactive environment. ① voltage-dependent potassium channels (K_v); ② voltage-dependent (VDCC), store-operated (SOC) and receptor-operated (ROC) calcium channels; ③ receptor-induced signalling via the inositol 1,4,5-trisphosphate (IP3)/diacylglycerol (DAG) pathway; ④ bone morphogenetic protein (BMP) signalling in endothelial and smooth muscle cells; ⑤ Angiopoietin-1 (Ang-1)/TIE2 signalling; ⑥ nitric oxide (NO) and prostacyclin (PGI_2) synthesis and secretion by endothelial cells; ⑦ Serotonin (5-hydroxytryptamine, 5-HT) signalling ⑧ G protein-coupled receptor (GPCR)-induced signalling via small GTPases (i.e. RhoA) and Rho-associated protein kinase (ROK = ROCK: Rho-associated, coiled-coil containing protein kinase); AVD: apoptotic volume decrease; BMP-R: BMP receptor; CaM: calmodulin; E_m: membrane potential; EGF: epidermal growth factor; ET-1: endothelin-1; GF: growth factor; HHV: human herpes virus; 5-HTT: 5-hydroxytryptamine (serotonin) transporter; MLC: myosin light chain; MLCK: myosin light chain kinase; MLCP: myosin light chain phosphatase; PDGF: platelet-derived growth factor; PIP_2: phosphatidylinositol biphosphate; PKC: protein kinase C; PLC: phospholipase C; ROS: reactive oxygen species; R-Smad: receptor-activated Smad; RTK: receptor tyrosine kinase; SR: sarcoplasmic reticulum. Adopted from Morrell et al., J Am Coll Cardiol. 2009 [29]

The therapeutic options currently available for PAH treatment mainly address the increased vascular tone by operating as vasodilators, but merely provide symptomatic remedy rather than an improved chance of survival. Since pathological vascular remodelling is the cause of pulmonary

arterial hypertension, drugs interfering with endothelial dysfunction, proliferation and apoptosis-resistance of smooth muscle cells may represent a promising therapeutic option.

B. MicroRNAs

1. The expanding universe of non-coding RNAs

Originally, RNA was regarded as the intermediary between DNA and protein. Non-protein-coding RNA was frequently thought to be transcriptional noise and junk. This view partially changed with the discovery that protein complexes involved in the conversion of these protein-coding RNAs, known as messenger RNAs (mRNAs), into proteins contain non-coding RNA (ncRNA) components to fulfil this task. Small nuclear RNAs (snRNAs) are part of the spliceosome and therefore essential for the removal of introns from the pre-mRNA. Transfer RNAs (tRNAs) match the individual amino acids with the respective codon in the mRNA during translation, whereas ribosomal RNA (rRNA) assists and catalyses protein synthesis. These findings showed that non-coding RNAs master crucial infrastructural and housekeeping tasks [34]. Moreover, small nucleolar RNAs (snoRNAs) and the only recently discovered small Cajal body-specific RNAs (scaRNAs), which are both snRNA subtypes, were shown to be involved in the modification (e.g. methylation, pseudouridylation) of different RNA species, including rRNAs, tRNAs and snRNAs and thus add another regulatory mechanism to RNA biology involving ncRNAs.

Although reports about the antisense phenomenon describing the observation that oligonucleotides complementary to endogenous RNA species interfere with biological processes, can be traced back to the 1980s, a major discovery regarding new ncRNA species was made in 1993, when Wightman et al. reported that RNA products of the lin-4 gene regulate lin-14 translation by binding to complementary sequences within the 3´ untranslated region (UTR) of lin-14 and thus determine temporal pattern formation during *C. elegans* development [35]. Lin-4 was the founding member of a novel class of ncRNAs in *C. elegans*, later termed microRNAs [36, 37]. In the following decades it became obvious, mainly by large-scale genome and transcriptome projects, that most of the genome of the studied model organisms is indeed transcribed. Surprisingly, complex organisms like humans and mice do not differ much from *C. elegans* in the number of protein-coding genes, but produce a much larger amount of ncRNA species [38]. The research efforts of the last decades support that some of these these ncRNAs execute crucial regulatory tasks and are required to orchestrate gene expression patterns during the development of complex organisms. They can be classified into long and small ncRNAs according to their size. Long ncRNAs are generally >200 nucleotides (nt) in size and have been shown to be capable of up- or

downregulating gene expression in processes such as dosage compensation, genomic imprinting, stress response as well as developmental patterning and differentiation [39].

Small ncRNAs arise from longer precursors by processing within the cell. Established classes of small ncRNAs in animals are Piwi-interacting RNAs (piRNAs), small interfering RNAs (siRNAs) and microRNAs (miRs). PiRNAs are ~25-30 nt long and seem to be exclusively expressed in germ cells and germ cell-associated somatic cells, where they serve as transcriptional gene silencers of retrotransposons and repetitive elements [39]. Endogenous siRNAs, which are ~21 nt in size, are produced from dsRNAs derived from virus replication, convergent transcription of transgenes or transposons, inverted repeats, transcripts with internal stem loop structures or mRNAs paired to natural antisense transcripts, and they were shown to mediate posttranscriptional silencing of mRNAs and transposons as well as transcriptional gene silencing [40]. Among the small ncRNAs, microRNAs are the most extensively studied and the subject of this work.

2. Biological significance of mammalian microRNAs

The research efforts of the last ten years have manifested the importance of microRNAs for cellular homeostasis since they were shown to modulate processes like apoptosis, cell fate decision, differentiation, migration and proliferation and are therefore crucial for the development of whole organisms. Not surprisingly, dysregulated microRNA expression has been observed in a variety of diseases and was proven to be associated with disease pathology. The reported disorders with microRNA contribution include cancer, autoimmune and neurodegenerative diseases, metabolic abnormalities, infection as well as diverse pulmonary and cardiovascular maladies [41]. Since microRNAs frequently target several components of a signalling pathway, the manipulation of microRNA expression promises immense therapeutic value. Moreover, microRNAs are detectable in different kinds of bodily fluids (e.g. blood) and are currently under investigation as new biomarkers for disease diagnosis and prognosis [42].

3. The discovery of RNA interference

In 1998, Fire et al. provided the first clues regarding the molecular pathway responsible for the antisense phenomenon, which they named RNA interference (RNAi), by demonstrating that in *C. elegans* double-stranded RNA (dsRNA) was more potent in interfering with gene expression than either strand individually [43]. At that time, it was proposed that RNAi served the defence of the host genome against mobile genetic elements (e.g. transposons) and viruses producing dsRNA during their replication. With the beginning of this millennium, the groups of David Bartel und Thomas Tuschl provided evidence for the RNase III-like processing of long dsRNA into short

siRNAs which were ~22 nt RNA in length and mediated mRNA degradation in an ATP-dependent manner in *Drosophila* in vitro systems [44, 45]. At the same time, the Hannon lab reported the partial purification of a protein complex from *Drosophila* which contained nuclease activity and was responsible for mRNA degradation. They named it the RNA-induced silencing complex (RISC) [46]. Moreover, they identified the RNase III nuclease mediating the digestion of long dsRNA into siRNA and called it Dicer [47]. Soon after, RNAi was observed in human cells [48]. Hutvágner et al. demonstrated that microRNAs are processed by Dicer [49]. One year later, they reported that microRNAs enter the RNAi pathway in mammalian cells [50]. In 2003, the RNase III enzyme Drosha was shown to initiate microRNA processing in the nucleus of human cells [51]. Almost simultaneously to the discovery of RNAi in animals, similar pathways of small RNA-induced posttranscriptional gene silencing (PTGS) were described in plants and shown to be involved in meristem function, organ polarity, vascular and leaf development, floral patterning as well as hormone and stress response [51]. The following section focuses on mammalian microRNA biogenesis.

4. MicroRNA biogenesis in mammals

MicroRNAs can be encoded in the introns of protein-coding genes as well as in the introns and exons of non-coding genes, but were also reported to arise from transposable elements or genome repeats [52]. Most microRNA genes are transcribed by RNA polymerase II and possess characteristic structural elements of ordinary mRNAs, namely a cap and a poly(A) tail. However, RNA polymerase III was demonstrated to be responsible for the transcription of certain microRNA genes [53]. Frequently, microRNAs appear in clusters within the genome and polymerase activity produces a polycistronic transcript. The initial transcript of individual microRNAs or microRNA clusters is termed pri-miR for primary microRNA. The primary transcript serves as a substrate for the Microprocessor multiprotein complex in the nucleus which consists at least of the RNase III enzyme Drosha and the essential cofactor DGCR8 (DiGeorge critical region 8) and processes the pri-miR into a ~60-70 nt long microRNA precursor (pre-miR) possessing a stem-loop structure with 5´-phosphate and a 2-nt hydroxylated 3' overhang. Several additional components of the microprocessor were described (e.g. helicases p68 and p72 [54]), but their involvement seems to depend on the primary microRNA to be processed. The pre-miR is subsequently exported from the nucleus into the cytoplasm by Exportin-5 in a Ran-GTP dependent manner. The pre-miR is then incorporated into the RISC loading complex (RLC) which consists of the RNase III endonuclease Dicer, Argonaute-2 (Ago2) and the dsRNA binding proteins TRBP (Tar RNA binding protein) and/or PACT (protein activator of PKR). Within the RLC, Dicer removes the loop of the

pre-miR leaving a 5´-phosphate and a 2-nt hydroxylated 3' overhang at the resulting ~22 nt microRNA duplex which is subsequently unwound by a helicase activity that seems not to be universal for all miRs. The mature microRNA (the guide strand) bound to an Ago protein forms the core of the microRNA-induced silencing complex (miRISC) and serves as a template to guide the miRISC to its targets which predominantly display partial complementary sequences within their 3´ UTR. The second strand of the miR duplex, the passenger strand or microRNA*, is generally discarded and degraded. In the established model for strand selection, the strand with the lower thermodynamic stability at the 5´-end is loaded into the RISC. Diederich and Haber additionally demonstrated that miR precursors with high complementarity in the stem are subject to the cleavage of the 3´-arm of the hairpin by Ago2 in the RLC before Dicer-mediated removal of the loop. The intact strand is selected as the guide, whereas the nicked strand is destined to be degraded [55]. Figure I.11 shows a schematic representation of canonical miR biogenesis.

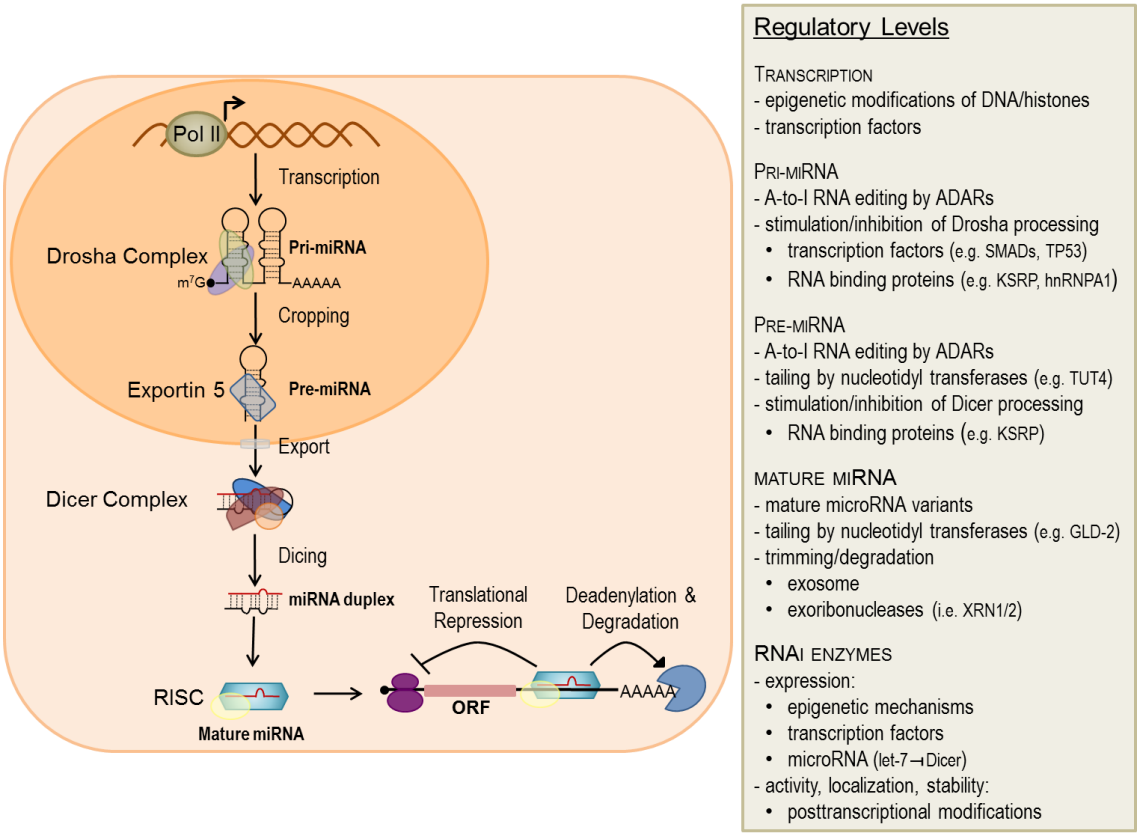

Figure I.11: **Canonical miR biogenesis and regulatory mechanisms.** MiR genes are mainly transcribed by RNA polymerase II into the primary microRNA transcript (Pri-miRNA) out of which the Drosha (microprocessor) complex in the nucleus excises one or several miR precursor molecules (Pre-miRNA). After export into the Cytoplasm, Dicer removes the loop to generate a miRNA duplex. The guide strand is incorporated into the RNA-induced silencing complex (RISC) to mediate mRNA silencing, whereas the passenger strand (miR*) is generally degraded. MicroRNA biogenesis is regulated by a variety of mechanisms affecting either the proteins involved in the biogenesis pathway or the microRNA itself. ADARs: adenosine deaminase, RNA-specific; TP53: tumour protein p53; KSRP: KH-type splicing regulatory protein; hnRNPA1: heterogeneous nuclear ribonucleoprotein A1; TUT4: terminal uridylyltransferase 4; GLD-2: regulatory cytoplasmic poly(A) polymerase; XRN1/2: 5'-3' exoribonuclease 1/2. The regulatory mechanisms are reviewed in Krol, Loedige & Filipowicz in Nat. Rev. Genet. 2010 [56]

Alternative ways of microRNA biogenesis by bypassing Drosha or Dicer have been described. Splicing of short introns with the potential to form hairpin structures, named mirtrons, can give rise to miR precursors without requiring Drosha [57]. In 2010, Cheloufi et al. reported Dicer-independent processing of the erythropoietic miR-451 involving Ago2 catalytic activity [58].
The research efforts of the last years have uncovered a variety of mechanisms which serve the regulation of microRNA biogenesis and impact microRNA action [56]. The fact that individual microRNAs of polycistronic transcripts are often observed to be differentially expressed in their mature form argue for posttranscriptional regulatory mechanisms.

5. Mechanisms of gene regulation by microRNAs

It is well established that miR target identification occurs via Watson-Crick base pairing and requires a certain degree but no absolute complementarity in animals. Due to empirical aspects and evolutionary conservation a contiguous segment of bases at the 5´ end covering the nucleotides 2-7 has been identified to be important for target recognition. This sequence was thought to represent the nucleation site where base pairing is initiated and is known as the ´seed´ sequence. However, functional ´non-seed´ target sites have been described, too [59]. Likewise, experimental evidence and evolutionary conservation are also the reason for the assumption that animal miRs target the 3´ UTR of transcripts. Nevertheless, there is no mechanistic aspect arguing against target sites in the 5´ UTR [60] and the existence of functional target sites in the open reading frame (ORF) has already been proven [61].

Members of the Argonaute protein family are responsible for the miRISC effector function. In mammals, there are 4 Ago proteins (Ago1, Ago2, Ago3 and Ago4), of which only Ago2 has an enzymatically active RNase H-like P-element-induced wimpy testis (Piwi) domain and is therefore capable of RNA cleavage. However, the direct endonucleolytic cleavage of the mRNA by Ago2 within the microRNA-mRNA base-paired region is rather uncommon since it requires full or at least high complementarity of the miR and the transcript [62], a condition that is frequently met in plants but only rarely applies to animal cells. Instead, microRNAs promote mRNA decay by triggering the removal of the 3´ poly(A) tail of partially complementary messages in the presence of the poly(A)-binding protein (PABP) by the CCR4-NOT deadenylase complex which leads to 5´ decapping and finally exonucleolytic degradation of the mRNA [63]. Figure I.12 shows a schematic representation of the mechanisms and proteins involved in the miR-mediated mRNA decay.

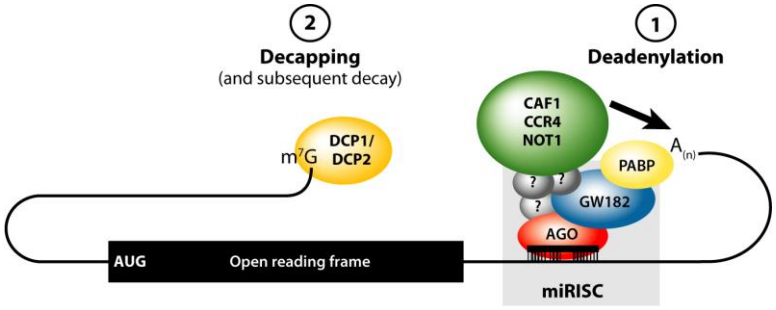

Figure I.12: **Schematic representation of miR-initiated mRNA decay.** ① Deadenylation of the mRNA poly(A) tail ($A_{(n)}$) requires recruitment of the CCR4-NOT1 deadenylase complex by the miRISC and direct interaction of the GW182 with the poly(A)-binding protein (PABP). ② After removal of the poly(A) tail, the cap (m^7G) at the 5′ end is eliminated by the DCP1/DCP2 decapping complex. AGO: Argonaute, CAF1: CCR4-associated factor, CCR4: carbon catabolite repression 4 protein, NOT1: negative on TATA-less. Adopted from Fabien et al., Annu Rev Biochem 2010 [64]

However, microRNAs often affect protein expression of their targets without changing mRNA abundance indicating that microRNAs cause inhibition of translation. Hitherto, existing reports indicate that microRNA-mediated translational repression is capable of affecting both the initiation and elongation phase (Fig. I.13).

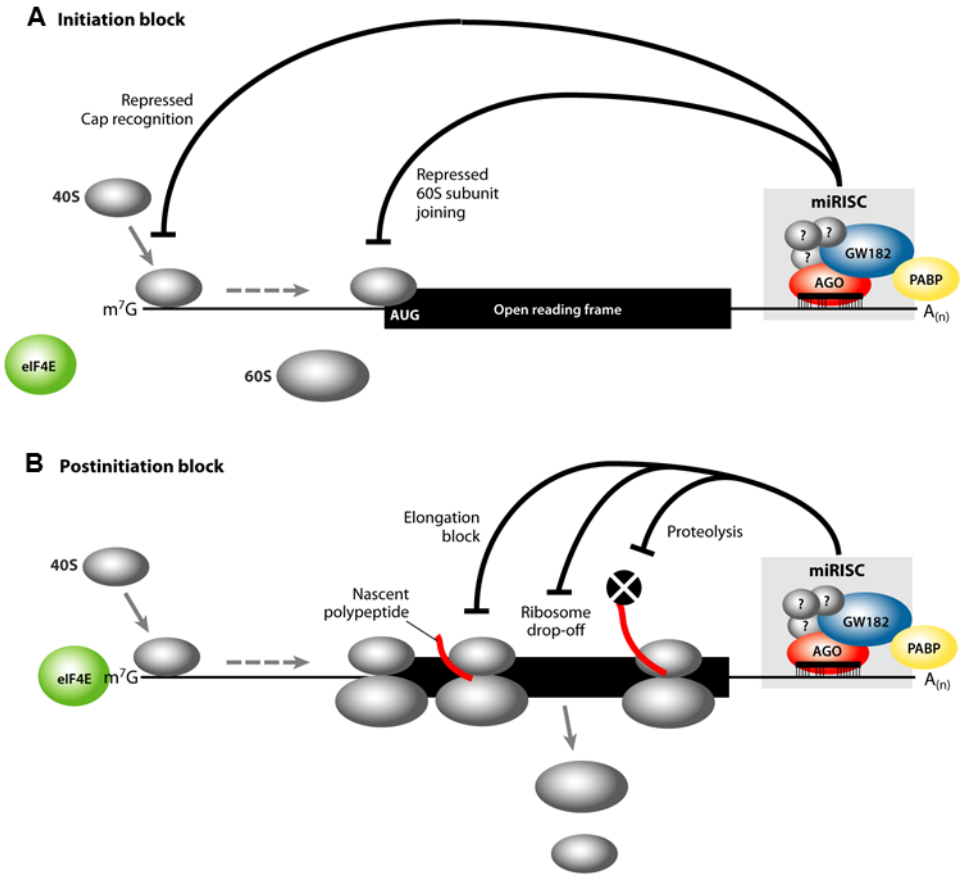

Figure I.13: **Schematic representation of miR-initiated translational repression. (A)** MiRISC blocks initiation of mRNA translation by preventing eIF4F-cap recognition and recruitment of the 40S ribosome subunit or by interfering with 60S ribosome subunit joining and 80S ribosome assembly. **(B)** Inhibition of mRNA translation in postinitiation phases potentially includes blunted ribosomal elongation, ribosome drop-off or enhanced proteolysis of nascent proteins. AGO: Argonaute, $A_{(n)}$: poly(A) tail, m^7G: the 5'-terminal cap. Adopted from Fabien et al., Annu Rev Biochem 2010 [64]

Inhibition of translational initiation occurs either due to impaired cap recognition or failing recruitment of the 60S ribosomal subunit. The mechanism for blocked protein elongation remains largely elusive, but possibly involves premature termination of translation followed by ribosome drop-off or degradation of the nascent polypeptides by recruited proteolytic enzymes. However, several studies provide evidence that miRNAs are capable of inhibiting protein synthesis in a poly(A) tail-dependent and -independent manner [64].

Both miRNA-mediated decay and translational repression require interaction of Ago with GW182 proteins. In mammals, three GW182 proteins are known, namely trinucleotide repeat containing 6A (TNRC6A), 6B (TNRC6B) and 6C (TNRC6C). An enrichment of translational repressed mRNAs has been observed in discrete and dynamic foci within the cytoplasm, namely GW or processing (P) bodies, which are probably also the location for the final stages of mRNA decay. P bodies do not accommodate ribosomes or most of the translation initiation factors, but contain Ago and GW182 proteins as well as enzymes involved in mRNA deadenylation, decapping and degradation [64].

RISC binding to the microRNA target sequence within the mRNA is influenced by several parameters. Alternative splicing and polyadenylation gives rise to different mRNA isoforms which might considerably differ in the length of their 3´ UTR and the number of microRNA target sites. Genes involved in basic cellular processes (housekeeping genes) tend to have shortened 3´ UTRs and are therefore less frequently regulated by microRNAs [65]. The association of transcripts with RNA binding proteins, such as human antigen R (HuR) or dead end homolog 1 (DND1), was shown to interfere with microRNA action by blocking the microRNA binding site or changing RNA secondary structure [66]. Moreover, importin 8 was reported to affect the association of Ago proteins with a diverse set of mRNA targets and is therefore necessary for microRNA-target interaction [67].

Although the majority of reports describe miR-mediated repression of gene expression on the posttranscriptional level, there are also a few reports documenting that microRNAs are able to promote translation of mRNAs under certain circumstances (e.g upon growth arrest or virus infection) [68, 69]. Additionally, microRNAs in the nucleus were shown to be capable of regulating transcription by targeting promoter sequences to either silence [70] or induce gene expression [71], perhaps depending on the degree of complementarity.

6. Role of microRNAs in the vasculature

In the first attempt to study the biological function of mammalian Dicer in vivo, the Hannon lab targeted the second of both RNase III domains of murine Dicer in transgenic mice to abrogate catalytic activity of the enzyme and prevent production of mature microRNAs. The loss of Dicer´s functional capability resulted in early embryonic lethality (before embryonic day E7.5) of homozygous animals probably due to defective maintenance of the stem cell population demonstrating Dicer´s necessity for proper mammalian development [72]. Since the first endothelial and hematopoietic cells emerge in the yolk sac blood islands in the developing mouse embryo at E7.0 [73], it might be possible that Dicer deletion also impaired differentiation of the endothelial and hematopoietic cell lineage in these mice.

First evidence for the involvement of Dicer in blood vessel formation during mammalian embryonic development was provided by Yang et al. who generated transgenic mice carrying hypomorphic Dicer alleles ($Dicer^{ex1/2}$) by deleting the first two exons of the murine dicer gene which code for a part of the helicase domain. The homozygous $Dicer^{ex1/2}$ embryos displayed retardation in growth and development compared to their wildtype littermates and died between embryonic day 12.5 and 14.5 possessing few blood vessels which were thin, small and less organized within the embryo and the yolk sac [74]. Consistently, maternal-zygotic dicer (MZdicer) zebrafish mutants in which the RNase III and dsRNA-binding domains were disrupted exhibited several abnormalities in morphogenesis including disturbed blood circulation [75]. Another viable, apparently healthy and normally developed hypomorphic Dicer mouse line ($Dicer^{d/d}$) did not produce offspring due to infertility of female homozygous mutant mice. Detailed analysis of the female mice revealed impaired blood vessel growth in the ovaries, a defect that could be partially restored by combined injection of miR-17-5p and let-7b which were shown to target both the anti-angiogenic factor tissue inhibitor of metalloproteinase 1 (TIMP1) [76]. In order to investigate the involvement of Dicer in postnatal angiogenesis, Suárez et al. generated two different endothelial specific Dicer deficient mouse lines, one inducible knockout and one hypomorphic mouse line. In both mouse lines, the endothelium specific Dicer deletion impaired angiogenesis in response to a variety of stimuli, including VEGF treatment, tumourigenesis, limb ischemia and wound healing [77].

In line with the in vivo observations, siRNA-mediated knockdown of Dicer in endothelial cells in vitro profoundly decreased proliferation and migration as well as tube forming and sprouting capacity [78, 79] indicating that Dicer plays an important role in endothelial cell function. In one study, the impaired capacity of Dicer deficient ECs to form tubes on Matrigel was rescued upon combined overexpression of miR-17-5p, -18a and -20a which are members of the miR-17-92 cluster [77]. Although siRNA elicited downregulation of Drosha also impaired capillary sprouting

and tube forming capacity of ECs, the effect of Dicer knockdown on in vitro angiogenesis was much more dramatic [78].

To identify microRNAs involved in endothelial cell biology, different research groups addressed microRNA expression in ECs of various origins by performing miR profilings. In total, 200 microRNAs were reported to be expressed in human endothelial cells [80]. Table I.1 shows a compilation of the microRNAs frequently detected or functionally analysed in ECs.

MiR name	Function in ECs	MiR name	Function in ECs
let-7a	n.d.	miR-101	anti-angiogenic [81]
let-7b	pro-angiogenic [76]	miR-103	n.d.
let-7c	n.d.	miR-106a	n.d.
let-7d	n.d.	miR-125a/b	control of vasomotor homeostasis [82]
let-7f	pro-angiogenic [78]	miR-126	pro-angiogenic [83-85], anti-inflammatory [86], anti-atherosclerotic [87], regulation of vascular integrity [83, 85, 88]
miR-10a	anti-inflammatory [89]	miR-130a	pro-angiogenic [90]
miR-15a/b	pro-apoptotic [91]	miR-132	pro-angiogenic, pro-proliferative [92]
miR-16	n.d.	miR-135a	regulation of leukotriene formation [93]
miR-17-3p (miR-17*)	anti-inflammatory [94]	miR-155	preeclamsia pathology [95]
miR-17-5p (miR-17)	pro-angiogenic [76], pro-proliferative [77]	miR-181a	endothelial cell fate decision [96]
miR-18a	pro-angiogenic [77]	miR-191	n.d.
miR-19a	anti-proliferative [97]	miR-199	maintainance of microcirculatory tone [98] regulation of leukotriene formation [93]
miR-20a	pro-angiogenic, pro-proliferative [77]	miR-200b	anti-angiogenic, vascular permeability [99]
miR-21	anti-apoptotic [100], anti-angiogenic [101]	miR-210	pro-angiogenic, pro-migratory [102] repression of mitochondrial respiration [103]
miR-23a	n.d.	miR-214	Anti-angiogenic [104]
miR-23b	anti-proliferative [105]	miR-217	promotes senescence, anti-angiogenic [106]
miR-24	anti-angiogenic, pro-apoptotic, anti-migratory, anti-proliferative [107]	miR-218	pro-proliferative, vascular patterning [108]
miR-27a	n.d.	miR-221	anti-angiogenic [109, 110] anti-proliferative [110]
miR-27b	pro-angiogenic [78]	miR-222	anti-angiogenic [110, 111] anti-proliferative [110]
miR-29a	n.d.	miR-296	pro-angiogenic [112]
miR-30a	n.d.	miR-301a	anti-thrombotic [113]
miR-30c	anti-thrombotic [113]	miR-320	anti-angiogenic, anti-migratory, anti-proliferative [114]
miR-31	anti-inflammatory [94]	miR-424	pro-angiogenic [115] anti-proliferative [116]
miR-34a	promotes senescence, anti-proliferative [117]	miR-503	anti-angiogenic, anti-proliferative, anti-migratory [118]
miR-92a	anti-angiogenic [119]	miR-519c	anti-angiogenic [120]
miR-100	anti-angiogenic, anti-proliferative [121]	miR-663	pro-inflammatory [122]

Table I.1: **Endothelial microRNAs and their biological functions.** The table shows microRNAs that are frequently detected in endothelial cells according to Heusschen et al. [80] as well as microRNAs that have been functionally studied in ECs so far. n.d.: not determined.

The function of a variety of miRs has already been studied in detail in the endothelium, thus contributing to their classification into pro- and anti-angiogenic miRs according to their effect on angiogenesis. MiR-126, the most prominent miR in the endothelial compartment, is encoded in an intron and is co-expressed with its host gene Egfl7 (EGF-like domain 7), a secreted peptide. Combined knockdown of miR-126 and miR-126* in zebrafish by morpholino-mediated targeting of pri-miR-126 did not affect overt morphology or vascular patterning of the animals but impaired vascular integrity promoting hemorrhage formation [83]. Correspondingly, genetic deletion of miR-126 in mice was frequently associated with embryonic or perinatal death due to systemic edema and leaky blood vessels resulting in multifocal hemorrhages [85]. Regarding the molecular mechanism, two negative regulators of VEGF signalling were identified to be directly regulated by miR-126, namely PIK3R2 (phosphoinositol-3 kinase regulatory subunit 2) and the sprouty-related protein SPRED1.

MiR-126 was also shown to control tumour necrosis factor-α (TNF-α)-induced vascular cell adhesion molecule 1 (VCAM1) expression and leukocyte adhesion to human umbilical vein endothelial cells (HUVECs) potentially implicating an involvement of miR-126 in the inflammatory response of the endothelium [86]. Finally, van Solingen et al. provided evidence for the requirement of miR-126 in ischemia-induced angiogenesis in vivo by combining a hindlimb ischemia model with the Antagomir-mediated inhibition of miR-126 [84].

MiR-221 and miR-222, which are transcribed in a single primary transcript and belong to the same miR family, were shown to downregulate protein expression of the stem cell factor (SCF) receptor v-kit Hardy-Zuckerman 4 feline sarcoma viral oncogene homolog (KIT) and displayed impaired tube forming and migratory capacity of endothelial cells [110].

Moreover, miR-221/222 partially normalized the increase in eNOS protein expression upon Dicer knockdown in the endothelial cell line EA.hy.926 [79]. Finally, Dentelli et al. provided evidence for the downregulation of miR-222 in ECs in response to the inflammatory cytokine interleukin-3 (IL-3) as well as decreased miR-222 levels in human atherosclerotic lesions. Additionally, signal transducer and activator of transcription (STAT) 5A was identified to be a direct miR-222 target and partially responsible for its inhibitory effect on neovascularization in vivo [111]. Other miRs whose functions have been studied in ECs are shown in Fig. I.14.

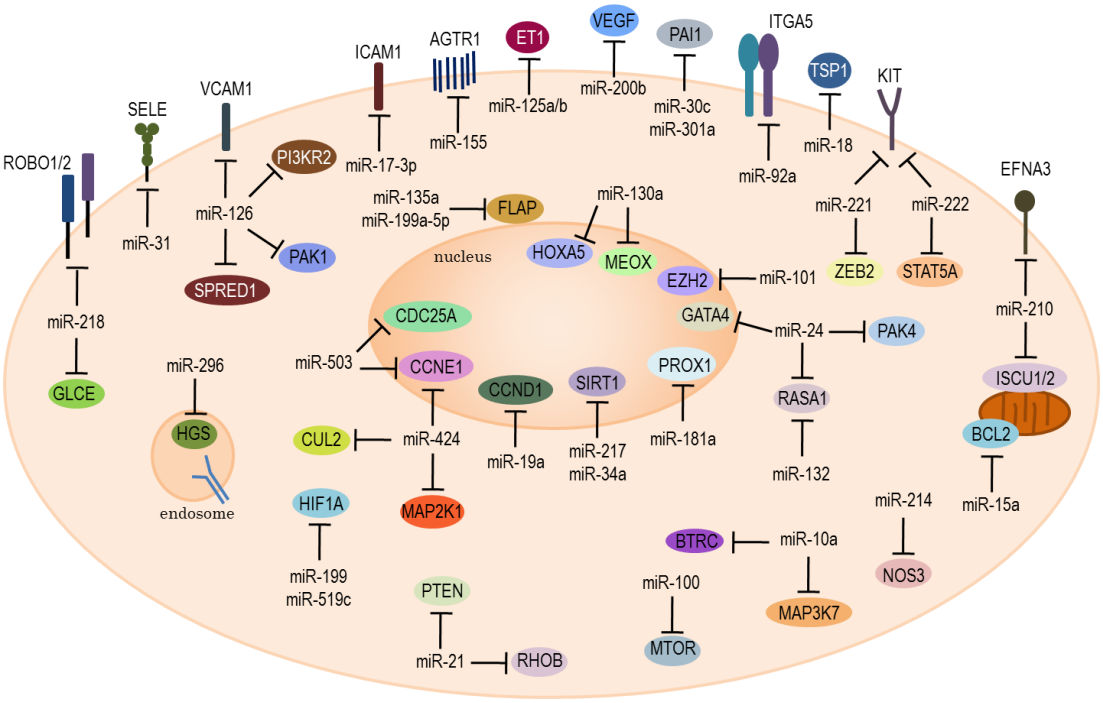

Figure I.14: **Endothelial microRNAs and their validated direct targets.** BTRC: beta-transducin repeat containing, MAP3K7: mitogen-activated protein kinase kinase kinase 7 [89]; BCL2: B-cell CLL/lymphoma 2 [91]; ICAM1: intercellular adhesion molecule 1, SELE: selectin E [94]; TSP1: thrombospondin-1 [77]; CCND1: Cyclin D1 [97]; PTEN: phosphatase and tensin homolog; RHOB: ras homolog gene family, member B [101]; GATA4: GATA binding protein 4, PAK4: p21 protein (Cdc42/Rac)-activated kinase 4, RASA1: RAS p21 protein activator 1 [92, 107]; PAI1: plasminogen activator inhibitor type 1 [113]; SIRT1: sirtuin 1 [106, 117]; ITGA5: integrin $\alpha 5$ [119]; MTOR: mechanistic target of rapamycin [121]; EZH2: enhancer of zeste homolog 2 [81]; ET1: endothelin 1 [82]; PAK1: p21 protein (Cdc42/Rac)-activated kinase 1, PI3KR2: phosphatidylinositol 3-Kinase regulatory subunit 2, SPRED1: sprouty-related, EVH1 domain containing 1 [83, 85, 88]; VCAM1: vascular cell adhesion molecule 1 [86]; MEOX: mesenchyme homeobox 2 (GAX), HOXA5: homeobox A5 [90]; FLAP: [93]; HIF1A: hypoxia inducible factor 1, alpha subunit [98, 120]; AGTR1: angiotensin II receptor, type 1 [95]; PROX1: prospero homeobox 1 [96]; VEGF: vascular endothelial growth factor [99]; EFNA3: Ephrin A3 [102]; ISCU1/2: iron-sulfur cluster scaffold homolog 1/2 [103]; NOS3: nitric oxide synthase 3, endothelial cell [104]; GLCE: glucuronic acid epimerase, ROBO1/2: roundabout 1/2 [108]; KIT: v-kit Hardy-Zuckerman 4 feline sarcoma viral oncogene homolog [110]; ZEB2: zinc finger E-box binding homeobox 2 [109]; STAT5A: signal transducer and activator of transcription 5A [111]; HGS: hepatocyte growth factor-regulated tyrosine kinase substrate [112]; CUL2: cullin 2 [115]; CCNE1: cyclin E1, MAP2K1: mitogen-activated protein kinase kinase 1 (MEK1), CDC25A: cell division cycle 25 homolog A [116, 118]

Only recently, Albinsson et al. reported the establishment of vascular smooth muscle cell specific Dicer knockout mice. The SM22α promoter driven inactivation of Dicer was embryonically lethal around day E16/17 as a result of vascular fragility associated with extensive hemorrhage formation. Thinning of the vascular wall due to reduced proliferation of smooth muscle cells and impaired contractility of umbilical vessels caused by downregulated expression of components of the contractile machinery and decreased stress fiber formation were documented. The expression of SMC-specific genes could be partially rescued by introducing miR-145 into Dicer knockout SMCs leading to restoration of actin polymerization [123], revealing the significance of miR-145 for smooth muscle cell differentiation. These findings are in line with the results of Cordes et al. who demonstrated that miR-145 was sufficient to differentiate multipotent neural crest stem cells

into vascular smooth muscle cells. Moreover, miR-145 was essential for the myocardin-induced conversion of fibroblasts into VSMCs. Although miR-145 biased VSMC differentiation, the genetically clustered and co-transcribed miR-143 was necessary to confine SMC proliferation and to promote SMC differentiation [124]. In vivo evidence for the essential role of the miR-143/145 cluster in smooth muscle phenotype determination was provided by Boettger et al. who generated miR-143/145 knockout mice. General deletion of the miR-143/145 cluster did not affect viability and fertility of the mutant mice, but they displayed a significant reduction in systolic blood pressure owing to reduced contractility of vascular smooth muscle cells which were largely locked in the synthetic phenotype [125]. So far, miR-143 and -145 are the most extensively studied microRNAs in vascular smooth muscle cells, but other miRs have also been shown to affect SMC phenotype. MiR-24 and miR-221 were both reported to be upregulated in response to PDGF which promotes the synthetic SMC phenotype, and both miRs interfered with the expression of contractile genes and cell cycle regulators to enhace cell proliferation [126, 127], just as the miR-221 family member miR-222 did [128]. Vice versa, BMP4 increased the level of mature miR-21 which caused an increase in the expression of contractile genes by downregulating programmed cell death 4 (PDCD4) [129]. Other microRNAs reported to affect cellular behavior of VSMCs are miR-1 [130], let-7d [131], miR-26a [132], miR-29b [133], and miR-146a [134].

7. The miR-17-92 cluster

The primary transcript of the miR-17-92 cluster, named Chromosome 13 open reading frame 25 (C13orf25), originally became famous for its upregulated expression in B-cell lymphoma as a consequence of chromosomal amplification [135], although the organization of the individual microRNAs in a cluster had already been described two years earlier [136].

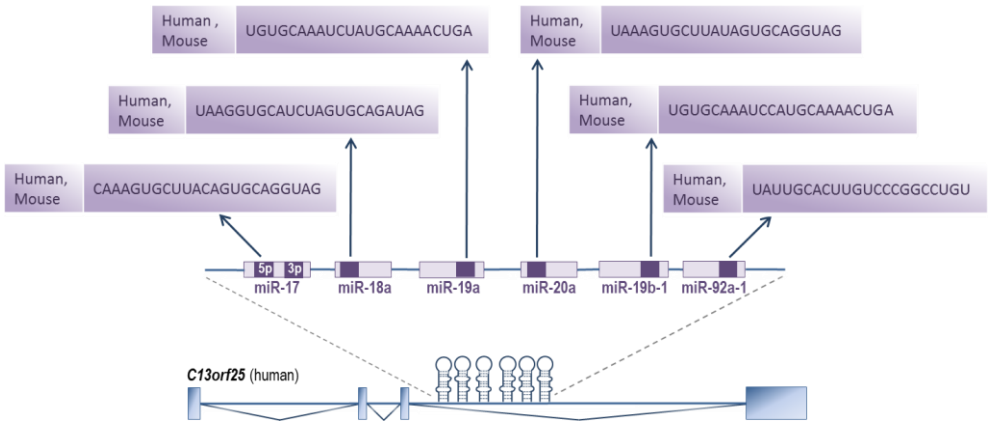

Figure I.15: **The miR-17-92 cluster.** The miR-17-92 cluster is highly conserved among species and encodes six microRNA precursors which give rise to the seven mature microRNAs miR-17-5p (miR-17), miR-17-3p (miR-17*), miR-18a, miR-19a, miR-20a, miR-19b-1 and miR-92a-1. Since miR-17-3p is often not detectable, its relevance as functional mature microRNA is questionable. In humans, the miR-17-92 cluster is located on chromosome 13. *C13orf25*: chromosome 13 open reading frame 25, 5p: 5 prime, 3p: 3 prime

C13orf25 harbors the 7 mature microRNAs miR-17-5p, miR-17-3p, miR-18a, miR-19a, miR-20a, miR-19b and miR-92a-1 which arise from 6 microRNA precursors (Fig. I.15). However, the biological significance of miR-17-3p is debatable since it is often not or only lowly expressed. Therefore, miR-17-3p is designated miR-17*, whereas miR-17-5p is also known as miR-17.

The miR-17-92 cluster is highly conserved among species and ancient gene duplications, deletions and mutations have given rise to two cluster paralogs in the mammalian genome, namely the miR-106a-363 and the miR-106b-25 cluster which are encoded on human chromosomes X and 7, respectively (Fig. I.16) [137]. The members of the miR-17-92 cluster and its paralogs can be categorized into four families based on the sequence of their seed region: the miR-17 family (miR-17, miR-20a/b, miR-106a/b, and miR-93), the miR-18 family (miR-18a/b), the miR-19 family (miR-19a/b) and the miR-25 family (miR-25, miR-92a, and miR-363) [138]. It is believed that members of the same seed family regulate a related set of genes and therefore execute similar biological functions.

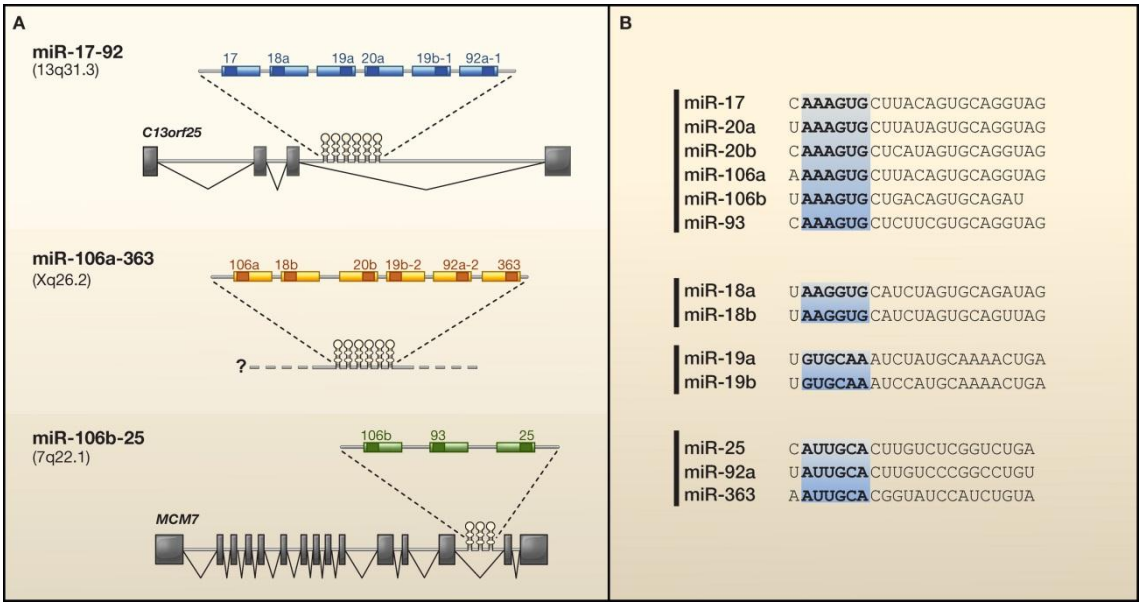

Figure I.16: **The miR-17-92 cluster paralogs. (A)** Genomic localization and organization of the human miR-17-92, miR-106a-363 and miR-106b-25 cluster paralogs. The structure of the primary transcript of the human miR-106a-363 cluster which is encoded on the X chromosome has not been defined yet, but contains the 6 mature microRNAs miR-106a, miR-18b, miR-20b, miR-19b-2, miR-92a-2 and miR-363. The miR-106b-25 cluster is localized in an intron of the *mcm7* gene on chromosome 7 and encodes miR-106b, miR-93 and miR-25. **(B)** Categorization of the microRNAs encoded by the three cluster paralogs into families according to their seed sequences (highlighted in blue). Adopted from Mendell, Cell 2008 [138]

He et al. proved in a B-cell lymphoma mouse model that overexpression of a transcript containing the precursors of the first five members of the miR-17-92 cluster (miR-17-19b) accelerated c-MYC-induced tumourigenesis. Due to the observed oncogenic potential of the miR-17-92 cluster, they suggested to name the primary transcript oncomiR-1 [139]. For this reason, the research efforts of subsequent years mainly focused on the role of the cluster in tumour biology as well as

its dissection with respect to the contribution of the individual members and resulted in a multitude of publications. The members of the miR-17-92 cluster were shown to control proliferation, senescence, survival, migration and invasion of cancer cells by targeting the cell cycle regulators cyclin-dependent kinase inhibitor (CDKN) 1A [140] and Cyclin D1 [141], the nuclear receptor coactivator amplified in breast cancer (AIB) 1 [142], Hif1α [143], the suppressor of cytokine signalling (SOCS) 1 [144], phosphatase and tensin homolog (PTEN) [145, 146], members of the E2F family of transcription factors [147] and the pro-apoptotic protein BIM (Bcl2L11) [140] as well as the suppressor of Wnt/β-catenin signalling HMG box-containing protein (HBP) 1 [148].

Moreover, BMPR2 [149] and TGFBR2 [150-153], have been proven to be regulated by miR-17 and miR-20a, and it was suggested that these microRNAs might be responsible for the observed downregulation of BMPR2 in non-genetic cases of pulmonary arterial hypertension [149]. Table I.2 summarizes the direct targets of the miR-17-92 cluster members that have been identified so far.

Gene symbol	Function	MicroRNA	References
BCL2	apoptosis	miR-17/20a	Beveridge et al. (2009) [154]
BCL2L11/BIM	apoptosis	miR-17/20a	Fontana et al. (2008) [140] Cloonan et al. (2008) [155]
	apoptosis	miR-19	Mavrakis et al. (2010) [156]
	apoptosis	miR-92a	Xiao et al. (2008) [157]
BMPR2	BMP signalling	miR-17/20a	Brock et al. (2009) [149]
CCND1	proliferation	miR-17/20a	Deshpande et al. (2009) [158] Yu et al. (2008) [141]
	proliferation	miR-19a	Qin et al. (2010) [97]
CDH1	metastasis	miR-92a	Chen et al. (2010) [159]
CDKN1A/p21	proliferation	miR-17/20a	Fontana et al. (2008) [140] Cloonan et al. (2008) [155]
CTGF	anti-angiogenic	miR-18a, miR-19	Dews et al. (2006) [150] Ernst et al. (2010) [160]
E2F1	proliferation	miR-17/20a	Scherr et al. (2007) [161] O´Donnell et al. (2005) [147]
ERBB4	neuronal development	miR-19a	Tsai et al (2010) [162]
ESR1	neuronal differentiation proliferation	miR-18a, miR-19a miR-18a	Loven et al. (2010) [163] Liu (2009) [164]
F3/TF	homeostasis	miR-19	Zhang et al. (2011) [165]
FN1	adhesion	miR-17	Shan et al. (2009) [166]
FNDC3A	adhesion	miR-17	Shan et al. (2009) [166]
GAB1	proliferation	miR-17	Cloonan et al. (2008) [155]
HBP1	metastasis	miR-17	Li et al. (2011) [148]
HIF1A	proliferation	miR-20a	Taguchi (2008) [143]
IL8	tumour metastasis	miR-17/20a	Yu et al (2010) [167]
IRF1	proliferation	miR-17	Cloonan et al. (2008) [155]
ITGA5	adhesion	miR-92a	Bonauer et al. (2008) [119]
KAT2B/PCAF	proliferation	miR-17	Cloonan et al. (2008) [155]
MAP3K12	neuronal differentiation	miR-17/20a	Beveridge et al. (2009) [154]
MAPK9	proliferation	miR-17	Cloonan et al. (2008) [155]

Gene symbol	Function	MicroRNA	References
MAPK14	lung branching morphogenesis	miR-17/20a	Carraro et al. (2009) [168]
MEF2D	neuronal differentiation	miR-17/20a	Beveridge et al. (2009) [154]
NCOA3	proliferation	miR-17	Hossain et al. (2006) [142] Cloonan et al. (2008) [155]
NR3C1/GR	stress habituation	miR-18a	Uchida et al (2008) [169]
NR4A2	neuronal differentiation	miR-19	Tsai et al (2010) [162]
NR4A3	proliferation	miR-17	Cloonan et al. (2008) [155]
PKD1	proliferation	miR-17	Cloonan et al. (2008) [155]
PKD2	proliferation	miR-17	Cloonan et al. (2008) [155] Sun et al (2010) [170]
PPP2R5E	proliferation	miR-19	Mavrakis et al. (2010) [156]
PPARA	proliferation	miR-17	Cloonan et al. (2008) [155]
PRKAA1	energy homeostasis	miR-19	Mavrakis et al. (2010) [156]
PTEN	apoptosis	miR-19	Lewis et al. (2003) [171] Olive et al. (2009) [145] Cloonan et al. (2008) [155] Mavrakis et al. (2010) [156]
PTPRO	proliferation	miR-17	Xu et al. (2008) [172]
RBL2/p130	proliferation	miR-17	Wang et al. (2008) [173]
RUNX1	proliferation	miR-17/20a	Fontana et al. (2007) [174]
SLC12A5/KCC2	neuronal homeostasis	miR-92a	Barbato et al. 2010 [175]
SMAD2	TGF-β signalling	miR-18a	Mestdagh et al. (2010) [151]
SMAD4	BMP/TGF-β signalling	miR-18a	Mestdagh et al. (2010) [151] Dews et al. (2010) [176]
SOCS1	STAT signalling inhibitor	miR-19	Pichiorri et al. (2008) [144]
STAT3	lung branching morphogenesis	miR-17/20a	Carraro et al. (2009) [168]
TGFBR2	TGF-β signalling	miR-17/20a	Volinia et al. (2006) [153] Tagawa et al. (2007) [152] Mestdagh et al. (2010) [151] Dews et al. (2010) [176]
TNF/TNFA	inflammation	miR-19a	Liu et al. (2011) [177]
TSG101	proliferation	miR-17	Cloonan et al. (2008) [155]
TP63/p63	proliferation	miR-92a	Manni et al. (2009) [178]
THBS1	anti-angiogenic	miR-18a	Dews et al. (2006) [150] Suarez et al. (2008) [77] Dogar et al (2011) [179]
VEGFA	angiogenic cytokine	miR-17	Ye et al (2008) [180]
ZNF512B/GAM	apoptosis proliferation	miR-17/20a, miR-92a	Tili et al (2010) [181]

Table I.2: Validated targets of the miR-17-92 cluster and their cellular function.

Moreover, Dews et al. reported in 2006 that Ras transformed colonocytes which additionally overexpress the miR-17-92 cluster form larger and better perfused tumours than the Ras transformed control cells. The tumour angiogenesis promoting activity of the miR-17-92 cluster was attributed to the downregulation of the anti-angiogenic proteins connective tissue growth factor (CTGF) and thrombospondin-1 (TSP-1) by miR-18 and miR-19 [150]. Two research groups addressed the contribution of the individual members to the overall tumourigenicity of the miR-17-92 cluster in two different B-cell lymphoma mouse models by genetic dissection. Both groups

identified miR-19 to be the miR in charge of the oncogenic potential of the miR-17-92 cluster and provided evidence that miR-19 promoted tumour cell survival by targeting regulators of apoptosis. However, the other members were thought to have auxiliary activities in tumour development [145, 146].

Lu et al. reported high expression of members of the miR-17-92 cluster in lung tissue of mouse embryos at E11.5 and observed perinatal lethality and an abnormal lung phenotype characterized by hyperproliferative and undifferentiated epithelial cells after specific overexpression of the miR-17-92 cluster in the distal lung epithelium [182]. Referring to this, miR-17 and its homologous family members miR-20a and miR-106b were shown to control lung branching morphogenesis by directly regulating the FGF10-FGFR2b downstream mediators mitogen-activated protein kinase 14 (MAPK14) and STAT3 in order to determine E-Cadherin (CDH1) levels in the epithelial cell membrane [168].

In 2008, the Tyler Jacks lab addressed the function of the individual paralogs of the miR-17-92 cluster in development by targeted deletion in mice. Expression analysis of members of the different paralogs in a variety of murine organs as well as embryonic stem (ES) cells revealed similar expression patterns for the miR-17-92 and the miR-106b-25 cluster, whereas members of the miR-106a-363 cluster could not be detected. Deletion of the miR-106b-25 and miR-106a-363 cluster neither impaired viability and fertility of the animals nor did they display any obvious abnormalities. In contrast, miR-17-92 knockout mice died immediately after birth exhibiting hypoplastic lungs, ventricular septal defects, signs of general growth retardation and impaired survival of B cell progenitors. To investigate redundancy of the paralogs, the lab generated double knockouts by simultaneously deleting miR-17-92 and miR-106b-25 as well as triple knockouts by deletion of all three paralogs. As a result, mutant animals died before embryonic day 15 (E15) suffering from severe heart defects as well as edema formation and vascular congestion. Thus, Ventura et al. presented evidence for essential and redundant functions of the miR-17-92 cluster and its paralogs during mammalian development [183].

Last year, Hackl et al. published miRNA expression profiles gained from different replicative cell and organismal aging sample sets including endothelial cells, replicated cytotoxic T cells, renal epithelial cells and skin fibroblasts as well as foreskin, mesenchymal stem cells and cytotoxic T cells from old and young donors. They observed a general downregulation of miR-17, miR-19b and miR-20a levels in all seven models, although the decrease of miR-19b in foreskin and cytotoxic T cells of old donors was not statistically significant, thus providing strong evidence for the involvement of members of the miR-17-92 cluster in aging [184].

Figure I.17 summarizes the regulatory involvement and effects of the miR-17-92 cluster in different biological systems.

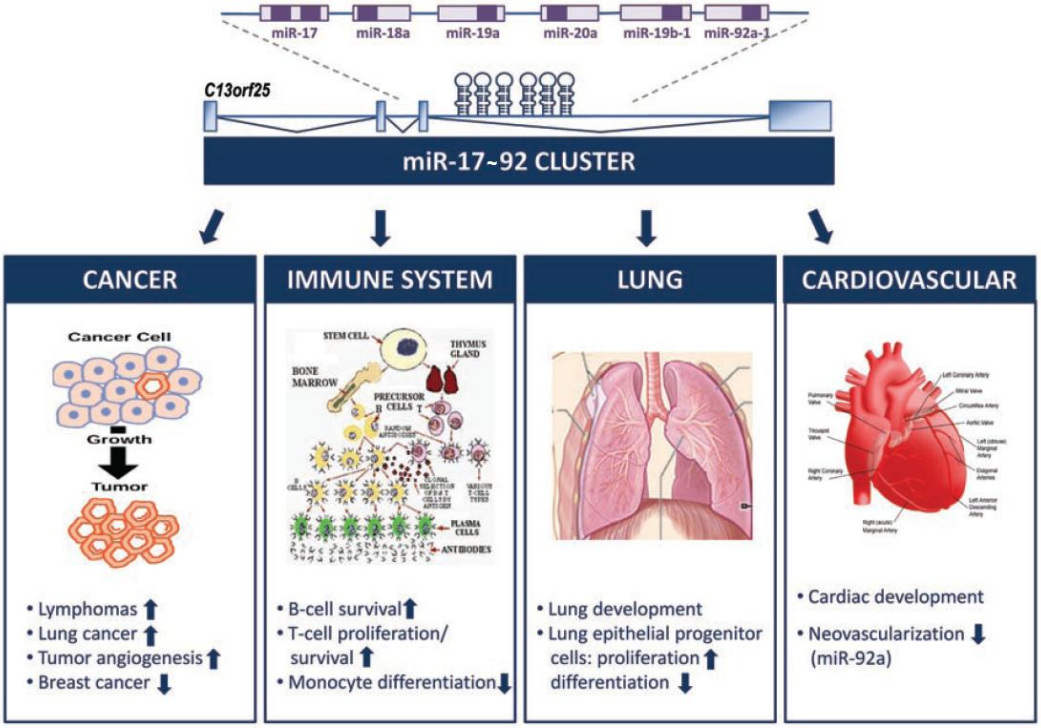

Figure I.17: **Summary of the versatile role of the miR-17-92 cluster in different biological systems.** Adapted from Bonauer & Dimmeler, Cell Cycle 2009 [185]

Concerning the transcriptional regulation, the proto-oncogene c-MYC [147], STAT3 and E2F1-3 [186] have been demonstrated to activate expression of the miR-17-92 cluster, whereas the tumour supressor p53 was shown to block it [187]. Additionally, there is substantial evidence that the individual members of the miR-17-92 cluster are differentially expressed and regulated [182]. Since they are transcribed together in a polycistronic mRNA, posttranscriptional processing or unequal stabilities of the mature miRNAs are probably responsible for this phenomenon. In line with this, Drosha processing of the miR-18a precursor in the primary transcript was discovered to be favoured in HeLa cells by binding of the heterogeneous nuclear ribonucleoprotein A1 (hnRNP A1) to a conserved sequence in the loop of pre-miR-18a in a context-dependent manner [188, 189]. It is very likely, that the processing of the other cluster members is also regulated, although the involved factors and mechanisms are not known yet, but will certainly be the matter of future investigations.

II. Objective

In recent years, microRNAs have gained considerable attention, since they were found to control almost every cellular process by regulating gene expression on the posttranscriptional level. Moreover, dysregulated microRNA expression has been observed in a variety of diseases and increasing evidence suggests that changes in microRNA levels substantially contribute to disease pathology. Therefore, microRNAs might represent a novel valuable target class for therapeutic intervention. However, in order to exploit a specific microRNA as a drug target, it is necessary to know its biological function.

The microRNA-17-92 cluster has become famous for its involvement in tumourigenesis and over-expression of the cluster in a mouse tumour model was shown to enhance vascularization of the tumours. Interestingly, our lab identified miR-92a as a negative regulator of angiogenesis in endothelial cells and a critical regulator of recovery in response to ischemic diseases.

So far, the function of the remaining members of the microRNA-17-92 cluster in vascular biology has not been specified in detail. Thus, the doctoral thesis at hand addresses the following two issues:

(1) The miR-17-92 cluster was dissected into the distinct members to analyse miR-17, -18a, -19a and -20a individually with respect to their function in endothelial cells and angiogenesis in vitro and in vivo. Moreover, we evaluated the effect of Antagomir-mediated inhibition of miR-17 on tumour angiogenesis in vivo.

(2) Pulmonary arterial hypertension (PAH) is a devastating disorder of the pulmonary vasculature frequently culminating in death due to right heart failure. Since some members of the miR-17-92 cluster were recently shown to be upregulated in animal models of pulmonary arterial hypertension, we studied the therapeutic applicability of Antagomir-mediated microRNA inhibition in experimental PAH. Since miR-17 inhibition turned out to be of therapeutic value, we further investigated the function of this miR in cells of the pulmonary vasculature.

III. Material and Methods

A. Material

1. Consumables

Item name	Manufacturer
Amicon Ultra centrifugal filter devices 3K	Millipore, Billerica, MA (USA)
Cell culture dishes (6 cm, 10 cm)	Greiner Bio-One GmbH, Frickenhausen (Germany)
Cell culture Flasks, 75T	Greiner Bio-One GmbH, Frickenhausen (Germany)
Combitips	Eppendorf AG, Hamburg (Germany)
Costar serological pipettes	Corning, Lowell, MA (USA)
Costar Stripette serological pipettes	Corning, Lowell, MA (USA)
Costar Transwell permeable support, 24 well plate, polycarbonate membrane 8.0 µm pores	Corning, Lowell, MA (USA)
Falkons (15 ml, 50 ml)	Greiner Bio-One GmbH, Frickenhausen (Germany)
Filter Tips TipOne RPT (10 µl, 100 µl, 1000 µl)	Starlab, Ahrensburg (Germany)
Hyperfilm ECL	Amersham, Buckinghamshire (GB)
Microcentrifuge Tubes TipOne (1.5 ml)	Starlab, Ahrensburg (Germany)
MicroWell™ Plates Nunc F96	Thermo Fisher Scientific Inc., Waltham, MA (USA)
Multiwell cell culture plates (6-, 12-,24-well)	Greiner Bio-One GmbH, Frickenhausen (Germany)
PCR tubes (0.5 ml)	Eppendorf AG, Hamburg (Germany)
Plastic cuvettes	Sarstedt, Nümbrecht (Germany)
PVDF membrane	Millipore, Billerica, MA (USA)
Safe-Lock Tubes (1.5 ml)	Eppendorf AG, Hamburg (Germany)
Safe-Lock Tubes (2 ml)	Eppendorf AG, Hamburg (Germany)
Whatman paper	Macherey-Nagel, Düren (Germany)

2. Electronic equipment

Item name	Type/Model	Manufacturer
Centrifuge	MIKRO 22R	Hettich, Tuttlingen (Germany)
	MIKRO 200R	Hettich, Tuttlingen (Germany)
	Biofuge 15	Heraeus Sepatech, Osterode (Germany)
	Multifuge 3S	Heraeus Instruments, Osterode (Germany)
	Megafuge 3.0R	Heraeus Sepatech, Osterode (Germany)
CO2 incubator		Heraeus Instruments, Osterode (Germany)
FACS	Canto II	BD, Franklin Lakes, NJ (USA)
GeneAmp PCR System	9700	Applied Biosystems, Foster City, CA (USA)
Gel documentation device		Vilber Lourmat, Marne-la-Vallée (France)
Homogenizer	FastPrep-24	MP Biomedicals, Solon, OH (USA)
	Tissue Tearor	Biospec products inc., Bartlesville, OK (USA)
Incubator	Function line	Heraeus Instruments, Osterode (Germany)
Laser Scanning Microscope	LSM510 META	Zeiss, Jena (Germany)

Item name	Type/Model	Manufacturer
Magnetic stirer	RCT basic	IKA, Staufen (Germany)
	MR 3001	Heidolph, Schwabach (Germany)
Microscope	Axiovert 100	Zeiss, Jena (Germany)
	Axiovert 100M	Zeiss, Jena (Germany)
Plate reader	Synergy HT	Biotek, Winooski, VT (USA)
Power supply	PowerPac HC	Bio-Rad, Munich (Germany)
	E865	Consort, Turnhout (Belgium)
Real-Time PCR System	StepOne Plus	Applied Biosystems, Foster City, CA (USA)
Refrigerated/Heating Circulator	F12	Julabo, Seelbach (Germany)
Safety Cabinet	HERAsafe	Heraeus, Hanau (Germany)
Shaking incubator	3033	GFL, Burgwedel (Germany)
Spectrophotometer	SmartSpec 3000	Bio-Rad, Munich (Germany)
	NanoDrop 1000	NanoDrop, Wilmington, DE (USA)
Table-top processor	CURIX 60	AGFA, Cologne (Germany)
Thermocycler	TPersonal	Biometra, Goettingen (Germany)
	TProfessional basic	Biometra, Goettingen (Germany)
Thermomixer	compact	Eppendorf, Hamburg (Germany)
Thermostat		Liebisch, Bielefeld (Germany)
Transilluminator	T2201	Sigma-Aldrich, St. Louis, MO (USA)
Tube luminometer	Lumat LB9507	Berthold technologies, Bad Wildbad (Germany)

3. Other equipment

Item name	Type/Model	Manufacturer
Adjustable-volume Pipettes	Reference	Eppendorf, Hamburg (Germany)
Adjustable-volume Pipettes	Pipetman	Gilson, Middleton, WI (USA)
Hemocytometer	Neubauer Improved	LO-Laboroptik GmbH, Bad Homburg (Germany)
Mini Gel Electrophoresis System	Owl EasyCast B2	Thermo Fisher Scientific Inc., Waltham, MA (USA)
Mini Gel Electrophoresis System	Protean 2	Bio-Rad, Munich (Germany)
Mini Gel Electrophoresis System	Protean 3	Bio-Rad, Munich (Germany)
Multipette	Plus	Eppendorf, Hamburg (Germany)
Multipette	Xstream	Eppendorf, Hamburg (Germany)
Quartz cuvette		Bio-Rad, Hercules, CA (USA)

4. Chemicals

Item name	Manufacturer
Acetic acid	J T Baker, Phillipsburg, NJ (USA)
Acrylamid solution (30%)	Applichem, Darmstadt (Germany)
Agarose	Roth, Karlsruhe (Germany)
Agarose high resolution	Roth, Karlsruhe (Germany)
Ampicillin	Roth, Karlsruhe (Germany)
APS	Roth, Karlsruhe (Germany)
Aqua ad iniectabilia	B. Braun AG, Melsungen (Germany)

Item name	Manufacturer
β-glycerolphosphate	ICN Biochemicals inc., Aurora, OH (USA)
β-Mercaptoethanol	Roth, Karlsruhe (Germany)
Brij 35	Sigma-Aldrich, St. Louis, MO (USA)
Bromophenol blue	Merck, Darmstadt (Germany)
Calcium chloride dihydrate	Merck, Darmstadt (Germany)
Chloroform	J T Baker, Phillipsburg, NJ (USA)
Complete Protease Inhibitor Cocktail Tablets	Roche, Indianapolis, IN (USA)
Disodium pyrophosphate	Sigma-Aldrich, St. Louis, MO (USA)
Distilled water RNA/DNA free	Invitrogen, San Diego, CA (USA)
Dithiothreitol (DTT)	Applichem, Darmstadt (Germany)
ECL Western Blotting Detection Reagents	Amersham, Buckinghamshire (GB)
Ethylenediamine tetraacetic acid (EDTA)	Sigma-Aldrich, St. Louis, MO (USA)
Ethylene glycol tetraacetic acid (EGTA)	Applichem, Darmstadt (Germany)
Ethanol absolute (EtOH abs.)	Sigma-Aldrich, St. Louis, MO (USA)
Ethidiumbromide	Roth, Karlsruhe (Germany)
Formaldehyde	Riedel-de Haën, Morristown, NJ (USA)
Glycerin	Applichem, Darmstadt (Germany)
Glycin	Applichem, Darmstadt (Germany)
HEPES	Roth, Karlsruhe (Germany)
Hydrochloric acid (HCl)	Sigma-Aldrich, St. Louis, MO (USA)
Isopropanol	Sigma-Aldrich, St. Louis, MO (USA)
Leupeptin	Sigma-Aldrich, St. Louis, MO (USA)
Magnesium acetate	Sigma-Aldrich, St. Louis, MO (USA)
Methanol	Sigma-Aldrich, St. Louis, MO (USA)
Methyl cellulose	Sigma-Aldrich, St. Louis, MO (USA)
Phast Gel Blue R350	GE Healthcare, Little Chalfont, Buckinghamshire (UK)
Phenylmethanesulfonylfluoride (PMSF)	Sigma-Aldrich, St. Louis, MO (USA)
PhosSTOP Phosphatase Inhibitor Cocktail Tablets	Roche, Indianapolis, IN (USA)
Potassium acetate	Merck, Darmstadt (Germany)
Potassium chloride (KCl)	Applichem, Darmstadt (Germany)
SDS	MP Biomedicals, Irvine, CA (USA)
Sodium acetate	Sigma-Aldrich, St. Louis, MO (USA)
Sodium chloride (NaCl)	J T Baker, Phillipsburg, NJ (USA)
Sodium ortho-vanadate (Na3VO4)	Sigma-Aldrich, St. Louis, MO (USA)
TEMED	Applichem, Darmstadt (Germany)
TRI Reagent	Sigma-Aldrich, St. Louis, MO (USA)
TRI Reagent BD	Sigma-Aldrich, St. Louis, MO (USA)
TRIS	Applichem, Darmstadt (Germany)
Triton X-100	Sigma-Aldrich, St. Louis, MO (USA)
Tween-20	Sigma-Aldrich, St. Louis, MO (USA)
Xylene cyanol	Merck, Darmstadt (Germany)
Xylol	Applichem, Darmstadt (Germany)

5. Other reagents

Name	Manufacturer
Bovine Serum Albumine (BSA) Fraction V	PAA laboratories, Pasching (Austria)
FITC-lectin	Sigma-Aldrich, St. Louis, MO (USA)
dNTP, 10 mM each	Promega, Madison, WI (USA)
Gelatine	Merck, Darmstadt (Germany)
Oligo(dT) primer	Invitrogen, San Diego, CA (USA)
Oligo(dT) primer	Roth, Karlsruhe (Germany)
Precision Plus Protein Standards	Bio-Rad, Munich (Germany)
Protein Assay	Bio-Rad, Munich (Germany)
RIPA	Sigma-Aldrich, St. Louis, MO (USA)
Sucofin skimmed milk powder	TSI GmbH & Co. KG, Zevem (Germany)
SYBR Green Fast Master Mix	Applied Biosystems, Foster City, CA (USA)
TaqMan Fast Master Mix	Applied Biosystems, Foster City, CA (USA)
4',6-Diamidin-2-phenylindol (DAPI)	Roche, Indianapolis, IN (USA)

6. Kits

Name	Manufacturer
Annexin V apoptosis detection kit	BD, Franklin Lakes, NJ (USA)
Cell Proliferation ELISA, BrdU (chemiluminescent)	Roche, Indianapolis, IN (USA)
Dual-Luciferase(R) Reporter 1000 Assay System	Promega, Madison, WI (USA)
FITC-BrdU Flow Kit	BD, Franklin Lakes, NJ (USA)
QIAquick gel extraction kit	Qiagen, Hilden (Germany)
QIAquick PCR Purification Kit	Qiagen, Hilden (Germany)
QIAprep spin mini kit	Qiagen, Hilden (Germany)
TaqMan MicroRNA Reverse Transcription kit	Applied Biosystems, Foster City, CA (USA)
Turbo DNA-free kit	Applied Biosystems, Foster City, CA (USA)

7. Enzymes

Name	Enzyme class	Manufacturer
HindIII	restriction enzyme	Roche, Indianapolis, IN (USA)
M-MLV	reverse transcriptase	Invitrogen, San Diego, CA (USA)
Proteinase K	endopeptidase	Sigma-Aldrich, St. Louis, MO (USA)
SpeI	restriction enzyme	Roche, Indianapolis, IN (USA)
T4 ligase	DNA-ligase	New England Biolabs, Frankfurt am Main (Germany)

8. Bacteria

Name/Strain	Genotype	Manufacturer
OmniMAX 2-T1R	F′ {*pro*AB+ *lacI*q *lacZ* Δ M15 *Tn*10(Tet$_R$) Δ (*ccd*AB)} *mcr*A Δ (*mrr-hsd*RMS-*mcr*BC) ϕ 80(*lacZ*) Δ M15 Δ (*lac*ZYA-*arg*F) U169 *end*A1 *rec*A1 *sup*E44 *thi*-1 *gyr*A96 *rel*A1 *ton*A *pan*D	Invitrogen, San Diego, CA (USA)

9. Bacterial Growth Media and Agar Plates

Name	Media formulation	pH	Manufacturer
LB Agar Capsules	1% Tryptone, 0.5% Yeast Extract-B, 1% NaCl, 1.5% Agar-B		MP Biomedicals, Irvine, CA (USA)
LB Medium Capsules	1% Tryptone, 0.5% Yeast Extract, 1% NaCl	6.7	MP Biomedicals, Irvine, CA (USA)
S.O.C. Medium	2% Tryptone, 0.5% Yeast Extract, 10 mM NaCl, 2.5 mM KCl, 10 mM MgCl2, 10 mM MgSO4, 20 mM glucose		Invitrogen, Carlsbad, CA (USA)

10. Plasmids

Name	Description	Reference/Manufacturer
pGl4	Renilla luciferase expression vector	Promega, Madison, WI (USA)
pMIR-REPORT	Firefly luciferase reporter vector	Ambion, Austin, TX (USA)
pMIR-REPORT-4xJak1/miR-17-MRE-wt	4x wt miR-17 MRE of Jak1 3´ UTR cloned into pMIR-REPORT via the HindIII and SpeI restriction sites	generated in the context of this study
pMIR-REPORT-4xJak1-miR-17-MRE-mut	4x mutated miR-17 MRE of Jak1 3´ UTR cloned into pMIR-REPORT via the HindIII and SpeI restriction sites	generated in the context of this study

11. Cell culture solutions and supplements

Name	Manufacturer
Collagen I	Chemicon, Billerica, MA (USA)
Collagen I, rat tail	BD, Franklin Lakes, NJ (USA)
DMEM Glutamax	Invitrogen, San Diego, CA (USA)
DMEM	PAA laboratories, Pasching (Austria)
EGM BulletKit (EBM medium + EGM SingleQuots)	Lonza, Verviers (Belgium)
EGM-2 MV BulletKit (EBM-2 + EGM-2 MV SingleQuots)	Lonza, Verviers (Belgium)
FCS	Invitrogen, San Diego, CA (USA)
FGF-2	Peprotech, Hamburg (Germany)
L-Glutamine	Invitrogen, San Diego, CA (USA)
GM-CSF	Peprotech, Hamburg (Germany)
HAT supplement	Biochrom AG, Berlin (Germany)
HEPES 1M	Invitrogen, San Diego, CA (USA)
IFN-α	Peprotech, Hamburg (Germany)
IL-6	Peprotech, Hamburg (Germany)
Lipofectamine 2000	Invitrogen, San Diego, CA (USA)
Lipofectamine RNAiMax	Invitrogen, San Diego, CA (USA)
MEM	Invitrogen, San Diego, CA (USA)
Matrigel	BD, Franklin Lakes, NJ (USA)
Medium M199	Sigma-Aldrich, St. Louis, MO (USA)
Non-essential amino acids	Invitrogen, San Diego, CA (USA)
OptiMEM	Invitrogen, San Diego, CA (USA)

Name	Manufacturer
PDGF-BB	Peprotech, Hamburg (Germany)
Penicillin-Streptomycin	Roche, Indianapolis, IN (USA)
Phosphate-buffered saline (PBS)	PAA laboratories, Pasching (Austria)
Phosphate-buffered saline (PBS)	Sigma-Aldrich, St. Louis, MO (USA)
Sodium hydroxide solution (NaOH) 5M	Applichem, Darmstadt (Germany)
Sodium pyruvate	PAA laboratories, Pasching (Austria)
Sphingosine-1-phosphate (S1P)	Sigma-Aldrich, St. Louis, MO (USA)
Trypsin-EDTA	Invitrogen, San Diego, CA (USA)

12. Primary cells and cell lines

Name	Species	Origin	Manufacturer
EA.Hy.926	*Homo sapiens*	HUVEC/A549 cell hybrid	Kindly provided by Prof. Ingrid Fleming, Cardiovascular Physiology, Goethe University Frankfurt
HEK293	*Homo sapiens*	kidney	Clontech, Mountain View, CA (USA)
HMVEC-L	*Homo sapiens*	lung	Lonza, Verviers (Belgium)
HUVEC	*Homo sapiens*	umbilical veins	Lonza, Verviers (Belgium)
LLC1	*Mus musculus*	lung carcinoma	ATCC, Manassas, VA (USA)

13. Animals

a) Mice

Name	Age	Experiment	Company
C57Bl/6	8 weeks	Tumour model	Charles River Laboratories, Sulzfeld (Germany)
C57Bl/6	8 weeks	Matrigel plug	Charles River Laboratories, Sulzfeld (Germany)
C57Bl/6J	8 weeks	Chronic hypoxia	Charles River Laboratories, Sulzfeld (Germany)

b) Rats

Name	Age	Sex	Experiment	Company
Sprague-Dawley rats	adult	male	MCT injury model	Charles River Laboratories, Sulzfeld (Germany)

B. Methods

1. Cell culture

a) Cell cultivation

Pooled human umbilical vein endothelial cells (HUVECs) were purchased from Lonza and cultured in endothelial basal medium (EBM; Lonza) supplemented with EGM SingleQuots (hydrocortisone, bovine brain extract, epidermal growth factor, gentamycin sulphate, amphotericin-B; Lonza) and 10% fetal calf serum (FCS; Invitrogen) until the third passage.

Ea.hy.926 cells were cultured in MEM (Invitrogen) containing 10% FCS (Invitrogen), 2 mM L-Glutamine (Invitrogen), 1 mM Sodium pyruvate (PAA laboratories), HAT supplement (100 µM Hypoxanthin, 16 µM Thymidin, 0.4 µM Aminopterin; Biochrom AG), 0.1 M non-essential amino acids (Invitrogen) and penicillin/streptomycin (Roche).

Human lung microvascular endothelial cells (HMVEC-L) were purchased from Lonza and cultured in EBM-2 medium supplemented with 10% FCS and the EGM-2 MV SingleQuots (ascorbic acid, hydrocortisone, epidermal growth factor, long R insulin-like growth factor-1, vascular endothelial growth factor, fibroblast growth factor-B, gentamycin sulphate, amphotericin-B; Lonza).

Lewis Lung Carcinoma Cells (LLC1, ATCC CRL-1642) were cultured in DMEM containing Glutamax™ and sodium pyruvate (Invitrogen) supplemented with 10% heat inactivated (56°C, 30 min) FCS and Penicillin/Streptomycin (P/S, Roche).

Human embryonic kidney (HEK) 293 cells (Clontech) were cultured in DMEM containing L-Glutamine (Invitrogen) supplemented with 10% FCS (Invitrogen) and 0.1 mM nonessential amino acids (Invitrogen).

b) Cell seeding

Cells were washed once with sterile PBS and trypsinized with Trypsin-EDTA at 37°C for 2-3 min. Trypsinization was stopped by addition of serum containing cell culture medium. Cells were transferred into Falkons and counted using a Neubauer glass chamber. The used seeding densities for the different cell types are shown in the table below.

Cell Type	Seeding density
HUVEC	3.5 or $4x10^5$/6 cm dish, $1.2x10^5$/10 cm dish
HEK293	$1.2x10^5$/12-well plate
LLC1	5 and $6x10^5$/6 cm dish
HPASMC	$2.5x10^3$/96-well plate $1.75x10^5$/6-well plate, $3.5x10^5$/6 cm well

Table III.1: Cell seeding desities

c) Transfection of cells with RNA molecules

Lyophilized miR precursors and siRNAs were dissolved in RNase-free water to a concentration of 20 µM, whereas PBS was used for the 20 µM stocks of the hairpin inhibitors. For overexpression of the individual miRs, 1 nM or 10 nM of specific precursor molecules for the members of the miR-17-92 cluster, miR-21, miR-27b and miR-126 as non-related controls or control pre-miR (Ambion) were used. Additionally, miR-17 was overexpressed by transfection of miR mimics. Inhibition of the different miRs in vitro was achieved by transfection of 50 nM miRIDIAN Hairpin Inhibitors (Dharmacon). For siRNA-mediated gene knockdown, HUVECs were transfected with 10 nM p21 or 40 nM JAK1 siRNA, AllStars Negative Control siRNA or a control siRNA directed

against firefly luciferase. Information on the miR precursors and inhibitors used as well as sequences of non-proprietary siRNAs are given in the tables below.

HUVECs and Lewis Lung Carcinoma Cells were transfected at 50-75% confluence with microRNA precursor molecules, hairpin inhibitors and/or siRNA using Lipofectamine RNAiMax (Invitrogen) according to the manufacturer´s protocol. For a 6 cm dish, the respective RNA molecules were mixed with 250 µl OptiMEM and incubated with 250 µl OptiMEM supplemented with 5 µl Lipofectamine RNAiMax for 15 min at RT. Cells were washed once with OptiMEM and 500 µl of the transfection mixture were added to 2.5 ml OptiMEM. Trifold volumes were used for cells in 10 cm dishes. For precursor transfection into SMCs in 96-well plates, 0.05 µl precursor molecule were added to 10 µl OptiMEM and mixed with 10 µl OptiMEM with 0.15 µl Lipofectamine RNAiMax. After washing, 20 µl transfection mixture were added to 80 µl OptiMEM. Medium changes were done 4 h after addition of the transfection reagents.

Pre-miR miRNA precursor name	Mature miR sequence	Manufacturer
Negative Control #1		Ambion, Austin, TX (USA) Cat# AM17110
hsa-miR-17	CAAAGUGCUUACAGUGCAGGUAG	Ambion, Austin, TX (USA) Cat# PM12412
hsa-miR-18a	UAAGGUGCAUCUAGUGCAGAUAG	Ambion, Austin, TX (USA) Cat# PM12973
hsa-miR-19a	UGUGCAAAUCUAUGCAAAACUGA	Ambion, Austin, TX (USA) Cat# PM10649
hsa-miR-20a	UAAAGUGCUUAUAGUGCAGGUAG	Ambion, Austin, TX (USA) Cat# PM10057
hsa-miR-27b	UUCACAGUGGCUAAGUUCUGC	Ambion, Austin, TX (USA) Cat# PM10750
hsa-miR-126	UCGUACCGUGAGUAAUAAUGCG	Ambion, Austin, TX (USA) Cat# PM12841

Table III.2: MicroRNA precursors

MiRIDIAN mimic name	Mature miR sequence	Manufacturer
Negative Control #1		Dharmacon, Lafayette, CO, USA Cat# CN-001000-01-05
hsa-miR-17-5p	CAAAGUGCUUACAGUGCAGGUAG	Dharmacon, Lafayette, CO, USA Cat# C-300485-05-0005

Table III.3: MicroRNA mimics

MiRIDIAN Hairpin inhibitor name	Mature miR sequence	Manufacturer
Negative Control #1		Dharmacon, Lafayette, CO, USA Cat# IN-001005-01
Negative Control #2		Dharmacon, Lafayette, CO, USA Cat# IN-002005-01
hsa-miR-17	CAAAGUGCUUACAGUGCAGGUAG	Dharmacon, Lafayette, CO, USA Cat# IH-300485-06-0005
hsa-miR-18a	UAAGGUGCAUCUAGUGCAGAUAG	Dharmacon, Lafayette, CO, USA Cat# IH-300487-06-0005

MiRIDIAN Hairpin inhibitor name	Mature miR sequence	Manufacturer
hsa-miR-19a	UGUGCAAAUCUAUGCAAAACUGA	Dharmacon, Lafayette, CO, USA Cat# IH-300488-05-0005
hsa-miR-20a	UAAAGUGCUUAUAGUGCAGGUAG	Dharmacon, Lafayette, CO, USA Cat# IH-300491-05-0005
hsa-miR-27b	UUCACAGUGGCUAAGUUCUGC	Dharmacon, Lafayette, CO, USA Cat# IH-300589-07-0005 Cat#

Table III.4: MicroRNA hairpin inhibitors

siRNA name	Sequence (sense/antisense)	Reference/Manufacturer
AllStars Negative Control siRNA	proprietary	Qiagen, Hilden (Germany); Cat# 1027280
Firefly luciferase siRNA	5´-CGUACGCGGAAUACUUCGAdTdT-3´ 5´-UCGAAGUAUUCCGCGUACGdTdT-3´	Sigma-Aldrich, St. Louis, MO (USA) according to Elbashir et al. Nature 2001 (411)
JAK1 HP validated siRNA	5´-CGGAUGAGGUUCUAUUUCAdTdT-3´ 5´-UGAAAUAGAACCUCAUCCGdGdT-3´	Qiagen, Hilden (Germany); Cat# SI00605514
p21 FlexiTube siRNA	5´-GGCAUUAGAAUUAUUUAAAdTdT-3´ 5´-UUUAAAUAAUUCUAAUGCCdAdG-3´	Qiagen, Hilden (Germany); Cat# SI00604905

Table III.5: siRNAs

d) 3D spheroid assay

24 hours after transfection cells were washed once with PBS, trypsinized with 0.5 ml Trypsin-EDTA for 2 min at 37°C and transferred into Falkons by addition of cell culture medium. Cells were pelleted by centrifugation at 1500 rpm (404 x g) for 5 min, resuspended in 1 ml cell culture medium and counted using a Neubauer glass chamber. 4.8 x 10^4 HUVECs were added to 12 ml EBM-methocel (80% EBM with 10% FCS and supplements + 20% Methocel) and 100 µl of the cell suspension per well were seeded in a 96-well U-bottom dish using an Eppendorf Multipette. Cells were incubated in the cell culture incubator overnight to accumulate in spheroids. The day after, spheroids were collected in a 50 ml Falkon, pelleted by centrifugation at 1000 rpm (179 x g) for 3 min and after suction of the medium supplied with 500 µl methocel-FCS (80% methocel, 20% FCS). Thereafter, 500 µl collagen gel was added, thoroughly mixed with the spheroid methocel-FCS suspension and 1 ml of the mixture was transferred into a well of a 24-well plate after incubation at RT for 2 min. The plate was incubated for 5 min in the cell culture incubator to allow the gel to solidify before the next spheroid gel was prepared. After completion of the last gel, the plate was incubated for 30 min in the incubator before 100 µl of cell culture medium were added per well. Spheroids were incubated for 24 h to allow capillary sprouting, before fixation with 500 µl 10% formaldehyde in PBS. In vitro angiogenesis was quantified by taking micro-graphs (Axiovert 100 M equipped with AxioCam camera, Carl Zeiss, Jena; 10x/0.3 objective) and measuring the cumulative length of all sprouts grown out of each spheroid using a digital imaging

software (Axiovision 4.6, Carl Zeiss Imaging Solutions GmbH, Munich) analyzing 10 spheroids per group and experiment.

collagen gel (1 ml)

10x M199 [µl]	100
Rat tail collagen I [µl]	800
1M Hepes [µl]	18
NaOH (0.2 M) [µl]	80-160 (until gel turns red)

e) Preparation of Methocel

A 1l bottle containing 6 g methylcellulose (Sigma-Aldrich) and a magnetic stir bar were autoclaved before 250 ml of prewarmed (60°C) EBM basal medium were aseptically added and stirred on a magnetic stirrer at 60°C for approximately 40 min. Subsequently, the remaining 250 ml EBM basal medium were added and the mixture was stirred at 4°C overnight. The next day, the lucent viscous solution was filled into 50 ml Falkons and centrifuged at 3500 rpm (2200 x g) or 4500 rpm (3636 x g) and RT for 2 h to pellet insoluble debris. The methocel without debris was transferred into new Falkons and stored in the fridge.

f) Test of paracrine pro-angiogenic activity using cell supernatants

HUVECs or Lewis Lung Carcinoma cells were transfected with 10 nM pre-miR as described above. After one day, cells were washed twice with serum-free medium and serum-free medium supplemented with 0.05% BSA was added to the cells. After further incubation of the cells for 24 h, the supernatants were transfered into 15 ml falcons and cell debris was removed by centrifugation at 1500 rpm (404 x g) and 4°C for 10 min. The cell-free supernatants were pipetted into the membrane equipped inserts of Amicon Ultra centrifugal filter devices (Millipore) and concentrated by centrifugation at 3500 rpm (2200 x g) and 4°C until the volume of the supernatants was tenfold reduced. 100 µl of the 10x concentrates were used for the spheroid sprouting assay instead of cell culture medium.

g) 2D endothelial tube network formation

48 h after transfection, HUVECs ($1x10^5$) were cultured in a 12-well plate (Greiner) coated with 200 µl Matrigel Basement Membrane Matrix (BD Biosciences). Tube length was quantified after 24 hours by measuring the cumulative tube length in five random microscopic fields (10x/0.3 objective) with a computer-assisted microscope (Axiovert 100 M equipped with AxioCam camera, Carl Zeiss, Jena) using Axiovision 4.6 (Carl Zeiss, Imaging Solutions GmbH, Munich).

h) Migration assay

To assess migratory capacity of endothelial cells, HUVECs were detached with trypsin 48 h after transfection, harvested and washed with serum-free medium by centrifugation at 1500 rpm

(404 x g) and RT for 5 min, resuspended in EBM with 0.1% BSA, counted and placed in the upper chamber of a modified Boyden chamber (5 x 10^4 cells per chamber, pore size 8 μm, BD Biosciences) coated with 1 μg/ml human Collagen I (Millipore). The chamber was placed in a 24-well culture dish containing EBM with 0.1% BSA in presence or absence of human vascular endothelial growth factor (VEGF, 50 ng/ml, Peprotech) or sphingosine-1-phosphate (S1P, Sigma-Aldrich). Lyophilized VEGF was dissolved in PBS + 0.1% BSA to a final stock concentration of 10 μg/ml. The S1P stock solution (1 mM) was generated by heating the lyophilized S1P in methanol to 50°C in a water bath for 2 h with occasional vortexing the mixture. Further dilutions were done in serum-free cell culture medium. After incubation for 4 h at 37°C, the cells on the lower side were fixed with 4% formaldehyde and the remaining non-migrating cells on the upper side of the chamber were mechanically removed with multiple moist cotton swabs and the inserts were washed three times with PBS. For quantification, cell nuclei were stained with 4',6-diamidinophenylidole (DAPI). Migrating cells on the bottom side of the chamber were counted manually in five random microscopic fields using a computer-assisted fluorescence microscope (Axiovert 100 M equipped with AxioCam camera, Carl Zeiss, Jena, 20x/0.4 objective)

i) Cytokine stimulation of HUVECs

40 h after siRNA transfection HUVECs were washed and serum starved in EBM containing 0.05% BSA for 9 h. Subsequently, the cells were left untreated or treated with IL-6 (100 ng/ml), FGF-2 (30 ng/ml), IFN-α (100 ng/ml) or GM-CSF (100 ng/ml) for 15 min. Proteins were isolated as described below. All cytokines were purchased from PeproTech and dissolved in PBS supplemented with 0.1% BSA.

j) BrdU FACS staining

48 h after transfection, BrdU was added to the culture medium for 45 min to a final concentration of 10 μM. Cells were harvested by trypsinization and once washed with PBS by centrifugation at 2000 rpm (380 x g) for 5 min at RT. A FITC-BrdU Flow Kit (BD Pharmingen) was used to stain the cells as follows. Fixation and permeabilization of the cells was achieved by incubating them for 30 min at RT in 100 μl Cytofix/Cytoperm buffer, followed by incubation on ice for 10 min in 100 μl CytopermPlus and 5 min in 100 μl Cytofix/Cytoperm buffer. Buffers were removed by washing the cells with 1 ml PermWash buffer combined with subsequent centrifugation at 4000 rpm (1520 x g) and RT for 3 min. After removing the final washing solution, cells were incubated with 100 μl DNase in PBS (300 μg/ml) for 1 h at 37°C. The DNase was removed by washing with PermWash buffer as described before. The cell pellets were resuspended in 50 μl PermWash buffer and incubated with 20 μl FITC-conjugated anti-BrdU antibody for 20 min at RT in the dark. After washing with PermWash buffer, the pellet was resuspended in 20 μl 7-AAD and

allowed to stand for 10 min. Finally, 300 µl PBS were added and FACS analysis was performed using a FACS Canto II device (BD). Unstained cells were used to perform the settings of the FACS.

k) BrdU ELISA

Cell proliferation of pulmonary smooth muscle cells was quantified using a chemiluminescent cell proliferation ELISA (Roche) according to the manufacturer´s protocol. In brief, 48 h after precursor transfection, medium was changed (growth medium w/o and with 30 ng/ml PDGF-BB or 10% FCS) and BrdU was added to the culture medium for 20 h to a final concentration of 10 µM. Cells were fixed with 200 µl FixDenat for 30 min at RT and removed by suction before the addition of 100 µl peroxidase conjugated anti-BrdU (anti-BrdU-POD) antibody for 90 min at RT. Non-bound antibody was removed by incubating the fixed cells three times with 200 µl 1x washing solution. 100 µl/well substrate solution were added and chemiluminescence was detected in triplicates with the Biotek Synergy HT plate reader. For data analysis the blank values were substracted from all other values to correct for unspecific binding of BrdU and anti-BrdU-POD antibody to the microplate.

l) Annexin V FACS staining

Apoptotic cell death of HUVECs was quantified using a FITC-Annexin V Apoptosis Detection Kit (BD Pharmingen) according to the manufacturer´s protocol. Shortly, 30 h after transfection 500 µM, 1 mM or no H_2O_2 was added to the cell culture medium for 14 h. Cells were trypsinized and collected with the initial cell culture medium by centrifugation at 1500 rpm (404 x g) and 4°C for 5 min. Cells were washed once with PBS and once with Annexin binding buffer before they were resuspended in 50 µl Annexin binding buffer and mixed with 2.5 µl Annexin V-FITC and 2.5 µl 7-AAD. Controls without Annexin V-FITC and/or 7-AAD were prepared to do the FACS settings. After incubation for 15 min in the dark, 200 µl binding buffer were added and subsequent FACS analysis was done using FACS Canto II (BD).

2. Molecular Biology

a) RNA isolation

For RNA isolation from cultured cells, the cell layer or pellet was washed once with PBS and lysed in 800 µl or 1 ml TRI Reagent (Sigma-Aldrich) for 5 min at room temperature (RT) to guarantee entire dissociation of ribonucleoprotein complexes. RNA isolation was either continued immediately after cell lysis or the samples were stored at -80°C. After addition of 1/5 of the initial volume of chloroform ($CHCl_3$), the samples were shaken vigorously for approximately 15 se-

conds, incubated for 3 min at RT and centrifuged for 15 min at 12000 x g and 4°C. The upper uncolored RNA containing aqueous phase was transferred into a new tube, mixed with an equal volume of isopropanol and incubated for 10 min at RT followed by centrifugation at 12000 x g and 4°C for 10 min. The resulting RNA pellet was washed with 75% ethanol (EtOH), vortexed and centrifuged for 5 min at 7500 x g and 4°C. After removal of the ethanol, the RNA pellet was air dried and solved in 30 µl or 50 µl of RNase-free water (H_2O). To facilitate dissolution, the RNA was incubated at 55°C for 10 min in an Eppendorf thermomixer.

In some RNA isolations, the aqueous phase was once more chloroform ($CHCl_3$) extracted after the initial phase separation and washed twice with 75% EtOH at the end of RNA isolation to get rid of residual phenol.

RNA isolation from mouse and rat organs was accomplished by homogenization of the organ or part of it in TRI Reagent using the Tissue Tearor (Biospec products inc) or the FastPrep-24 instrument (MP Biomedicals) and ceramic spheres. The volume of TRI Reagent was adapted to tissue size.

b) RNA isolation from paraffin sections

RNA isolation from paraffin embedded tumours was done according to a published protocol [190]. Shortly, 4-5 tissue sections, each 30 µm thick, were cut with a microtome and transferred into 1.5 ml tubes. Deparaffinization was achieved by rinsing the slices twice with 500 µl xylene for 5 min at 57°C followed by centrifugation at 10000 x g and RT for 2 min. Afterwards, the tissue was washed twice with 100% ethanol and centrifuged for 10 min at 10000 x g, RT. After removal of the ethanol, 500 µl digestion buffer B (500 mM Tris-HCl pH 7.6, 10 mM NaCl, 20 mM EDTA, 1% SDS) and 5 µl of a proteinase K solution (50 µg/µl) were added followed by incubation of the mixture at 55°C for 3 h. Proteinase K was inactivated by heating the reaction for 7 min to 100°C. Subsequently, the RNA was isolated from the supernatant with TRI Reagent BD (Sigma-Aldrich) as follows. One volume of supernatant was vigorously mixed with 3 volumes TRI Reagent BD (Sigma-Aldrich) followed by incubation at RT for 5 min. After addition of 1/5 of the volume of chloroform, the mixture was again vigorously mixed, allowed to stand for 3 min at RT and centrifuged at 12000 x g and 4°C for 15 min. The aqueous phase was transferred into a new tube, mixed with an equal volume of isopropanol and incubated at RT for 10 min followed by centrifugation (12000 x g, 8 min, 4°C). After washing once with 75% EtOH at 7500 x g and 4°C for 5 min and vaporization of residual ethanol, 20 µl RNase-free water was added and dissolving of RNA was forced by incubating at 55°C for 10 min.

c) Determination of RNA/DNA concentration

In the beginning, 1 µl of RNA were mixed with 99 µl RNase-free H_2O and filled into a quartz cuvette to measure the absorbance at 260 nm with the SmartSpec PlusSpectrophotometer (Bio-Rad Laboratories) which automatically calculated the RNA concentration.

Later on, RNA and DNA concentrations were determined with the NanoDrop 1000 spectrophotometer by pipetting 2 µl of the nucleic acid solution onto the optical pedestal.

Both spectrophotometers were blanked with pure water before performing the measurements.

d) MicroRNA detection by real-time PCR

In the course of the initial project, microRNAs were quantified according to a stem loop reverse transcription qPCR method published by Wu et al. [1]. The principle of the detection method is shown in Figure III.1. First, the microRNA is reverse transcribed using a stem loop primer which contains the binding sites for the universal reverse primer and the Taqman universal probe needed for qPCR detection as well as six nucleotides at its 3´ end that are complementary to the 3´-terminal nucleotides of the microRNA. In the second step, the reverse transcription product is quantified by real-time PCR using a miR specific forward primer covering the remaining nucleotides of the miR, the Taqman probe and a universal reverse primer.

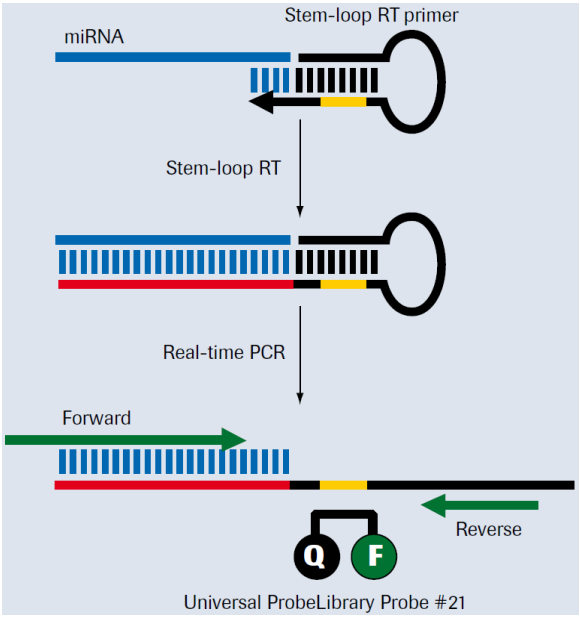

Figure III.1: **Real-time PCR quantification of microRNAs using a universal probe.** The binding site of the universal probe #21 is shown in yellow. Adopted from Wu et al. [1]

The primers were designed according to the miR sequences listed in the Sanger miR base (http://www.mirbase.org/). The microRNA and primer sequences are given in Table III.6.

hsa-miR-17	miR sequence	CAAAGUGCUUACAGUGC**AGGUAG**
	stem loop primer	GTTGGCTCTGGTGCAGGGTCCGAGGTATTCGCACCAGAGCCAACCTACCT
	forward primer	GCGCCAAAGTGCTTACAGTGC
hsa-miR-18a	miR sequence	UAAGGUGCAUCUAGUGC**AGAUAG**
	stem loop primer	GTTGGCTCTGGTGCAGGGTCCGAGGTATTCGCACCAGAGCCAACCTATCT
	forward primer	CGCCTAAGGTGCATCTAGTGC
hsa-miR-19a	miR sequence	UGUGCAAAUCUAUGCAA**AACUGA**
	stem loop primer	GTTGGCTCTGGTGCAGGGTCCGAGGTATTCGCACCAGAGCCAACTCAGTT
	forward primer	CGCGTGTGCAAATCTATGCAA
hsa-miR-20a	miR sequence	UAAAGUGCUUAUAGUGC**AGGUAG**
	stem loop primer	GTTGGCTCTGGTGCAGGGTCCGAGGTATTCGCACCAGAGCCAACCTACCT
	forward primer	GCGCCTAAAGTGCTTATAGTGC
RNU48	RNU sequence	AGUGAUGAUGACCCCAGGUAACUCUGAGUGUGUCGCUGAUGCCAUCACC GCAGCGCU**CUGACC**
	stem loop primer	GTTGGCTCTGGTGCAGGGTCCGAGGTATTCGCACCAGAGCCAACGGTCAG
	forward primer	GAGTGATGATGACCCCAGGTAA
Universal reverse primer		GTGCAGGGTCCGAGGT

Table III.6: Primer sequences for miR quantification via stem loop RT and qPCR

The composition of the reactions and the amplification programs were as follows:

Stem loop reverse transcription

	1x			
Stem loop Primer (0.5 µM) [µl]	1	30 min	16°C	
dNTPs (10 µM each) [µl]	0.25	30 sec	30°C	60 cycles
M-MLV Reverse Transcriptase (200 U/µl) [µl]	0.25	30 sec	42°C	
DTT[µl]	1	1 sec	50°C	
5x first strand buffer[µl]	2	15 min	70°C	
H_2O [µl]	1.5	∞	4°C	
RNA (25 ng/µl) [µl]	4			
Total volume [µl]	**10**			

In the stem loop RT 100 ng total RNA were reverse transcribed. RNU48 served as endogenous control for human RNA, whereas snoRNA202 was used for murine samples. Every miR and the endogenous control were reverse transcribed in separate reactions. The resulting cDNA was diluted 1:5 with water before usage in the real-time quantification.

Taqman real-time PCR

	1x			
2x Fast Universal Taqman Master [µl]	10	20 sec	95°C	
Universal probe #21 [µl]	2	1 sec	95°C	40-50 cycles
Forward primer (10 µM) [µl]	1	20 sec	60°C	
Universal reverse primer (10 µM) [µl]	1			
H_2O [µl]	1			
cDNA (1:5 diluted) [µl]	5			
Total volume [µl]	**20**			

For the second project, miRs were exclusively quantified using the more specific TaqMan MicroRNA Assays offered by Applied Biosystems. The assay principle is shown in Figure III.2.

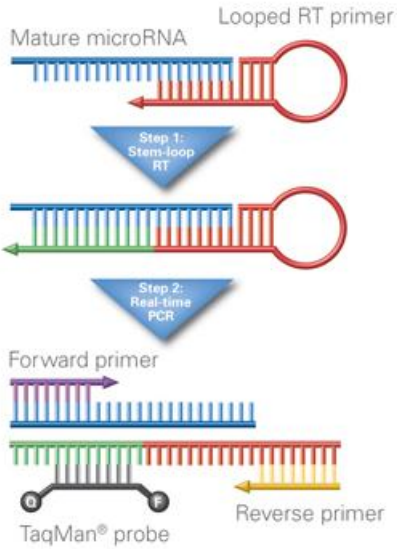

Figure III.2: **Real-time PCR quantification of microRNAs using TaqMan MicroRNA Assays.** The commercially available TaqMan MicroRNA Assays have a high specificity as they use a microRNA specific TaqMan probe. Adopted from the Applied Biosystems web site [191]

The assays we used are listed in table III.7. MicroRNA expression levels were generally normalized to an endogenous control. For mouse samples we used snoRNA202, for rat samples U6 snRNA and for human samples U6 snRNA or RNU48 as endogenous control.

Stem loop reverse transcription microRNA assays

	1x		
H_2O [µl]	3.10	30 min	16°C
100 mM dNTPs [µl]	0.10	30 min	42°C
10x RT Buffer [µl]	1.00	30 sec	85°C
RNase Inhibitor [µl]	0.13	∞	4°C
MultiScribe Reverse Transcriptase [µl]	0.67		
Total Master [µl]	**5.00**		
5x Primer [µl]	2.00		
RNA (2.5 ng/µl) [µl]	3.00		
Total volume [µl]	**10.00**		

If the primers for different miRs and the loading control were compatible with each other according to the Applied Biosystems multiplex primer pool list, up to four distinct primers were used in one RT reaction in which the volume of each primer was lowered to 1 µl and the water quantity was adapted to the final volume of 10 µl.

Taqman real-time PCR microRNA assays

	1x			
2x Fast Universal Taqman Master [µl]	10	20 sec	95°C	
20x primer [µl]	1	1 sec	95°C	40-50 cycles
H_2O [µl]	4	20 sec	60°C	
cDNA (1:5 diluted) [µl]	5			
Total volume [µl]	**20**			

All quantitative real-time PCRs were done on a StepOne Plus device (Applied Biosystems). The relative miR expression levels were calculated according to the formula $2^{-\Delta CT}$ with $\Delta C_T = C_T^{miR} - C_T^{endogenous\ control}$

Assay name	Assay ID	Target sequence
hsa-miR-17	002308	CAAAGUGCUUACAGUGCAGGUAG
hsa-miR-20a	000580	UAAAGUGCUUAUAGUGCAGGUAG
hsa-miR-21	000397	UAGCUUAUCAGACUGAUGUUGA
hsa-miR-92a	000431	UAUUGCACUUGUCCCGGCCUGU
snoRNA202	001232	GCUGUACUGACUUGAUGAAAGUACUUUUGAACCCUUUUCCAUCUGAUG
U6 snRNA	001973	GUGCUCGCUUCGGCAGCACAUAUACUAAAAUUGGAACGAUACAGAGAAGAUUAG CAUGGCCCCUGCGCAAGGAUGACACGCAAAUUCGUGAAGCGUUCCAUAUUUUUA CUGCCCUCCAUGCCCUGCCCCACAAACGCUCUGAUAACAGUCUGUCCCUGUCUC UCUCCUGCUGCUCCUAUGGAAGCGAAGUUUUCCGCUCCUGCAGAAAGCAAAGUU ACGACUCAGAGACGGCUGAGGAUGACAUCAGCGAUGUGCAGGGAACCCAGCGCC UGGAGCUUCGGGAUGACGGGGCCUUCAGCACCCCCACGGGGGGUUCUGACACC CUGGUGGGCACCUCCCUGGACACACCCCCGACCUCCGUGACAGGCACCUCAGAG GAGCAAGUGAGCUGGUGGGGCAGCGGGCAGACGGUCCUGGAGCAGGAAGCGGG CAGUGGGGGUGGCACCCGCCGCCUCCCGGGCAGCCCAAGGCAAGCACAGGCAA CCGGGGCCGGGCCACGGCACCUGGGGGUGGAGCCGCUGGUGCGGGCAUCUCG AGCUAAUCUGGUGGG
RNU48	001006	GAUGACCCCAGGUAACUCUGAGUGUGUCGCUGAUGCCAUCACCGCAGCGCUCUG ACC

Table III.7: TaqMan MicroRNA Assays for microRNA quantification by real-time PCR. Assays were purchased from Applied Biosystems, Foster City, CA (USA).

e) DNase digestion

Before reverse transcription of RNA into cDNA for analysis of gene expression via real-time PCR, residual DNA was removed by DNase digestion using the Ambion Turbo DNA-free kit (Applied Biosystems). After mixing the RNA in aqueous solution with 0.1 volume of 10x Turbo DNase buffer and 2 units Turbo DNase in a 0.5 ml PCR tube, the reaction was incubated at 37°C for 30 min. Enzyme inactivation was achieved by addition of 0.1 volume of DNase inactivation reagent and subsequent incubation for 5 min at room temperature with occasional mixing. Finally, the reaction was centrifuged at 10000 x g for 1.5 min to pellet the inactivation reagent and the RNA containing supernatant was transferred into a new tube.

f) Reverse transcription

250 ng RNA were reverse transcribed in a 20 µl reaction using 0.5 mM of each dNTP (Promega), 0.5 µg $Oligo(dT)_{12-18}$ primer (Invitrogen or Roth) and 200 units M-MLV reverse transcriptase in the corresponding first-strand buffer supplemented with 10 mM DTT (Invitrogen) for 50 min at 37°C followed by heat inactivation at 70°C for 15 min. The resulting cDNA was diluted 1:5 with water before employment in the SYBR Green real-time reaction.

g) SYBR Green real-time PCR

SYBR Green real-time PCR

	1x			
2x Fast SYBR Green Master [µl]	10	20 sec	95°C	
Forward primer (10 µM) [µl]	1	3 sec	95°C	40 cycles
Reverse primer (10 µM) [µl]	1	30 sec	60°C	
H_2O [µl]	3	15 sec	95°C	melt curve
cDNA (1:5 diluted) [µl]	5	1 min	60°C	
Total volume [µl]	**20**	15 sec	95°C	

All quantitative real-time PCRs were done on a StepOne Plus device (Applied Biosystems). Primer sequences were determined with NCBI Primer-Blast or adopted from the literature as indicated. Primers were ordered from Sigma-Aldrich.

Gene	Spezies	NCBI mRNA accession number/ Reference	Forward and reverse primer sequences
CDKN1A	*Homo sapiens*	NM_000389.4 NM_134440.1	5´-GACTCTCAGGGTCGAAAACG-3´ 5´-GGATTAGGGCTTCCTCTTGG-3´
BMPR2	*Homo sapiens*	Brock et al.	5´-AGCCCAACAGTCAATCCAATG-3´ 5´-GGTTGCGTTCATTCTGCATAG-3´
SMAD5	*Homo sapiens*	NM_001001419.1	5´-ACTGGGATTACAGGACTTGACCCAA-3´ 5´-AGTCAGTGGCTACCGAAAGAACAGA-3´
EFNB1	*Homo sapiens*	NM_004429.4	5´-CGGTGCCGGTTGCGTCATCT-3´ 5´-CGCTGCTGTGTGTGCTTGCG-3´
TGFBR2	*Homo sapiens*	NM_003242.5 NM_001024847.2	5´-CTGTGGATGACCTGGCTAA-3´ 5´-CATTTCCCAGAGCACCAGAG-3´
ACTA2	*Homo sapiens*	NM_001613.2 NM_001141945.1	5´-CCCTGGCATTGCCGACCGAA-3´ 5´-GGCCAGGATGGAGCCACCGA-3´
CNN1	*Homo sapiens*	NM_001299.4	5´-GCGGAAATTCGAGCCGGGGA-3´ 5´-CTGTGCCCAGCTTGGGGTCG-3´
SMTN	*Homo sapiens*	NM_134270.1 NM_134269.1 NM_006932.3	5´-GGGCGTCCCAACAGTGGCTC-3´ 5´-TGGCTGGTGCCTTCAGGGGT-3´
RPLP0	*Homo sapiens*	NM_001002.3 NM_053275.3	5´-AGCCTGGAAAAAGGAGGTCTTC-3´ 5´-ACTGTGCCAGCCCAGAACA-3´
TGFBR2	*Rattus norvegicus*	NM_031132.3	5´-AGTTTTGCGACGTGACACTG-3´ 5´-TCTCACAGATGGAGGTGACG-3´
BMPR2	*Rattus norvegicus*	NM_080407.1	5´-GGCGAAAAGATCAAGAGACG-3´ 5´-CACTGCCATTGTTGTTGACC-3´
CDKN1A	*Rattus norvegicus*	NM_080782.3	5´-TAGGACTTCGGGGTCTCCTT-3´ 5´-GCTCTGGACGGTACGCTTAG-3´
SMAD5	*Rattus norvegicus*	NM_021692.1	5´-CCAGGCGGCACATCGGGAAA-3´ 5´-ACAGACGGTGGTGGGGTGGA-3´
ID1	*Rattus norvegicus*	NM_012797.2	5´-AGACTCCTCCGCGCCTCTCC-3´ 5´-ACCAAGCACCACTTCGCCCG-3´
EFNB1	*Rattus norvegicus*	NM_017089.2	5´-AGGCCTCTGGGCTCTGTGGG-3´ 5´-GCAGGGCCAGGGGGCTATCT-3´
BACT	*Rattus norvegicus*	NM_031144.2	5´-AGCCATGTACGTAGCCATCC-3´ 5´-ACCCTCATAGATGGGCACAG-3´

Table III.8: Primer sequences for SYBR Green real-time PCR.

The formula $2^{-\Delta CT}$ with $\Delta C_T = C_T^{gene} - C_T^{endogenous\ control}$) was used to calculate the relative gene expression. The large ribosomal protein P0 (RPLP0) was chosen as endogenous control for human samples and β-actin (BACT) for rat tissue. Primer sequences are listed in the table below.

h) Gene expression profiling by microarrays

3.5 x 10^5 HUVECs were seeded into a 6 cm cell culture dish and transfected with 10 nM Pre-17 or control pre-miRNA (Pre-Co) the next day. Total RNA was isolated 24 h after transfection using TRI Reagent (Sigma-Aldrich) as described above. RNA samples were sent to Prof. Dr. med. Wolf-Karsten Hofmann in Berlin who organized the microarray analysis. Gene expression profile using 10 µg of total RNA was assessed with the GeneChip® Human Genome U133 Plus 2.0 Array (Affymetrix, Santa Clara, CA) using standard hybridization protocols. GeneChip image analysis was performed using GCOS Version 1.3 (Affymetrix, Santa Clara, CA). Data analysis was done with GeneSpringVersion 4.2 (Agilent Technologies, Santa Clara, CA) as described previously [192].

i) Cloning of the luciferase reporter construct

Synthetic oligonucleotides bearing 4x the miR-17 recognition element of the JAK1 mRNA 3´ UTR or a mutated version of the sequence and the respective antisense strands all containing HindIII and SpeI restriction sites (Table III.9) were designed on the basis of the sequence predicted to be the miR-17 target site by the TargetScan algorithm (Fig. III.3)

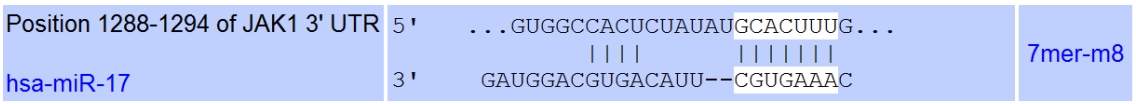

Figure III.3: **Predicted miR-17 binding site in the 3´ UTR of JAK1.** Adopted from the TargetScan web site [193]

Oligonucleotides were ordered from Sigma-Aldrich and dissolved in water at a concentration of 1 µg/µl. Annealing of the complementary strands was achieved by heating 2 µg of each oligonucleotide in a 50 µl reaction containing 1x annealing buffer (30 mM HEPES pH 7.4, 100 mM potassium acetate, 2 mM magnesium acetate) to 90°C for 3 min followed by incubation at 37°C for one hour.

The oligonucleotide inserts were purified with the QIAquick PCR Purification Kit (Qiagen, Hilden) according to the manufacturer´s protocol. Briefly, 5 volumes buffer PB (250 µl) were mixed with the annealing reactions followed by addition of 10 µl of 3 M sodium acetate (pH 5.0). The resulting mixtures were applied to QIAquick columns in 2 ml collection tubes and centrifuged for 1 min at 17900 x g and RT. The flow-through was discarded and columns were washed with 0.75 ml buffer PE by centrifugation (1 min, 17900 x g, RT). After removal of the flow-through, the columns were again centrifuged to get rid of residual EtOH contained in buffer PE. The 2 ml col-

lection tubes were discarded and replaced by 1.5 ml tubes. To elute the oligonucleotides 30 µl water were added to the QIAquick membrane and allowed to stand for 1 min. After centrifugation (1 min, 17900 x g, RT), the eluate was once more added to the column and centrifuged. Samples of the purified oligonucleotides (5 µl + 1 µl 6x loading dye) were analysed and compared with the single stranded oligonucleotides (1 µg oligonucleotide + 4 µl H_2O + 1 µl 6x loading dye) on a 3% high resolution agarose-TAE (40 mM Tris-Acetate, 1 mM EDTA) gel. Oligonucleotides were stored at -20°C.

6x loading dye
0.1% (w/v) bromophenol blue
0.1% (w/v) xylene cyanol
10 mM EDTA
40% (v/v) glycerol

Oligonucleotide name	Oligonucleotide sequence (sense/antisense)
4x wt JAK1 MRE for miR-17	5´- CTAGTCTGTGGCCACTCTATATGCACTTTGTTCTGTGGCCACTCTATATGCACTTT- GTTCTGTGGCCACTCTATATGCACTTTGTTCTGTGGCCACTCTATATGCACTTTGT- TA-3´ 5´- AGCTTAACAAAGTGCATATAGAGTGGCCACAGAACAAAGTGCATATA- GAGTGGCCACAGAACAAAGTGCATATAGAGTGGCCACAGAACAAAGTGCATATA- GAGTGGCCACAGA-3´
4x mutated JAK1 MRE for miR-17	5´- CTAGTCTGTGGCTAATCTATATGTAATTTGTTCTGTGGCTAATCTATATGTAATTT- GTTCTGTGGCTAATCTATATGTAATTTGTTCTGTGGCTAATCTATATGTAATTTGTTA- 3´ 5´- AGCTTAACAAATTACATATAGATTAGCCACAGAACAAATTACATATAGATTAGCCA- CAGAACAAATTACATATAGATTAGCCACAGAACAAATTACATATAGATTAGCCACA- GA-3´

Table III.9: **Sequences of the inserts used for the luciferase assay.** The Nukleotides corresponding to the SpeI and HindIII restriction sites are shown in orange and the seed sequence in red. Mutated nucleotides are highlighted in yellow. MRE: microRNA recognition element

5 µg of the pMIR-REPORT firefly luciferase vector were linearized in a double digest with HindIII and SpeI to guarantee unidirectional ligation of the insert.

pMIR-REPORT restriction digest

pMIR-REPORT (0.807 µg/µl) [µl]	6.2	1.5 h	37°C
Buffer M [µl]	2	15 min	65°C
H_2O [µl]	10.8		
Spe I [µl]	0.5		
Hind III [µl]	0.5		
Total volume [µl]	**20**		

Double digested vector was mixed with 4 µl 6x loading dye and separated from partially or non-digested vector by agarose gel (1% agarose-TAE) electrophoresis. Subsequent purification of the vector was done with the QIAquick Gel Extraction Kit according to the manufacturer´s protocol. In

brief, the DNA fragment corresponding to the linearized vector was excised from the agarose gel on an UV table with a scalpel, transferred into a 1.5 ml tube and weighed (384.5 mg). Three volumes of buffer QC (1154 µl) were added and incubated in an Eppendorf Thermomixer Compact at 50°C with agitation until the gel slice had completely dissolved. Thereafter, 10 µl 3 M sodium acetate were added and the solution was transferred into a 2 ml tube followed by the addition of one gel volume (384.5 µl) isopropanol. The mixture was transferred into a QIAquick column in a 2 ml collection tube, which was centrifuged at 17900 x g and RT for 1 min. After discarding the flow through, the column was treated with another 500 µl of buffer QC and centrifuged to remove traces of the agarose gel. Then, the column was washed with 750 µl buffer PE and and additionally centrifuged at 17900 x g and RT for 1 min. To elute the vector from the column, 30 µl H_2O were added and incubated for 1 min at RT before final centrifugation (17900 x g, RT, 1 min).
For ligation of the oligonucleotide inserts into the vector, the following reactions were prepared and incubated at 4°C overnight:

Ligation	
Linearized pMIR-REPORT [µl]	4
Annealed insert wt or mutated [µl]	1
10x ligase reaction buffer [µl]	2
T4 ligase [µl]	2
H_2O [µl]	11
Total volume [µl]	**20**

A no-insert ligation was done in parallel as negative control.

The ligation reactions were transformed into One Shot OmniMAX 2-T1R chemically competent *E. coli* according to the manufacturer´s protocol. Briefly, *E. coli* were thawed on ice, gently mixed with 5 µl of the ligation reaction and incubated on ice for 30 min. Thereafter, bacterial cells were subjected to a heat-shock for 30 sec at 42°C in a water bath. After 2 min incubation on ice, 250 µl of pre-warmed SOC medium were added and the cells were horizontally shaken at 37°C and 225 rpm for 1 hour in a bacterial incubator. Before plating, the cells were pelleted by centrifugation at 5000 rpm (2370 x g) for 1 min, 150 µl medium were removed and the cells were resuspended in the remaining medium. Cells were spread on pre-warmed agar plates supplemented with 50 µg/ml ampicillin and incubated at 37°C overnight. Per construct material from 12 colonies were picked and used to inoculate 3 ml LB medium supplemented with 50 µg/ml ampicillin. Propagation of cells was achieved by incubation at 37°C and 225 rpm in a bacterial incubator.
Small scale DNA purification was done with the QIAprep Spin Miniprep Kit according to the manufacturer´s protocol. Shortly, 2.5 ml *E. coli* culture were pelleted by centrifugation at 6800 x g for 3 min. The pellets were resuspended in buffer P1 containing RNase A and mixed with 250 µl buffer P2 by inverting the tube several times. Thereafter, 350 µl buffer N3 were added and

distributed by inverting followed by centrifugation of the mixtures (17900 x g, 10 min, RT). The supernatants were applied to QIAprep spin columns by decanting and centrifuged at 17900 x g and RT for 1 min. Then, columns were washed with 0.5 ml buffer PB and centrifuged twice while removing the flow-through after the first round. DNA was eluted with 30 µl H_2O.

For sequencing 6 µl DNA were mixed with 1 µl M13 (-20) sequencing primer and sent to Seqlab in Göttingen for HotShot sequencing of around 300 bases. Constructs with successful sequencing results were used for the luciferase reporter assay.

Oligonucleotide name	sequence
M13 (-20) primer	5´-GTAAAACGACGGCCAG-3´

Table III.10: Sequencing primer sequence

j) Luciferase reporter assay

Two days after seeding, HEK293 cells were transfected with 0.02 ng Luciferase plasmid, 0.2 ng pGL4 Renilla plasmid (Promega) as control for the transfection efficiency and 10 pmol Pre-17 or control pre-miR (Pre-Co) using Lipofectamine 2000 (Invitrogen) according to the manufacturer´s protocol.

HEK transfection

Mix 1:		Mix 2:	
OptiMEM [µl]	100	OptiMEM [µl]	100
pGl4 (0.1 ng/µl) [µl]	2	Lipofectamine 2000	3
pMIR-REPORT-4x MRE (0.01 ng/µl) [µl]	2	→ 5 min at RT	
Precursor (20 µM) [µl]	1		

Mixing of both 1:1 → 5 min at RT → 20 min at RT
800 µl HEK medium + 200 µl transfection mixture

48 h after transfection cells were washed once with PBS and lysed with 250 µl 1x PLB buffer for 15 min at room temperature on an orbital shaker. After transfer into 1.5 ml tubes, cell debris was removed by centrifugation at 13000 rpm (16060 x g) and 4°C for 2 min. 20 µl of the supernatant were used to measure firefly and renilla luciferase activity with the Dual-Luciferase® Reporter 1000 Assay System (Promega) and the Lumat LB 9507 (Berthold Technologies).

3. Protein biochemistry

a) Protein extraction from mammalian cells

HUVECs were lysed in RIPA lysis buffer (Sigma-Aldrich) containing protease and/or phosphatase inhibitors (Roche) for 15 min on ice. After centrifugation for 15 min at 14000 rpm (18620 x g) and 4 °C, the supernatant was transferred into a new tube.

b) Protein extraction from animal organs

Tissue slices of animal organs were transferred into tubes with screw caps containing a ceramic sphere (MP Biomedicals) and homogenized in RIPA buffer (Sigma-Aldrich) supplemented with protease and phosphatase inhibitors (Roche) using a FastPrep automated homogenizer (MP Biomedicals). After incubation on ice for 15 min, the lysates were centrifuged for 15 min at 14000 rpm (18620 x g) and 4 °C.

c) Determination of protein concentration

The Bradford method was used to determine protein concentrations colorimetrically. A bovine serum albumin (BSA) standard curve was prepared using a BSA stock solution (10 mg/ml) which was diluted to yield solutions with 0.1, 0.2, 0.4, 0.6, 0.8 and 1 mg/ml BSA. 10 µl of each solution was mixed with 990 µl 1x Bradford reagent (diluted with aqua dest) in triplicate in plastic cuvettes and incubated for at least 5 min at RT. The standard curve was automatically created by the SmartSpec 3000 spectrophotometer (Bio-Rad) after measurement of the absorption of the standard samples at 595 nm.

To determine protein concentrations 1-2 µl of protein were mixed with 1ml 1x Bradford reagent in triplicate, allowed to stand for at least 5 min at RT and absorption was measured with the spectrophotometer.

d) Immunoblot (Western blot)

Equal amounts of protein (30-50 µg) were mixed with 4x protein loading dye and boiled at 95°C for 5 min to denature the proteins. After cooling and short spin down of the samples, proteins were separated on discontinuous SDS-polyacrylamide gels using the Mini Protean II Tetra electrophoresis system (Bio-Rad) at 80 V at the beginning and at 130 V as soon as the samples entered the resolving gel.

SDS-PAGE gel composition:

	Stacking gel	Resolving gel (15 ml)		
	5%	8%	10%	14%
Components				
H_2O [ml]	5.45	7.1	6.1	4.1
30% acrylamid [ml]	1.7	4	5	7
Stacking/Resolving buffer [ml]	2.5	3.75	3.75	3.75
10% APS [µl]	125	150	150	150
TEMED [µl]	12.5	6	6	6

4x protein loading dye
250 mM Tris-HCl pH 8.0
8% SDS
40% Glycerin
0.04% bromphenol blue
200 mM DTT

stacking buffer
0.5 M Tris-HCl pH 6.8
0.4% SDS

resolving buffer
1.5 M Tris-HCl pH 8.8
0.4% SDS

running buffer
25 mM Tris
96 mM Glycin
1% SDS

Proteins were blotted for 1.5 h at 20 W by wet transfer in a Mini Trans-Blot Cell (Bio-Rad) onto polyvinylidene fluoride (PVDF) membranes (Millipore), which were activated in methanol for 1 min and rinsed with H_2O before use. Unspecific binding of antibodies to the membrane was blocked by incubation in 5% nonfat dry milk or BSA in TBS with 0.1% Tween-20 (TBS-T) for 1 h at RT. After washing the membranes three times for 10 min with TBS-T, they were incubated overnight at 4°C with the primary antibody as indicated in the table. The next day, membranes were again washed three times with TBS-T and incubated with the horseradish peroxidase-conjugated secondary antibody at RT for 1.5 h. After washing the membranes three times with TBS-T, the blots were incubated with enhanced chemiluminescence (ECL) reagent according to the manufacturer´s instructions (Amersham). After transferring the blots into a plastic envelope in a film cassette, films were added to the cassette and exposed to the membrane in the dark room for various time points. Films were developed in a CURIX 60 processor (AGFA). Developed films were scanned with an EPSON Perfection 2480 PHOTO scanner and bands were densiometrically quantified using Scion Image for Windows – Release Alpha 4.0.3.2 (Scion Image Corporation, Frederick, MD, USA).

Primary antibody name	Blocking	Dilution	Manufacturer
rabbit polyclonal anti-BIM	5% milk	1:100 in 3% milk	BD, Franklin Lakes, NJ (USA)
rabbit monoclonal anti-JAK1 6G4	5% milk	1:1000 in 5% BSA	Cell Signaling, Danvers, MA (USA)
goat polyclonal anti-CTGF	5% BSA	1:250 in 5% BSA	Santa Cruz Biotechnology, Santa Cruz, CA (USA)
mouse monoclonal anti-Thrombospondin AB-3	5% BSA	1:250 in 5% BSA	Calbiochem, Darmstadt (Germany)
mouse monoclonal anti-pSTAT3 (Tyr 705) (3E2)	5% milk	1:1000 in 5% milk	Cell Signaling, Danvers, MA (USA)
mouse monoclonal anti-STAT3 (124H6)	5% milk	1:1000 in 5% milk	Cell Signaling, Danvers, MA (USA)
rabbit monoclonal anti-STAT3 (79D7)	5% milk	1:1000 in 5% BSA	Cell Signaling, Danvers, MA (USA)
mouse monoclonal anti-Tubulin alpha Ab-2	5% BSA or milk	1:1500 in 3% BSA or milk	NeoMarkers, Fremont, CA (USA)
mouse anti-p21	5% BSA	1:1000 in 3% BSA	BD, Franklin Lakes, NJ (USA)

Table III.11: Primary antibodies

Secondary antibody name	Dilution	Manufacturer
peroxidase-conjugated rabbit anti-mouse IgG	1:8000	Jackson ImmunoResearch, Newmarket (England)
peroxidase-conjugated goat anti-rabbit IgG	1:8000	Jackson ImmunoResearch, Newmarket (England)
donkey anti-goat IgG-HRP	1:10000	Santa Cruz Biotechnology, Santa Cruz, CA (USA)

Table III.12: Secondary antibodies

e) Stripping of membranes

To remove antibodies from PVDF membranes, blots were transferred into a 50 ml Falkon filled with 10 ml stripping buffer and incubated for 30 min at 50°C in a hybridization oven. After stripping, blots were washed 3x in TBS-T and blocked for the reprobe with another antibody.

stripping buffer
62.5 mM Tris-HCl
2% SDS
0.1 M β-mercaptoethanol

f) Zymography

48 h after transfection or Antagomir addition, HUVECs were washed once and incubated in serum-free EBM medium. After 24 h supernatants were collected, dead cells were pelleted by centrifugation at 2000 rpm (719 x g) and 4°C for 5 min and 10x concentrates were generated using Amicon Ultra centrifugal filter devices (Millipore) at 3300 rpm (1960 x g). Additionally, cells were washed twice with cold PBS and lysed in 1x JNK buffer supplemented with 1 mM PMSF (200 mM stock in EtOH absolut) for 15 min on ice. After removal of cell debris by centrifugation at 14000 rpm (18620 x g) and 4°C for 15 min, protein concentration was determined according to the Bradford method. 25 µl 10x supernatants and 50 µg cell lysate were mixed with equal volumes 2x zymography loading dye. Proteins were separated on SDS-polyacrylamide gels containing 1 mg/ml gelatin at 160 V using the Mini Protean II Tetra electrophoresis system (Bio-Rad). Gels were incubated twice for 20 min at RT in renaturation buffer followed by overnight incubation in activation buffer at 37°C. After washing the gels once briefly with aqua dest, proteins were visualized by incubation in staining solution. Active matrix metalloproteinases resulted in clear bands on the blue stained gel.

10x JNK buffer
20 mM Tris-HCl pH 7.4
150 mM NaCl
1 mM EDTA pH 8.0
1 mM EGTA pH 8.0
1% Triton X-100
2.5 mM disodium pyrophosphate
1 mM β-glycerolphosphate
1 mM Na_3VO_4
1 µg/ml Leupeptin

2x loading dye
125 mM Tris-HCl pH 6.8
20% glycerol
4% SDS
0.005% bromphenol blue

1x running buffer
24 mM Tris base pH 8.3
192 mM Glycin
0.1% SDS

renaturation buffer
2.5% Triton X-100 in H_2O

1x activation buffer
10 mM Tris-HCl pH 7.5
1.25% Triton X-100
5 mM $CaCl_2$
200 mM NaCl
0.05% Brij 35

staining solution
1 vol acetic acid
3 vol methanol
6 vol H_2O
1 vol 0.2% Phast Gel Blue R350

Gels were scanned with an EPSON Perfection 2480 PHOTO scanner and bands were densiometrically quantified using Scion Image for Windows – Release Alpha 4.0.3.2 (Scion Image Corporation, Frederick, MD, USA).

4. Bioinformatics

a) In silico microRNA target prediction

To find predicted targets of miR-17 and the other members of the miR-17-92 cluster as well as the location of the predicted binding site in the 3´ UTR, the TargetScanHuman web interface (http://www.targetscan.org/) with releases 4.2 (April 2008) and 5.1 (April 2009) was used.

5. In vivo experiments

Animal experiments in our department were done by the technical assistants Ariane Fischer, Susanne Heydt and Tino Röxe. The local ethic committees approved all animal experiments.

a) Antagomir administration

Antagomirs were synthesized by VBC Biotech, Vienna according to the information given by Krutzfeldt et al. [194]. In brief, all Antagomirs were single-stranded 2'-*O*-methyl-modified RNA oligonucleotides containing two phosphorothioate linkages at the 5´-end and four phosphorothioate linkages at the 3´ end as well as a cholesterol moiety at the 3´ end. A schematic representation of an Antagomir is shown in Figure III.4.

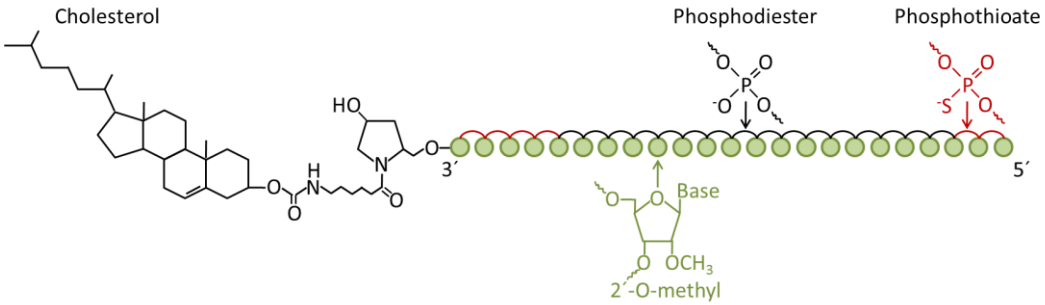

Figure III.4: **Composition of an Antagomir.** The sequence of an Antagomir is generally reverse complementary to the microRNA to be targeted. The 2´-O-methyl modification of the bases and the phosphotioate bonds at both ends protect the Antagomirs from degradation by nucleases. The cholesterol moiety at the 3´ end facilitates cellular uptake.

The sequences of the Antagomirs are given in table III.13. To analyse the specificity and efficiency of the Antagomirs, tissue was snap-frozen and stored at -80°C for RNA analysis. RNA isolation and real-time PCR was performed as described above.

Antagomir name	Mature miR sequence	Antagomir sequence
Antagomir-Co		5`-AAGGCAAGCUGACCCUGAAGUU-3`
Antagomir-17	5´-CAAAGUGCUUACAGUGCAGGUAG-3´	5`-CUACCUGCACUGUAAGCACUUUG-3`
Antagomir-18a	5´-UAAGGUGCAUCUAGUGCAGAUAG-3´	5`-CUAUCUGCACUAGAUGCACCUUA-3`
Antagomir-19a	5´-UGUGCAAAUCUAUGCAAAACUGA-3´	5`-UCAGUUUUGCAUAGAUUUGCACA-3`
Antagomir-20a	5´-UAAAGUGCUUAUAGUGCAGGUAG-3´	5`-CUACCUGCACUAUAAGCACUUUA-3`
Antagomir-21	5´-UAGCUUAUCAGACUGAUGUUGA-3´	5´-UCAACAUCAGUCUGAUAAGCUA-3´
Antagomir-92a	5´-UAUUGCACUUGUCCCGGCCUG-3´	5´-CAGGCCGGGACAAGUGCAAUA-3´

Table III.13: Antagomirs

b) Matrigel plug assay

Eight-week-old mice were injected subcutaneously with two Matrigel basement matrix (BD) plugs (200 µl each) at day 0. Antagomir-Co, Antagomir-17, Antagomir-18a, Antagomir-19a or Antagomir-20a were injected i.v. at day 0 (after Matrigel implantation) and at day 2 and day 4. All Antagomirs were administered at doses of 8 mg per kg body weight (bw) with 0.2 ml per injection. Matrigel plugs were harvested at day 7. In order to analyse perfused capillaries, 200 µl FITC-conjugated lectin (1 mg/ml) was injected i.v. 30 min before harvest. Lectin positive structures were counted manually in five microscopic fields (5x/0.25 objective) using a computer-assisted fluorescence microscope (Axiovert 100 M equipped with AxioCam camera, Carl Zeiss, Jena). Images were taken with a laser scanning microscope (LSM510 META with Software Release 4.0 SP2, Carl Zeiss, Jena) using the Plan-Neofluar 40x/1.3 Oil objective.

c) Tumour model

Lewis lung carcinoma (LLC) cells were cultured as described above and 1 million cells were injected subcutaneously in C57Bl/6 mice by Alexander Scholz at the Edinger Institute in Frankfurt. Tumour volume was measured daily with a Thorpe caliper (Horex, Germany) and was calculated as d_1 x d_2. 30 min before harvest, FITC-conjugated lectin was i.v. injected. After explantation, tumours were weighted and 3D tumour volume was calculated using the formula d_1 x d_2 x d_3, where d_n represent the three orthogonal diameter measurements. Tumour specimens were fixed in 4% formalin and were histologically examined. Sections were stained with an anti-endomucin antibody (eBioscience; 1:100) followed by an anti-rat Alexa Fluor 555 antibody (Invitrogen). Pictures were taken with a laser scanning microscope (LSM510 META with Software Release 4.0 SP2, Carl Zeiss, Jena) using the Plan-Neofluar 40x/1.3 Oil objective (Endomucin staining) or Plan-Neofluar 20x/0.5 objective (FITC-Lectin). Lectin positive structures were counted manually in three images per tumour slice and for the Endomucin staining five images were evaluated automatically using Axiovision 4.6 (Zeiss Imaging Solutions GmbH, Munich). Immunostainings and data acquisition were done by Marion Muhly-Reinholz.

d) PAH animal models

All work regarding the PAH models were done by our collaboration partners of the Gießen University Lung Centre. The following description of the methods was provided by Dr. Soni Pullamsetti.

Animals and experimental design: chronic hypoxia mouse model

Adult C57Bl/6J mice were obtained from Charles River Laboratories. Animals were housed under controlled temperature (~22°C) and lighting (12/12-hour light/dark cycle), with free access to food and water. The animals were exposed to chronic hypoxia (10% O_2) in a ventilated chamber, as described previously. The level of hypoxia was held constant by an auto regulatory control unit (model 4010, O_2 controller, Labotect; Göttingen, Germany) supplying either nitrogen or oxygen. Excess humidity in the recirculating system was prevented by condensation in a cooling system. CO_2 was continuously removed by soda lime. Cages were opened once a day for cleaning as well as for food and water supply. The chamber temperature was maintained at 22-24°C. Normoxic mice were kept under identical conditions. Mice were exposed to hypoxia for 28 days and were treated with Antagomirs directed against miR-17, miR-21, miR-92a, a control Antagomir or the solvent PBS (10 animals each) intravenously (tail vein) at day 14, day 17, day 20, day 23 and day 26.

Animals and experimental design: monocrotaline lung injury model

Adult male Sprague-Dawley rats (300-350 g in body weight; Charles River Laboratories, Sulzfeld, Germany) were randomized for treatment 21 days after a subcutaneous injection of 60 mg/kg monocrotaline (MCT, Sigma-Aldrich) to induce pulmonary arterial hypertension as described previously [195]. Healthy control rats received a saline injection instead of monocrotaline. For Antagomir treatment, 21 days MCT injected rats were divided into 5 groups (10 animals each) and were treated with Antagomirs against miR-17, a control Antagomir or solvent (PBS) intravenously (tail vein) at day 22 and day 29.

Hemodynamic and right ventricular hypertrophy (RVH) measurements

Hemodynamic measurements were performed as previously described [195]. Briefly, rats and mice were anesthetized, tracheotomized and artificially ventilated using a positive end expiratory pressure (PEEP) of 1 cm of H_2O column. The left carotid artery was isolated and cannulated with a polyethylene cannula connected to a fluid-filled force transducer and the systemic arterial pressure (SAP) was measured. A catheter was inserted through the right jugular vein into the right ventricle for measurement of right ventricular systolic pressure (RVSP). The animals were

exsanguinated and the lungs were flushed with sterile saline. The left lung was fixed for histology in 3.5% neutral buffered formalin and the right lung was snap frozen in liquid nitrogen. The heart was isolated and dissected under microscope. The right ventricular wall was separated from the left ventricular wall and ventricular septum. Dry weight of the right ventricle, free left ventricular wall and ventricular septum was determined. Right ventricular hypertrophy was expressed as the ratio of weight of the right ventricular (RV) wall and that of the free left ventricular wall and ventricular septum (LV+S).

High-resolution echocardiography

Anesthesia was induced with 3% isoflurane gas and maintained with 1.0-1.5% isoflurane in room air supplemented with 100% O_2. Animals were laid supine on a heating platform with all legs taped to ECG electrodes for heart rate (HR) monitoring. Body temperature was monitored via a rectal thermometer (Indus Instruments, Houston, TX) and maintained at 36.5-37.5°C using a heating pad. The chest of the rats and mice was shaved and treated with a chemical hair remover to reduce ultrasound attenuation. To provide a coupling medium for the transducer, a pre-warmed ultrasound gel was spread over the chest wall.

Transthoracic echocardiography was performed and analysed with a Vevo770 high-resolution imaging system equipped with a 30-MHz transducer (VisualSonics, Toronto, Canada) to determine the pulmonary artery acceleration time (PAAT). An experienced sonographer who was blinded to results of invasive and morphometric studies performed all studies.

Histology and pulmonary vascular morphometry

The formalin-fixed lungs were subjected to paraffin embedding. The paraffin-embedded tissues were cut into 3 µm thick slices. Elastica staining was performed according to common histopathological procedures. The degree of muscularization of small peripheral pulmonary arteries was assessed by double-staining the 3 µm sections with an anti-α-smooth muscle actin antibody (dilution 1:900, clone 1A4, Sigma-Aldrich, Saint Louis, Missouri) and anti-human von Willebrand factor antibody (vWF, dilution 1:900, Dako, Hamburg, Germany) followed by analysis of the vessels using a computerized morphometric analysis system (QWin; Leica, Wetzlar, Germany) to determine the degree of pulmonary artery muscularization. In each rat, 80 to 100 intra-acinar arteries (25 to 50 µm diameter) were categorized as muscular, partially muscular or non-muscular. Arteries of the same size were additionally analysed for the medial wall thickness as previously described [195]. In mouse sections, 80-100 intra-acinar vessels at a size between 20 and 70 µm accompanying either alveolar ducts or alveoli were analysed. All analyses were done in a blinded fashion.

6. Data analysis

Data are expressed as mean ± standard error of the mean (SEM). Calculations were made with Microsoft Excel 2007 and 2010. The Kolmogorov-Smirnov test was used to analyse the datasets for normality. Two treatment groups were statistically compared by Mann-Whitney U test (if datasets did not exhibit a normal distribution) or student´s t-test (if datasets exhibited a normal distribution). Multiple group comparisons were done by ANOVA and Dunn´s (if datasets did not exhibit a normal distribution), Dunnett´s or Newman-Keuls (if datasets exhibited a normal distribution) posthoc analysis. For statistical analysis GraphPad Prism version 5.00 for Windows (GraphPad Software, San Diego, CA, USA) or SPSS Statistics 17.0 (SPSS Inc., Chicago, IL, USA) were used. Results were considered statistically significant when $P < 0.05$.

IV. Results

Since previous research in our lab demonstrated that the individual members of the miR-17-92 cluster are expressed in human umbilical vein endothelial cells (HUVECs) and that miR-92a displays anti-angiogenic capacity in ECs and controls recovery in response to ischemic diseases [119], we decided to characterize the biological function of the other members of the miR-17-92 cluster, namely miR-17, miR-18a, miR-19a and miR-20a, in endothelial cells and EC-dependent physiological and pathophysiological processes. MiR-19b was neglected in this study since it just differs by one nucleotide from miR-19a, so that both microRNAs are bioinformatically predicted to target the same gene expression pattern and might therefore be functionally redundant. Furthermore, we evaluated the applicability of miR-17, -21 and -92a inhibition by systemic administration of the respective Antagomirs as therapeutic approach in pulmonary arterial hypertension in a collaborational project within the Excellence Cluster Cardio-Pulmonary System (ECCPS) with the group of Dr. Ralph Schermuly in Gießen.

A. Functional role of members of the miR-17-92 cluster in endothelial cells and angiogenesis

1. Individual members of the miR-17-92 cluster affect angiogenesis in vitro

To gain first insights into the cell-intrinsic function of the members of the miR-17-92 cluster in endothelial cells, miR-17, -18a, -19a and -20a were overexpressed in HUVECs by transfection of commercially available miR precursor (pre-miR) molecules, and the cells were analysed in an in vitro angiogenesis assay regarding their sprout formation capacity. In Pre-18a, -19a and -20a transfected HUVECs a specific increase in the respective mature miR was detected by a universal probe based qPCR detection method, whereas in Pre-17 treated cells not only a profound rise of mature miR-17 but also of miR-20a was measured (Fig. IV.1A). Potentially, the determined augmentation of mature miR-20a is a detection artefact due to the limited specificity of the real-time method we initially used to quantify mature microRNAs. Owing to the high sequence similarity of miR-17 and miR-20a, reverse transcription of both miRs was achieved with the identical stem loop primer, followed by the real-time quantification in which the specificity of the reaction was solely dictated by the miR specific forward primer as the reverse primer and the TaqMan probe were universal for all miRs. Individual overexpression of all the cluster members significantly reduced endothelial cell sprouting of spheroids in the three-dimensional (3D) angiogenesis

assay, although miR-17 exhibited the strongest effect (Fig. IV.1B/C). In order to determine, whether the inhibitory effect of miR-17 on in vitro angiogenesis is concentration dependent, we transfected HUVECs with 10 nM, 1 nM and 0.1 nM miR-17 or control precursor molecules and assessed the sprouting capacity in the spheroid model. Indeed, miR-17 inhibited spheroid sprouting in a concentration dependent manner (Fig. IV.1D). To confirm the effect of miR-17 on spheroid sprouting, we repeated the assay with a miR-17 mimic from another company. As for the miR-17 precursor, sprouting of spheroids was dramatically impaired after transfection of the miR-17 mimic (Fig. IV.1E).

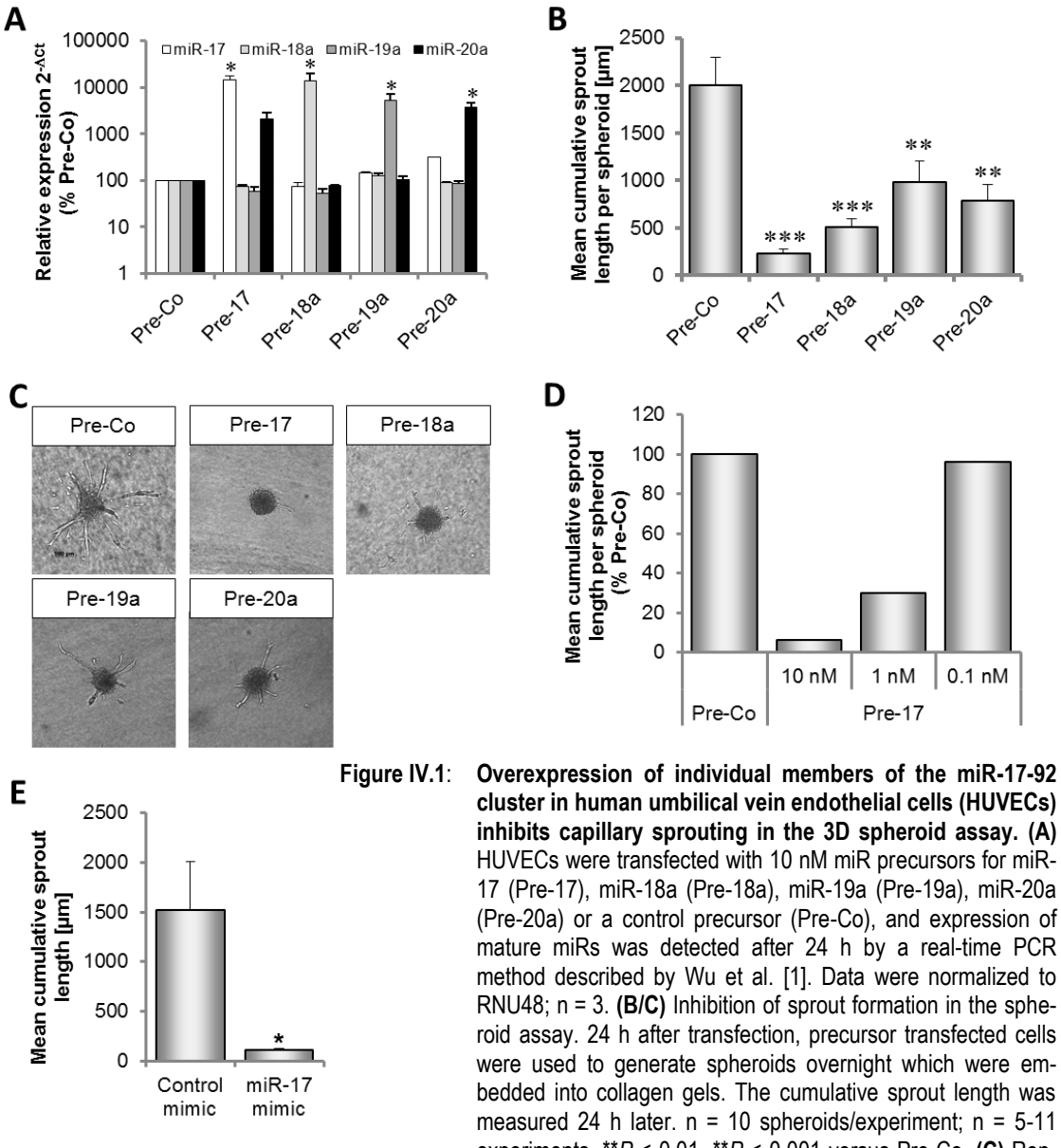

Figure IV.1: **Overexpression of individual members of the miR-17-92 cluster in human umbilical vein endothelial cells (HUVECs) inhibits capillary sprouting in the 3D spheroid assay. (A)** HUVECs were transfected with 10 nM miR precursors for miR-17 (Pre-17), miR-18a (Pre-18a), miR-19a (Pre-19a), miR-20a (Pre-20a) or a control precursor (Pre-Co), and expression of mature miRs was detected after 24 h by a real-time PCR method described by Wu et al. [1]. Data were normalized to RNU48; n = 3. **(B/C)** Inhibition of sprout formation in the spheroid assay. 24 h after transfection, precursor transfected cells were used to generate spheroids overnight which were embedded into collagen gels. The cumulative sprout length was measured 24 h later. n = 10 spheroids/experiment; n = 5-11 experiments. $^{**}P < 0.01$, $^{**}P < 0.001$ versus Pre-Co. **(C)** Representative images. Scale bar represents 100 µm. **(D)** HUVECs were transfected with different concentrations of miR-17 precursor or a control precursor (Pre-Co) as indicated. Sprouting capacity of the cells was analysed in the spheroid assay as described before. n = 10 spheroids/condition, n = 1 experiment. **(E)** Effect of 10 nM miR-17 mimic on spheroid sprouting. n = 10 spheroids/experiment; n = 3 experiments.

We further analysed the effect of the individual miR-17-92 cluster members in a second angiogenesis assay, namely the two-dimensional (2D) tube network formation on Matrigel in which the endothelial cells assemble in capillary-like structures. Surprisingly, a comparatively slight and nonsignificant reduction of the length of the tube networks was observed after overexpression of miR-17, -18a, -19a and miR-20a compared to the control precursor treated cells (Fig. IV.2A). Since endothelial cell migration is an essential process in angiogenesis, we addressed the migratory capacity of precursor transfected endothelial cells in collagen I coated Boyden chambers. Consistent with the results gained from the tube network formation assay, overexpression of miR-17, -18a, and -19a slightly, but nonsignificantly, impaired the migratory capacity of ECs under basal conditions and in response to VEGF, whereas miR-20a reduced EC migration by trend only upon VEGF stimulation but not under basal conditions (Fig. IV.2B).

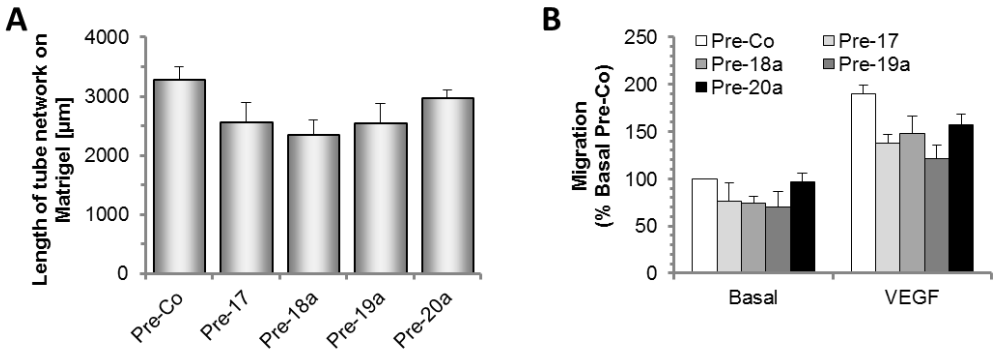

Figure IV.2: **Overexpression of individual members of the miR-17-92 cluster slightly impairs tube formation and migratory capacity of human umbilical vein endothelial cells (HUVECs).** HUVECs were transfected with 10 nM miR precursor for miR-17 (Pre-17), miR-18a (Pre-18a), miR-19a (Pre-19a), miR-20a (Pre-20a) or a control precursor (Pre-Co) and seeded onto Matrigel coated dishes to quantify tube formation capacity or collagen I coated boyden chambers to address migration 48 h after transfection. **(A)** Effect of cluster members on tube network formation on Matrigel. Tube networks were quantified 24 h after cell seeding. n = 5. **(B)** Effect of cluster members on basal and VEGF-induced migration in modified Boyden chambers. Migrated cells were counted 4 h after cell seeding. n = 4.

Furthermore, inhibition of endothelial cell apoptosis occurs during angiogenesis to ensure cell survival. In hematopoetic and tumour cells, anti-apoptotic activity has been attributed to the miR-17-92 cluster [145, 157]. To analyse the impact of miR-17, -18a, -19a and -20a on apoptosis in endothelial cells, we again overexpressed the miRs in HUVECs by precursor transfection and measured the percentage of apoptotic cell death by staining the cells with fluorescently labelled annexin V for FACS (fluorescence activated cell sorting) analysis of cell surface exposed phosphatidylserine (Fig. IV.3). Oxidative stress was excerted by addition of low (200 µM) and high concentrations (1 mM) of hydrogen peroxide (H_2O_2) to promote endothelial cell apoptosis. Whereas overexpression of miR-17, -19a and -20a did not affect EC apoptosis under standard culture conditions or upon treatment with a low dose of H_2O_2, Pre-18a transfected ECs displayed a significantly increased apoptotic rate under standard culture conditions and showed a trend

towards enhanced apoptotic cell death in response to 200 µM H_2O_2. Under high oxidative stress, miR-17 showed a trend, but no statistically significant effect, towards reduction of apoptotic cell death. In contrast, miR-18a, -19a and -20a displayed no definite effect on EC apoptosis under this condition.

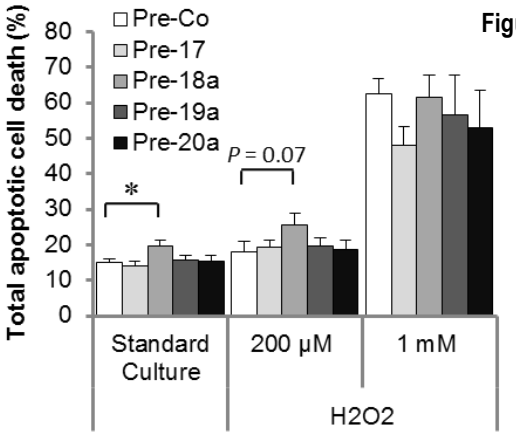

Figure IV.3: **Effect of miR-17, -18a, -19a and -20a on EC apoptosis.** Overexpression of the individual miRs in HUVECs was accomplished by transfection of miR precursor molecules. 48 h after transfection, cells were stained with FITC-conjugated annexin and 7-AAD to determine the number of apoptotic cells by FACS analysis. Cells were exposed to oxidative stress by addition of H_2O_2 to the cell culture medium 14 h before analysis of apoptotic cell death. n = 3 - 11 experiments. **P* < 0.05.

Finally, proliferation of endothelial cells is a critical event during blood vessel formation. To address the effect of the individual miRs on EC proliferation, we determined the cell cycle profile of HUVECs overexpressing the different miRs by FACS analysis of BrdU incorporation 48 h after precursor transfection. As shown in Fig. IV.4A, the number of cells in the S phase of the cell cycle was significantly increased after overexpression of miR-17 and miR-20a indicating that these two miRs stimulate proliferation of ECs. In contrast, miR-18a and miR-19a had no effect on the number of proliferating cells. Transfection of HUVECs with four different concentrations of miR-17 and control precursor revealed that the pro-proliferative effect of miR-17 was concentration dependent (Fig. IV.4B).

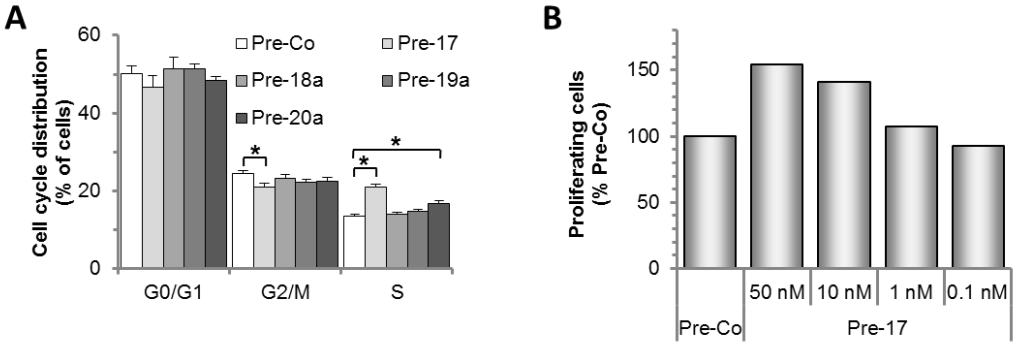

Figure IV.4: **MiR-17 and miR-20a enhance proliferation of endothelial cells. (A)** 48 h after transfection of HUVECs with 10 nM miR-17, -18a, -19a and -20a precursor, BrdU was added to the cell culture medium for 45 min and cells were stained with an anti-BrdU antibody and 7-AAD before measurement of the cell cycle profile via fluorescence activated cell sorting (FACS). n = 4-8. **P* < 0.05 **(B)** HUVECs were transfected with different concentrations of miR-17 and control precursor as indicated. 48 h after transfection BrdU incorporation was measured by FACS staining. n = 1.

To verify that the members of the miR-17-92 cluster indeed play a role in angiogenesis in vitro, we addressed the effect of blocking the endogenous miRs individually by transfection of commercially available hairpin inhibitors in the 3D spheroid assay. Although ECs were transfected with the same amount of each miR specific inhibitor, considerable differences in the knockdown efficiency of the individual miRs by the respective inhibitor were observed. Whereas the levels of miR-18a and miR-19a were profoundly decreased 24 h after inhibitor transfection, the reduction of mature miR-17 and miR-20a was rather moderate. The hairpin inhibitor targeting miR-27b, which was applied as an additional non-related control in the spheroid assay, also displayed an efficient knockdown capability (Fig. IV.5A). Inhibition of miR-17, -18a and -20a significantly enhanced spheroid sprouting about 1.5 fold, whereas the hairpin inhibitor against miR-19a increased the in vitro angiogenic response only slightly. Conversely, the miR-27b hairpin inhibitor significantly impaired angiogenic sprouting (Fig. IV.5B) as previously reported [78].

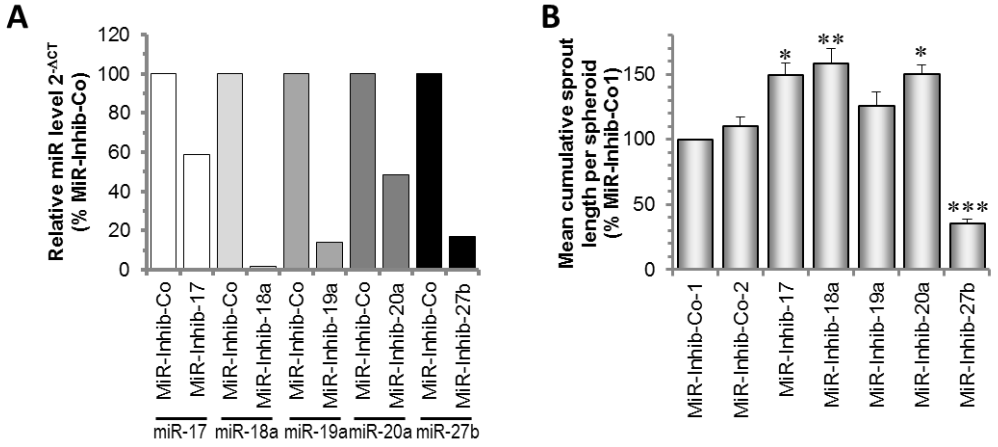

Figure IV.5: **Inhibition of individual members of the miR-17-92 cluster in human umbilical vein endothelial cells (HUVECs) promotes capillary sprouting in the 3D spheroid assay**. HUVECs were transfected with 50 nM miR inhibitors targeting individual members of the miR-17-92 cluster and miR-27b as indicated. 24 h after transfection spheroids were generated overnight and embedded into collagen gels. Another 24 h later, capillary sprout length was quantified. **(A)** Confirmation of microRNA knockdown 24 h after inhibitor transfection. MiR expression in control inhibitor treated cells (MiR-Inhib-Co) represents the mean of both control inhibitors (MiR-Inhib-Co-1, miR-Inhib-Co-2) used. MiR levels were normalized to RNU48. n = 1. **(B)** Effect of miR inhibition on spheroid sprouting. n = 10 spheroids/experiment; n = 6 experiments. **P* < 0.05, ***P* < 0.01, ****P* < 0.001 versus MiR-Inhib-Co-2.

2. Combined inhibition of miR-17 and miR-20a by Antagomir-17 augments neovascularization in vivo

Having shown that the individual members of the miR-17-92 cluster affect the angiogenic activity of endothelial cells in vitro, we next addressed their relevance for blood vessel formation in vivo. Since there has been up to now no non-transgenic approach to upregulate microRNAs in vivo and as for therapeutic angiogenesis it would be preferable to downregulate anti-angiogenic miRs, we decided to use previously established microRNA inhibitors, referred to as Antagomirs, to

inhibit the individual members of the miR-17-92 cluster in vivo. Antagomirs which were first described by Krutzfeldt et al. in 2005 are RNA oligonucleotides that are fully complementary to the respective microRNA carrying phosphorothioate linkages to improve stability and a cholesterol moiety to facilitate cellular uptake [194]. Antagomirs targeting the members of the miR-17-92 cluster were designed on the basis of the sequences of hsa-miR-17, hsa-miR-18a, hsa-miR-19a and hsa-miR-20a given in the Sanger miRBase database. Since the miR-17-92 cluster is highly conserved across species, the individual members do not differ between human and mouse.

To study the impact of the individual cluster members on blood vessel formation in vivo, we combined the Matrigel plug angiogenesis mouse model with the systemic administration of Antagomirs by i.v. injection into the tail vein. The detailed experimental setup is shown in Fig. IV.6D.

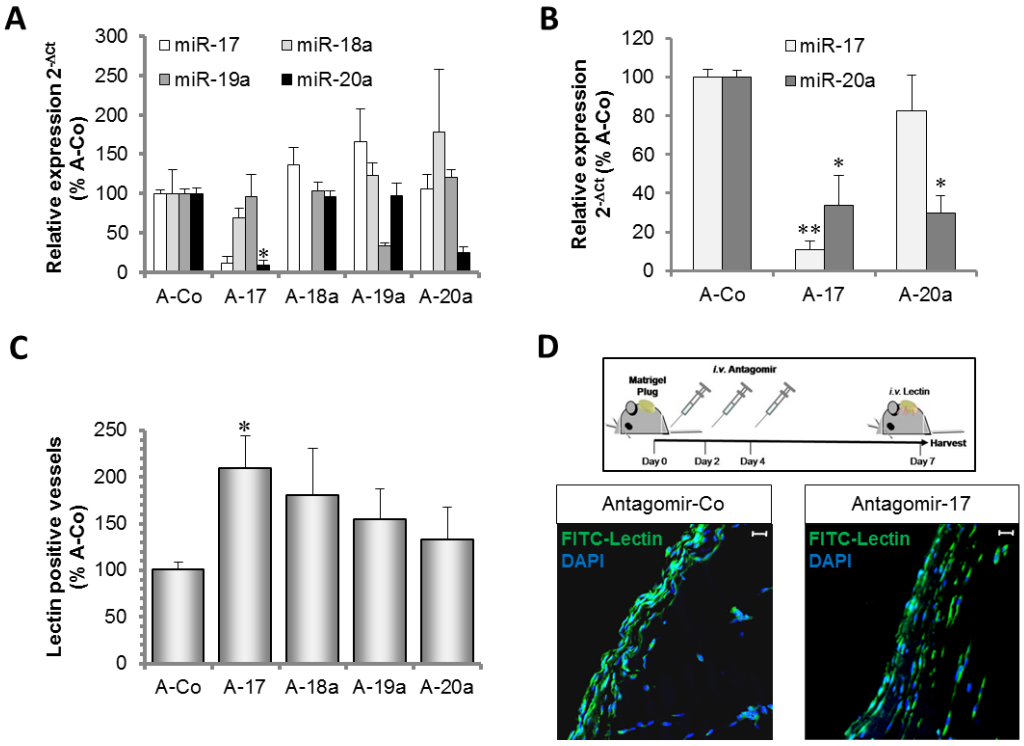

Figure IV.6: **Antagomir-mediated inhibition of miR-17 enhances angiogenesis in mice. (A-B)** Effect of systemic infusion of three intravenous (i.v.) injections of Antagomirs (8 mg/kg body weight per injection) targeting miR-17 (A-17), miR-18a (A-18a), miR-19a (A-19a), and miR-20a (A-20a) or a control Antagomir (A-Co) on miR expression in hearts harvested 7 days after the first injection. n = 3-6 mice per group. MiR expression was detected by a real-time PCR method using a universal TaqMan probe in combination with a miR-specific forward primer (A) and a TaqMan miRNA assay with higher specificity (B). SnoRNA202 was used as endogenous control. **(C-D)** Effect of Antagomir intravenous infusion at days 0, 2, and 4 on the number of lectin-perfused vessels in Matrigel plugs in vivo after 7 days. Analysis of Matrigel plugs was done by Tino Röxe. n = 4-10 mice per group, n = 2 plugs per mouse. **P* < 0.05, ***P* < 0.01 versus A-Co. (D) Schematic drawing of the experimental design and representative images of Matrigel plug sections of Antagomir-Co and Antagomir-17 treated mice. Scale bars represent 20 µm.

Shortly before harvest, Lectin-FITC was i.v. infused into the mice to enable visualization of perfused vessels in the Matrigel plugs. Three injections of 8mg/kg body weight Antagomir at the day of Matrigel plug implantation as well as two and four days afterwards resulted in an efficient and

specific knockdown of miR-18a, -19a and -20a after one week in the hearts of the animals treated with the respective Antagomirs (Fig. IV.6A). Only Antagomir-17 revealed an off-target effect by significantly blocking the closely related miR-20a besides its intended target miR-17.

Since mature miR expression was measured by a qPCR method in which the specificity is only determined by the forward primer, whereas the reverse primer and the TaqMan probe are universal, we additionally measured the expression of miR-17 and miR-20a with a second method that uses a miR specific TaqMan probe for improved specificity. This method verified the finding that Antagomir-17 blocked both miRs, miR-17 and miR-20a (Fig. IV.6B). MiR-17 and miR-20a only differ in two nucleotides and off-target effects of different miR-17 inhibitors on members of the miR-17 seed family are reported in the literature [168, 196]. Three injections of Antagomir-17 significantly increased the number of perfused vessels invading the Matrigel plug in vivo, whereas specific inhibition of miR-18a, -19a and -20a showed a trend towards enhanced neovascularization but no statistical significance (Fig. IV.6C/D).

To see whether one dose of each Antagomir sufficiently blocks the respective microRNA to promote neovascularization, we repeated the Matrigel plug assay with one Antagomir injection at day one after Matrigel plug implantation (Fig. IV.7).

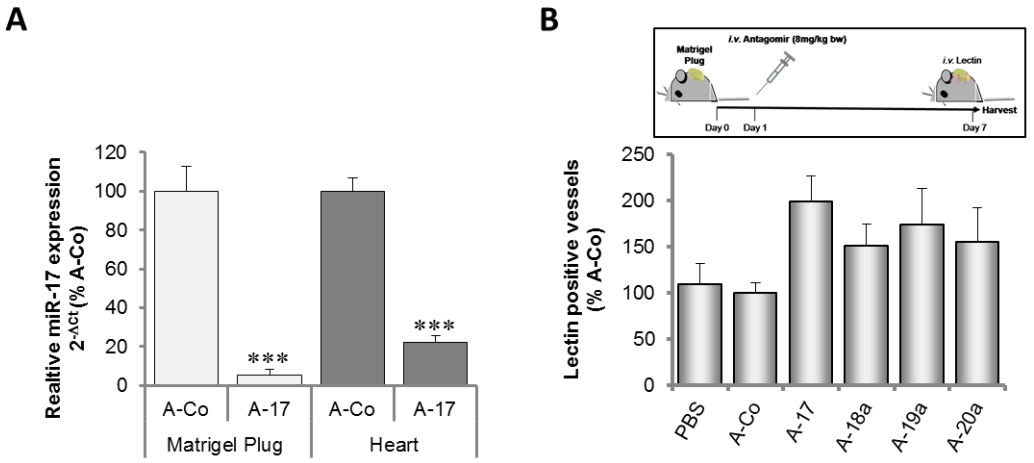

Figure IV.7: **Effect of one injection of Antagomir on neovascularization of Matrigel plugs in vivo. (A)** After implantation of Matrigel plugs by subcutaneous injection of Matrigel supplemented with 0.5 µg/ml FGF-2, mice were treated with one i.v. injection of Antagomir-17 (8 mg/kg bw). After three days Matrigel plugs and the hearts of the mice were harvested and total RNA was isolated using TRI Reagent. MiR-17 expression was measured using the respective MicroRNA Assay kit (Applied Biosystems). SnoRNA202 was used as endogenous control. n = 8. ****P* < 0.001 versus A-Co. **(B)** Effect of one single Antagomir infusion (8 mg/kg bw) at day 1 on the number of lectin-perfused vessels in Matrigel plugs in vivo. Analysis of Matrigel plugs was done by Tino Röxe. n = 4-8 per group, n = 2 plugs per mouse.

Analysis of miR-17 expression in the Matrigel plugs and the hearts of Antagomir-17 treated mice three days after Antagomir administration revealed a miR-17 knockdown by nearly 90% in the Matrigel plugs and 80% in the hearts of the animals (Fig. IV.7A). Regarding neovascularization of

Matrigel plugs, the effects were akin to that observed in animals treated with three Antagomir injections, although the profound increase of perfused vessels in animals receiving one dose of Antagomir-17 did not reach statistical significance (Fig. IV.7B). In summary, these data demonstrate that the combined inhibition of miR-17 and miR-20a by Antagomir-17 enhances blood vessel formation in vivo.

3. Impact of the miR-17-92 cluster members on tumour angiogenesis

Dews et al. previously reported that tumour cells overexpressing the miR-17-92 cluster form larger and better perfused tumours in mice. The tumour angiogenesis promoting effect of the miR-17-92 cluster in this model was attributed to the suppression of anti-angiogenic factors produced by tumour cells, namely connective tissue growth factor (CTGF) and thrombospondin-1 (TSP-1), which might act in a paracrine manner on endothelial cells to control blood vessel formation [150]. Since in our hands the individual members of the miR-17-92 cluster inhibited angiogenesis in vitro upon overexpression in ECs, we next addressed the effect of these miRs on the paracrine angiogenic activity of endothelial cells in comparison to tumour cells. We used the murine Lewis Lung Carcinoma 1 (LLC1) cell line which displayed compared to HUVECs a similar level of mature miR-17 which we measured as a representative member of the miR-17-92 cluster by real-time PCR in both cell types (Fig. IV.8).

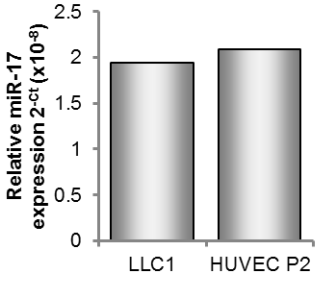

Figure IV.8: **MiR-17 is equally expressed in LLC1 and endothelial cells.** RNA was isolated using TRI Reagent and miR-17 levels in LLC1 cells and HUVEC in the 2nd passage (P2) were determined by real-time PCR with the respective MicroRNA Assay kit (Applied Biosystems). n = 1

To analyse the impact of the individual miRs on paracrine angiogenic activity, we overexpressed miR-17, miR-18a, miR-19a and miR-20a in HUVECs and LLC1 cells by transfection of the respective precursor molecules. Serum-free conditioned medium was generated one day after transfection, tenfold concentrated by centrifugation the following day and applied to untreated collagen-embedded EC spheroids (Fig.IV.9A). The mean cumulative sprout length of individual spheroids in each condition was quantified as a measure for the angiogenic activity of the conditioned media. As a result, conditioned medium of LLC1 tumour cells overexpressing miR-17, miR-19a and miR-20a (Fig. IV.9B) slightly enhanced angiogenic sprouting of endothelial cells compared to the medium of control precursor transfected LLC1 cells. In contrast, conditioned medium derived from endothelial cells transfected with the precursors for miR-17, miR-18a or

miR-19a showed a trend towards reduced angiogenic activity of endothelial cells (Fig. IV.9C) in comparison with the Pre-Co treated HUVECs. Nevertheless, the observed differences were statistically not significant. Overall, the angiogenic activity of the supernatants differed the most between LLC1 and endothelial cells after overexpression of miR-17, -18a and -19a.

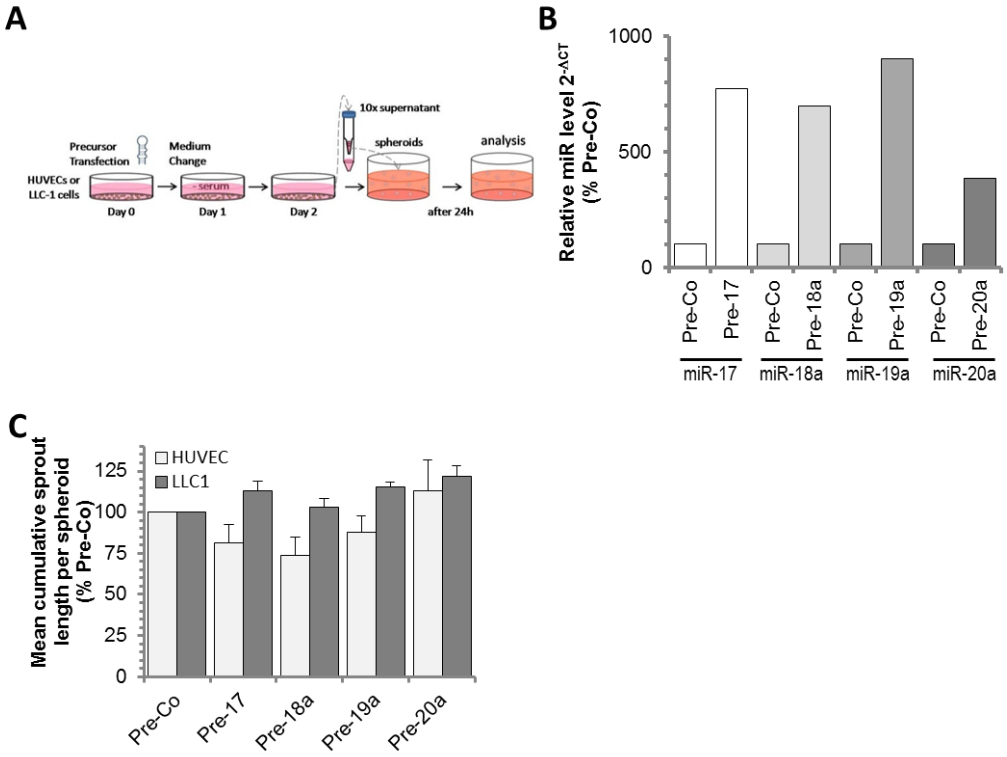

Figure IV.9: **Effect of members of the miR-17-92 cluster on paracrine activity of tumour cells in vitro. (A)** Schematic drawing of experimental design. HUVECs or LLC1 tumour cells were transfected with the respective precursors. Medium was changed to Dulbecco modified Eagle medium with 0.05% bovine serum albumin after 1 day. Conditioned medium was collected at day 2, and 10x concentrates were transferred to collagen-embedded spheroids with non-transfected HUVECs. Quantification of spheroid sprout length was performed after incubation of the spheroids with the conditioned medium for 24 h. **(B)** Confirmation of miR overexpression in LLC1 cells 48 h after precursor transfection. MiR levels were normalized to snoRNA202. n = 1. **(C)** Effect of 10x supernatants of precursor transfected HUVECs and LLC1 cells on sprouting capacity of non-transfected HUVECs. n = 3 for HUVECs, n = 4 for LLC1.

To see whether the members of the miR-17-92 cluster affect CTGF and TSP-1 expression in endothelial cells, we analysed cell lysates of precursor transfected HUVECs by Western blotting. The precursor for miR-126 was used as an additional non-related control. Overexpression of miR-18a and miR-19a slightly lowered CTGF levels, whereas miR-17, miR-20a, miR-92a and the non-related miR-126 had no effect (Fig. IV.10A). A visible decrease of TSP-1 occurred only upon miR-19a overexpression, but not in ECs transfected with precursors of the other miRs (Fig. IV.10B). Overall, our results suggest that the members of the miR-17-92 cluster act in a cell-context dependent manner to regulate angiogenesis in vitro.

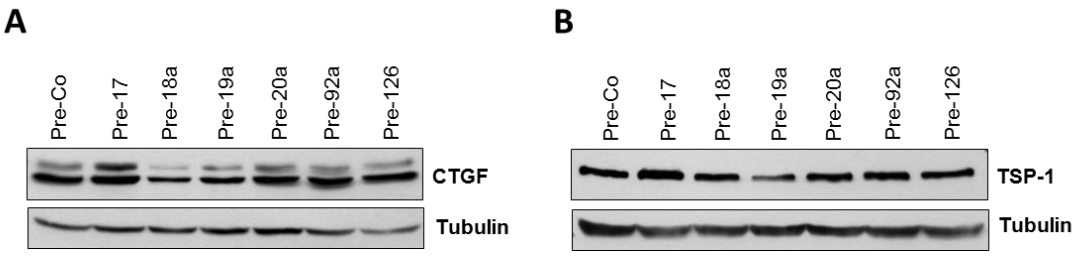

Figure IV.10: **Effect of miR overexpression on CTGF (A) and TSP-1 (B) protein expression.** HUVECs were transfected with the indicated miR precursors, and after 48 h cells were lysed with radio immunoprecipitation assay (RIPA) buffer supplemented with protease inhibitors to extract proteins. Connective tissue growth factor (CTGF) and thrombospondin-1 (TSP-1) expression was determined by Western blot analysis. Pre-126 served as a non-related control. Representative results out of 4 independent experiments are shown. Tubulin served as loading control.

Since Antagomir-17 had the strongest effect on neovascularization of Matrigel plugs in vivo, we analysed the effect of this Antagomir on tumour growth and vascularization in a Lewis lung carcinoma tumour model. Two series of experiments with different injection protocols were performed.

In the first series, mice received one dose of Antagomir i.v. at day 5 after subcutaneous (s.c.) inoculation of LLC1 cells into both flanks of the mice (Fig. IV.11A). Analysis of the miR-17 level in the explanted tumours at the end of the experiment (day 13) still showed a decrease of miR-17 by 28.1 ± 7.9% in the Antagomir-17 treated animals (Fig. IV.11B). Tumour size, volume and weight were increased, although the observed differences were statistically not significant (Fig. IV.11A/C/D). Nevertheless, tumour vascularization was not elevated as addressed by quantifying lectin-FITC positive and endomucin-stained vessels (Fig. IV.11E/F).

In the second series, mice were treated with two doses of Antagomir-17 at day 5 and 10 after LLC1 inoculation (Fig. IV.12A) resulting in half the expression of miR-17 in the tumours of Antagomir-17 compared to control Antagomir injected animals at the end of the experiment (Fig. IV.12B). Using this treatment protocol, we could not detect differences in tumour size, volume and weight (Fig. IV.12A/C/D). Moreover, quantification of endomucin-positive capillaries within the tumours did not reveal any effect of Antagomir-17 on tumour vascularization (Fig. IV.12E).

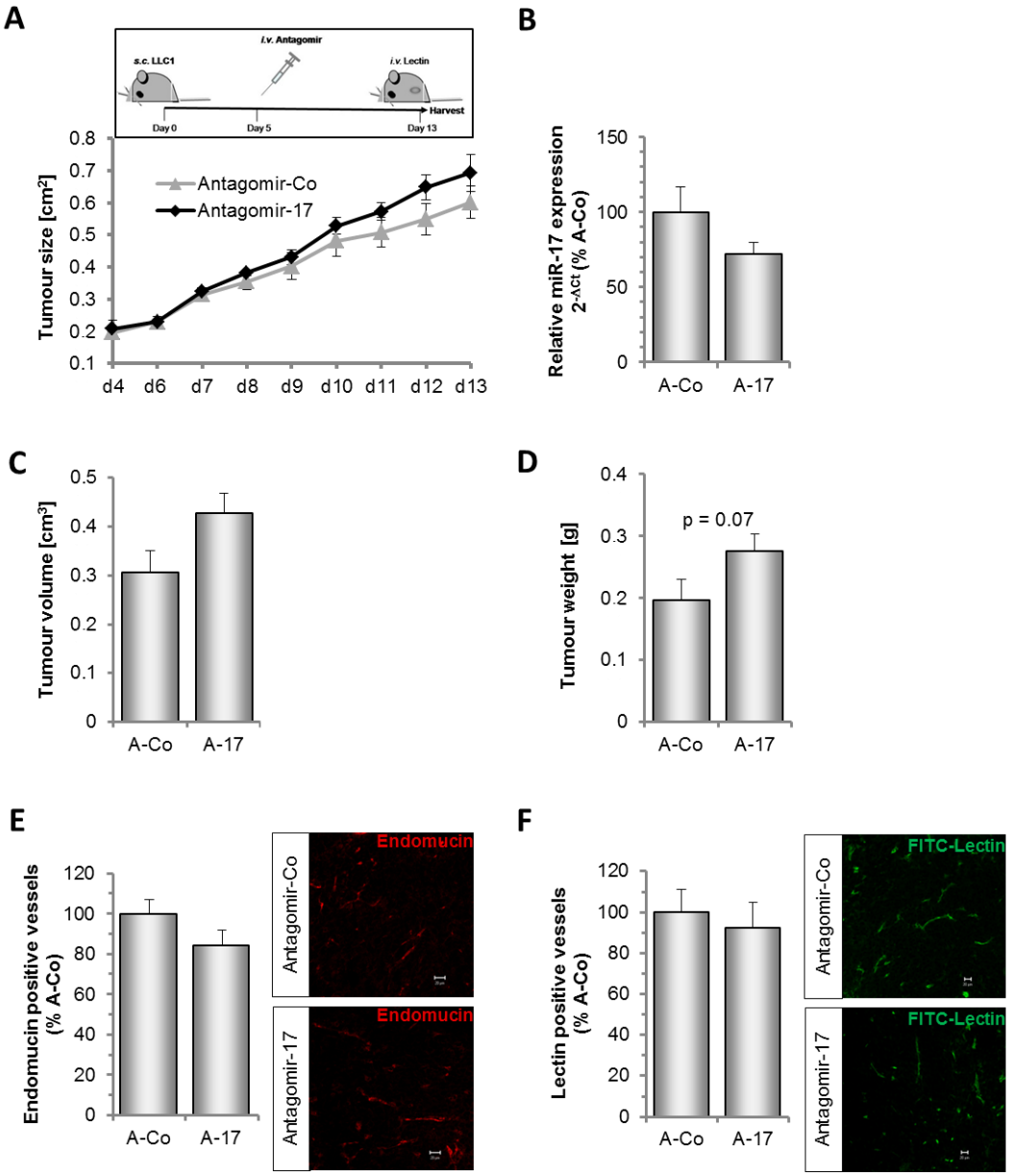

Figure IV.11: **Effect of one injection of Antagomir-17 on tumour growth and angiogenesis. (A)** Schematic drawing of experiment design. LLC1 cells were subcutaneously injected at day 0 and mice were treated once with Antagomir-17 (8 mg/kg bw i.v.) at day 5. Tumours were harvested at day 13. n = 7 for Antagomir-Co and n = 6 for Antagomir-17. Analysis of tumour size, volume and weight was done by Ariane Fischer. Immunostainings were performed and evaluated by Marion Muhly-Reinholz. **(B)** Expression of miR-17 in LLC1-derived tumours after 1 i.v. injection of Antagomir at day 5. Total RNA was isolated using TRI Reagent from slices of paraffin embedded tumours as described in the method section. MiR-17 expression was detected by a real-time PCR method previously described by Wu et al. [1]. **(C)** Volume of explanted tumours. 3D tumour volume was calculated by multiplying the three orthogonal diameter measurements (d_1 x d_2 x d_3). **(D)** Weight of explanted tumours. **(E)** Tumour angiogenesis was detected in sections stained with the endothelial marker endomucin. A secondary antibody conjugated to Alexa Fluor 555 was used. The number of vessels was counted manually. **(F)** Perfused vessels were detected by intravenous infusion of fluorescein isothiocyanate (FITC)-conjugated lectin and were quantified by automatic measurement of the pixel region in each section. Scale bars represent 20 µm.

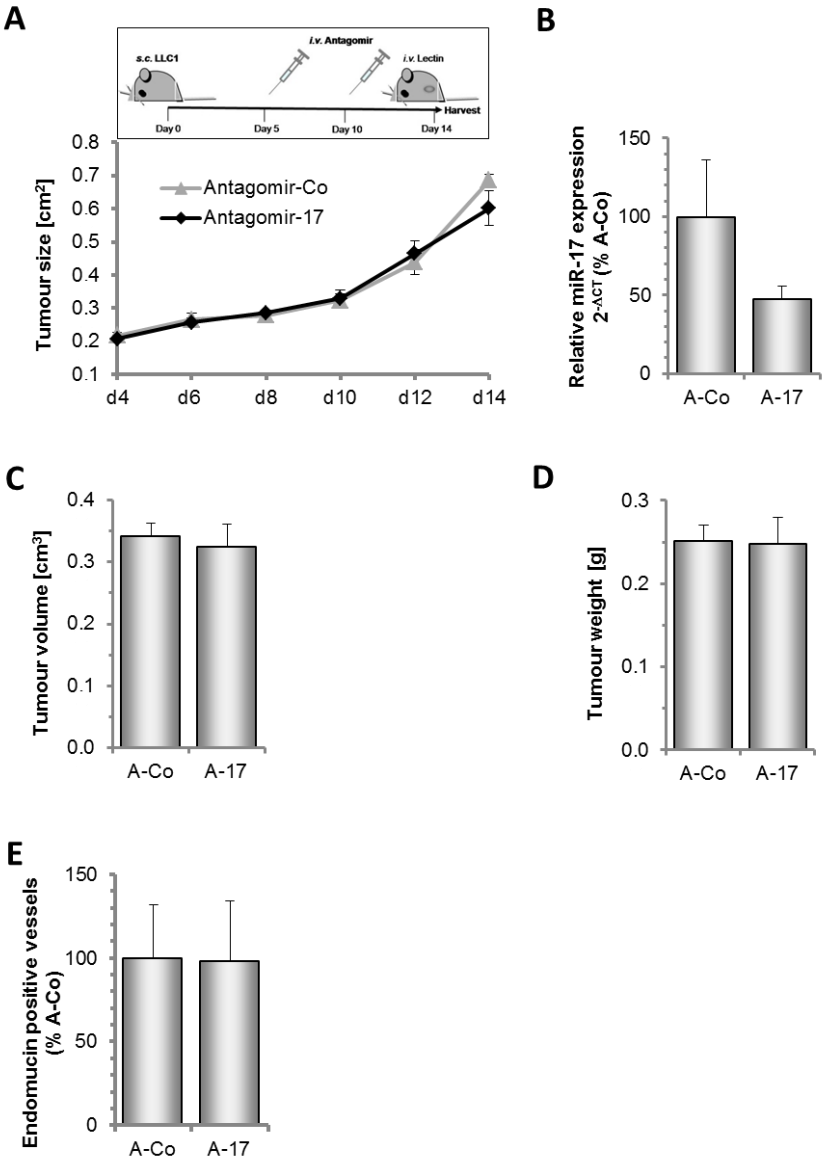

Figure IV.12: **Effect of two injections of Antagomir-17 on tumour growth and angiogenesis. (A)** Schematic drawing of experiment design. LLC1 cells were subcutaneously injected at day 0 and mice were treated with Antagomir-17 (8 mg/kg bw i.v.) at days 5 and 10. Tumours were harvested at day 14. Analysis of tumour size, volume and weight was mainly done by Ariane Fischer. Immunostainings were performed and evaluated by Marion Muhly-Reinholz. n = 6 for Antagomir-Co, n = 5 for Antagomir-17. **(B)** Expression of miR-17 in LLC1-derived tumours after two i.v. injections of Antagomir-17 at day 5 and 10. Total RNA was isolated using TRI Reagent from a piece of tumour that was removed during the tumour harvest. MiR-17 expression was detected by a real-time PCR method published by Wu et al. [1]. **(C)** Volume of explanted tumours. 3D tumour volume was calculated by multiplying the three orthogonal diameter measurements (d_1 x d_2 x d_3). **(D)** Weight of explanted tumours. **(E)** Tumour angiogenesis was detected in sections stained with the endothelial marker endomucin. A secondary antibody conjugated to Alexa Fluor 555 was used. The number of vessels was quantified by automatic measurement of the pixel region in each section.

Consistently, blocking miR-17 by treatment of LLC1 cells in vitro with different concentrations of Antagomir-17 did not affect proliferation of these cells as determined by FACS measurement of BrdU incorporation, although miR-17 expression was efficiently decreased in the cells treated with 2.5 µM A-17 (Fig. IV.13A/B).

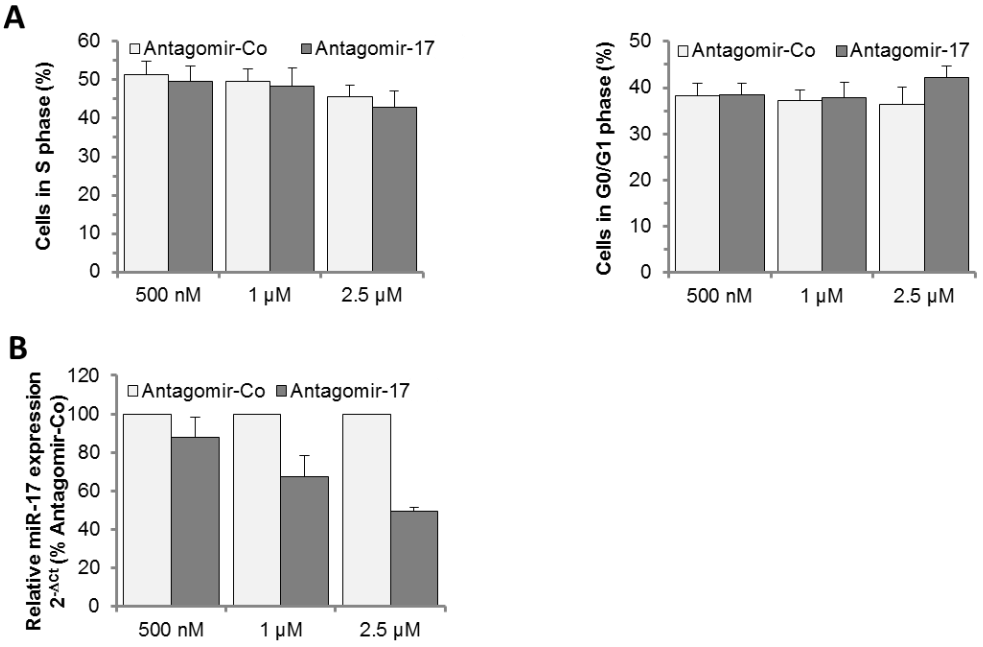

Figure IV.13: **Effect of Antagomir-17 on LLC1 proliferation and miR-17 expression in vitro.** LLC1 cells were treated with different concentrations of Antagomir-17 as indicated. **(A)** 48 h after Antagomir addition, cell cycle activity was quantified by FACS analysis of anti-BrdU-FITC/7-AAD stained cells. **(B)** Quantification of miR-17 knockdown. Total RNA was isolated with TRI Reagent 48 h after Antagomir addition. MiR-17 expression was detected by a real-time PCR method using a universal TaqMan probe in combination with a miR specific forward primer as previously described by Wu et al. [1]. SnoRNA202 was used as endogenous control. n = 3.

4. Targets of the members of the microRNA-17-92 cluster in endothelial cells

a) The pro-apoptotic protein BIM is no relevant target of the miR-17-92 cluster in ECs

Several reports identified known regulators of cell cycle progression and apoptosis to be targets of the members of the miR-17-92 cluster in tumour and hematopoetic cells. Among others, the pro-apoptotic protein BIM (BCL2L11) is a described target of the miR-17-92 cluster, which controls apoptosis of lymphocytes and tumour cells [140, 157]. To test whether the members of the miR-17-92 cluster regulate BIM expression in endothelial cells, we overexpressed the individual members by precursor transfection and analysed protein cell lysates for BIM expression by Western blotting. Only miR-20a significantly downregulated BIM protein level, whereas miR-17, -18a and -19a only marginally decreased its expression (Fig. IV.14). Since the members of the miR-17-92 cluster only slightly affected BIM expression and did not promote cell survival as shown in Fig. IV.3, BIM seems not to be a functionally relevant target of the miR-17-92 cluster in endothelial cells.

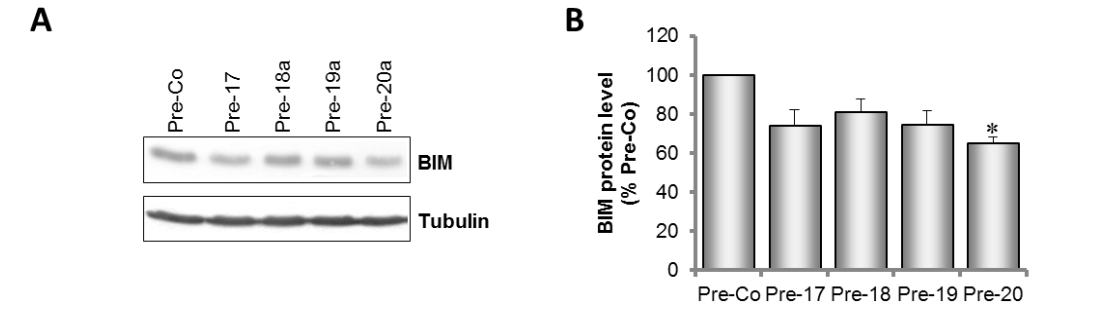

Figure IV.14: **Effect of members of the miR-17-92 cluster on BIM expression. (A)** Expression of the pro-apoptotic protein BIM in HUVECs 48 h after transfection with precursors for the indicated miRs. A representative Western blot is shown. **(B)** Summarized quantification of BIM protein expression of n = 3 experiments. Tubulin was used to normalize BIM expression.

b) Identification of targets of miR-17 in endothelial cells

Among the members of the miR-17-92 cluster investigated in this study, miR-17 was most effective in regulating angiogenesis in vitro and in vivo. Analysis of the miR-17 expression pattern in different cell types of the cardiovascular system revealed ubiquitous expression of miR-17 in mouse cardiomyocytes, the non-cardiomyocyte fraction of murine hearts and murine lung endothelial cells (Fig. IV.15A) as well as the endothelial cell line EA.hy.926, human microvascular endothelial cells (HMVEC) and HUVECs of different passages (Fig. IV.15B).

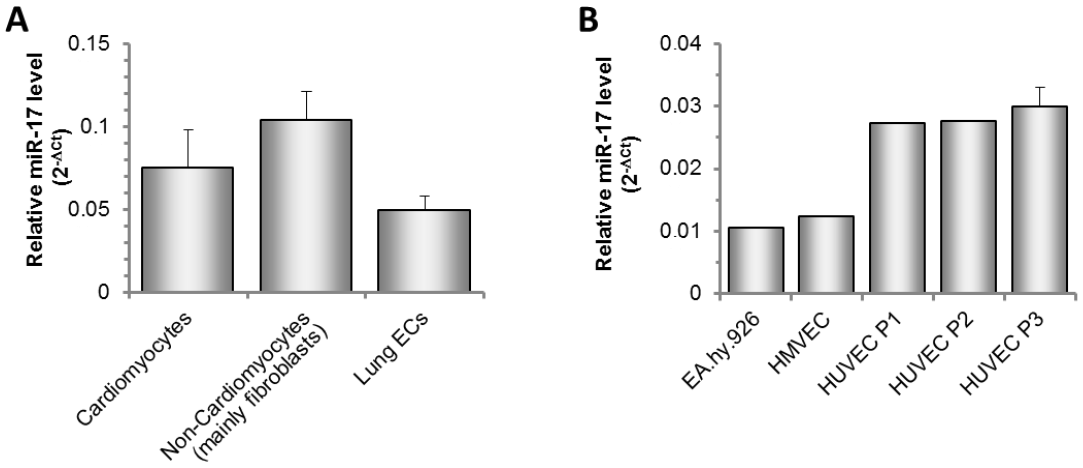

Figure IV.15: **MiR-17 is expressed in endothelial cells of different origin. (A)** MiR-17 expression in murine cardiomyocytes, the non-cardiomyocyte fraction of the heart and lung endothelial cells (ECs). RNA of freshly isolated cardiomyocytes (n = 4) and the non-cardiomyocyte fraction of mouse hearts was provided by Dr. A. Bonauer. The non-cardiomyocyte fraction (n = 3) comprised the cells that were adherent after 1.5 h of pre-plating (of the cardiomyocyte supernatant) and predominantly consisted of fibroblasts but also cardiac endothelial cells. RNA of cultured murine lung ECs (n = 5) was provided by Dr. C. Urbich. MiR-17 expression was measured using the respective MicroRNA Assay kit (Applied Biosystems). SnoRNA202 was used as endogenous control. **(B)** MiR-17 expression in the human endothelial Ea.hy.926 cell line, human microvascular endothelial cells (HMVEC) and human umbilical vein endothelial cells (HUVEC) of different passages (P1-P3).The different endothelial cell types were cultured as described in the method section. Total RNA was isolated using TRI Reagent and miR expression was detected by a real-time PCR method using a universal TaqMan probe in combination with a miR specific forward primer as previously described by Wu et al. [1]. RNU48 was used as endogenous control. n = 1 for EA.hy.926, HMVEC, HUVEC P1, HUVEC P2; n = 3 for HUVEC P3.

Moreover, we were interested in identifying targets of miR-17 relevant for the profound anti-angiogenic activity observed in endothelial cells in vitro. For this purpose, we overexpressed

miR-17 in HUVECs by precursor transfection for 24 h, isolated total RNA from these and the control precursor transfected cells. RNA of three independent experiments was analyzed using oligonucleotide based microarrays. With this method, we were able to analyse the relative expression levels of approximately 47,000 transcripts corresponding to more than 38,500 human genes. To find primarily direct targets of miR-17, we matched the downregulated genes with miR-17 targets that were predicted by the targetscan algorithm. Among these, several validated miR-17 targets appeared like the transforming growth factor receptor beta II (TGFBR2), the cell cycle regulator cyclin-dependent kinase inhibitor 1A (CDKN1A, p21), polycystic kidney disease 2 (PKD2), the E2F transcription factor 1 (E2F1), the nuclear receptor coactivator 3 (NCOA3), Cyclin D1 (CCND1) and the hypoxia inducible factor 1α (HIF1A). Predicted but not yet validated miR-17 targets downregulated in our microarray and potentially involved in angiogenesis were the sphingosine-1-phosphate receptor 1 (S1PR1, EDG1), platelet derived growth factor D (PDGFD), tumour necrosis factor alpha-induced protein 1 (TNFAIP1), and the protein Janus kinase 1 (JAK1), of which the latter was more than two fold downregulated (Table IV.1).

Symbol	Product	Genbank	Affymetrix	fold change (pre-17/pre-Co)	p-value
FYCO1	FYVE and coiled-coil domain containing 1	NM_024513	218204_s_at	0.284	0.0426
JAK1	Janus kinase 1	AL039831	201648_at	0.382	0.0040
PLEKHA3	pleckstrin homology domain containing, family A (phosphoinositide binding specific) member 3	BE550332 AF286162 BE550332	227659_at 223370_at 227658_s_at	0.458	0.0002
TGFBR2	transforming growth factor, beta receptor II (70/80kDa)	D50683 NM_003242	208944_at 207334_s_at	0.477	0.0460
EIF2C1	eukaryotic translation initiation factor 2C, 1	AW071829 NM_012199	222576_s_at 218287_s_at	0.493	0.0010
TNFAIP1	tumour necrosis factor, alpha-induced protein 1 (endothelial)	BC001643 NM_021137	201208_s_at 201207_at	0.509	0.0013
PDGFD	platelet derived growth factor D	NM_025208	219304_s_at	0.533	0.0384
PKD2	polycystic kidney disease 2 (autosomal dominant)	NM_000297	203688_at	0.555	0.0434
S1PR1	sphingosine-1-phosphate receptor 1	NM_001400	204642_at	0.556	0.0513
CDKN1A	cyclin-dependent kinase inhibitor 1A (p21, Cip1)	NM_000389	202284_s_at	0.565	0.0238
ZFYVE26	zinc finger, FYVE domain containing 26	AB002319 AB002319	37943_at 213073_at	0.631	0.0196
RBL2	retinoblastoma-like 2 (p130)	NM_005611	212332_at 212331_at	0.638	0.0182
E2F1	E2F transcription factor 1	NM_005225 M96577	204947_at 2028_s_at	0.659	0.0294
DYNC1LI2	dynein, cytoplasmic 1, light intermediate chain 2	NM_006141	203590_at	0.674	0.0718
FAM129A	family with sequence similarity 129, member A	AF288391 NM_022083	217967_s_at 217966_s_at	0.688	0.0003
NCOA3	nuclear receptor coactivator 3	AL034418 AF012108 NM_006534 AF012108 U80737	233555_s_at 209060_x_at 207700_s_at 209061_at 211352_s_at	0.690	0.0002
CYBRD1	cytochrome b reductase 1	AL136693 NM_024843	222453_at 217889_s_at	0.692	0.1230
CCND1	cyclin D1	M73554 BC000076	208712_at 208711_s_at	0.696	0.0094

Symbol	Product	Genbank	Affymetrix	fold change (pre-17/pre-Co)	p-value
FNDC3A	fibronectin type III domain containing 3A	NM_014923	202304_at	0.708	0.0830
HIF1A	hypoxia inducible factor 1, alpha subunit	NM_001530	200989_at	0.756	0.0188
VASP	vasodilator-stimulated phosphoprotein	NM_003370	202205_at	0.761	0.1107
ZNF264	zinc finger protein 264	NM_003417	205917_at	0.808	0.0031
BCL2L11	BCL2-like 11 (apoptosis facilitator)	AA629050	222343_at	0.812	0.4465
RUFY2	RUN and FYVE domain containing 2	NM_017987 AB040970 AB040970	219957_at 233192_s_at 233191_at	0.822	0.0290
EPHA4	EPH receptor A4	NM_004438	206114_at	0.828	0.0210
EIF5A2	eukaryotic translation initiation factor 5A2	NM_020390 AF262027	220198_s_at 223598_at	0.938	0.5513
FN1	fibronectin 1	BC005858 X02761 AJ276395 AK026737 AF130095 AJ276395	211719_x_at 212464_s_at 214702_at 216442_x_at 210495_x_at 214701_s_at	0.961	0.1770
BMPR2	bone morphogenetic protein receptor, type II (serine/threonine kinase)	BF247383	238516_at	1.012	0.5036
ITGB8	integrin, beta 8	BC002630 BF513121	211488_s_at 226189_at	1.020	0.7805
RUNX1	runt-related transcription factor 1	NM_001754 D43968 D43967	208129_x_at 209360_s_at 210365_at	1.020	0.9333
PTEN	phosphatase and tensin homolog	U96180 NM_000314	204053_x_at 204054_at	1.082	0.5734
MAPK9	mitogen-activated protein kinase 9	AI808345 U35002 W37431	225781_at 210570_x_at 203218_at	1.090	0.4463
KAT2B	K (lysine) acetyltransferase 2B, PCAF	AV727449	203845_at	1.116	0.8439
STAT3	signal transducer and activator of transcription 3	BC000627 AA634272	208992_s_at 208991_at	1.209	0.0082
MAPK14	mitogen-activated protein kinase 14	NM_001315 L35253 AF100544	202530_at 211561_x_at 210449_x_at	1.474	0.0007

Table IV.1: Affymetrix microarray gene expression analysis after miR-17 overexpression – effect on selected predicted targets. HUVECs were transfected with 10 nM Pre-17 or a control precursor (Pre-Co) and after 24 h total RNA was isolated. Gene expression was analysed with Affymetrix 3' Gene Expression Analysis Arrays. Predicted targets that have been validated in previous publications are shaded in grey. In case of 2 or more probes for one gene the mean fold change was calculated. n = 3.

c) MiR-17 does not affect matrix metalloproteinase activity in endothelial cells

Angiogenesis is an invasive process involving proteolysis of the extracellular matrix. The enzyme family of matrix metalloproteinases (MMPs) comprises extracellular endopeptidases that degrade specific ECM components and participate in the angiogenic response. MMP-1, MMP-2, MMP-9, and the membrane inserted MT-1-MMP are reported to be expressed in endothelial cells of which MMP-2 and MT-1-MMP are primarily investigated for their involvement in angiogenesis [197]. Consistently, all these MMPs were found to be expressed on the mRNA level in our microarray. Two members of the MMP family are predicted to be miR-17 targets by the Targetscan algorithm, namely the membrane inserted MMP24 (MT5-MMP) and MMP2.

Consistent with the literature stating that MMP24 is brain specific [198], MMP24 mRNA was not expressed in HUVECs according to the microarray. In contrast, MMP2 mRNA was expressed in HUVECs and slightly but nonsignificantly downregulated after miR-17 overexpression (Fig. IV.16).

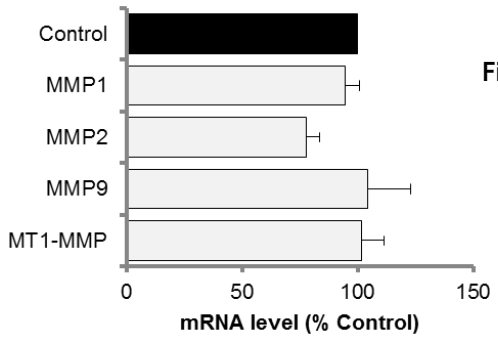

Figure IV.16: **Effect of miR-17 on transcript levels of endothelial matrix metalloproteinases.** HUVECs were transfected with 10 nM Pre-17 or Pre-Co and after 24 h total RNA was isolated. Gene expression was analyzed with Affymetrix 3' Gene Expression Analysis Arrays. In case of 2 or more probes for one gene the mean fold change was calculated. n = 3.

To investigate whether microRNA-17 affects MMP expression, we decided to perform gelatin zymography after overexpression and Antagomir-mediated inhibition of miR-17 in HUVECs to test for MMP enzyme activity.

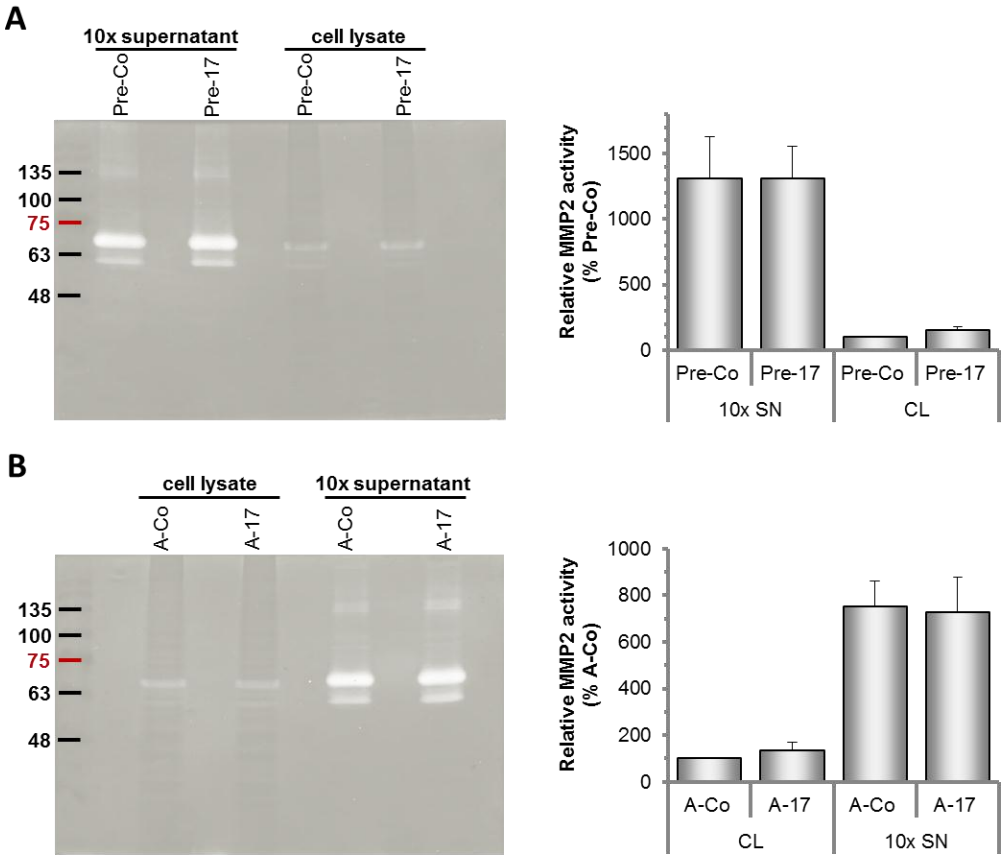

Figure IV.17: **MiR-17 does not affect proteolytic activity of MMP2.** HUVECs were transfected with 10 nM control and miR-17 precursor molecules **(A)** or treated with 2.5 µM control and miR-17 Antagomir **(B)**. Medium was changed to serum-free medium after 48 h for 24 h. 10x concentrates of cell supernatants were generated by centrifugation using centrifugal filter units and equal volumes were loaded onto the gel. Cells were lysed in JNK buffer and equal amounts of protein (50 µg) were analysed on the gel. CL: cell lysate, SN: supernatant. Representative zymographies and the quantification of MMP2 activity of three independent experiments are shown.

Since MMP2 is secreted by endothelial cells, we analysed 10x concentrates of the cell supernatant as well as cell lysates. Three bands appeared around the 63 kD marker band that probably result from a latent (pro-form, ~ 68 kD), an intermediate (~ 64 kD) and an active (~ 62 kD) form of MMP2 (Fig. IV.17). Nevertheless, we could not detect any major differences in MMP2 activity using gelatin, neither upon miR-17 overexpression nor after miR-17 inhibition.

d) MiR-17-mediated repression of p21 expression influences endothelial cell function in angiogenesis in vitro

As mentioned before, endothelial cell proliferation plays an important role in angiogenesis. Hence, we addressed the function of the described miR-17 target and cell cycle regulator p21 in endothelial cells (Fig. IV.18).

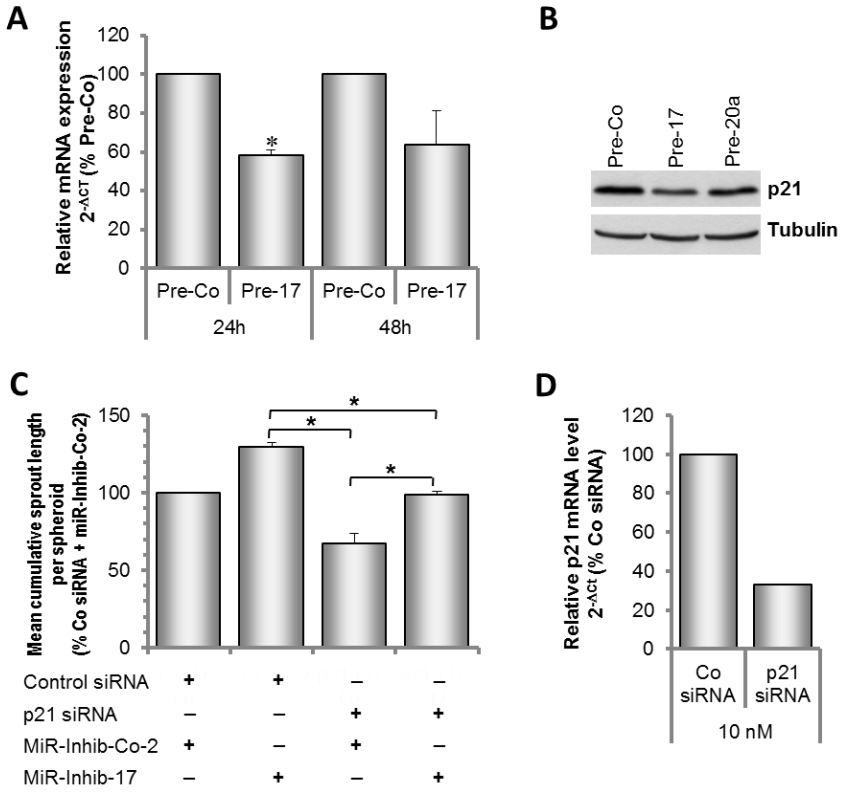

Figure IV.18: **MiR-17 regulates the cell cycle regulator p21 and proliferation of endothelial cells. (A)** MiR-17 decreases p21 mRNA expression. MiR-17 was overexpressed in HUVECs by transfection of 10 nM miR-17 precursor molecules (Pre-17). RNA was isolated with TRI Reagent 24 h and 48 h after transfection, DNase digested and reverse transcribed. cDNA was analysed for p21 mRNA expression using real-time PCR. The large ribosomal protein P0 (RPLP0) was used as endogenous control. n = 3 **(B)** MiR-17 downregulates p21 protein. Pre-17 and Pre-20a as well as control precursor (10 nM each) transfected HUVECs were lysed in RIPA buffer supplemented with protease inhibitors and protein lysates were used for p21 Western blot analysis. A representative Western blot out of 5 independent experiments is shown. Tubulin was used as endogenous control. **(C)** MiR-17 inhibition rescues the impaired angiogenic sprouting of p21 depleted HUVECs. HUVECs were transfected with p21 siRNA (10 nM), miR-17 inhibitor (50 nM), and the respective controls as indicated. Spheroids were generated and sprouting was quantified. n = 3. **P* < 0.05. **(D)** Confirmation of p21 mRNA knockdown in siRNA transfected HUVEC. 24 h after transfection RNA was isolated, DNase digested, reverse transcribed and assayed for p21 mRNA expression via real-time PCR. p21 mRNA levels were normalized to RPLP0. n = 1.

To confirm the inhibitory effect of miR-17 on p21 expression, real time PCR was used to determine p21 mRNA levels 24 h and 48 h after precursor transfection. Indeed, p21 mRNA was almost twofold decreased at the first time point measured (Fig. IV.18A). Furthermore, a reduction of p21 protein could be observed in miR-17 overexpressing HUVECs (Fig. IV.18B). To ascertain that p21 represents a miR-17 target in angiogenesis in vitro, we co-transfected HUVECs with an inhibitor against miR-17 and p21 siRNA as well as the corresponding oligonucleotide controls and used the cells in the 3D spheroid sprouting assay. As observed previously, blocking miR-17 increased the angiogenic response of ECs, whereas a modest knockdown of p21 slightly decreased sprouting of spheroids, an effect that could be partially rescued by concomitant miR-17 inhibition (Fig. IV.18C/D). In context with the altered cell cycle profile observed after miR-17 overexpression in HUVECs, these results suggest that miR-17 impairs in vitro angiogenesis at least to some extent by affecting p21-mediated regulation of EC proliferation.

e) MiR-17 does not affect chemotaxis of endothelial cells in response to sphingosine-1-phosphate

The sphingosine-1-phosphate receptor 1 (S1PR1) is a member of the endothelial differentiation gene (Edg) family of G protein-coupled receptors and was originally found to be highly induced in endothelial cells undergoing differentiation [199]. Furthermore, Edg-1 knockout mice die before birth due to severe vascular defects [200]. In general, Edg receptors initiate diverse cellular events upon sphingolipid metabolite stimulation like migration, morphogenesis, proliferation, and survival [201]. To check if the miR-17-mediated downregulation of Edg-1 observed in the microarray affects the response of HUVECs towards its ligand sphingosine-1-phosphate (S1P), we analysed the S1P stimulated migration of precursor transfected ECs in a Boyden chamber assay (Fig. IV.19).

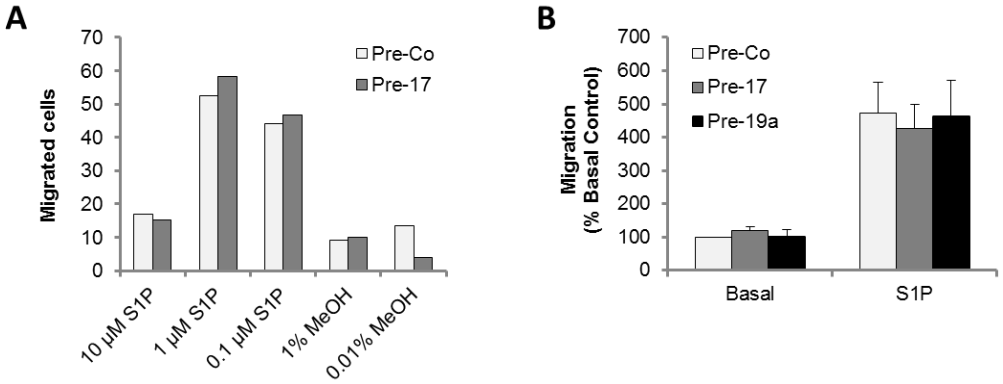

Figure IV.19: **Effect on sphingosin-1-phosphate (S1P)-induced endothelial cell migration. (A)** Dose dependent effect of S1P on endothelial cell migration. Methanol (MeOH) served as solvent control. The graph shows for each condition the mean value of 5 visual fields. n = 1. **(B)** Effect of overexpression of miR-17 and miR-19a on S1P (1 µM) induced migration in a collagen I coated boyden chamber. Experiments were done 48 h after transfection and cells were allowed to migrate for 4 h. n = 5.

In a dose-response experiment with 10 µM, 1 µM and 0.1 µM S1P, we observed a dose dependent regulation of EC migration towards the sphingolipid stimulus with a maximal effect at a concentration of 1 µM S1P (Fig. IV.19A). Nevertheless, overexpression of miR-17 and miR-19a, which also was predicted to target Edg-1, did not alter the chemotaxis and migratory capacity of ECs towards S1P (Fig. IV.19B). These results implicate that the miR-17-mediated decrease of Edg-1 may not be sufficient to disturb S1P signalling in endothelial cells.

f) Janus kinase 1 (JAK1) is a novel direct target of miR-17 in endothelial cells

The Janus kinase family of intracellular, non-receptor associated tyrosine kinases transduce signals from a plethora of cytokines to the nucleus mainly via phosphorylation and activation of the signal transducers and activators of transcription (STATs). In general, the JAK/STAT pathway is composed of the four Janus kinases JAK1, JAK2, JAK3 and TYK2 and the seven STAT transcription factors STAT1, STAT2, STAT3, STAT4, STAT5a, STAT5b and STAT6. According to the microarray, the transcripts of JAK1, JAK2 and TYK2 as well as STAT1, STAT3, STAT5b and STAT6 were expressed in HUVECs. JAK1 and TYK2 mRNA were both significantly reduced upon miR-17 overexpression in the microarray, but compared to the profound effect on the JAK1 transcript, expression of TYK2 was only marginally affected (Fig. IV.20).

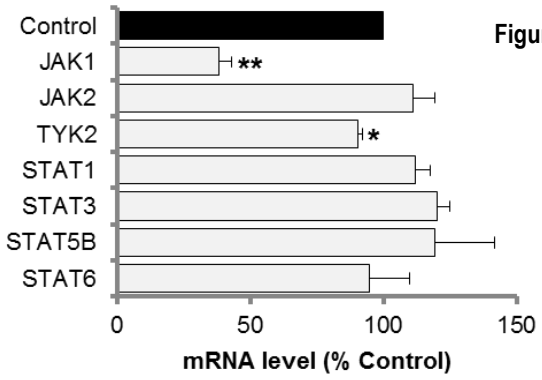

Figure IV.20: **Effect of miR-17 on transcript level of components of the JAK/STAT pathway.** HUVECs were transfected with 10 nM Pre-17 or a control pre-miR and after 24 h total RNA was isolated. Gene expression was analyzed with Affymetrix 3' Gene Expression Analysis Arrays. In case of 2 or more probes for one gene the mean fold change was calculated. n = 3. **P* < 0.05, ***P* < 0.01.

JAK1 knockout mice suffered from severely impaired lymphocytic development, died shortly after birth and analysis of different cell types isolated from JAK1$^{-/-}$ mice revealed impaired biological responses of three major cytokine receptor subfamilies, namely the class II cytokine receptors, γ_c subunit utilizing cytokine receptors and gp130 associated receptors [202]. So far, little is known about the specific function of JAK1 in the angiogenic response of endothelial cells.

Overexpression of the individual members of the miR-17-92 cluster and the non-related miR-126 resulted in specific downregulation of JAK1 protein in endothelial cells overexpressing miR-17 and the related cluster member miR-20a (Fig. IV.21A/B). Moreover, inhibition of miR-17 increased JAK1 protein level (Fig. IV.21C). In order to verify a direct regulatory effect of miR-17 on JAK1 expression, the miR-17 binding site in the JAK1 3´ UTR was cloned in four replicates in the

3´ UTR of a luciferase reporter gene and luciferase activity was measured after miR precursor transfection. A construct in which four nucleotides of the miR-17 binding site were mutated was used as a control. Overexpression of miR-17 decreased luciferase activity of the construct with the wild type binding sequence but not of the plasmid with the mutated binding sites indicating that the JAK1 3´ UTR indeed contains a functional miR-17 binding site (Fig. IV.21D).

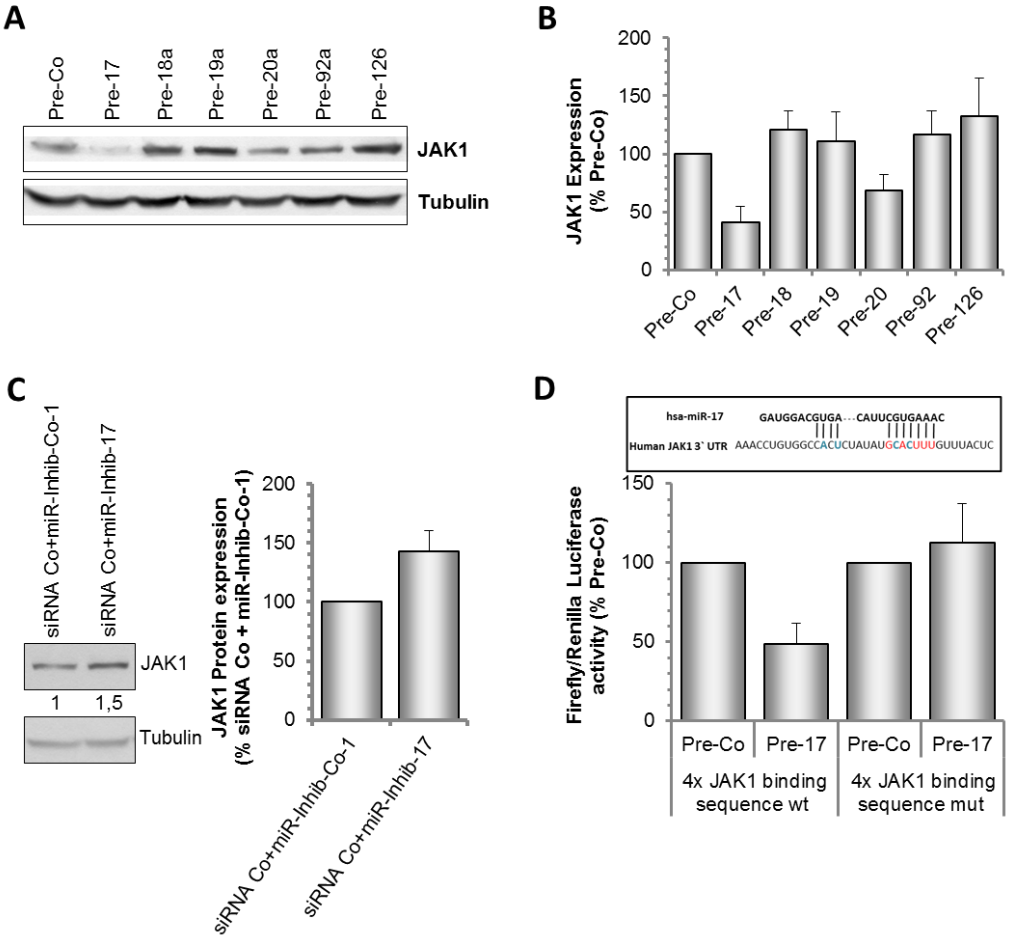

Figure IV.21: **JAK1 is a novel target of miR-17 in endothelial cells. (A/B)** MiR-17 and miR-20a downregulate JAK1 protein expression in endothelial cells. Precursor transfected HUVECs were lysed with RIPA buffer supplemented with protease inhibitors 48 h after transfection and proteins were probed for JAK1 using Western blot analysis. Tubulin served as endogenous control. A representative Western blot is shown in (A) and the quantification of n = 4 experiments in (B). **(C)** HUVECs were transfected with a combination of control siRNA (40 nM) and control miR inhibitor (50 nM) or control siRNA (40 nM) and miR-17 inhibitor (50 nM). 72 h after transfection cells were lysed in RIPA buffer and the extracted proteins were probed for Jak1 by Western blotting. Tubulin was used as loading control. The blots were densiometrically analysed using Scion Image. JAK1 protein levels were normalized to Tubulin expression. The graph shows the results of 3 independent experiments. A representative blot is shown. **(D)** JAK1 is a direct target of miR-17. Four copies of the miR-17 binding sequence found in the 3´ UTR of JAK1 were cloned downstream of a Firefly luciferase reporter gene and co-transfected with control or miR-17 precursor molecules into HEK cells. 48 h after transfection Firefly luciferase normalized to Renilla luciferase activity was measured in HEK cell homogenates. A mutated luciferase construct (mutations were applied to nucleotides written in blue) was used as negative control. wt: wildtype, mut: mutated. n = 4.

To address the function of JAK1 in endothelial cells, we used a specific siRNA to silence its expression and analysed the cells regarding their sprouting capacity in the 3D spheroid assay as

well as the downstream signalling in response to different cytokines and growth factors based on STAT3 phosphorylation. Indeed, silencing of JAK1 impaired angiogenic sprouting of spheroids (Fig. IV.22A) and suppressed phosphorylation of STAT3 in untreated as well as cytokine stimulated HUVECs (Fig. IV.22B).

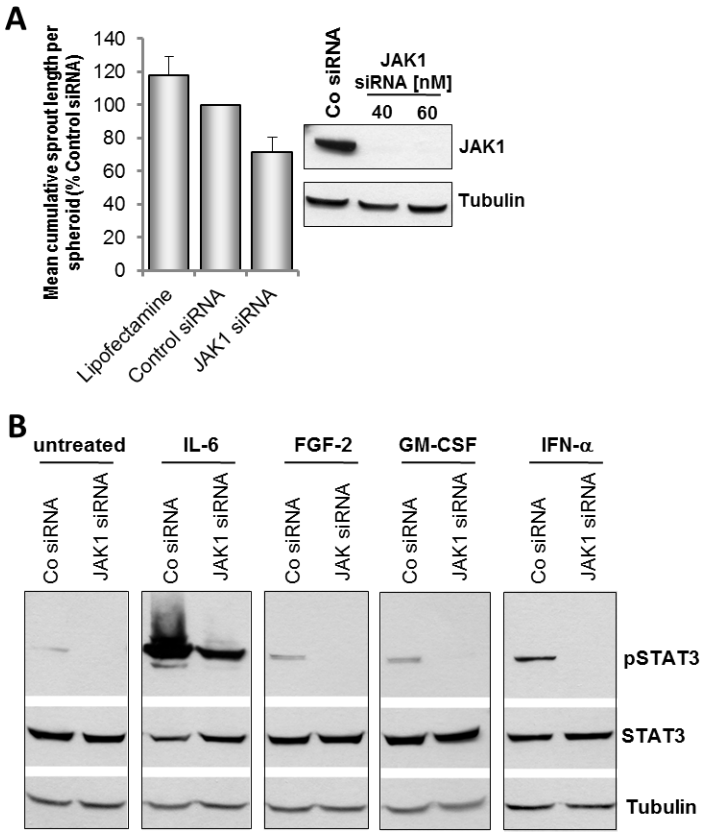

Figure IV.22: **JAK1 depletion impairs spheroid sprouting and phosphorylation of STAT3 in response to different cytokines. (A)** Effect of JAK1 silencing using 40 nM siRNA on spheroid sprouting. A siRNA directed against firefly luciferase or cells treated with the transfection reagent was used as control. n = 5-6. Downregulation of JAK1 protein 48 h after siRNA transfection is shown in the Western blot. Tubulin served as loading control. n = 1. **(B)** HUVECs were transfected with 40 nM JAK1 siRNA or control siRNA. After incubation of 9 h in serum-free medium supplemented with 0.05% BSA, cells were stimulated with IL-6 (100 ng/ml), FGF-2 (30 ng/ml), IFN-α (100 ng/ml), or GM-CSF (100 ng/ml) for 15 min. STAT3 phosphorylation (pSTAT3) was detected by Western blot analysis. Tubulin was used as loading control. Representative blots are shown.

To validate that JAK1 actually represents a downstream target of miR-17 in these cellular processes we transfected HUVECs with combinations of a miR-17 inhibitor and JAK1 siRNA or the respective control oligonucleotides. In fact, silencing of JAK1 prevented the pro-angiogenic effect (Fig. IV.23A) mediated by the miR-17 inhibitor and suppressed enhanced STAT3 phosphorylation (Fig. IV.23B/C). In summary, we identified JAK1 as a novel target of miR-17 in endothelial cells which is involved in angiogenesis in vitro as well as signal transduction in response to some cytokines and growth factors.

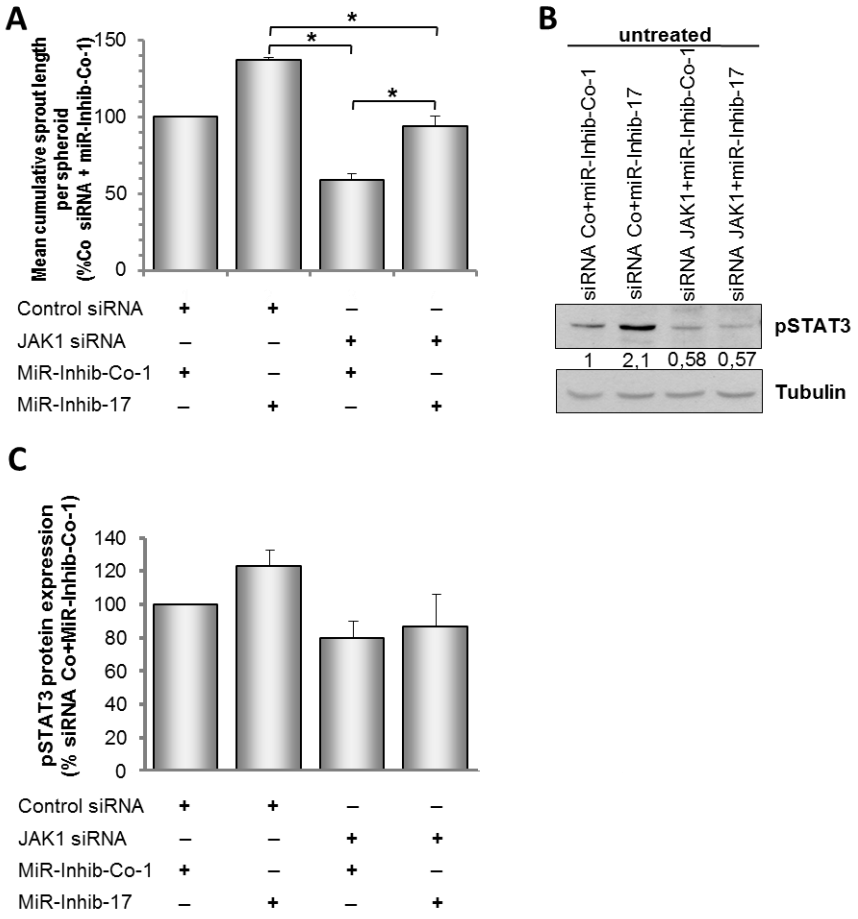

Figure IV.23: **JAK1 siRNA reduces the pro-angiogenic effect of miR-17 inhibition.** HUVECs were transfected with JAK1 siRNA (40 nM), miR-17 inhibitor (50 nM), and the respective controls as indicated. **(A)** Spheroids were generated and sprouting was quantified; n = 3. **P* < 0.05. **(B/C)** 40 h or 64 h after transfection cells were kept in serum-free medium for further 8 h. Thereafter, cells were left untreated or stimulated with 100 ng/ml IFN-α for 15 min. Cell lysates were probed for STAT3 phosphorylation by Western blot analysis. Tubulin was used as loading control. The blots were densitometrically analysed using Scion Image. Phospho-STAT3 (pSTAT3) levels were normalized to tubulin expression. The representative blot of three independent experiments in (A) shows the phosphorylation of STAT3 in untreated cells 48 h after transfection. The graph in (C) summarizes the results of three independent experiments with IFN-α stimulated cells 72 h after transfection.

B. Applicability of microRNA inhibition as therapeutic approach for pulmonary arterial hypertension

Pulmonary arterial hypertension (PAH) is a disorder of the lung vasculature associated with pulmonary vasoconstriction and extensive vascular remodelling leading to hypertrophy of the right ventricle and ultimately right heart failure. In 2010, Caruso et al. demonstrated that among others members of the miR-17-92 cluster and miR-21 are dysregulated in two classical rat models of pulmonary arterial hypertension in a time-dependent manner [203]. Since miR-17 and miR-92a exerted the most impressive effects on the vascular system in this and a previously published study [119], and both were shown to be upregulated in the lungs of diseased animals, we evaluated the impact of systemic miR-17 and miR-92a inhibition by the corresponding Antagomirs in

experimental pulmonary arterial hypertension. The project was done in collaboration with the group of Dr. Ralph Schermuly from the University of Gießen Lung Centre who provided the expertise in two animal models of pulmonary arterial hypertension, namely hypoxia-induced PAH in mice and the monocrotaline injury model in rats. Since right-sided heart failure is part of the disease pattern in pulmonary arterial hypertension and Thum et al. provided evidence that specific inhibition by Antagomir-21 improved cardiac function in animal models of heart failure [204], we additionally tested the effect of Antagomir-21 on functional parameters in experimental PAH.

1. Effect of miR-17, -21 and -92a inhibition on chronic hypoxia-induced pulmonary arterial hypertension in mice

To determine the efficiency of the individual Antagomirs in murine lungs, mice received one i.v. injection of 8 mg/kg body weight Antagomir-17, -21 or -92a and lungs were harvested 3 days after the injection to determine the microRNA expression level. Antagomir-17 reduced the expression of miR-17 by 41.6 ± 6.7%, Antagomir-21 the level of miR-21 by 50.1 ± 3.4%, and Antagomir-92a abolished miR-92a expression almost completely (98.6 ± 0.1%) in lung tissue of mice treated with the respective Antagomirs compared to control Antagomir treated mice (Fig. IV.24). Neither Antagomir affected the expression of the other two microRNAs. From this experiment we concluded that injecting the Antagomirs every third day is sufficient to achieve an adequate knockdown in the lung.

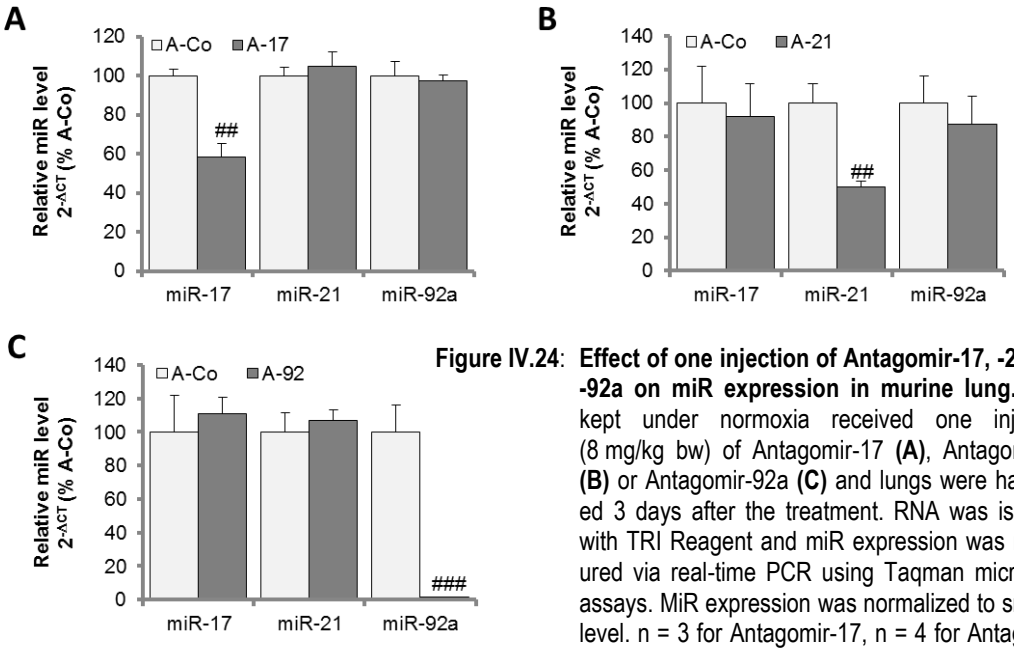

Figure IV.24: **Effect of one injection of Antagomir-17, -21 and -92a on miR expression in murine lung.** Mice kept under normoxia received one injection (8 mg/kg bw) of Antagomir-17 **(A)**, Antagomir-21 **(B)** or Antagomir-92a **(C)** and lungs were harvested 3 days after the treatment. RNA was isolated with TRI Reagent and miR expression was measured via real-time PCR using Taqman microRNA assays. MiR expression was normalized to sno202 level. n = 3 for Antagomir-17, n = 4 for Antagomir-21 and -92a. ##*P* < 0.01, ###*P* < 0.001 vs A-Co.

Mice for the chronic hypoxia-induced PAH model were exposed to hypoxia for 14 days before they were i.v. injected with a total of 5 doses (8 mg/kg bw) of Antagomir-17, -21 or -92a at inter-

vals of three days. Control animals were treated with PBS or a control Antagomir. After 27 days of hypoxia, hemodynamic and functional parameters were determined, and organs were harvested to confirm the miR knockdown. A scheme of the experimental setup is shown in Fig. IV.25A.

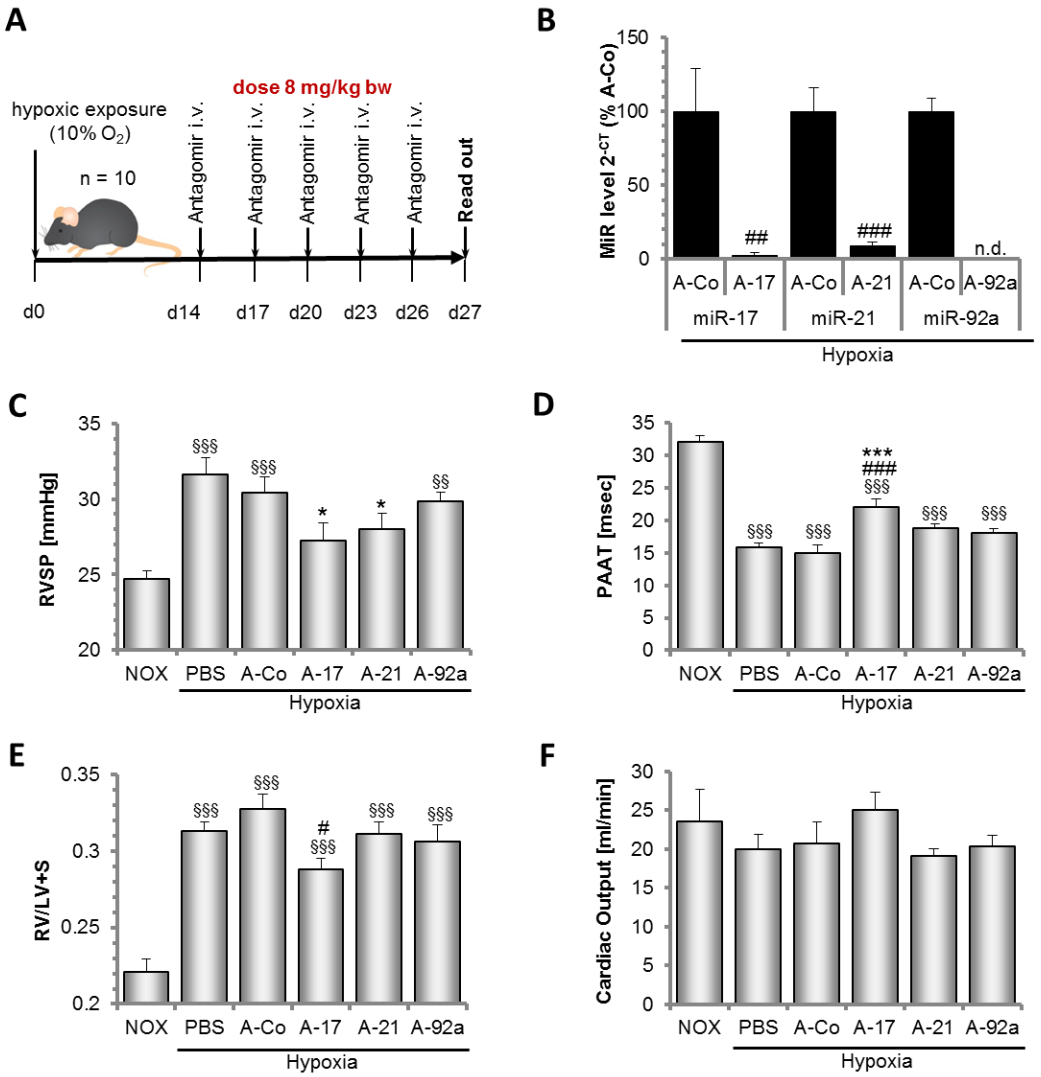

Figure IV.25: **Effects of Antagomir-17, -21 and -92a on hemodynamics and heart function in chronic hypoxic mice. (A)** Schematic drawing of experimental design. Mice were exposed to hypoxia for 2 weeks before they were treated with one injection (8 mg/kg bw) of Antagomir-17, Antagomir-21 or Antagomir-92a every third day until day 26. PBS and control Antagomir were used as controls. Hemodynamics and cardiac function were analysed at day 27. Organs were harvested to analyse miR knockdown and vascular histomorphometry in the lungs. **(B)** Knockdown efficiency of A-17, A-21 and A-92a in the liver of Antagomir-treated animals exposed to chronic hypoxia. RNA was isolated from murine liver tissue with the Qiagen miRNeasy Mini kit and miR expression was analysed using the respective TaqMan MicroRNA assays. Work was done by Ariane Fischer. n = 4-5. **(C)** Right ventricular systolic pressure (RVSP). n = 8-9. **(D)** Pulmonary artery acceleration time (PAAT). n = 4-5. **(E)** Right-heart hypertrophy estimated by calculating the weight ratio of right ventricle to left ventricle plus septum (RV/LV+S). n = 8-10 **(F)** Cardiac output (CO) measured by high-resolution echocardiography. n = 4-5. Results expressed as mean ± SEM. Experiments were done by our collaboration partners at the University of Gießen Lung Centre. n.d.: not determined. §§P < 0.01, §§§P < 0.001 vs HC, *P < 0.05 vs PBS, #P< 0.05, ## P< 0.01, ###P < 0.001 vs A-Co.

Analysis of miR-17, -21 and -92a levels by real-time PCR showed an efficient knockdown in the animals treated with the respective Antagomir (Fig. IV.25B). Analysis of hemodynamics revealed a dramatic rise in right ventricular systolic pressure (RVSP) in chronic hypoxic mice indicating that they suffered from PAH (Fig. IV.25C). Only Antagomir-17 and Antagomir-21 medicated mice showed a significant decrease in RVSP compared to the PBS controls (Fig. IV.25C) without any change in systemic arterial pressure (SAP, data not shown). Antagomir-17 was the sole Antagomir analysed that significantly improved pulmonary artery acceleration time (PAAT) as determined by high-resolution echocardiography (Fig. IV.25D). Consistently, the hypoxia-induced increase in right-sided heart hypertrophy as a consequence of impaired pulmonary hemodynamics in PAH was significantly lower in Antagomir-17 compared to control Antagomir treated mice resulting in a normalization of cardiac output (Fig. IV.25E/F). Antagomir-92a did not reveal a significant effect on any of the measured parameters. Taken together, Antagomir-17 displayed the most beneficial effect of the three tested Antagomirs on hemodynamic parameters as well as cardiopulmonary function.

2. Antagomir-17, -21 and -92a influence muscularization of the lung vasculature in chronic hypoxic mice

One hallmark of the molecular pathobiology of pulmonary arterial hypertension is an increase in muscularization of pulmonary arteries [27]. To see whether inhibition of miR-17, -21 and -92a by the corresponding Antagomirs affects the morphology of the lung vasculature, sections of murine lungs were stained for smooth muscle actin (SMA) and von Willebrand factor (vWF) to visualize the intima and media of pulmonary vessels (Fig. IV.26). In both control groups (PBS and Antagomir-Co treated) chronic hypoxia caused a dramatic rise in the fraction of non-muscularized intra-acinar arteries accompanied by a strong decline of the number of partially and fully muscularized vessels. All tested Antagomirs partially reversed the hypoxia-induced structural changes of the pulmonary vasculature. In detail, Antagomir-17 and -21 significantly decreased the number of fully muscularized and increased the fraction of non-muscularized vessels, whereas Antagomir-92a only reduced the percentage of fully muscularized arteries in a statistically significant manner. In summary, all three Antagomirs influenced vascular muscularization, although Antagomir-17, -21 and -92a significantly differed in their effects on hemodynamic and functional parameters as demonstrated before.

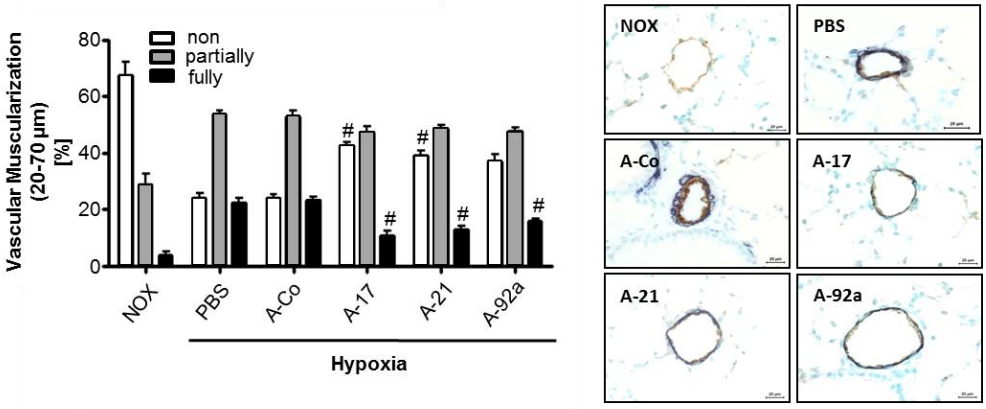

Figure IV.26: **Antagomir-17, -21 and -92a affect muscularization of pulmonary arteries.** Lung sections were immunostained for von Willebrand factor (vWF in brown indicate ECs) and α-smooth muscle actin (SMA in purple; SMCs) for morphometric analysis of pulmonary vessels. The graph shows the proportion of non-, partially or fully muscularized pulmonary arteries (sized 20-70 µm). Each bar represents mean ± SEM. n = 5. #$P < 0.05$ versus A-Co. Representative images of immunostained pulmonary arteries from normoxia (NOX) and hypoxic mice treated with PBS, Antagomir control (A-Co), Antagomir-17 (A-17), -21 (A-21) and -92a (A-92a) are shown. Scale bar: 20 µm. Analysis of pulmonary vasculature was performed by our collaboration partners at the University of Gießen Lung Centre.

3. Antagomir-17 benefits cardiopulmonary function in monocrotaline-induced PAH in rats

Since Antagomir-17 had the most favorable effect on hypoxia-induced PAH in mice, we addressed its therapeutic benefit in a second animal model, namely the monocrotaline-induced PAH in rats. To initiate the disease, rats were subcutaneously injected with 60 mg/kg bw monocrotaline. Antagomir treatment was started at day 22 by i.v. injection of 5 mg/kg bw followed by a second Antagomir administration at day 29. Hemodynamics and functional parameters were measured at day 34/35. Animals were sacrificed afterwards to harvest the organs. A scheme of the experimental setup is shown in Fig. IV.27A.

Although we had reduced the dose and frequency of Antagomir injections compared to the mouse model for financial reasons, we could detect an almost complete knockdown of miR-17 in lung tissue of Antagomir-17 treated rats indicating that the dosage was adequate (Fig. IV.27B). The animals of the two MCT injected control groups had a dramatically increased right ventricular systolic pressure (RVSP) compared to the healthy controls demonstrating the presence of pulmonary arterial hypertension (Fig. IV.27C). In accordance with the results gained from the mouse model, Antagomir-17 significantly lowered RVSP (Fig. IV.27C) without impairing systemic arterial pressure (SAP, data not shown) in MCT treated rats. Consistently, the MCT-induced rise of the total pulmonary vascular resistance index (TPVRi) was almost abolished in Antagomir-17 injected rats compared to the diseased controls (data not shown). Likewise, animals that had received Antagomir-17 displayed a significantly improved pulmonary artery acceleration time (PAAT) as to

the MCT control groups (Fig. IV.27D). Although the estimation of right-heart hypertrophy by calculating the ratio of the right ventricle to the left ventricle with septum did not indicate a statistically significant decline of hypertrophy in A-17 medicated rats (Fig. IV.27E), cardiac output was recovered to the level of the healthy controls (Fig. IV.27F). In summary, we confirmed the beneficial effect of Antagomir-17 observed in the chronic hypoxia mouse model on hemodynamics and cardiopulmonary function in the rat model of MCT-induced PH.

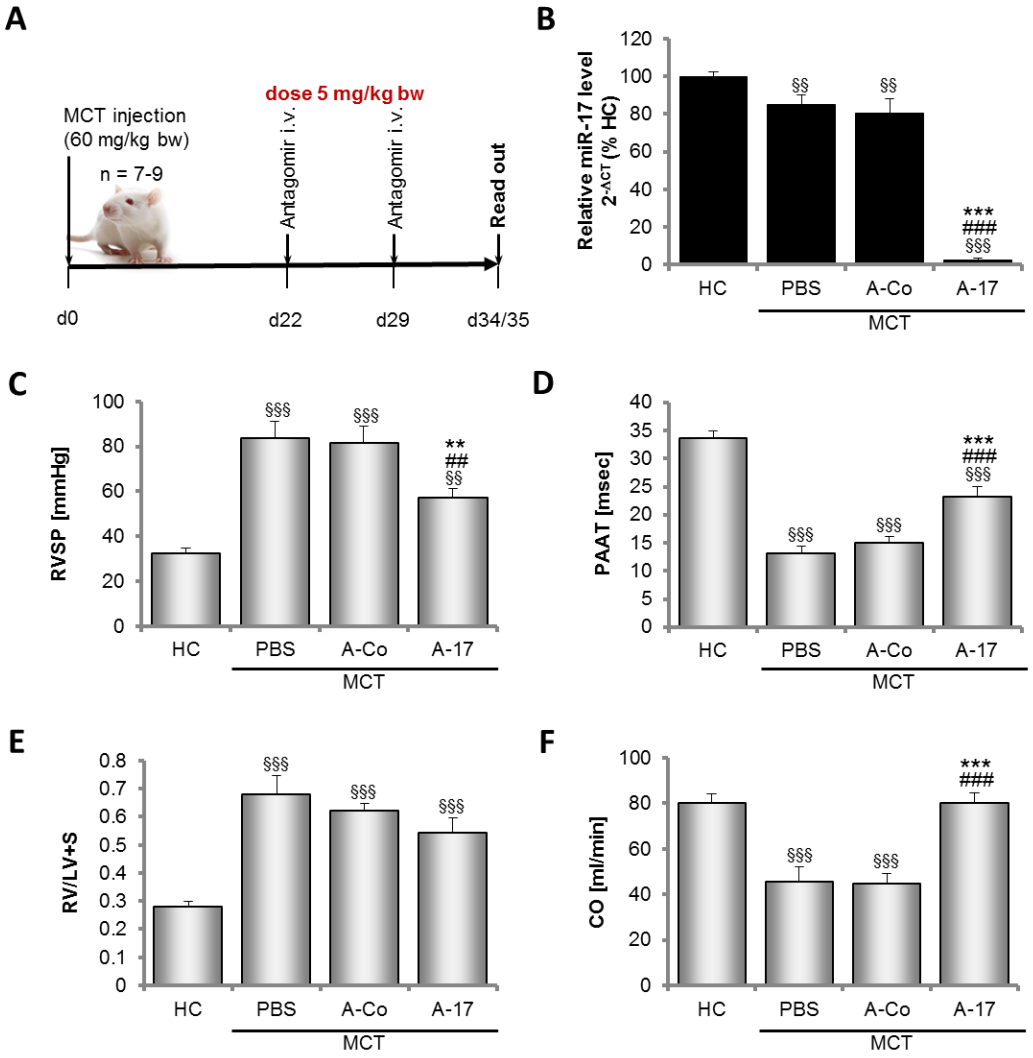

Figure IV.27: **Antagomir-17 ameliorates disease pattern in a rat model of MCT-induced PAH. (A)** Scheme of experimental setup. Development of pulmonary arterial hypertension (PAH) was initiated by subcutaneous injection of 60 mg/kg monocrotaline (MCT). Subsequently, Rats received two injections (5mg/kg bw) of Antagomir-17, control Antagomir or PBS at day 22 and 29. Hemodynamics and heart function were measured by high-resolution echocardiography at day 34/35. Lungs and hearts were harvested for analysis of miR-17 knockdown, muscularization of pulmonary arteries and hypertrophy of the right ventricle. **(B)** Expression of miR-17 in the lungs of the MCT and Antagomir treated rats, n = 5-10, **(C)** Right ventricular systolic pressure (RVSP). n = 7-9. **(D)** Pulmonary artery acceleration time (PAAT). n = 8-9. **(E)** Right-heart hypertrophy expressed as the weight ratio of right ventricle to left ventricle plus septum (RV/LV+S). n = 8-9. **(F)** Cardiac output (CO). n = 7-9. Each bar represents mean ± SEM. Experiments were done by our collaboration partners at the University of Gießen Lung Centre. §§*P* < 0.01, §§§*P* < 0.001 vs HC, ***P* < 0.01, ****P* < 0.001 vs PBS, ##*P* < 0.01, ###*P* < 0.001 vs A-Co.

4. Antagomir-17 improves muscularization pattern of the lung vasculature in the MCT-induced PAH rat model

Again, lung sections were analysed by histology to investigate the effect of Antagomir-17 on pulmonary vascular remodelling this time by quantifying both the degree of muscularization and the medial wall thickness of peripheral pulmonary arteries. The lungs of the diseased control animals exhibited a significant higher percentage of fully muscularized and a dramatically decreased amount of non-muscularized intra-acinar arteries compared to the healthy controls. Antagomir-17 treatment resulted in a reduction of fully muscularized and a significant rise in partially muscularized vessels but did not increase the number of non-muscularized arteries with respect to the MCT injected control groups (Fig. IV.28).

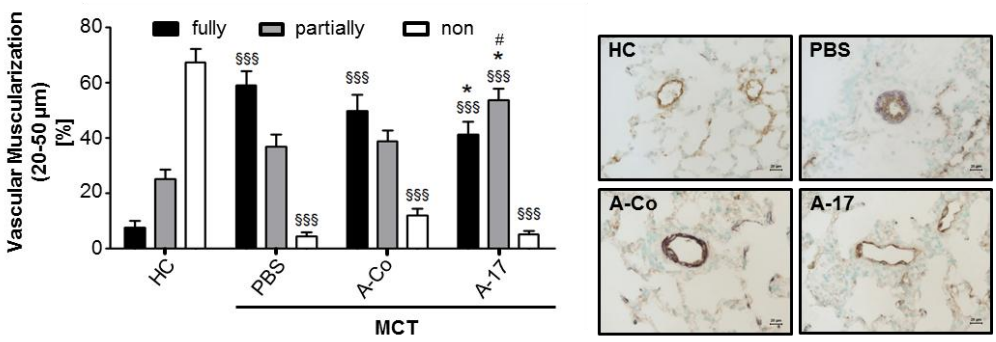

Figure IV.28: **Antagomir-17 affects muscularization of pulmonary arteries in MCT treated rats.** Lung sections were stained for von Willebrand factor (vWF in brown; ECs) and α-smooth muscle actin (SMA in purple; SMCs) and 80-100 intraacinar vessels were analysed in each animal. Proportion of fully (black bars), partially (grey bars), or non-muscularized (white bars) pulmonary arteries, as percentage of total pulmonary artery cross section (sized 20–50 µm). Representative pictures of the immunostaining. Bar graph: 20 µm. Histomorphometric analysis of pulmonary vasculature was done by our collaboration partners at the University of Gießen Lung Centre. §§§P < 0.001 vs HC, *P < 0.05 vs PBS, #P < 0.05 vs A-Co.

Consistently, medial wall thickness of small (<50 µm), medium (50-100 µm) and large (>100 µm) peripheral arteries was drastically elevated in sick control rats as to healthy controls. In A-17 injected rats, the medial wall thickness of small and medium-sized vessels was significantly reduced compared to the MCT treated control groups (data not shown) suggesting that inhibition of miR-17 affects vascular smooth muscle cells within the lung.

5. Identification of miR-17 targets involved in the beneficial effect of Antagomir-17 in vivo

To gain first insights into the molecular mechanism by which A-17 excerts its beneficial effect on cardiopulmonary function in experimental PAH, we analysed the rat lungs for the mRNA levels of

various validated and predicted targets of miR-17 that have previously been associated with the pathogenesis of the disease (Fig. IV.29).

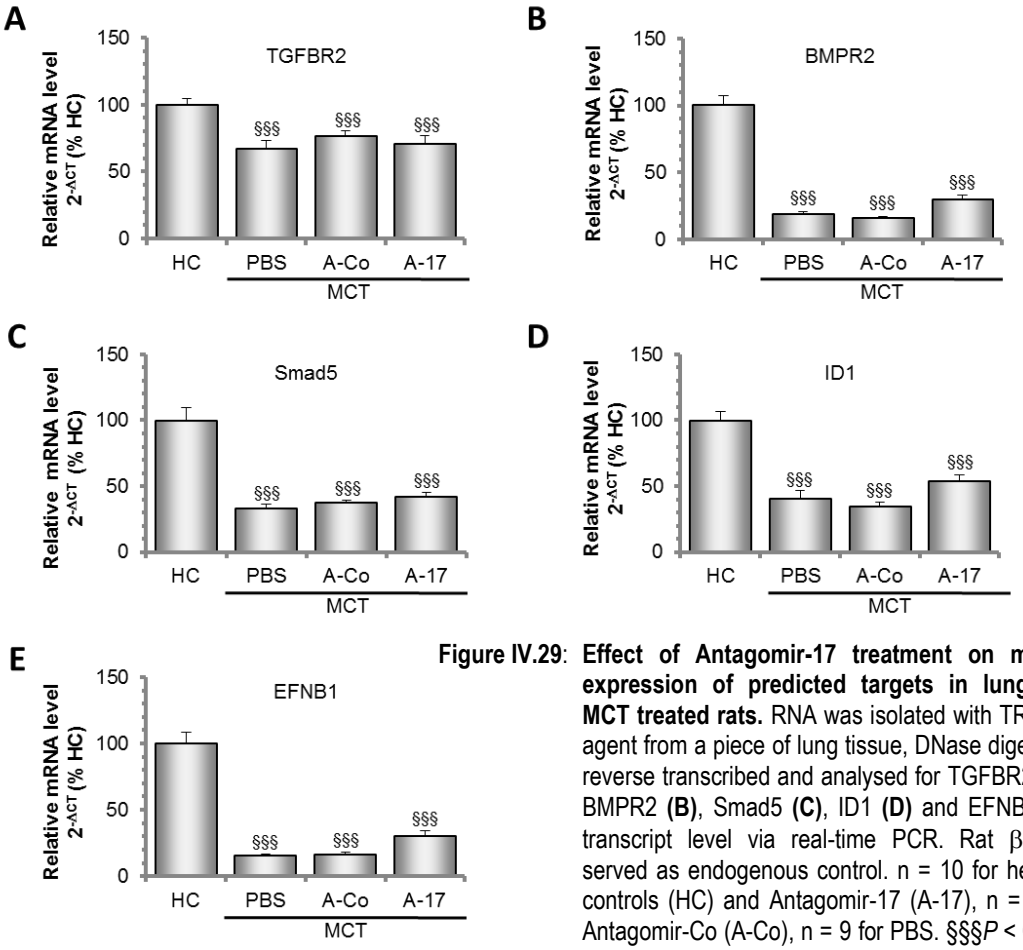

Figure IV.29: **Effect of Antagomir-17 treatment on mRNA expression of predicted targets in lungs of MCT treated rats.** RNA was isolated with TRI Reagent from a piece of lung tissue, DNase digested, reverse transcribed and analysed for TGFBR2 **(A)**, BMPR2 **(B)**, Smad5 **(C)**, ID1 **(D)** and EFNB1 **(E)** transcript level via real-time PCR. Rat β-actin served as endogenous control. n = 10 for healthy controls (HC) and Antagomir-17 (A-17), n = 5 for Antagomir-Co (A-Co), n = 9 for PBS. §§§$P < 0.001$ vs HC.

Several reports demonstrate dysregulated TGF-β/BMP signalling in patients suffering from PAH and in PAH animal models [33, 205]. Both, the bone morphogenetic protein receptor II (BMPR2) and the transforming growth factor receptor II (TGFBR2), transmembrane type II receptors for the TGF- β superfamily of growth factors, were shown to be regulated by miR-17 in transformed cell lines [149, 151-153, 176]. Whereas TGFBR2 mRNA level in the lungs of the Antagomir-17 treated rats was comparable to that of the PBS and A-Co treated controls (Fig. IV.29A), the expression of BMPR2 mRNA was marginally increased compared to control Antagomir injected animals (Fig. IV.29B). However, the observed differences were not statistically significant. Smad5, a downstream mediator of BMPR2 signalling, was also predicted to be a target of miR-17 by the Targetscan prediction algorithm, but real-time PCR analysis of Smad5 mRNA expression did not reveal any profound differences between Antagomir-17 treated and control animals (Fig. IV.29C). The inhibitor of DNA binding 1 (ID1), which was shown to be a BMP/Smad target in ECs [206], was also slightly upregulated on mRNA level (Fig. IV.29D) but again the differences

revealed no statistical significance. The mRNA level of another predicted miR-17 target, Ephrin B1 (EFNB1), which was demonstrated to be enriched in freshly isolated lung ECs [207], was also insignificantly increased in the A-17 treated rats as compared to the control animals (Fig. IV.29E).

Overall, we could not observe any statistically significant alterations of TGFBR2, BMPR2, Smad5, ID1 and EFNB1 on the mRNA level by Antagomir-17 treatment. Unfortunately, all efforts to detect BMPR2 protein by Western blotting failed.

Finally, the transcript of the cyclin-dependent kinase inhibitor p21, a validated miR-17 target, was most profoundly increased in the lungs of the A-17 injected rats compared to the controls (Fig. IV.30A). The increase of p21 was confirmed on the protein level by Western blot analysis, which showed a strong increase of this miR-17 target in the lungs of A-17 treated rats (Fig. IV.30B).

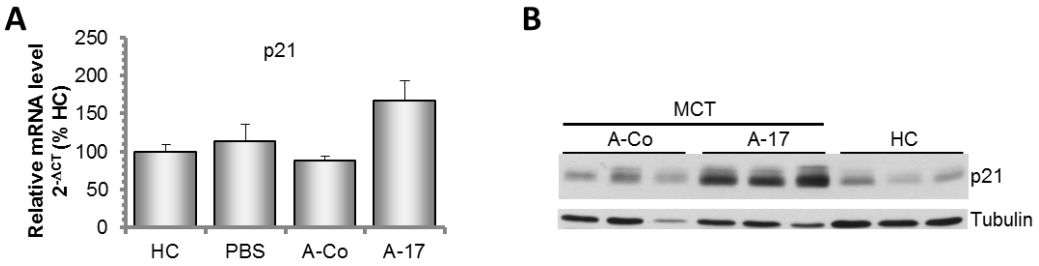

Figure IV.30: **Antagomir-17 treatment increases p21 expression in lungs of MCT treated rats. (A)** Effect on p21 mRNA. RNA was isolated with TRI Reagent from a piece of lung tissue, DNase digested, reverse transcribed and analysed for p21 transcript level. Rat β-actin served as endogenous control. n = 10 for healthy controls (HC) and Antagomir-17 (A-17), n = 5 for Antagomir-Co (A-Co), n = 9 for PBS. **(B)** Protein lysates from pieces of lung tissue were prepared in RIPA buffer supplemented with protease and phosphatase inhibitors. Equal amounts of protein (50 µg) were probed for p21 expression by Western blotting. Samples of n = 3 animals were analysed per group in the Western blot shown. Sample preparation and Western blot analysis were done by Natalja Reinfeld.

6. MiR-17 regulates p21 expression and proliferation of pulmonary smooth muscle cells

PAH is a multifactorial disease that affects various cell types including ECs and SMCs. Real-time PCR analysis of miR-17 level in cultured human and rat PASMC and HUVEC revealed higher expression of miR-17 in ECs compared to SMCs (Fig. IV.31).

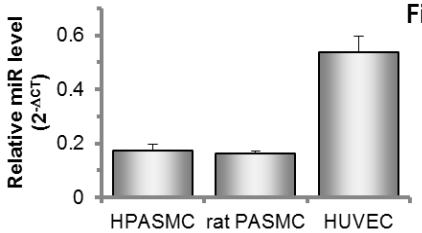

Figure IV.31: **MiR-17 expression in smooth muscle cells and endothelial cells.** Human pulmonary artery smooth muscle cells (HPASMCs), rat pulmonary artery smooth muscle cells (PASMCs) and HUVECs were cultured as described in the methods section. RNA was isolated with TRI Reagent and miR-17 expression was measured using the respective TaqMan microRNA assay. RNU6 was used as endogenous control. n = 3 for rat PASMC, n = 6 for HPASMC and HUVEC.

In the first part, we demonstrated that inhibition of miR-17 improves the angiogenic capacity of ECs. However, the influence on SMCs has not been studied so far. The decreased muscularization of the pulmonary vasculature in the A-17 treated animals in the in vivo experiments and the upregulated p21 expression in the rat lungs suggested that miR-17 might influence the proliferation of PASMCs. Therefore, we used Antagomirs to inhibit miR-17 (Fig. IV.32A) and transfected precursor molecules to overexpress miR-17 (Fig. IV.32D) in HPASMCs in vitro and determined the impact on p21 expression and proliferation of these cells. Indeed, miR-17 inhibition resulted in an increase of p21 mRNA and protein expression (Fig. IV.32B/C). Vice versa, p21 mRNA was significantly lowered in cells transfected with 10 nM Pre-17 (Fig. IV.32E).

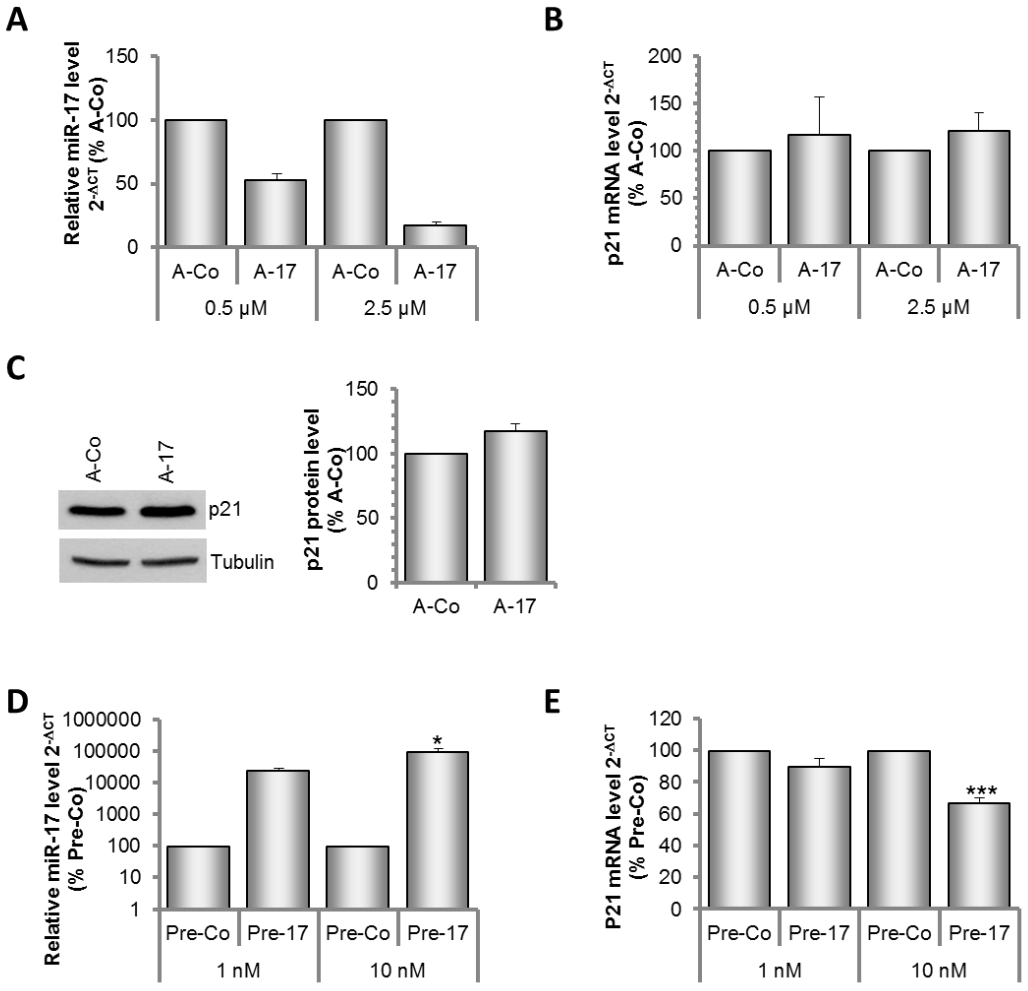

Figure IV.32: **MiR-17 regulates p21 expression in human pulmonary artery smooth muscle cells (HPASMCs). (A/B)** HPASMCs were treated with 0.5 µM and 2.5 µM control or miR-17 Antagomir and RNA was isolated after 24 h and DNase digested. (A) MiR-17 level was quantified using the TaqMan microRNA assay and normalized to RNU48. n = 6 (B) p21 mRNA was quantified by real-time PCR using gene specific primers. The large ribosomal protein P0 (RPLP0) was used as endogenous control. n = 6 **(C)** HPASMCs subjected to 2.5 µM Antagomir were lysed in RIPA buffer supplemented with protease inhibitors and equal amounts of protein lysates were probed for p21 by Western blotting. Tubulin was used as endogenous control. A representative Western blot and the summarized quantification of five independent experiments are shown. **(D)** HPASMCs were transfected with 1 nM and 10 nM control or miR-17 precursor molecule and RNA was isolated after 24 h. After DNase digestion of the RNA, miR-17 expression and p21 mRNA level were measured as described above. n = 5 for 1 nM and n = 6 for 10 nM precursor. **P* < 0.05, ****P* < 0.001

To address the impact of miR-17 on SMC proliferation, BrdU incorporation during DNA replication of precursor transfected SMCs was measured using a cell proliferation ELISA. In accordance with the lowered p21 abundance, the cells overexpressing miR-17 had an enhanced proliferation rate under standard culture conditions and upon stimulation with platelet derived growth factor-BB (PDGF-BB) as shown in Fig. IV.33.

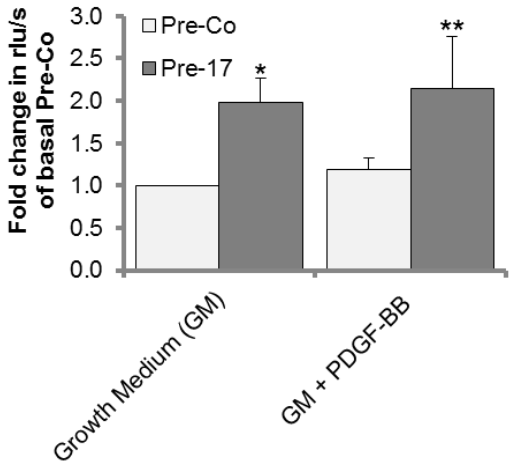

Figure IV.33: **MiR-17 increases proliferation of HPASMCs.** HPASMCs were transfected with 10 nM control (Pre-Co) and miR-17 precursor molecule (Pre-17), and after 48 h medium was changed to growth medium (GM) and GM supplemented with 30 ng/ml PDGF-BB. Cells were incubated for 20 h with BrdU, and the degree of BrdU labeling was determined with a chemilumincent cell proliferation ELISA. Different conditions were done in triplicates in every experiment. Results are given in relative light units per second (rlu/s). n = 3 experiments. *$P < 0.05$, **$P < 0.01$.

7. MiR-17 controls TGFBR2 expression in pulmonary smooth muscle cells

Having demonstrated that miR-17 influences p21 expression and proliferation of HPASMCs in vitro, we additionally addressed the impact of miR-17 on the expression of other miR-17 targets in these cells. Previous studies showed that miR-17 represses the BMPR2 in HEK cells [149]. However, in our hands BMPR2 mRNA was not reduced upon miR-17 overexpression in HPASMCs (Fig. IV.34A) despite a tremendous increase of mature miR-17 (Fig. IV.32D). Unfortunately, we did not succeed in detecting BMPR2 protein in HPASMCs via Western blotting.

Likewise, Pre-17 transfected HUVECs did not display impaired BMPR2 mRNA or protein levels (Fig. IV.34B/C), although mature miR-17 expression was significantly raised (Fig. IV.34D).

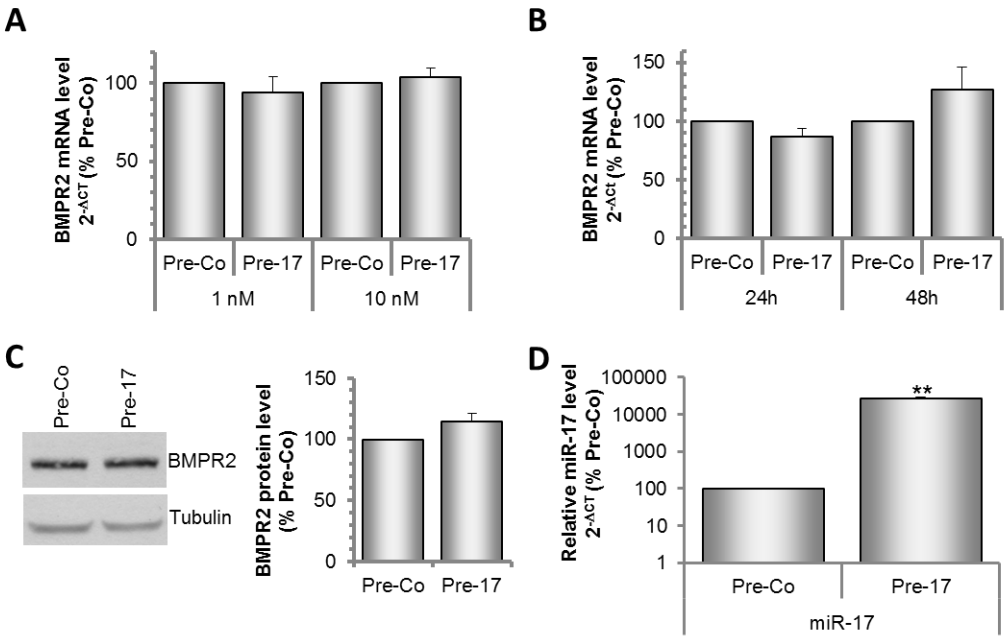

Figure IV.34: **MiR-17 does not regulate BMPR2 expression in HPASMCs and HUVECs. (A)** Effect of miR-17 on BMPR2 mRNA in SMCs. HPASMCs were transfected with 1 nM and 10 nM control (Pre-Co) or miR-17 precursor molecule (Pre-17) and RNA was isolated after 24 h. After DNase digestion of the RNA, BMPR2 mRNA level was measured by real-time PCR. n = 5 for 1 nM and n = 6 for 10 nM precursor. (B-D)Effect of miR-17 on BMPR2 expression in ECs. HUVECs were transfected with 10 nM control or miR-17 precursor. **(B)** RNA was isolated with TRI Reagent after 24 h and 48 h, DNase digested and analysed for BMPR2 mRNA. n = 3. **(C)** Proteins were extracted after 48 h using RIPA buffer supplemented with protease inhibitors and equal amounts of protein lysates were probed for BMPR2 by Western blotting. Tubulin was used as endogenous control. A representative Western blot and the summarized quantification of three independent experiments are shown. **(D)** Confirmation of miR-17 overexpression 24 h after precursor transfection in RNA of HUVECs used to measure BMPR2 mRNA level in (B). n = 3. $^{**}P < 0.01$

Similarly Smad5 and EFNB1 mRNA levels were not decreased in miR-17 overexpressing HPASMCs (Fig. IV.35A/B).

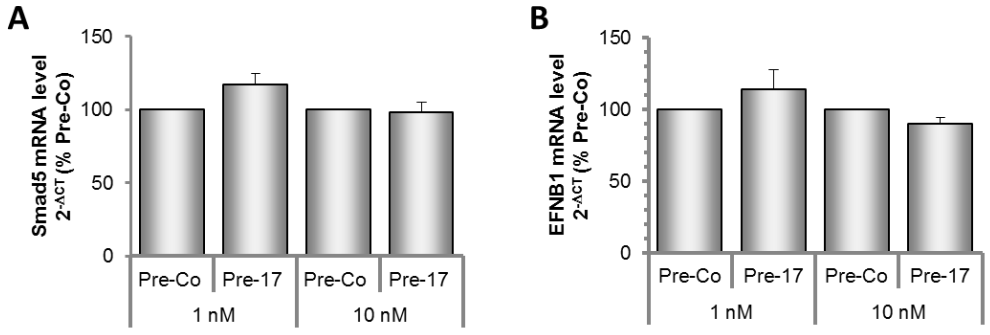

Figure IV.35: **MiR-17 does not affect Smad5 and EFNB1 transcript levels in HPASMCs.** HPASMCs were transfected with 1 nM and 10 nM control (Pre-Co) or miR-17 precursor molecule (Pre-17) and RNA was isolated after 24 h. DNase digested RNA was reverse transcribed and BMPR2 mRNA level was measured by real-time PCR. Effect of miR-17 on Smad5 **(A)** and EFNB1 **(B)** mRNA expression. The large ribosomal protein P0 (RPLP0) was used as endogenous control. n = 5 for 1 nM and n = 6 for 10 nM precursor.

The most drastic effect of miR-17 in vitro was observed for TGF-ß receptor 2 (TGFBR2), which was profoundly downregulated in miR-17 overexpressing HPASMCs on mRNA (Fig. IV.36A) and

protein level (Fig. IV.36B). Consistently, inhibiting miR-17 expression induced TGFBR2 expression (Figure IV.36C/D).

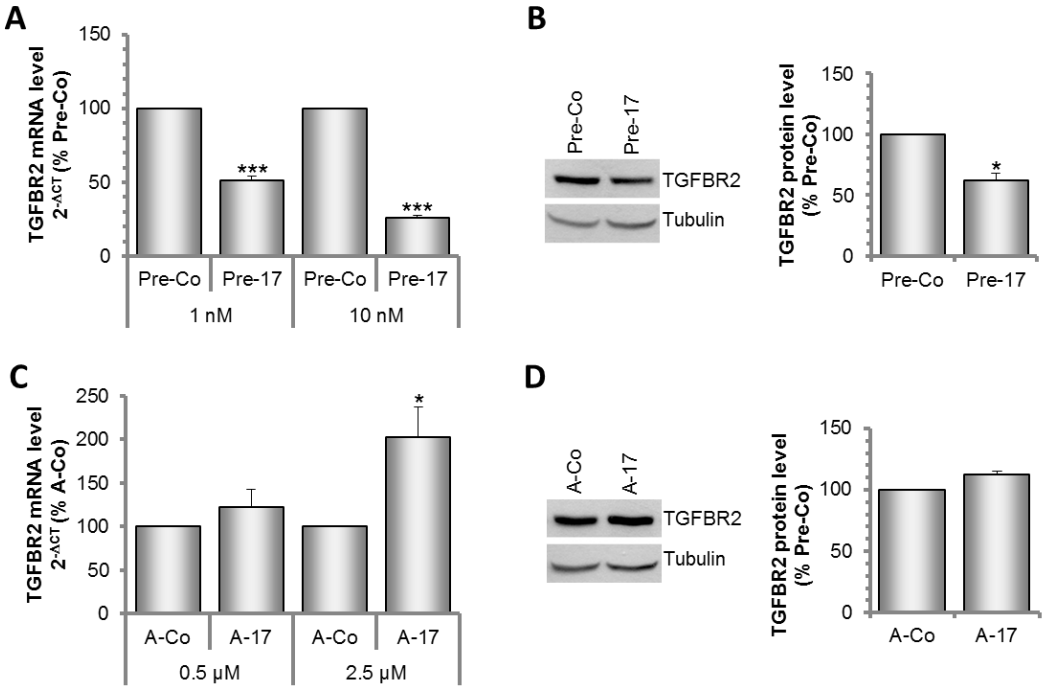

Figure IV.36: **MiR-17 regulates TGFBR2 in HPASMCs.** HPASMCs were transfected with 1 nM and 10 nM control (Pre-Co) or miR-17 precursor molecule (Pre-17) or treated with 0.5 µM and 2.5 µM control or miR-17 Antagomir and RNA was isolated after 24 h. For analysis of TGFBR2 protein level, 10 nM of each precursor or 2.5 µM of each Antagomir were used. Proteins were isolated with RIPA buffer 48 h after transfection and analysed by Western blotting. **(A)** Effect of miR-17 overexpression on TGFBR2 mRNA. n = 5-6. **(B)** Effect of miR-17 overexpression on TGFBR2 protein. n = 3. **(C)** Effect of miR-17 inhibition on TGFBR2 mRNA. n = 6. (D) Effect of miR-17 inhibition on TGFBR2 protein. n = 3. *$P < 0.05$, ***$P < 0.001$.

In recent years, various reports provided evidence for the involvement of TGF-β superfamily (including BMPs and TGFs) signalling in vascular smooth muscle cell differentiation into the contractile phenotype. Last year, Inamoto et al. demonstrated that aortic SMCs from patients harbouring mutations in the TGFBR2 display impaired expression of a variety of marker proteins for the contractile phenotype [208]. Since TGFBR2 was profoundly affected by miR-17 overexpression or inhibition in HPASMCs in our hands, we analysed these cells for the transcript levels of the three contractile proteins α-actin 2 (ACTA2), calponin 1 (CNN1) and smoothelin (SMTN). ACTA2 mRNA was higher expressed in HPASMCs than transcript levels of CNN1 and SMTN and remained constant in contrast to both others (Fig. IV.37A-C). However, the differences observed in CNN1 and SMTN levels were not statistically significant.

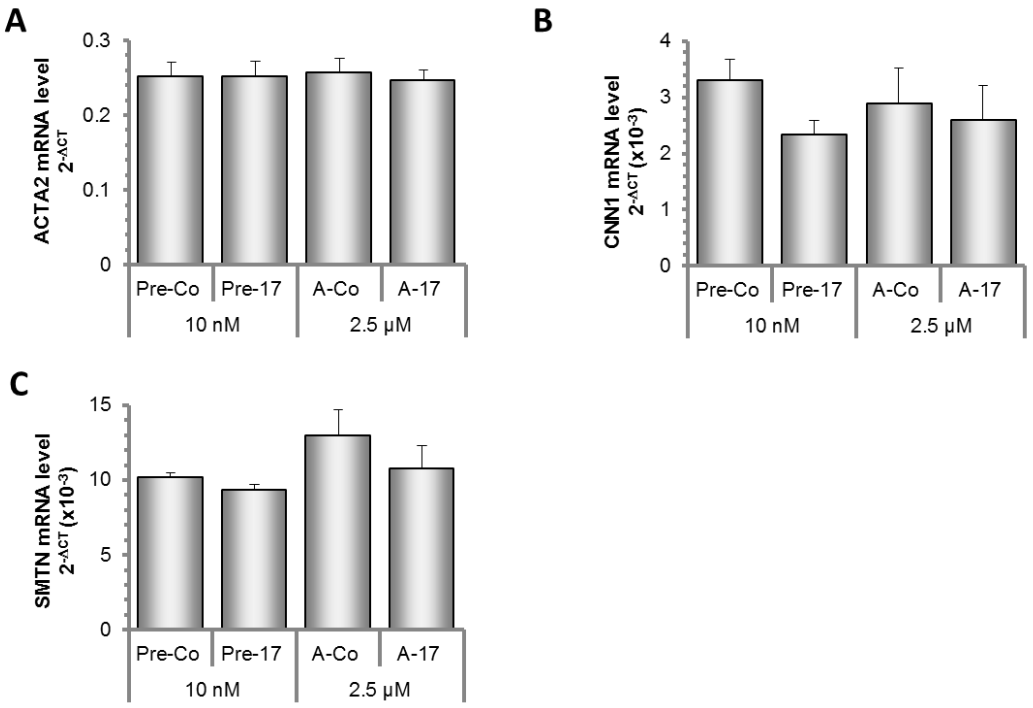

Figure IV.37: **MiR-17 does not change transcript levels of contractile proteins in HPASMCs.** RNA of HPASMCs transfected with 10 nM precursor molecules or treated with 2.5 µM Antagomirs was analysed for the expression of contractile proteins **(A)** α-actin 2 (ACTA2), **(B)** calponin 1 (CNN1) and **(C)** smoothelin (SMTN) via real-time PCR. n = 3.

V. Discussion

MicroRNAs are known to regulate gene expression on the posttranscriptional level by inducing mRNA degradation or blocking translation and therefore represent important regulators of cell behaviour in higher organisms. Due to their crucial role in controlling processes like cell migration, proliferation and survival, microRNAs participate in orchestrating the development of whole organisms and govern tissue homeostasis in the adult. A variety of microRNAs have been shown to be expressed in diverse cell types of the cardiovascular system regulating heart, vessel and blood development as well as the response to stress conditions. Not surprisingly, dysregulated microRNA expression has been described in various diseases and is associated with disease pathology.

The microRNA-17-92 cluster has originally become famous for its involvement in tumourigenesis since the primary transcript is frequently amplified in different types of solid tumours and leukemia [135, 153]. In 2006, Dews et al. showed that overexpression of the miR-17-92 cluster in transformed colonocytes promoted tumour growth and vascularization in a mouse tumour model [150]. Our lab previously demonstrated the expression of the individual members of the miR-17-92 cluster in human umbilical vein endothelial cells (HUVECs) and provided evidence that the last member of the cluster, miR-92a, has anti-angiogenic activity in ECs and represents a crucial regulator of recovery after ischemia [119]. At that time, little was known about the function of the remaining members of the miR-17-92 cluster in the endothelium. In this thesis, the miR-17-92 cluster was dissected to analyse the members individually regarding their biological role in endothelial cells in vitro and angiogenesis in vitro and in vivo.

A. Functional role of members of the miR-17-92 cluster in endothelial cells and angiogenesis

To study the biological role of the individual cluster members in vitro, we used commercially available miR precursor molecules to overexpress miR-17, -18a, -19a and -20a in endothelial cells in vitro and analysed the effects of the miRs in functional assays addressing the angiogenic and migratory capacity as well as proliferation and apoptosis of ECs. Vice versa, we blocked miR-17, -18a, -19a and -20a with specific inhibitors to investigate the impact of depletion of the individual miRs on angiogenesis in vitro. To address the relevance of the different members of the miR-17-92 cluster for blood vessel formation in vivo, we inhibited the different miRs by Antagomirs in the Matrigel plug mouse model of neovascularization. Since miR-17 was most effective in regulating angiogenesis, we identified miR-17 targets in ECs and evaluated the impact of

Antagomir-mediated inhibition of miR-17 on tumour angiogenesis in a mouse tumour model. We neglected to investigate miR-19b in this project since it just differs by one nucleotide from miR-19a and is probably functionally redundant.

1. Cell-intrinsic anti-angiogenic activity of individual members of the miR-17-92 cluster in vitro

In contrast to the reported tumour angiogenesis promoting activity of the miR-17-92 cluster when overexpressed in tumour cells [150], we demonstrate in this study that overexpression of the individual miR-17-92 cluster members miR-17, -18a, -19a and -20a significantly blocks angiogenic sprouting of endothelial cells in the 3D spheroid model in vitro. However, the ability of the endothelial cells to form capillary networks on Matrigel is only marginally and nonsignificantly reduced after overexpression of each individual miR. The formation of capillary-like structures in the spheroid sprouting and the tube formation assay is a multistep process involving endothelial cell migration, proliferation and survival. Enhanced expression of miR-17, -18a, -19a and -20a results in a statistically nonsignificant reduction of EC migratory capacity on collagen I. With respect to EC survival, overexpression of miR-17, -19a and -20a does not affect the percentage of apoptotic cells under standard cell culture conditions and after exposure of the cells to low oxidative stress. However, miR-18a significantly enhances apoptotic cell death of ECs under standard cell culture conditions, and also under low oxidative stress, apoptosis of miR-18a overexpressing ECs is by trend still increased. Nevertheless, under conditions of high oxidative stress, overexpression of miR-18a has no effect on EC apoptosis and neither has overexpression of miR-19a and -20a. Only miR-17 overexpressing ECs tend to undergo less apoptotic cell death under this condition. EC proliferation is significantly enhanced after overexpression of miR-17 and miR-20a, whereas miR-18a and miR-19a do not affect the proliferation rate of ECs. Although overexpression of each individual miR significantly impaired EC spheroid sprouting, only inhibition of miR-17, -18a and -20a significantly enhanced capillary sprouting of spheroids in vitro. Blocking of miR-19a showed just a minor trend towards an increased angiogenic response. In vivo, combined downregulation of miR-17 and miR-20a with three injections of Antagomir-17 significantly promotes vascularization of Matrigel plugs, whereas individual inhibition of miR-18a, -19a and -20a increases the number of perfused vessels within the Matrigel plug just by trend.

Up to now, there is no in vitro assay to model the complex morphogenetic event of angiogenesis as it occurs in vivo. Most assays mimic certain steps of the angiogenic process. In contrast to the tube formation assay which illustrates events occurring at later stages of angiogenesis, namely the assembly of an interconnected capillary-like network, the spheroid model mimics vascular

sprouting, an initial event in the formation of a new vessel from a pre-existing one. The two assays also differ in the importance of the cellular events involved. The tube formation assay mainly focuses on adhesion, migration and integration of individual cells into a network. Endothelial cell proliferation seems to be of minor importance and invasion of cells into the substratum does not occur since the cells are seeded on top of a very thin layer of Matrigel restricting them to two-dimensional movement. The spheroid assay depicts a 3D model of branching morphogenesis, which was postulated on the basis of airway branching in *Drosophila*, involving a tip cell which guides the nascent sprout at the front and stalk cells that serve sprout elongation. Whereas the task of the tip cell is to invade the surrounding by matrix degradation and migration, the stalk cells are specialized on proliferation [209]. In vivo, quiescent blood vessels are enclosed by a continuous basement membrane which separates them from the surrounding interstitial matrix. During sprouting angiogenesis, the activated endothelial cell secretes proteolytic enzymes to degrade the vascular basement membrane matrix of the interstitium. The basement membrane next to nonangiogenic cells consists of collagen IV, laminin, nidogen/entactin and perlecan whereas the ECM of the vascular interstitium mainly contains collagen I and fibronectin [210].

Since endothelial cell behavior is largely determined by the matrix environment, the different matrices used in the two angiogenesis assays must also be taken into account. In the spheroid assay collagen I was employed, whereas in the tube network formation assay Matrigel was applied to coat the cell culture dish. Matrigel is a complex basement membrane extract derived from the mouse Engelbreth-Holm-Swarm (EHS) sarcoma mainly consisting of laminin (56%), collagen IV (31%) and nidogen/entactin (8%) [211]. Thus, the spheroid model mimics angiogenic sprouting within the interstitium and the tube network formation assay is based on the interactions of the endothelium with the underlying vascular basement membrane. Although we observed a profound impairment of sprouting in the spheroid assay, migration on collagen I was only slightly reduced indicating that the endothelial cells did not fail to interact with the matrix.

There are two reports contradicting our results at first sight since they demonstrate that miR-17 together with let-7b [76] or miR-18a and -20a [77] rescues impaired angiogenesis caused by Dicer deficiency and therefore exerts pro-angiogenic activity. Deletion of Dicer leads to abolished maturation of most microRNAs leading probably to profound alterations of a variety of cellular processes. Therefore, one may speculate that the re-introduction of single microRNAs has other consequences than in non-modified cells. Moreover, Suarez et al. demonstrated that VEGF upregulates miR-17, -18a and -20a in HUVECs isolated from umbilical cords and that combined inhibition of miR-17, -18a and -20a in these HUVECs impaired tube forming capacity on Matrigel [77]. In the commercially available HUVECs that we used for this study, VEGF treatment did not

change mature levels of the members of the miR-17-92 cluster (data not shown). Although we did not address the effects of combinatorial overexpression or inhibition of members of the miR-17-92 cluster, it is unlikely that their joint action results in opposite effects with respect to angiogenesis. Therefore, the different origin of the cells as well as the distinct culture and assay conditions are probably the reason for the discrepant results. Combined overexpression of miR-17 and let-7b also promoted tube forming capacity of SV40 transformed lymphatic endothelial cells (SVEC) of murine origin. Since SVEC do not express miR-126 [85], which is generally regarded to be EC enriched, the comparability of SVEC with ECs derived from blood vessels might be problematic. Additionally, it is well established that the miR-17-92 cluster is capable of executing pleiotropic effects due to the different target specificities of the individual cluster members and the possibility of regulating targets with opposing effects.

2. The miR-17-92 cluster in tumour angiogenesis

We were surprised by our findings that enhanced expression of each member of the miR-17-92 cluster individually suppressed the angiogenic capacity of endothelial cells since Dews et al. observed increased tumour vascularization in mice after transplanting transformed colonocytes that overexpressed the whole miR-17-92 cluster. In detail, Dews et al. demonstrated that miR-18 and miR-19 downregulate the anti-angiogenic proteins connective tissue growth factor (CTGF) and thrombospondin-1 (TSP-1) which are both members of the thrombospondin type 1 repeat (TSR) superfamily [150]. Moreover, a subsequent report provided evidence that the cluster indirectly decreases expression of a third TSR protein, clusterin, by miR-17/20-mediated repression of TGFBR2 and Smad4 downregulation via miR-18a, thus blunting TGF-β signalling [176]. As the three TSR proteins are all secreted factors, we speculated that the pro-angiogenic effect of the miR-17-92 cluster observed in tumours might be due to alterations in the secretome of tumour cells. Indeed, supernatants of tumour cells overexpressing miR-17, -18a, -19a or -20a individually displayed a trend towards enhancing EC spheroid sprouting activity in vitro compared with supernatants of similar treated HUVECs. Indeed, we observed only a minor decrease of CTGF and TSP-1 in HUVECs after miR-18a or -19a expression. In contrast, Suaréz et al demonstrate in the endothelial cell line Ea.hy.926 a decrease of TSP-1 protein to 17% of the control cells after miR-18a overexpression and a doubling in TSP-1 protein level upon miR-18a inhibition [77]. Ea.hy.926 cells are hybrid cells originally generated by polyethylene glycol (PEG)-induced fusion of primary human umbilical vein endothelial cells (HUVECs) and the human lung carcinoma cell line A549 [212]. Various publications verify endothelial cell characteristics of Ea.hy.926 cells (e.g. presence of Weibel-Palade bodies [213]), but nevertheless Ea.hy.926 cells possess more

chromosomes (around eighty) than the cells from which they were derived (A549: 61 chromosomes, HUVEC: 46 chromosomes) including a marker chromosome from the A549 cell line [212]. Actually, it is questionable if this cell line can really be regarded as endothelial cells. But the fact that Ea.hy.926 cells contain genetic material of tumour cells seems to be a plausible explanation for the different effects of miR-18a on TSP-1 expression observed in Ea.hy.926 by Suaréz et al. and primary HUVECs in our hands. These results imply that the simultaneous presence of the microRNA and the target mRNA does not predispose the target to be affected by the microRNA and that other factors co-decide the fate of the target, e.g. tissue specific RNA binding proteins that mask the binding site of the microRNA in the target mRNA. Likewise, miR-19a was shown to exert an anti-proliferative effect in EA.Hy926 cells, whereas in our study miR-19a did not affect proliferation of HUVECs [97] indicating that the effect of a given microRNA depends on the cellular context and might even differ in related cell types.

Since Antagomir-17 mediated inhibition of miR-17/20 profoundly enhanced vascularization of Matrigel plugs, we investigated the effect of Antagomir-17 on tumour growth and angiogenesis in vivo. Although one injection of Antagomir-17 slightly, but nonsignificantly, increased tumour weight and volume, no increase in tumour vascularization was observed. These results were quite surprising since the same dose of Antagomir-17 in the Matrigel plug model resulted in a doubling of perfused vessels within the plug suggesting that Antagomir-17 differentially affects neovascularization of Matrigel plugs and tumour angiogenesis. In the tumour, Antagomir-17 probably alters the composition of the secretome of the tumour cells, e.g. by increasing TGF-β–induced expression of TSR protein clusterin via the TGFBR2, and thus balances the pro-angiogenic effect that Antagomir-17 probably exerts in the endothelial cells. The slight rise in tumour weight and volume might be due to effects on Cyclin D1, which was shown to be targeted by miR-17/20 in breast cancer cells and generally promotes cell cycle progression [141]. Application of an additional dose of Antagomir-17 to increase the knockdown of miR-17 within the tumour did not reveal any effect, neither on tumour size and volume nor on tumour angiogenesis. Accordingly, Antagomir mediated inhibition of miR-17 in LLC1 cells in vitro did not affect their proliferation rate. In contrast, Fontana et al. reported that application of Antagomir-17 to neuroblastoma cells in vitro or direct injection into the tumour in vivo abolished tumour cell growth and induced apoptosis of tumour cells [140]. Inhibition of tumour cell proliferation by miR-17/20 inhibitors was demonstrated to be dependent on the expression level of the miRs in tumour cells, tumour cells overexpressing the miR-17-92 cluster responded to inhibitor treatment with decreased cell growth whereas proliferation of tumour cells with lower miR-17-92 levels remained unchanged [214]. We did not compare the miR-17 expression level in LLC1 cells to that of other

tumour cells but the fact that the level of miR-17 in LLC1 was comparable to that of HUVECs suggests that LLC1 cells do not overexpress the miR-17-92 cluster and their proliferation is therefore less affected by Antagomir-17. Eventually, the net effect of Antagomir-17 on tumour growth and tumour angiogenesis depends on the impact of the Antagomir on the endothelial cells, the tumour cells and paracrine, cell-nonautonomous mechanisms (Fig. V.1)

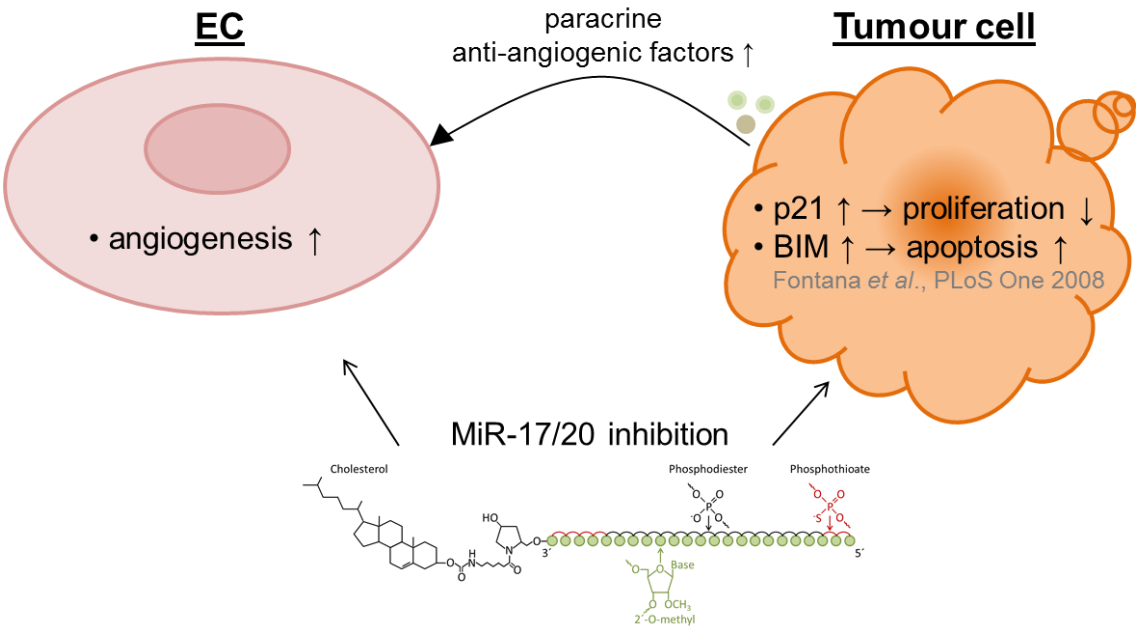

Figure V.1: **Effects of Antagomir-17 on tumour cells and endothelium.** The net effect of Antagomir-17 on tumour growth and tumour angiogenesis is determined by its effects on the tumour cells, the endothelium and paracrine signalling.

The members of the miR-17-92 cluster seem not to be the only microRNAs regulating angiogenesis in a context-dependent manner by differential intrinsic (cell-autonomous) and paracrine (cell-nonautonomous) mechanisms (Fig. V.2). Sohail Tavazoie from the Rockefeller University in New York presented data at a recent Keystone Symposium that showed that miR-126 in cancer cells suppresses tumour angiogenesis associated endothelial cell recruitment by downregulating insulin-like growth factor binding protein 2 (IGFBP2), thus impairing the tumour cells´ insulin-like growth factor 1 (IGF1) secretion which is a chemoattractant for endothelial cells [215]. In contrast, miR-126 was demonstrated to have angiogenesis promoting activity in endothelial cells by enhancing VEGF signalling [83, 85]. At present, much research effort is invested in identifying proteins (e.g. RNA binding proteins) or cellular mechanisms (e.g. alternative mRNA 3´ UTRs, miR binding site polymorphisms) responsible for the tissue and cell type specific effects of microRNAs. Although our understanding of the mechanisms that regulate microRNA action are still limited at the moment, the forthcoming years will certainly bring our understanding forward concerning this matter.

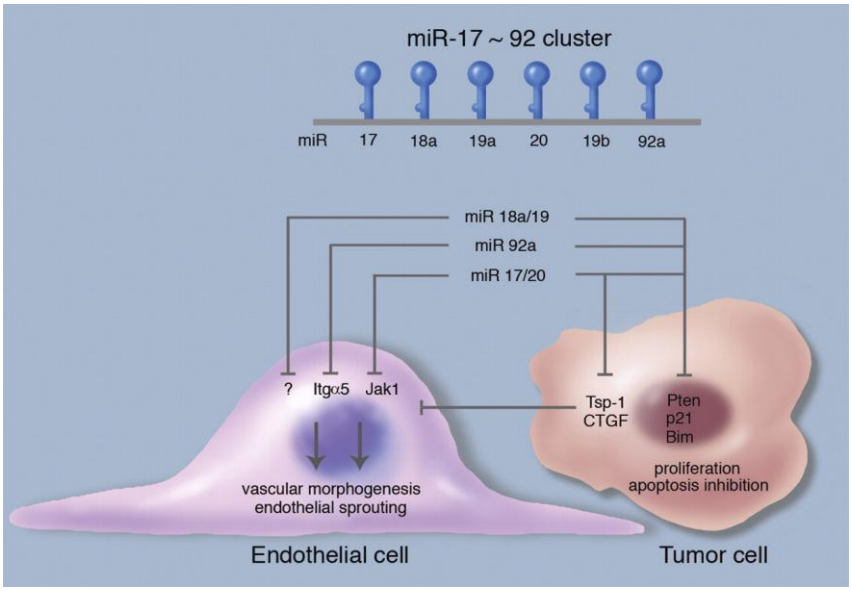

Figure V.2: **Involvement of the miR-17-92 cluster in the regulation of angiogenesis.** In tumour cells, miR-18 and miR-19 downregulate the anti-angiogenic, secreted proteins thrombospondin-1 (TSP-1) and connective tissue growth factor (CTGF), thereby creating a pro-angiogenic environment which promotes angiogenesis in the close-by tumour endothelium in a cell-nonautonomous manner. In endothelial cells, miR-17/20 and miR-92a block angiogenesis cell-autonomously by repressing Janus kinase 1 (JAK1) and Integrin α5 (ITGα5). The members of the miR-17-92 cluster also enhance proliferation and survival of tumour cells by targeting phosphatase and tensin homolog (PTEN), p21 and Bim. Adopted from Kuhnert & Kuo, Blood 2010 [216]

3. Targets of the members of the miR-17-92 cluster in endothelial cells

a) The pro-apoptotic protein BIM

Up to now, more than 40 targets of the miR-17-92 cluster have been described in tumour cells and other cell types (see Table I.2 in the introduction). Among them are well known regulators of apoptosis and cell proliferation. We first addressed the effect of the individual cluster members on the pro-apoptotic protein BIM since all of them, except for miR-18a, were predicted to target BIM according to the targetscan algorithm. In several tumour studies, expression of the miR-17-92 cluster was inversely correlated with expression of the pro-apoptotic protein BIM. In detail, miR-17/20 [140], miR-19 [156] and miR-92a [157] have already been validated to target BIM in tumour cells. In our hands, only miR-20a had a statistically significant effect on BIM protein expression, but a trend towards reduction could be observed for all members of the cluster including miR-18a. But since miR-18a reduced BIM expression the least, one may speculate that this might be the reason for the increase in apoptosis observed in Pre-18a transfected cells under normal culture conditions. Under high oxidative stress, miR-17 overexpressing HUVECs showed a trend towards reduction of cellular apoptosis which might be due to its regulatory activity regarding BIM. But the fact that the anti-apoptotic effect of miR-20a was less pronounced under these conditions, although it had the stronger effect on BIM protein expression, argues for the involvement of other proteins. Further research activities are needed to elucidate the mechanism determining target

specificity of highly similar microRNAs, especially those belonging to the same seed family like miR-17 and miR-20a.

b) Identification of targets of miR-17 in endothelial cells

MicroRNA target identification is a major issue in microRNA biology since the regulated targets dictate the biological function of a given microRNA. Due to the initial observation that microRNAs in animal cells frequently reduce protein expression without affecting mRNA level of their targets, it was thought for a long time that animal miRs rather act by translational repression than by initiation of mRNA degradation. However, studies employing microarray analysis demonstrated that some miRs downregulate their targets to a large extent on the transcript level [217]. Indeed, various research groups compared microarray mRNA data with results from proteomic approaches and observed both mRNA destabilization and block of translation [218-220]. It was proposed that the contribution of each mechanism to target downregulation depends on the respective miR-mRNA pair [219]. Nevertheless, it is still not known how the relative contributions of translational inhibition and mRNA degradation to target regulation by microRNAs are determined.

In order to identify direct targets of miR-17 in ECs, we performed microarray analysis of HUVECs after miR-17 overexpression and matched the downregulated transcripts with the miR-17 targets predicted by the targetscan algorithm. Indeed, we found several predicted targets to be downregulated on the mRNA level, some of which have already been validated in other cell types like the cell cycle regulator CDKN1A/p21 [140] or the TGF-β receptor 2 [151-153, 176].

c) Effect of miR-17 on the cyclin dependent kinase inhibitor 1A

In contrast to the reported effects of miR-17 in the rat endothelial cell line [166], miR-17 and miR-20a significantly increased proliferation of HUVECs in our hands. For miR-17, we demonstrated that the stimulatory effect on proliferation is concentration dependent by transfecting different amounts of precursor molecules. Several reports ascribe a pro-proliferative effect to miR-17 in a variety of cell types which was attributed to some extent to the downregulation of the cell cycle regulator CDKN1A/p21 [140, 155]. However, Yu et al. described a negative feedback loop in which Cyclin D1 induces miR-17 and -20a expression, which in turn regulate Cyclin D1 expression to limit proliferation of breast cancer cells [141]. Surprisingly, according to our microarray analysis miR-17 overexpression significantly decreased transcript expression of both, CDKN1A/p21 and Cyclin D1, although they have opposing effects on cell cycle progression. Nevertheless, we observed enhanced cell proliferation after miR-17 overexpression indicating that miR-17 alters the balance between pro- and anti-proliferative factors within the cell. Polycystic kidney disease 2 (PKD2) is a predicted miR-17 target proposed to regulate proliferation of human embryonic kidney (HEK) cells in culture [170] and known to act together with PKD1 as

sensory transducer in primary cilia of renal epithelial cells [221]. Interestingly, humans and mice with mutated polycystin alleles display vascular defects [222, 223]. Consistently, both polycystin genes were demonstrated to be expressed in endothelial cells and PKD2 was proposed to regulate NO biosynthesis in response to shear stress [224] suggesting a crucial role of PKD2 in the vascular system. Indeed, our microarray analysis revealed a downregulation of PKD2 by almost 50% upon miR-17 overexpression. Since the function of PKD2 in cultured endothelial cells has not been investigated so far, further experiments are needed to clarify the impact of PKD2 on EC proliferation in the absence of laminar shear stress.

It is likely that other proteins, either direct miR-17 targets or proteins indirectly affected by the change in miR-17 level, are involved in this pro-proliferative shift. Consistently, Cloonan et al. observed an increased proliferation of HEK293T cells upon miR-17 overexpression and proved that a rise of pro-proliferative transcripts due to secondary and tertiary effects was the cause [155].

Moreover, cell cycle regulators like p21 as a member of the family of CDK inhibitors or cyclin D1 have been shown to function in cellular events beyond cell cycle control such as cell migration [225, 226]. Impaired expression of these proteins as observed upon Pre-17 transfection may disorganize vessel growth by causing an imbalance between proliferation and migration. This aspect might explain the stronger effects of miR-17 and miR-20a in the spheroid model mimicking tip and stalk cell guided angiogenic sprouting compared to those in the tube formation assay. Since the effect of p21 on endothelial cell proliferation and apoptosis was shown to critically depend on p21 expression level [227] and this also might be true for Cyclin D1, determining the exact contributions of both genes to coordinated vessel growth represents a challenge. The fact that microRNAs often target genes with opposing function, but nevertheless push the cell in a specific direction, illustrates the complexity of the processes determining cell fate and emphasizes once more one of the basic principles in cell biology that the ratio of oponent activities determines the outcome.

d) Effect of miR-17 on extracellular matrix and endothelial matrix metalloproteinases

In transgenic mice overexpressing miR-17, Shan et al. documented a profound reduction of high molecular weight fibronectin and fibronectin type-III domain containing 3A (FNDC3A) in different organs of the animals. Fibronectin protein was also downregulated after miR-17 overexpression in a rat endothelial cell line implying that miR-17 can affect ECM composition [166]. Functionally, overexpression of miR-17 resulted in impaired cell adhesion, migration and proliferation in these cells. Indeed, our microarray analysis revealed a 1.4 fold downregulation of FNDC3A and a 1.25 fold decrease of FNDC3B upon miR-17 overexpression, which are both predicted miR-17

targets according to the targetscan algorithm, although these changes were statistically not significant. Fibronectin 1 is not predicted to be a miR-17 target and FN1 mRNA was not changed in the microarray after Pre-17 transfection into HUVECs. As microRNAs are capable of controlling translation of target mRNAs without changing the mRNA level, western blot analysis is necessary to shed light on the regulation of fibronectin and both fibronectin type-III domain containing proteins by miR-17 in HUVECs.

Since MMP2, a secreted matrix metalloproteinase, which is involved in angiogenesis and degrades collagen I, is a predicted miR-17 target and was slightly downregulated on the mRNA level after miR-17 overexpression, we performed gelatin zymography to test whether miR-17 inhibition or overexpression affects MMP2 activity. The three most prominent clear bands were attributed to the latent pro-MMP2 (68 kD), the intermediate MMP2 (64 kD) and the active MMP2 (62 kD). However, we could not detect any differences in MMP2 activity in gelatin zymography implicating that miR-17 does not affect collagen degradation at least not under normal culture conditions and when collagen is used in its hydrolysed state as gelatin.

e) JAK1 as a novel target of miR-17 in endothelial cells and angiogenesis

Microarray analysis after miR-17 overexpression revealed a profound downregulation of the Janus Kinase (JAK) 1 mRNA and this downregulation could reproducibly be detected on the protein level. Cloning of four copies of the miR-17 binding site found in the 3´ UTR of JAK1 mRNA into a luciferase reporter vector verified a direct regulatory effect of miR-17. JAK1 is one of four members (JAK1, JAK2, JAK3 and TYK2) of the Janus kinase family of non-receptor tyrosine kinases which transduce cytokine signals from membrane receptors via phosphorylation of Signal Transducers and Activators of Transcription (STATs) into the nucleus to alter gene expression. JAK1 knockout in mice resulted in growth retardation during embryonic development, perinatal lethality and severe adverse effects on lymphocyte development. Moreover, macrophages, embryonic fibroblasts and cardiomyocytes isolated from JAK1 knockout offspring revealed hindered responses to cytokines that bind to class II cytokine receptors, cytokine receptors that utilize the γ_c subunit for signalling, and the gp130 subunit dependent family of cytokine receptors manifesting non-redundant roles of JAK1 in the signalling that arises in this subset of receptors [202]. JAK1 was reported to be essential for the IL-6-induced phosphorylation of STAT1 and STAT3 in fibrosarcoma cells [228]. Moreover, Shimoda et al. demonstrated a critical role for JAK1 in G-CSF-mediated STAT3 and STAT5 phosphorylation in myeloid cells [229]. STAT3 affects a variety of biological processes including apoptosis, proliferation and inflammation. Cardiomyocyte restricted knockout of STAT3 resulted in reduced myocardial capillary density in the postnatal mouse heart due to paracrine inhibition of endothelial cell proliferation [230]. We analysed JAK1

function in endothelial cells by siRNA-mediated inhibition and observed decreased sprouting of spheroids in vitro and blunted phosphorylation of STAT3 in nonstimulated HUVECs and in response to the cytokines IL-6, FGF-2, GM-CSF and IFN-α. We did not look at the phosphorylation status of the other STAT transcription factors expressed in HUVECs, although JAK1 probably also accomplishes phosphorylation of STAT1, STAT5b and STAT6. STAT3 itself was reported to be targeted by miR-17 in lung epithelial cells [168], but overexpression of miR-17 did neither reduce STAT3 mRNA nor protein in ECs in our hands (data not shown). Since after depletion of JAK1 a considerable signal for phosphorylated STAT3 remained in the IL-6 stimulated ECs, other kinases must be involved in IL-6-induced STAT3 phosphorylation in endothelial cells. Besides JAK1, JAK2 and TYK2 are also expressed in endothelial cells and are probably responsible for phosphorylation of STAT3 in response to IL-6 in the absence of JAK1. JAK3 expression is rather restricted to hematopoetic cells [231]. In endothelial cells, JAK1 and TYK2 were shown to mediate the hypoxia independent upregulation of Hif-1α in response to IFN-α [232] and are involved in urokinase-type plasminogen activator (uPA)-induced phosphorylation of STAT1 [233], a signalling pathway that might control EC proliferation and/or migration during angiogenesis caused by vascular injury. By using a siRNA and microRNA inhibitor double transfection approach, we could demonstrate that JAK1 depletion reduced the pro-angiogenic activity of miR-17 inhibition and validated therewith the causal relationship of miR-17 and JAK1 in angiogenesis. To our knowledge, this is the first study that addressed the function of JAK1 in angiogenesis in vitro.

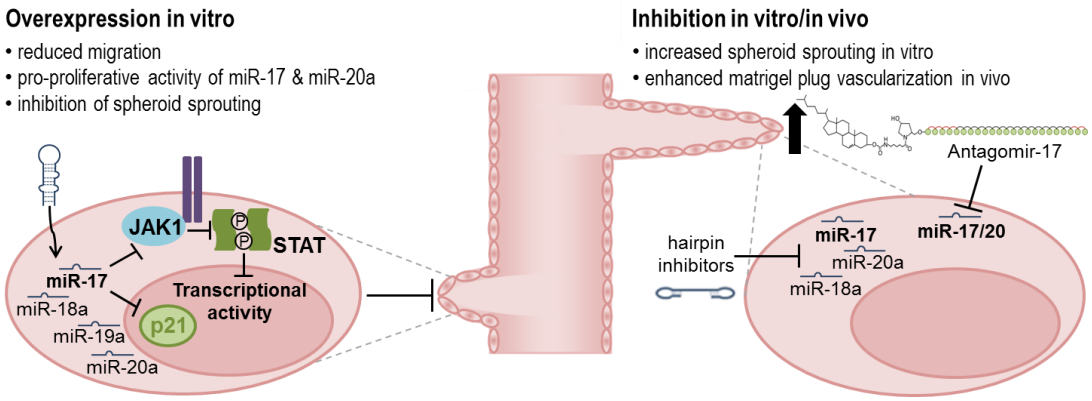

Figure V.3: **Cell-intrinsic effect of members of the miR-17-92 cluster on angiogenic capacity of endothelial cells.** Overexpression of miR-17, -18a, -19a and -20a impairs angiogenic sprouting in vitro. At least in part, the anti-angiogenic activity of miR-17 is based on the direct regulation of the cell cycle dependent kinase inhibitor p21 and the Janus kinase 1 (JAK1) which results in decreased signaling via STAT proteins. Vice versa, inhibition of miR-17, -18a and -20a promotes angiogenic sprouting in vitro. Only combined inhibition of miR-17 and miR-20a by Antagomir-17 enhances vascularization in vivo.

Generally, we observed stronger effects for miR-17 than for miR-20a overexpressing ECs in assays addressing miR function and on common miR-17/20 downstream targets (e.g. JAK1, p21); BIM represented an exception to this rule. Although we used similar concentrations of Pre-17 and

Pre-20a to overexpress both miRs in HUVECs in vitro, less mature miR-20a could be detected compared with mature miR-17. Differences in overexpression efficiency of both miRs may account for the distinct effects of miR-17 and -20a on downstream targets. But it is essential to mention, that at the beginning of the study we used a miR detection method employing a universal TaqMan probe and self-designed primers. Since amplification of miR-17 and miR-20a in the reverse transcription reaction was achieved with the identical stem-loop primer, and the qPCR detection was based on a universal TaqMan probe and a universal reverse primer, the detection specifity was determined by the forward primer. Due to differences in sequence, the forward primers for miR-17 and miR-20a might have had different amplification efficiencies accounting for the differences in mature miR levels detected. Therefore, we used the commercially available TaqMan MicroRNA Assays which promised higher specificity by applying miR specific forward primer and TaqMan probes in the qPCR quantification step. Using this method, we confirmed that Antagomir-17 not only blocked microRNA-17 but also miR-20a in vivo. This is consisted with reports of several other groups which observed knockdown of other members of the miR-17 seed family when using inhibitors targeting miR-17 [168, 196]. However, we did not measure the side effects of Antagomir-17 towards other members of the miR-17 seed family except for miR-20a. At least the miRs of the paralogous miR-106a-363 cluster seem frequently not to be expressed [168, 183], of which miR-106a and miR-20b belong to the miR-17 seed family.

B. Applicability of microRNA inhibition as therapeutic approach for pulmonary arterial hypertension

1. Evaluation of different Antagomirs in animal models of PAH

The research efforts of recent years manifested dysregulated microRNA expression in a variety of diseases and provided evidence that disease pathology can partially be attributed to the dysregulation of specific miRs. In 2010, Caruso et al. published their microRNA expression profiles gained by screening lung tissue of chronic hypoxic and monocrotaline (MCT) treated rats [203]. Among others, they observed time dependent alterations of members of the miR-17-92 cluster and miR-21 during the course of disease progression. Whereas miR-21 levels were not significantly changed in the lungs of chronic hypoxic rats but profoundly lowered in MCT treated rats, levels of the miR-17-92 cluster members miR-17, -19b, -20a and -92a were elevated at specific time points in both rat models. Since microRNAs affect whole signalling pathways and cellular processes by regulating the expression of several genes at the same time, they represent an

attractive therapeutic target. The current medical treatment of PAH patients is largely restricted to vasodilators such as endothelin-receptor antagonists, phosphodiesterase-5 inhibitors and prostanoids (prostacyclin and analogues) which provide only symptomatic relief. Drugs that intervene with pathological remodelling of the pulmonary vasculature by targeting endothelial dysfunction, apoptosis-resistance and proliferation of pulmonary smooth muscle cells may render beneficial effects and provide a valuable therapeutic option. Hence, we aimed to elucidate the applicability of microRNA inhibition by Antagomirs in animal models of pulmonary arterial hypertension in a collaborational project within the Excellence Cluster Cardiopulmonary Systems (ECCPS) with the group of Dr. Ralph Schermuly from the University of Gießen Lung Centre. Antagomirs, which are chemically modified and cholesterol conjugated antisense molecules of microRNAs, were shown to be effective in downregulating miR expression in vivo in a variety of organs [194]. Due to the fact that miR-17 and miR-92a were both shown to be upregulated in lung tissue of pulmonary hypertensive rats, we employed Antagomir-17 and Antagomir-92a in the study. MiR-21 is upregulated in fibroblasts of the failing heart and Antagomir-21 was shown to reduce cardiac fibrosis, thereby preventing dilatation of the left ventricle and normalizing fractional shortening in a mouse model of left-heart hypertrophy [204]. Since the increased pulmonary vascular resistance in PAH leads to right-heart hypertrophy, we also analysed the effects of Antagomir-21 in the PAH animal models.

First, we tested all three Antagomirs in chronic hypoxia-induced pulmonary arterial hypertension in mice. Low oxygen tension causes constriction of pulmonary vessels to reduce blood flow to less ventilated regions of the lung, thereby ensuring the ventilation-perfusion match. If the entire lung experiences hypoxia, pulmonary vasoconstriction leads to a rise in pulmonary vascular resistance. Chronic hypoxia results in increased muscularization of pulmonary arteries by stimulating proliferation of smooth muscle cells. Due to increased pulmonary vascular resistance, mice suffer from right heart hypertrophy. However, the pathological changes are largely reversible upon return of the animals to normoxic conditions [234]. Therefore, chronic hypoxia elicits a rather mild form of PAH.

Although the knockdown efficiency after one injection of the individual Antagomirs varied considerably in the lungs of normoxic mice, miR-17, -21 and -92a were all efficiently and significantly decreased in tissue of chronic hypoxic mice treated with 5 injections of the individual Antagomirs.

Regarding hemodynamics, Antagomir-17 revealed the most beneficial effects by significantly decreasing right ventricular systolic pressure (RVSP) and increasing pulmonary artery acceleration time (PAAT). Antagomir-21 also decreased RVSP, whereas Antagomir-92a did not affect any hemodynamic parameter. Right heart hypertrophy was significantly reduced in A-17 but not in

A-21 and A-92a treated mice. Interestingly, all three Antagomirs improved the muscularization pattern of the pulmonary arteries. MiR-17 is well-known to enhance proliferation of different cell types [140, 155, 170]. MiR-21 was shown to be upregulated in response to hypoxia in PASMCs and promoted their proliferation which could be confined by miR-21 inhibition [235], thus explaining the beneficial effect of Antagomir-21 on arterial muscularization. So far, the biological function of miR-92a has not been studied in vascular smooth muscle cell, but it was reported that miR-92a promotes proliferation of myeloid cells [178] but had no effect on endothelial cell growth [119].

Since Antagomir-17 achieved the most beneficial effect in chronic hypoxia-induced PAH, we additionally addressed the therapeutic value of this Antagomir in a second PAH animal model, i.e. the monocrotaline injury model. Monocrotaline is a phytotoxin found in seeds of the plant *Crotalaria spectabilis*. Monocrotaline is metabolized by liver resident mixed function oxidases producing the reactive bifunctional cross-linking compound MCT pyrrole. Since the lungs are the first eminent vascular bed distal to the liver, MCT mainly harms the pulmonary vasculature. The detailed mechanism of PAH induction by MCT is not known, but pathology involves direct damage of the endothelium, strong inflammatory response and structural remodelling that includes enhanced muscularization of pulmonary arteries [236]. Although we reduced Antagomir dose to 5 mg/kg bw and the number of injections to 2 in the rats, miR-17 was still almost completely depleted in lung tissue of the examined animals. Similar to the chronic hypoxia mouse model, we observed a significant improvement of RVSP and PAAT upon Antagomir-17 treatment. Although the effect of Antagomir-17 on right heart ventricular hypertrophy was not statistically significant, cardiac output was completely recovered. Antagomir-17 treatment also partially reversed the MCT-induced changes in the muscularization pattern of the pulmonary arteries supporting an involvement of miR-17 in the regulation of SMC proliferation and/or survival.

2. Mechanism of action of Antagomir-17 in PAH

To gain first hints towards the mechanism responsible for the beneficial effects of Antagomir-17 in experimental PAH, we analysed the rat lungs for miR-17 targets. Since BMPR2 expression and BMP signalling were shown to be frequently decreased in patients suffering from PAH and in PAH animal models [33, 205], we focused on analyzing the expression of BMPR2, Smad5 and the BMP downstream target ID1. Additionally, we measured the transcript level of TGFBR2 which is known to be involved in the activation of contractile protein expression in SMCs in response to TGF-β [208]. De-differentiation of SMCs into the proliferative phenotype is frequently associated with vascular diseases. EFNB1 mRNA expression was determined since it was demonstrated to

be highly expressed in freshly isolated lung ECs [207] and was profoundly downregulated in lung tissue of monocrotaline treated rats according to a microarray analysis of our collaboration partners (data not shown). Compared to the transcripts of BMPR2, Smad5, ID1 and EFNB1 which were decreased by more than 50% in MCT treated rats, the decline of TGFBR2 mRNA was rather moderate. Whereas the mRNAs for BMPR2, Smad5, ID1 and EFNB1 were slightly increased in Antagomir-17 treated rats, TGFBR2 transcript remained unchanged compared to the control animals. Unfortunately, we did not succeed in detecting BMPR2 protein via Western blot analysis of total lung lysate. This might be due to the fact that BMPR2 expression seemed to be restricted to cells of the pulmonary vasculature, mainly endothelial cells [33] which constitute around 1/3 of an entire rat lung [237]. Perhaps the fraction of BMPR2 of the total protein amount is too low to detect it via Western blot analysis. Immunohistochemistry could be used as an alternative method. Although Brock et al. demonstrated that BMPR2 is targeted by miR-17 and miR-20a in HEK cells [149], BMPR2 mRNA was neither altered on the mRNA level after overexpression of miR-17 in HPASMCs nor on mRNA and protein level in miR-17 overexpressing HUVECs. These results suggest that BMPR2 might be no target of miR-17 in HPASMCs and endothelial cells. BMPR2 protein could not be detected in HPASMCs which is consistent with the literature reporting low expression of BMPR2 in arterial smooth muscle in healthy human lung tissue [33].

In contrast to the BMPR2, the TGFBR2 was indeed targeted by miR-17 in HPASMCs. TGF-β1 is known to promote lung fibrosis by inducing the differentiation of fibroblasts into myofibroblast which secrete large amounts of collagen [238]. In vascular smooth muscle cells TGF-β signalling is crucial for the differentiation of SMCs into the contractile phenotype. Aortic SMCs from individuals carrying heterozygous mutations of the TGFBR2 gene, display reduced expression of a variety of contractile proteins [208]. However, alterations of TGFBR2 levels in HPASMCs had no profound effects on the expression of the contractile proteins α-actin 2, calponin 1 and smoothelin under standard culture conditions. To finally clarify the impact of miR-17-mediated regulation of TGFBR2 on expression of contractile proteins, further experiments are needed involving TGF-β1 stimulation of HPASMCs.

However, Antagomir-17 treatment of pulmonary hypertensive rats profoundly upregulated mRNA and protein expression of the cell cycle inhibitor p21. Since Antagomir-17 ameliorated muscularization of pulmonary arteries in both animal models, we further addressed the biological function of miR-17 in pulmonary artery smooth muscle cells. Upon miR-17 overexpression, the proliferation of HPASMCs was dramatically increased and impaired p21 expression was observed. Vice versa, p21 was slightly upregulated in Antagomir-17 treated SMCs. According to the literature, p21 is a well established regulator of SMC proliferation [239, 240]. Therefore, we suggest that

Antagomir-17 improves pulmonary hemodynamics by increasing the expression of the cell cycle inhibitor p21 in smooth muscle cells, thus interfering with pathological muscularization of pulmonary arteries.

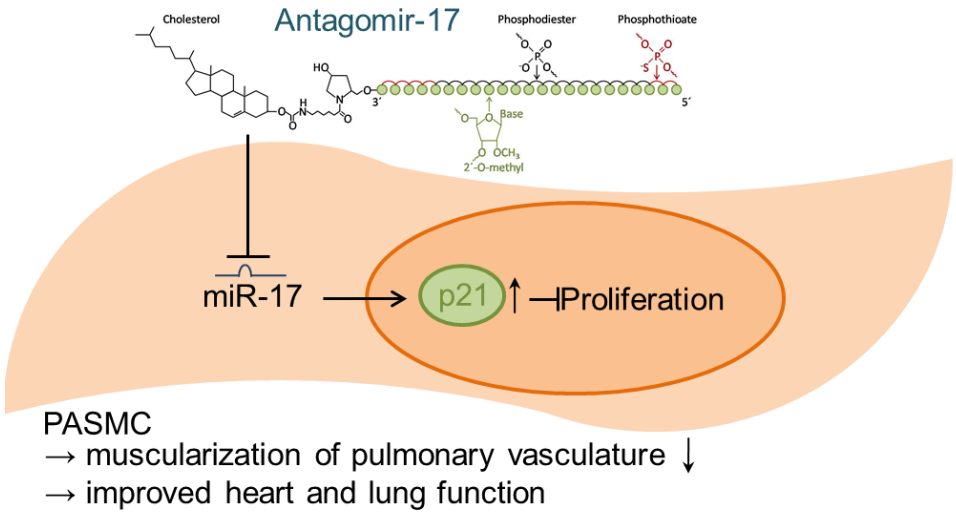

Figure V.4: **Antagomir-17 represses proliferation of smooth muscle cells by increasing the cyclin dependent kinase inhibitor p21.**

VI. Conclusion

Almost two decades ago, microRNAs were discovered as novel posttranscriptional regulators of gene expression. Since then, research efforts have uncovered their involvement in the control of various cellular processes including migration, proliferation and cell survival. Even more complex events, such as the formation of new blood vessels or organ development, have been shown to be tightly regulated and orchestrated by microRNAs. Due to their crucial regulatory role in tissue homeostasis in vertebrates, it does not come as a big surprise that dysregulated microRNA expression is associated with pathology of diverse diseases. In this regard, the miR-17-92 cluster is a prime example since it has become famous for its amplified expression in tumours and its oncogenic potential. Our lab demonstrated the expression of the members of the miR-17-92 cluster, namely miR-17, -18a, -19a, -20a, -19b and -92a, in endothelial cells and provided evidence for the anti-angiogenic activity of miR-92a in ECs as well as its important regulatory role in tissue recovery after ischemia.

In this work we addressed the function of the remaining members of the miR-17-92 cluster, i.e. miR-17, miR-18a, miR-19a and miR-20a, in endothelial cells and angiogenesis. Surprisingly, the individual members all displayed anti-angiogenic properties in endothelial cells in vitro, although overexpression of the whole cluster in transformed colonocytes was shown to promote tumour angiogenesis in a mouse model. In this context, we provide evidence that the individual miRs differentially affect the paracrine angiogenic activity of endothelial and tumour cells. Moreover, Antagomir-mediated inhibition of miR-17/20 in a mouse tumour model did not affect tumour angiogenesis, although miR-17/20 inhibition profoundly increased vascularization of Matrigel plugs. Thus, our research efforts suggest a differential involvement of the members of the miR-17-92 cluster in physiological and tumour angiogenesis. Additionally, we identified Janus kinase (JAK) 1 as a novel miR-17 target in endothelial cells and demonstrated the involvement of JAK1 in angiogenesis and in the phosphorylation of STAT3 in response to different cytokines in vitro. Overall, inhibition of specific members of the miR-17-92 cluster might represent an attractive therapeutic strategy to enhance angiogenesis in ischemic diseases.

In the second part of the present work we investigated the therapeutic value of Antagomir-mediated microRNA inhibition in animal models of pulmonary arterial hypertension. Collectively, inhibition of miR-17 by the respective Antagomir revealed a significant improvement of pulmonary hemodynamics and cardiac function in both the chronic hypoxia mouse model and the monocrotaline-induced lung injury rat model. Histomorphometric analysis of the lungs of the pulmonary hypertensive mice and rats uncovered a significant reduction of disease associated musculariza-

tion of pulmonary arteries in Antagomir-17 treated animals compared to the control animals indicating interference with smooth muscle cell proliferation or survival. Probing of lung tissue of the pulmonary hypertensive rats for selected miR-17 targets uncovered a profound increase in the expression of the cyclin dependent kinase inhibitor p21 in the Antagomir-17 treated rats suggesting that inhibition of miR-17 impairs proliferation by impeding cell cycle progression. Analysis of miR-17 function in human smooth muscle cells in vitro corroborated the results from the animal experiments by demonstrating pro-proliferative activity of miR-17 and decreased levels of p21 in these cells. Collectively, our results indicate that Antagomir-17 improves pulmonary hemodynamics and cardiac function by interfering with vascular remodelling within the lung. Hence, inhibition of miR-17 might be of therapeutic value to ameliorate the disease pattern in pulmonary arterial hypertension.

In summary, the present work provides insights into the regulatory functions of members of the miR-17-92 cluster, especially miR-17, in blood vessels and suggests that specific inhibition of members of the miR-17-92 cluster might be a novel option to treat vascular diseases.

FUNKTIONELLE CHARAKTERISIERUNG VON MITGLIEDERN DES MICRORNA-17-92-CLUSTERS IM BLUTGEFÄßSYSTEM

Dissertation

zur Erlangung des Doktorgrades der Naturwissenschaften

vorgelegt beim Fachbereich Biochemie, Chemie und Pharmazie (FB 14)

der Goethe-Universität in Frankfurt am Main

von Carmen Döbele

aus Waldshut

Frankfurt am Main 2011

(D30)

VII. Zusammenfassung

MicroRNAs (miRs) sind eine Klasse von nicht codierenden RNA-Molekülen, die in Vertebraten endogen exprimiert werden und in ihrer maturen Form die Genexpression auf posttranskriptioneller Ebene regulieren, indem sie die mRNA-Translation inhibieren oder den Abbau der mRNA induzieren. Die Forschung der letzten zwei Jahrzehnte hat gezeigt, dass miRs in die Regulation zellulärer Prozesse, wie Apoptose, Proliferation und Differenzierung, involviert sind und eine dysregulierte miR-Expression mit diversen Krankheiten assoziiert sein kann. Der miR-17-92-Cluster beinhaltet die sieben maturen MicroRNAs miR-17-5p (miR-17), miR-17-3p (miR-17*), miR-18a, miR-19a, miR-20a, miR-19b und miR-92a, die durch Prozessierung durch den kernständigen Drosha- und den cytosolischen Dicer-Multienzymkomplex aus demselben polycistronischen Primärtranskript hervorgehen. Der miR-17-92-Cluster wurde ursprünglich aufgrund seines oncogenen Potentials identifiziert, das zum Teil auf die Tumorangiogenese-fördernde Wirkung von miR-18 und miR-19 sowie den pro-proliferativen Effekt von miR-17 and miR-20a zurückgeführt wurde. Die konstitutive Deletion des miR-17-92-Clusters in Mäusen führt zu postnataler Letalität aufgrund von Herz- und Lungendefekten, was auf eine funktionelle Bedeutung des Clusters in der Entwicklung beider Organe hindeutet. Unsere Arbeitsgruppe hat bereits nachgewiesen, dass das miR-17-92-Clustermitglied miR-92a in Endothelzellen anti-angiogene Eigenschaften besitzt und eine Inhibition dieser MicroRNA mittels Antagomirs die Bildung von Blutgefäßen fördert und somit die Geweberegeneration nach ischämischen Erkrankungen im Mausmodell unterstützt. Hingegen ist die Funktion der übrigen Clustermitglieder im vaskulären System größtenteils ungeklärt.
Das Ziel der vorliegenden Arbeit war die funktionelle Charakterisierung der einzelnen Clustermitglieder miR-17, miR-18a, miR-19a und miR-20a in Endothelzellen und endothelzellabhängigen Prozessen.

Funktion der miR-17-92-Clustermitglieder in physiologischer Angiogenese

Um die Wirkung der einzelnen miRs auf Angiogenese *in vitro* zu untersuchen, wurden miR-17, miR-18a, miR-19a und miR-20a durch Transfektion von kommerziell erhältlichen Vorläufermolekülen (Precursor) in Endothelzellen aus humanen Nabelschnüren (HUVEC) überexprimiert und ihr Einfluss auf die kapillare Aussprossung im 3D-Sphäroidmodell untersucht. Die Überexpression jeder einzelnen miR führte zu einer signifikanten Reduktion der kapillaren Aussprossungen, wobei miR-17 den stärksten Effekt aufwies. Umgekehrt hatte die Inhibition von miR-17, miR-18a and miR-20a durch Transfektion von kommerziell erhältlichen Hairpin-Inhibitoren eine verstärkte kapillare Aussprossung im Sphäroid-Modell zur Folge.

Um die Funktion der einzelnen Clustermitglieder in der Angiogenese *in vivo* zu untersuchen, wurde das Matrigelplug-Mausmodell mit der systemischen Gabe von spezifischen Cholesterin-konjugierten microRNA-Inhibitoren, so genannten Antagomirs, kombiniert. Drei Injektionen Antagomir-17, Antagomir-18a, Antagomir-19a und Antagomir-20a in einer Dosis von jeweils 8 mg/kg Körpergewicht führten in den Herzen der behandelten Tiere zu einer spezifischen Reduktion der entsprechenden maturen miRs. Lediglich Antagomir-17 hemmte nicht nur miR-17-5p, sondern auch miR-20a, die sich in ihrer Sequenz lediglich in zwei Nukleotiden voneinander unterscheiden. Vermutlich aufgrund der kombinierten Inhibition von miR-17 und miR-20a erzielte Antagomir-17 bei Verwendung von drei Injektionen einen signifikanten Anstieg der Vaskularisierung der Matrigelplugs, wohingegen Antagomir-18a, -19a und -20a bei gleicher Dosierung keine signifikanten Effekte aufwiesen. Auch bei Verwendung von nur einer Injektion Antagomir-17, konnte eine erhöhte Vaskularisierung der Matrigelplugs verzeichnet werden, obgleich die Daten keine statistische Signifikanz erreichten.

Funktion der miR-17-92-Clustermitglieder in der Tumorangiogenese

Die in dieser Studie beobachtete zellintrinsische anti-angiogene Wirkung der einzelnen Mitglieder des miR-17-92-Clusters in Endothelzellen steht im Widerspruch zu der bereits in der Literatur dokumentierten Erhöhung der Tumorangiogenese nach Implantation von Tumorzellen, die den gesamten Cluster verstärkt exprimieren. Um zu untersuchen, ob diese unterschiedlichen Beobachtungen auf einer differentiellen Regulation der parakrinen Aktivität von Tumor- und Endothelzellen durch die miR-17-92-Clustermitglieder beruhen, transfizierten wir Lewis Lung Carcinoma 1 (LLC1)-Zellen und HUVEC mit den einzelnen miR-Precursorn und testeten die Wirkung des konditionierten Mediums auf die kapillare Ausprossung von HUVEC im *in vitro*-Sphäroidmodell. Tatsächlich zeigte das konditionierte Medium der Tumorzellen im Vergleich zu dem der Endothelzellen nach Überexpression von miR-17, miR-18a oder miR-19a eine leicht verstärkte angiogene Aktivität im Späroidmodell. Diese Daten deuten auf zelltypspezifische Unterschiede der Clustermitglieder in Tumor- und Endothelzellen hin.

Da Überexpression und Inhibition von miR-17 im Sphäroidmodell *in vitro* und die Antagomir-17 vermittelte Hemmung von miR-17/20 *in vivo* ingesamt die stärksten Effekte auf Angiogenese erzielt hatten, untersuchten wir die Wirkung von Antagomir-17 auf Tumorwachstum und -angiogenese durch Kombination des LLC1-Maustumormodells mit der systemischen Antagomir-Gabe. Eine Injektion Antagomir-17 führte zu einer moderaten Reduktion der miR-17-Expression im Tumorgewebe und hatte einen leichten Anstieg des Tumorwachstums zur Folge, jedoch ohne die Vaskularisierung der Tumore zu fördern, obwohl mit der gleichen Dosis an Antagomir-17 im

Matrigelplug-Modell eine verstärkte Plug-Vaskularisierung erzielt wurde. Auch eine stärkere Reduktion der miR-17-Expression im Tumorgewebe durch zwei Injektionen Antagomir-17 zeigte keinen pro-angiogenen Effekt auf die Tumorvaskulatur und führte zu keinem veränderten Tumorwachstum. Ebenso zeigte die Behandlung von LLC1-Zellen *in vitro* mit Antagomir-17 keine Veränderung der Proliferationsrate. Zusammenfassend deuten unsere Daten darauf hin, dass eine Inhibition von miR-17 unter physiologischen Bedingungen die Bildung neuer Blutgefäße fördert, jedoch Tumorangiogenese vermutlich aufgrund von kompensatorischen Effekten in den Tumorzellen nicht beeinflusst.

Zielgene von miR-17 in Endothelzellen

Aufgrund des signifikanten Effekts von miR-17-Überexpression und -Inhibition auf Angiogenese *in vitro* und *in vivo* galt unser Interesse der Identifikation von Angiogenese relevanten Zielgenen dieser MicroRNA. Aus diesem Grund führten wir eine Microarray-Genexpressionsanalyse nach Überexpression von miR-17 in HUVECs durch und verglichen die herunterregulierten Transkripte mit den Zielgenen, die durch den Targetscan-Algorithmus für miR-17 vorhergesagt wurden, um möglichst direkte Zielgene zu identifizieren. Unter den signifikant herunterregulierten Transkripten befanden sich miR-17-Zielgene, die bereits in anderen Zelltypen validiert wurden, wie die Serin/Threonin-Rezeptorkinase TGFBR2 (TGF-β-Rezeptor Typ 2), der Transkriptionsfaktor E2F1 und der Zellzyklusinhibitor p21.

Die Proliferation von Endothelzellen stellt eine wichtige Komponente im Angiogenese-Prozess dar. Die Überexpression von miR-17 und miR-20a führte zu einer verringerten Expression des Zellzyklusinhibitors p21 auf mRNA- und Proteinebene und verursachte einen signifikanten Anstieg des Anteils an Endothelzellen in der S-Phase des Zellzyklus. Doppeltransfektionsexperimente mit MicroRNA-Hairpin-Inhibitoren und siRNA ergaben, dass die siRNA vermittelte Reduktion von p21 dem pro-angiogenen Effekt der miR-17-Inhibition entgegenwirkte und demonstrierten somit die Beteiligung von p21 in Angiogenese *in vitro*.

Zu den am stärksten herunterregulierten Transkripten zählte die Janus Kinase 1 (JAK1). JAK1 ist ein Mitglied der rezeptorassoziierten Janus-Tyrosinkinasen. Diese dienen im Cytoplasma als Antwort auf diverse Cytokine der Phosphorylierung verschiedener Mitglieder der signal transducer and activator of transcription (STAT)-Transkriptionsfaktoren, die im Anschluss als Dimere im Zellkern die Genexpression regulieren. STAT3 ist für seinen regulatorischen Einfluss auf Apoptose, Proliferation und Inflammation bekannt. miR-17 und miR-20a waren die einzigen Mitglieder des miR-17-92 Cluster, die nach ihrer Überexpression eine deutliche Reduktion von JAK1 auf Proteinebene bewirkten. Umgekehrt führte die Inhibition von miR-17 in Endothelzellen zu

einem Anstieg des JAK1-Proteinlevels. Durch Einführung von vier Kopien der miR-17-Bindestelle aus der 3´ untranslatierten Region (UTR) der JAK1-mRNA und einer mutierten Variante im Anschluss an ein Luciferase-Reportergen bestätigte sich, dass es dabei tatsächlich um eine funktionale miR-17-Bindestelle handelt. Somit konnten wir JAK1 als neues Zielgen von miR-17 in Endothelzellen validieren.

Funktionell führte die siRNA vermittelte Reduktion von JAK1 zu vermindertem Sprouting im Sphäroid-Modell *in vitro* und beeinträchtigte die Phosphorylierung von STAT3 unter basalen Bedingungen und besonders nach Stimulation mit den inflammatorischen Cytokinen Interleukin-6 (IL-6) und Interferon-α (IFN-α). Doppeltransfektionsexperimente mit MicroRNA-Hairpin-Inhibitoren und siRNA bestätigten, dass eine Reduktion der JAK1-Expression den pro-angiogenen Effekt der miR-17-Inhibition im *in vitro* Sphäroid-Modell und die verstärkte STAT3-Phosphorylierung verhinderte. Folglich ist JAK1 in Endothelzellen auch funktionell relevant.

Zusammenfassend weisen unsere Daten darauf hin, dass der anti-angiogene Effekt von miR-17 durch die Dysregulation einer Vielzahl von Proteinen zustande kommt und zumindest für den Zellzyklusregulator p21 und die Januskinase 1 konnten wir eine Beteiligung an Angiogenese *in vitro* nachweisen.

MicroRNA-Inhibition als therapeutische Strategie in arteriellem Lungenbluthochdruck

Der zweite Teil der Arbeit zeigt Daten aus einem Kollaborationsprojekt mit dem Lungenzentrum der Universität Gießen, in dem das therapeutische Potential der Antagomir-vermittelten Inhibition von miR-17, miR-21 und miR-92a in Tiermodellen des arteriellen Lungenbluthochdrucks (pulmonal-arterielle Hypertonie: PAH) untersucht wurde. Die PAH ist eine Erkrankung des pulmonalen Gefäßsystems, die durch eine Erhöhung des Lungengefäßwiderstandes und dem damit verbundenen Anstieg des Bluthochdrucks im Lungenkreislauf charakterisiert ist. Als Folge der erhöhten Belastung des Herzens kommt es zur Rechts-Herzinsuffizienz, die letztendlich zum Tod durch Herzversagen führt. Auf zellulärer Ebene lässt sich die Erkrankung auf eine extensive Umstrukturierung der Lungengefäße zurückführen, die vor allem durch verengte Lungenarterien und erhöhte Gefäßmuskularisierung sowie gelegentlicher Thrombus-Bildung gekennzeichnet ist. Im letzten Jahr wurde in zwei Rattenmodellen der pulmonalen Hypertonie gezeigt, dass die Expression von Mitgliedern des miR-17-92-Clusters sowie miR-21 in Lungengewebe der erkrankten Ratten einer zeitabhängigen Dysregulation unterliegt. Daher untersuchten wir zuerst das therapeutische Potential von Antagomir-17, Antagomir-21 und Antagomir-92a in der Hypoxie-induzierten pulmonalen Hypertonie in Mäusen. Obwohl alle drei Antagomirs bei Verwendung von fünf Injektionen den Hypoxie induzierten Anstieg der Arterien-Muskularisierung signifikant reduzierten, zeigte lediglich

Antagomir-17 eine generelle Verbesserung der Hämodynamik innerhalb der Lunge und eine reduzierte Hypertrophie des rechten Ventrikels. Die positiven Effekte von Antagomir-17 auf Lungen- und Herzfunktion wurden in einem zweiten Tiermodell, der Monocrotalin-induzierten PAH in Ratten, bestätigt.

Die Untersuchung des Lungengewebes der Ratten belegte einen starken Anstieg des Zellzyklusinhibitors p21 sowohl auf mRNA- als auch Proteinebene. In *in vitro*-Experimenten mit humanen Gefäßmuskelzellen aus der Lunge konnten wir zeigen, dass die Überexpression von miR-17 zu einer deutlichen Reduktion von p21-mRNA führt und eine Erhöhung der Zellproliferation zur Folge hatte. Umgekehrt führte die Antagomir-vermittelte Inhibition von miR-17 zu einem Anstieg von p21-mRNA und -Protein in den Gefäßmuskelzellen. Basierend auf diesen Daten schlussfolgerten wir, dass Antagomir-17 vermutlich durch Steigerung der p21-Expression die Proliferation der Gefäßmuskelzellen in der Lunge bremst und somit die Muskularisierung der Lungenarterien reduziert, was zu einer Verbesserung der Hämodynamik in der Lunge beiträgt. In den Gefäßmuskelzellen *in vitro* beobachteten wir zusätzlich einen starken regulatorischen Effekt von miR-17 auf die Expression der Serin/Threonin-Rezeptorkinase TGFBR2, für die in der Literatur eine Funktion bei der Regulation des kontraktilen Phänotyps von Gefäßen beschrieben ist. Allerdings konnten wir unter normalen Zellkulturbedingungen keine signifikanten Veränderungen in den mRNA-Leveln der kontraktilen Proteine α-Aktin 2, Calponin 1 and Smoothelin durch miR-17-Überexpression und -Inhibition in den Gefäßmuskelzellen detektieren.

Ingesamt zeigen die Daten dieser Arbeit, dass miR-17 regulatorische Funktionen in Blutgefäßen erfüllt und eine Inhibition dieser MicroRNA bei Herz-Kreislauferkrankungen von therapeutischem Nutzen sein könnte.

VIII. References

1. Wu, R.-M., et al. *Real-Time PCR Quantification of Plant miRNAs Using Universal Probe Library Technology*. Biochemica, 2007. **2**, 12-15.
2. Wang, Y. and G. Oliver, *Current views on the function of the lymphatic vasculature in health and disease.* Genes Dev, 2010. **24**(19): p. 2115-26.
3. Tortora, G.J. and B.H. Derrickson, *Essentials of Anatomy and Physiology*. 8th International student edition ed2010, New York: John Wiley & Sons Ltd.
4. *Human Anatomy*. Available from: http://academic.kellogg.edu/herbrandsonc/bio201_mckinley/Cardiovascular_System.htm.
5. *Education Program in Anatomy - MacAnatomy* Available from: http://macanatomy.mcmaster.ca/index.php?option=com_content&view=article&id=233%3Aarteries-capillaries-and-veins&catid=47%3Acardiovascular-anatomy&Itemid=169.
6. Krstic, R.V., *Human Microscopic Anatomy: An Atlas for Students of Medicine and Biology* 1997, Berlin: Springer.
7. Adams, R.H., *Molecular control of arterial-venous blood vessel identity.* J Anat, 2003. **202**(1): p. 105-12.
8. Webb, R.C., *Smooth muscle contraction and relaxation.* Adv Physiol Educ, 2003. **27**(1-4): p. 201-6.
9. Jain, R.K., *Molecular regulation of vessel maturation.* Nat Med, 2003. **9**(6): p. 685-93.
10. Ramcharan, K.S., et al., *The endotheliome: A new concept in vascular biology.* Thromb Res, 2010.
11. Sumpio, B.E., J.T. Riley, and A. Dardik, *Cells in focus: endothelial cell.* Int J Biochem Cell Biol, 2002. **34**(12): p. 1508-12.
12. Senger, D.R., et al., *Tumor cells secrete a vascular permeability factor that promotes accumulation of ascites fluid.* Science, 1983. **219**(4587): p. 983-5.
13. Michiels, C., *Endothelial cell functions.* J Cell Physiol, 2003. **196**(3): p. 430-43.
14. Dejana, E., *Endothelial cell-cell junctions: happy together.* Nat Rev Mol Cell Biol, 2004. **5**(4): p. 261-70.
15. Wamhoff, B.R., D.K. Bowles, and G.K. Owens, *Excitation-transcription coupling in arterial smooth muscle.* Circ Res, 2006. **98**(7): p. 868-78.
16. Beamish, J.A., et al., *Molecular regulation of contractile smooth muscle cell phenotype: implications for vascular tissue engineering.* Tissue Eng Part B Rev, 2010. **16**(5): p. 467-91.
17. Rensen, S.S., P.A. Doevendans, and G.J. van Eys, *Regulation and characteristics of vascular smooth muscle cell phenotypic diversity.* Neth Heart J, 2007. **15**(3): p. 100-8.
18. Strilic, B., et al., *Electrostatic cell-surface repulsion initiates lumen formation in developing blood vessels.* Curr Biol, 2010. **20**(22): p. 2003-9.
19. Strilic, B., et al., *The molecular basis of vascular lumen formation in the developing mouse aorta.* Dev Cell, 2009. **17**(4): p. 505-15.
20. Carmeliet, P., *Angiogenesis in life, disease and medicine.* Nature, 2005. **438**(7070): p. 932-6.
21. le Noble, F., et al., *Flow regulates arterial-venous differentiation in the chick embryo yolk sac.* Development, 2004. **131**(2): p. 361-75.
22. Lin, F.J., M.J. Tsai, and S.Y. Tsai, *Artery and vein formation: a tug of war between different forces.* EMBO Rep, 2007. **8**(10): p. 920-4.
23. Ribatti, D., B. Nico, and E. Crivellato, *Morphological and molecular aspects of physiological vascular morphogenesis.* Angiogenesis, 2009. **12**(2): p. 101-11.
24. Nussenbaum, F. and I.M. Herman, *Tumor angiogenesis: insights and innovations.* J Oncol, 2010. **2010**: p. 132641.
25. Chung, A.S., J. Lee, and N. Ferrara, *Targeting the tumour vasculature: insights from physiological angiogenesis.* Nat Rev Cancer, 2010. **10**(7): p. 505-14.
26. Battegay, E.J., *Angiogenesis: mechanistic insights, neovascular diseases, and therapeutic prospects.* J Mol Med, 1995. **73**(7): p. 333-46.
27. Rabinovitch, M., *Molecular pathogenesis of pulmonary arterial hypertension.* J Clin Invest, 2008. **118**(7): p. 2372-9.
28. Davies, R.J. and N.W. Morrell, *Molecular mechanisms of pulmonary arterial hypertension: role of mutations in the bone morphogenetic protein type II receptor.* Chest, 2008. **134**(6): p. 1271-7.
29. Morrell, N.W., et al., *Cellular and molecular basis of pulmonary arterial hypertension.* J Am Coll Cardiol, 2009. **54**(1 Suppl): p. S20-31.

30. Sartore, S., et al., *Contribution of adventitial fibroblasts to neointima formation and vascular remodeling: from innocent bystander to active participant.* Circ Res, 2001. **89**(12): p. 1111-21.
31. Jurasz, P., et al., *Role of apoptosis in pulmonary hypertension: from experimental models to clinical trials.* Pharmacol Ther, 2010. **126**(1): p. 1-8.
32. Eickelberg, O. and R.E. Morty, *Transforming growth factor beta/bone morphogenic protein signaling in pulmonary arterial hypertension: remodeling revisited.* Trends Cardiovasc Med, 2007. **17**(8): p. 263-9.
33. Atkinson, C., et al., *Primary pulmonary hypertension is associated with reduced pulmonary vascular expression of type II bone morphogenetic protein receptor.* Circulation, 2002. **105**(14): p. 1672-8.
34. Amaral, P.P. and J.S. Mattick, *Noncoding RNA in development.* Mamm Genome, 2008. **19**(7-8): p. 454-92.
35. Wightman, B., I. Ha, and G. Ruvkun, *Posttranscriptional regulation of the heterochronic gene lin-14 by lin-4 mediates temporal pattern formation in C. elegans.* Cell, 1993. **75**(5): p. 855-62.
36. Lau, N.C., et al., *An abundant class of tiny RNAs with probable regulatory roles in Caenorhabditis elegans.* Science, 2001. **294**(5543): p. 858-62.
37. Lagos-Quintana, M., et al., *Identification of novel genes coding for small expressed RNAs.* Science, 2001. **294**(5543): p. 853-8.
38. Mattick, J.S., *The genetic signatures of noncoding RNAs.* PLoS Genet, 2009. **5**(4): p. e1000459.
39. Brosnan, C.A. and O. Voinnet, *The long and the short of noncoding RNAs.* Curr Opin Cell Biol, 2009. **21**(3): p. 416-25.
40. Ghildiyal, M. and P.D. Zamore, *Small silencing RNAs: an expanding universe.* Nat Rev Genet, 2009. **10**(2): p. 94-108.
41. Tsai, L.M. and D. Yu, *MicroRNAs in common diseases and potential therapeutic applications.* Clin Exp Pharmacol Physiol, 2010. **37**(1): p. 102-7.
42. Scholer, N., et al., *Serum microRNAs as a novel class of biomarkers: a comprehensive review of the literature.* Exp Hematol, 2010. **38**(12): p. 1126-30.
43. Fire, A., et al., *Potent and specific genetic interference by double-stranded RNA in Caenorhabditis elegans.* Nature, 1998. **391**(6669): p. 806-11.
44. Zamore, P.D., et al., *RNAi: double-stranded RNA directs the ATP-dependent cleavage of mRNA at 21 to 23 nucleotide intervals.* Cell, 2000. **101**(1): p. 25-33.
45. Elbashir, S.M., W. Lendeckel, and T. Tuschl, *RNA interference is mediated by 21- and 22-nucleotide RNAs.* Genes Dev, 2001. **15**(2): p. 188-200.
46. Hammond, S.M., et al., *An RNA-directed nuclease mediates post-transcriptional gene silencing in Drosophila cells.* Nature, 2000. **404**(6775): p. 293-6.
47. Bernstein, E., et al., *Role for a bidentate ribonuclease in the initiation step of RNA interference.* Nature, 2001. **409**(6818): p. 363-6.
48. Elbashir, S.M., et al., *Duplexes of 21-nucleotide RNAs mediate RNA interference in cultured mammalian cells.* Nature, 2001. **411**(6836): p. 494-8.
49. Hutvagner, G., et al., *A cellular function for the RNA-interference enzyme Dicer in the maturation of the let-7 small temporal RNA.* Science, 2001. **293**(5531): p. 834-8.
50. Hutvagner, G. and P.D. Zamore, *A microRNA in a multiple-turnover RNAi enzyme complex.* Science, 2002. **297**(5589): p. 2056-60.
51. Lee, Y., et al., *The nuclear RNase III Drosha initiates microRNA processing.* Nature, 2003. **425**(6956): p. 415-9.
52. Smalheiser, N.R. and V.I. Torvik, *Mammalian microRNAs derived from genomic repeats.* Trends Genet, 2005. **21**(6): p. 322-6.
53. Borchert, G.M., W. Lanier, and B.L. Davidson, *RNA polymerase III transcribes human microRNAs.* Nat Struct Mol Biol, 2006. **13**(12): p. 1097-101.
54. Fukuda, T., et al., *DEAD-box RNA helicase subunits of the Drosha complex are required for processing of rRNA and a subset of microRNAs.* Nat Cell Biol, 2007. **9**(5): p. 604-11.
55. Diederichs, S. and D.A. Haber, *Dual role for argonautes in microRNA processing and posttranscriptional regulation of microRNA expression.* Cell, 2007. **131**(6): p. 1097-108.
56. Krol, J., I. Loedige, and W. Filipowicz, *The widespread regulation of microRNA biogenesis, function and decay.* Nat Rev Genet, 2010. **11**(9): p. 597-610.
57. Berezikov, E., et al., *Mammalian mirtron genes.* Mol Cell, 2007. **28**(2): p. 328-36.
58. Cheloufi, S., et al., *A dicer-independent miRNA biogenesis pathway that requires Ago catalysis.* Nature, 2010. **465**(7298): p. 584-9.
59. Brodersen, P. and O. Voinnet, *Revisiting the principles of microRNA target recognition and mode of action.* Nat Rev Mol Cell Biol, 2009. **10**(2): p. 141-8.

60. Lytle, J.R., T.A. Yario, and J.A. Steitz, *Target mRNAs are repressed as efficiently by microRNA-binding sites in the 5' UTR as in the 3' UTR.* Proc Natl Acad Sci U S A, 2007. **104**(23): p. 9667-72.
61. Qin, W., et al., *miR-24 regulates apoptosis by targeting the open reading frame (ORF) region of FAF1 in cancer cells.* PLoS One, 2010. **5**(2): p. e9429.
62. Yekta, S., I.H. Shih, and D.P. Bartel, *MicroRNA-directed cleavage of HOXB8 mRNA.* Science, 2004. **304**(5670): p. 594-6.
63. Piao, X., et al., *CCR4-NOT deadenylates mRNA associated with RNA-induced silencing complexes in human cells.* Mol Cell Biol, 2010. **30**(6): p. 1486-94.
64. Fabian, M.R., N. Sonenberg, and W. Filipowicz, *Regulation of mRNA translation and stability by microRNAs.* Annu Rev Biochem, 2010. **79**: p. 351-79.
65. Stark, A., et al., *Animal MicroRNAs confer robustness to gene expression and have a significant impact on 3'UTR evolution.* Cell, 2005. **123**(6): p. 1133-46.
66. Kedde, M. and R. Agami, *Interplay between microRNAs and RNA-binding proteins determines developmental processes.* Cell Cycle, 2008. **7**(7): p. 899-903.
67. Weinmann, L., et al., *Importin 8 is a gene silencing factor that targets argonaute proteins to distinct mRNAs.* Cell, 2009. **136**(3): p. 496-507.
68. Vasudevan, S., Y. Tong, and J.A. Steitz, *Switching from repression to activation: microRNAs can up-regulate translation.* Science, 2007. **318**(5858): p. 1931-4.
69. Orom, U.A., F.C. Nielsen, and A.H. Lund, *MicroRNA-10a binds the 5'UTR of ribosomal protein mRNAs and enhances their translation.* Mol Cell, 2008. **30**(4): p. 460-71.
70. Kim, D.H., et al., *MicroRNA-directed transcriptional gene silencing in mammalian cells.* Proc Natl Acad Sci U S A, 2008. **105**(42): p. 16230-5.
71. Place, R.F., et al., *MicroRNA-373 induces expression of genes with complementary promoter sequences.* Proc Natl Acad Sci U S A, 2008. **105**(5): p. 1608-13.
72. Bernstein, E., et al., *Dicer is essential for mouse development.* Nat Genet, 2003. **35**(3): p. 215-7.
73. McGrath, K.E., et al., *Circulation is established in a stepwise pattern in the mammalian embryo.* Blood, 2003. **101**(5): p. 1669-76.
74. Yang, W.J., et al., *Dicer is required for embryonic angiogenesis during mouse development.* J Biol Chem, 2005. **280**(10): p. 9330-5.
75. Giraldez, A.J., et al., *MicroRNAs regulate brain morphogenesis in zebrafish.* Science, 2005. **308**(5723): p. 833-8.
76. Otsuka, M., et al., *Impaired microRNA processing causes corpus luteum insufficiency and infertility in mice.* J Clin Invest, 2008. **118**(5): p. 1944-54.
77. Suarez, Y., et al., *Dicer-dependent endothelial microRNAs are necessary for postnatal angiogenesis.* Proc Natl Acad Sci U S A, 2008. **105**(37): p. 14082-7.
78. Kuehbacher, A., et al., *Role of Dicer and Drosha for endothelial microRNA expression and angiogenesis.* Circ Res, 2007. **101**(1): p. 59-68.
79. Suarez, Y., et al., *Dicer dependent microRNAs regulate gene expression and functions in human endothelial cells.* Circ Res, 2007. **100**(8): p. 1164-73.
80. Heusschen, R., et al., *MicroRNAs in the tumor endothelium: novel controls on the angioregulatory switchboard.* Biochim Biophys Acta, 2010. **1805**(1): p. 87-96.
81. Smits, M., et al., *Down-regulation of miR-101 in endothelial cells promotes blood vessel formation through reduced repression of EZH2.* PLoS One, 2011. **6**(1): p. e16282.
82. Li, D., et al., *MicroRNA-125a/b-5p inhibits endothelin-1 expression in vascular endothelial cells.* J Hypertens, 2010. **28**(8): p. 1646-54.
83. Fish, J.E., et al., *miR-126 regulates angiogenic signaling and vascular integrity.* Dev Cell, 2008. **15**(2): p. 272-84.
84. van Solingen, C., et al., *Antagomir-mediated silencing of endothelial cell specific microRNA-126 impairs ischemia-induced angiogenesis.* J Cell Mol Med, 2009. **13**(8A): p. 1577-85.
85. Wang, S., et al., *The endothelial-specific microRNA miR-126 governs vascular integrity and angiogenesis.* Dev Cell, 2008. **15**(2): p. 261-71.
86. Harris, T.A., et al., *MicroRNA-126 regulates endothelial expression of vascular cell adhesion molecule 1.* Proc Natl Acad Sci U S A, 2008. **105**(5): p. 1516-21.
87. Zernecke, A., et al., *Delivery of microRNA-126 by apoptotic bodies induces CXCL12-dependent vascular protection.* Sci Signal, 2009. **2**(100): p. ra81.
88. Zou, J., et al., *Two functional microRNA-126s repress a novel target gene p21-activated kinase 1 to regulate vascular integrity in zebrafish.* Circ Res, 2011. **108**(2): p. 201-9.

89. Fang, Y., et al., *MicroRNA-10a regulation of proinflammatory phenotype in athero-susceptible endothelium in vivo and in vitro.* Proc Natl Acad Sci U S A, 2010. **107**(30): p. 13450-5.
90. Chen, Y. and D.H. Gorski, *Regulation of angiogenesis through a microRNA (miR-130a) that down-regulates antiangiogenic homeobox genes GAX and HOXA5.* Blood, 2008. **111**(3): p. 1217-26.
91. Yin, K.J., et al., *Peroxisome proliferator-activated receptor delta regulation of miR-15a in ischemia-induced cerebral vascular endothelial injury.* J Neurosci, 2010. **30**(18): p. 6398-408.
92. Anand, S., et al., *MicroRNA-132-mediated loss of p120RasGAP activates the endothelium to facilitate pathological angiogenesis.* Nat Med, 2010. **16**(8): p. 909-14.
93. Gonsalves, C.S. and V.K. Kalra, *Hypoxia-mediated expression of 5-lipoxygenase-activating protein involves HIF-1alpha and NF-kappaB and microRNAs 135a and 199a-5p.* J Immunol, 2010. **184**(7): p. 3878-88.
94. Suarez, Y., et al., *Cutting edge: TNF-induced microRNAs regulate TNF-induced expression of E-selectin and intercellular adhesion molecule-1 on human endothelial cells: feedback control of inflammation.* J Immunol, 2010. **184**(1): p. 21-5.
95. Cheng, W., et al., *microRNA-155 regulates angiotensin II type 1 receptor expression in umbilical vein endothelial cells from severely pre-eclamptic pregnant women.* Int J Mol Med, 2011. **27**(3): p. 393-9.
96. Kazenwadel, J., M.Z. Michael, and N.L. Harvey, *Prox1 expression is negatively regulated by miR-181 in endothelial cells.* Blood, 2010. **116**(13): p. 2395-401.
97. Qin, X., et al., *MicroRNA-19a mediates the suppressive effect of laminar flow on cyclin D1 expression in human umbilical vein endothelial cells.* Proc Natl Acad Sci U S A, 2010. **107**(7): p. 3240-4.
98. Yeligar, S., H. Tsukamoto, and V.K. Kalra, *Ethanol-induced expression of ET-1 and ET-BR in liver sinusoidal endothelial cells and human endothelial cells involves hypoxia-inducible factor-1alpha and microrNA-199.* J Immunol, 2009. **183**(8): p. 5232-43.
99. McArthur, K., et al., *MicroRNA-200b Regulates Vascular Endothelial Growth Factor-Mediated Alterations in Diabetic Retinopathy.* Diabetes, 2011.
100. Weber, M., et al., *MiR-21 is induced in endothelial cells by shear stress and modulates apoptosis and eNOS activity.* Biochem Biophys Res Commun, 2010. **393**(4): p. 643-8.
101. Sabatel, C., et al., *MicroRNA-21 Exhibits Antiangiogenic Function by Targeting RhoB Expression in Endothelial Cells.* PLoS One, 2011. **6**(2): p. e16979.
102. Fasanaro, P., et al., *MicroRNA-210 modulates endothelial cell response to hypoxia and inhibits the receptor tyrosine kinase ligand Ephrin-A3.* J Biol Chem, 2008. **283**(23): p. 15878-83.
103. Chan, S.Y., et al., *MicroRNA-210 controls mitochondrial metabolism during hypoxia by repressing the iron-sulfur cluster assembly proteins ISCU1/2.* Cell Metab, 2009. **10**(4): p. 273-84.
104. Chan, L.S., et al., *Role of microRNA-214 in ginsenoside-Rg1-induced angiogenesis.* Eur J Pharm Sci, 2009. **38**(4): p. 370-7.
105. Wang, K.C., et al., *Role of microRNA-23b in flow-regulation of Rb phosphorylation and endothelial cell growth.* Proc Natl Acad Sci U S A, 2010. **107**(7): p. 3234-9.
106. Menghini, R., et al., *MicroRNA 217 modulates endothelial cell senescence via silent information regulator 1.* Circulation, 2009. **120**(15): p. 1524-32.
107. Thum, T., *MicroRNAs as Therapeutic Targets during Cardiac Remodeling*, in *Keystone Symposium MicroRNAs and Human Disease*2011: Fairmont Banff Springs.
108. Small, E.M., et al., *MicroRNA-218 regulates vascular patterning by modulation of Slit-Robo signaling.* Circ Res, 2010. **107**(11): p. 1336-44.
109. Chen, Y., et al., *Regulation of the expression and activity of the antiangiogenic homeobox gene GAX/MEOX2 by ZEB2 and microRNA-221.* Mol Cell Biol, 2010. **30**(15): p. 3902-13.
110. Poliseno, L., et al., *MicroRNAs modulate the angiogenic properties of HUVECs.* Blood, 2006. **108**(9): p. 3068-71.
111. Dentelli, P., et al., *microRNA-222 controls neovascularization by regulating signal transducer and activator of transcription 5A expression.* Arterioscler Thromb Vasc Biol, 2010. **30**(8): p. 1562-8.
112. Wurdinger, T., et al., *miR-296 regulates growth factor receptor overexpression in angiogenic endothelial cells.* Cancer Cell, 2008. **14**(5): p. 382-93.
113. Patel, N., et al., *Involvement of miR-30c and miR-301a in immediate induction of plasminogen activator inhibitor-1 by placental growth factor in human pulmonary endothelial cells.* Biochem J, 2011. **434**(3): p. 473-82.
114. Wang, X.H., et al., *MicroRNA-320 expression in myocardial microvascular endothelial cells and its relationship with insulin-like growth factor-1 in type 2 diabetic rats.* Clin Exp Pharmacol Physiol, 2009. **36**(2): p. 181-8.

115. Ghosh, G., et al., *Hypoxia-induced microRNA-424 expression in human endothelial cells regulates HIF-alpha isoforms and promotes angiogenesis.* J Clin Invest, 2010. **120**(11): p. 4141-54.
116. Nakashima, T., et al., *Down-regulation of mir-424 contributes to the abnormal angiogenesis via MEK1 and cyclin E1 in senile hemangioma: its implications to therapy.* PLoS One, 2010. **5**(12): p. e14334.
117. Ito, T., S. Yagi, and M. Yamakuchi, *MicroRNA-34a regulation of endothelial senescence.* Biochem Biophys Res Commun, 2010. **398**(4): p. 735-40.
118. Caporali, A., et al., *Deregulation of microRNA-503 contributes to diabetes mellitus-induced impairment of endothelial function and reparative angiogenesis after limb ischemia.* Circulation, 2011. **123**(3): p. 282-91.
119. Bonauer, A., et al., *MicroRNA-92a controls angiogenesis and functional recovery of ischemic tissues in mice.* Science, 2009. **324**(5935): p. 1710-3.
120. Cha, S.T., et al., *MicroRNA-519c suppresses hypoxia-inducible factor-1alpha expression and tumor angiogenesis.* Cancer Res, 2010. **70**(7): p. 2675-85.
121. Grundmann, S., et al., *MicroRNA-100 Regulates Neovascularization by Suppression of Mammalian Target of Rapamycin in Endothelial and Vascular Smooth Muscle Cells.* Circulation, 2011. **123**(9): p. 999-1009.
122. Ni, C.W., H. Qiu, and H. Jo, *MicroRNA-663 upregulated by oscillatory shear stress plays a role in inflammatory response of endothelial cells.* Am J Physiol Heart Circ Physiol, 2011.
123. Albinsson, S., et al., *MicroRNAs are necessary for vascular smooth muscle growth, differentiation, and function.* Arterioscler Thromb Vasc Biol, 2010. **30**(6): p. 1118-26.
124. Cordes, K.R., et al., *miR-145 and miR-143 regulate smooth muscle cell fate and plasticity.* Nature, 2009. **460**(7256): p. 705-10.
125. Boettger, T., et al., *Acquisition of the contractile phenotype by murine arterial smooth muscle cells depends on the Mir143/145 gene cluster.* J Clin Invest, 2009. **119**(9): p. 2634-47.
126. Chan, M.C., et al., *Molecular basis for antagonism between PDGF and the TGFbeta family of signalling pathways by control of miR-24 expression.* EMBO J, 2010. **29**(3): p. 559-73.
127. Davis, B.N., et al., *Induction of microRNA-221 by platelet-derived growth factor signaling is critical for modulation of vascular smooth muscle phenotype.* J Biol Chem, 2009. **284**(6): p. 3728-38.
128. Liu, X., et al., *A necessary role of miR-221 and miR-222 in vascular smooth muscle cell proliferation and neointimal hyperplasia.* Circ Res, 2009. **104**(4): p. 476-87.
129. Davis, B.N., et al., *SMAD proteins control DROSHA-mediated microRNA maturation.* Nature, 2008. **454**(7200): p. 56-61.
130. Chen, J., et al., *Induction of microRNA-1 by myocardin in smooth muscle cells inhibits cell proliferation.* Arterioscler Thromb Vasc Biol, 2011. **31**(2): p. 368-75.
131. Yu, M.L., et al., *Vascular Smooth Muscle Cell Proliferation Is Influenced by let-7d MicroRNA and Its Interaction With KRAS.* Circ J, 2011. **75**(3): p. 703-9.
132. Leeper, N.J., et al., *MicroRNA-26a is a novel regulator of vascular smooth muscle cell function.* J Cell Physiol, 2011. **226**(4): p. 1035-43.
133. Chen, K.C., et al., *OxLDL up-regulates microRNA-29b, leading to epigenetic modifications of MMP-2/MMP-9 genes: a novel mechanism for cardiovascular diseases.* FASEB J, 2011.
134. Sun, S.G., et al., *miR-146a and Kruppel-like factor 4 form a feedback loop to participate in vascular smooth muscle cell proliferation.* EMBO Rep, 2011. **12**(1): p. 56-62.
135. Ota, A., et al., *Identification and characterization of a novel gene, C13orf25, as a target for 13q31-q32 amplification in malignant lymphoma.* Cancer Res, 2004. **64**(9): p. 3087-95.
136. Mourelatos, Z., et al., *miRNPs: a novel class of ribonucleoproteins containing numerous microRNAs.* Genes Dev, 2002. **16**(6): p. 720-8.
137. Tanzer, A. and P.F. Stadler, *Molecular evolution of a microRNA cluster.* J Mol Biol, 2004. **339**(2): p. 327-35.
138. Mendell, J.T., *miRiad roles for the miR-17-92 cluster in development and disease.* Cell, 2008. **133**(2): p. 217-22.
139. He, L., et al., *A microRNA polycistron as a potential human oncogene.* Nature, 2005. **435**(7043): p. 828-33.
140. Fontana, L., et al., *Antagomir-17-5p abolishes the growth of therapy-resistant neuroblastoma through p21 and BIM.* PLoS One, 2008. **3**(5): p. e2236.
141. Yu, Z., et al., *A cyclin D1/microRNA 17/20 regulatory feedback loop in control of breast cancer cell proliferation.* J Cell Biol, 2008. **182**(3): p. 509-17.
142. Hossain, A., M.T. Kuo, and G.F. Saunders, *Mir-17-5p regulates breast cancer cell proliferation by inhibiting translation of AIB1 mRNA.* Mol Cell Biol, 2006. **26**(21): p. 8191-201.
143. Taguchi, A., et al., *Identification of hypoxia-inducible factor-1 alpha as a novel target for miR-17-92 microRNA cluster.* Cancer Res, 2008. **68**(14): p. 5540-5.

144. Pichiorri, F., et al., *MicroRNAs regulate critical genes associated with multiple myeloma pathogenesis.* Proc Natl Acad Sci U S A, 2008. **105**(35): p. 12885-90.
145. Olive, V., et al., *miR-19 is a key oncogenic component of mir-17-92.* Genes Dev, 2009. **23**(24): p. 2839-49.
146. Mu, P., et al., *Genetic dissection of the miR-17~92 cluster of microRNAs in Myc-induced B-cell lymphomas.* Genes Dev, 2009. **23**(24): p. 2806-11.
147. O'Donnell, K.A., et al., *c-Myc-regulated microRNAs modulate E2F1 expression.* Nature, 2005. **435**(7043): p. 839-43.
148. Li, H., et al., *miR-17-5p promotes human breast cancer cell migration and invasion through suppression of HBP1.* Breast Cancer Res Treat, 2011. **126**(3): p. 565-75.
149. Brock, M., et al., *Interleukin-6 modulates the expression of the bone morphogenic protein receptor type II through a novel STAT3-microRNA cluster 17/92 pathway.* Circ Res, 2009. **104**(10): p. 1184-91.
150. Dews, M., et al., *Augmentation of tumor angiogenesis by a Myc-activated microRNA cluster.* Nat Genet, 2006. **38**(9): p. 1060-5.
151. Mestdagh, P., et al., *The miR-17-92 microRNA cluster regulates multiple components of the TGF-beta pathway in neuroblastoma.* Mol Cell, 2010. **40**(5): p. 762-73.
152. Tagawa, H., et al., *Synergistic action of the microRNA-17 polycistron and Myc in aggressive cancer development.* Cancer Sci, 2007. **98**(9): p. 1482-90.
153. Volinia, S., et al., *A microRNA expression signature of human solid tumors defines cancer gene targets.* Proc Natl Acad Sci U S A, 2006. **103**(7): p. 2257-61.
154. Beveridge, N.J., et al., *Down-regulation of miR-17 family expression in response to retinoic acid induced neuronal differentiation.* Cell Signal, 2009. **21**(12): p. 1837-45.
155. Cloonan, N., et al., *The miR-17-5p microRNA is a key regulator of the G1/S phase cell cycle transition.* Genome Biol, 2008. **9**(8): p. R127.
156. Mavrakis, K.J., et al., *Genome-wide RNA-mediated interference screen identifies miR-19 targets in Notch-induced T-cell acute lymphoblastic leukaemia.* Nat Cell Biol, 2010. **12**(4): p. 372-9.
157. Xiao, C., et al., *Lymphoproliferative disease and autoimmunity in mice with increased miR-17-92 expression in lymphocytes.* Nat Immunol, 2008. **9**(4): p. 405-14.
158. Deshpande, A., et al., *3'UTR mediated regulation of the cyclin D1 proto-oncogene.* Cell Cycle, 2009. **8**(21): p. 3584-92.
159. Chen, Z.L., et al., *microRNA-92a promotes lymph node metastasis of human esophageal squamous cell carcinoma via E-cadherin.* J Biol Chem, 2010.
160. Ernst, A., et al., *De-repression of CTGF via the miR-17-92 cluster upon differentiation of human glioblastoma spheroid cultures.* Oncogene, 2010. **29**(23): p. 3411-22.
161. Scherr, M., et al., *Lentivirus-mediated antagomir expression for specific inhibition of miRNA function.* Nucleic Acids Res, 2007. **35**(22): p. e149.
162. Tsai, Z.Y., et al., *Identification of microRNAs regulated by activin A in human embryonic stem cells.* J Cell Biochem, 2010. **109**(1): p. 93-102.
163. Loven, J., et al., *MYCN-regulated microRNAs repress estrogen receptor-alpha (ESR1) expression and neuronal differentiation in human neuroblastoma.* Proc Natl Acad Sci U S A, 2010. **107**(4): p. 1553-8.
164. Liu, W.H., et al., *MicroRNA-18a prevents estrogen receptor-alpha expression, promoting proliferation of hepatocellular carcinoma cells.* Gastroenterology, 2009. **136**(2): p. 683-93.
165. Zhang, X., et al., *MicroRNA-19 (miR-19) regulates tissue factor expression in breast cancer cells.* J Biol Chem, 2011. **286**(2): p. 1429-35.
166. Shan, S.W., et al., *MicroRNA MiR-17 retards tissue growth and represses fibronectin expression.* Nat Cell Biol, 2009. **11**(8): p. 1031-8.
167. Yu, Z., et al., *microRNA 17/20 inhibits cellular invasion and tumor metastasis in breast cancer by heterotypic signaling.* Proc Natl Acad Sci U S A, 2010. **107**(18): p. 8231-6.
168. Carraro, G., et al., *miR-17 family of microRNAs controls FGF10-mediated embryonic lung epithelial branching morphogenesis through MAPK14 and STAT3 regulation of E-Cadherin distribution.* Dev Biol, 2009. **333**(2): p. 238-50.
169. Uchida, S., et al., *Characterization of the vulnerability to repeated stress in Fischer 344 rats: possible involvement of microRNA-mediated down-regulation of the glucocorticoid receptor.* Eur J Neurosci, 2008. **27**(9): p. 2250-61.
170. Sun, H., et al., *MicroRNA-17 post-transcriptionally regulates polycystic kidney disease-2 gene and promotes cell proliferation.* Mol Biol Rep, 2010. **37**(6): p. 2951-8.
171. Lewis, B.P., et al., *Prediction of mammalian microRNA targets.* Cell, 2003. **115**(7): p. 787-98.

172. Xu, X., et al., *Protein tyrosine phosphatase receptor-type O (PTPRO) is co-regulated by E2F1 and miR-17-92.* FEBS Lett, 2008. **582**(19): p. 2850-6.
173. Wang, Q., et al., *miR-17-92 cluster accelerates adipocyte differentiation by negatively regulating tumor-suppressor Rb2/p130.* Proc Natl Acad Sci U S A, 2008. **105**(8): p. 2889-94.
174. Fontana, L., et al., *MicroRNAs 17-5p-20a-106a control monocytopoiesis through AML1 targeting and M-CSF receptor upregulation.* Nat Cell Biol, 2007. **9**(7): p. 775-87.
175. Barbato, C., et al., *MicroRNA-92 modulates K(+) Cl(-) co-transporter KCC2 expression in cerebellar granule neurons.* J Neurochem, 2010. **113**(3): p. 591-600.
176. Dews, M., et al., *The myc-miR-17~92 axis blunts TGF{beta} signaling and production of multiple TGF{beta}-dependent antiangiogenic factors.* Cancer Res, 2010. **70**(20): p. 8233-46.
177. Liu, M., et al., *TNF-alpha is a novel target of miR-19a.* Int J Oncol, 2011. **38**(4): p. 1013-22.
178. Manni, I., et al., *The microRNA miR-92 increases proliferation of myeloid cells and by targeting p63 modulates the abundance of its isoforms.* FASEB J, 2009. **23**(11): p. 3957-66.
179. Dogar, A.M., H. Towbin, and J. Hall, *Suppression of latent TGF-beta1 restores growth inhibitory TGF-beta signaling through microRNAs.* J Biol Chem, 2011.
180. Ye, W., et al., *The effect of central loops in miRNA:MRE duplexes on the efficiency of miRNA-mediated gene regulation.* PLoS One, 2008. **3**(3): p. e1719.
181. Tili, E., et al., *GAM/ZFp/ZNF512B is central to a gene sensor circuitry involving cell-cycle regulators, TGF{beta} effectors, Drosha and microRNAs with opposite oncogenic potentials.* Nucleic Acids Res, 2010. **38**(21): p. 7673-88.
182. Lu, Y., et al., *Transgenic over-expression of the microRNA miR-17-92 cluster promotes proliferation and inhibits differentiation of lung epithelial progenitor cells.* Dev Biol, 2007. **310**(2): p. 442-53.
183. Ventura, A., et al., *Targeted deletion reveals essential and overlapping functions of the miR-17 through 92 family of miRNA clusters.* Cell, 2008. **132**(5): p. 875-86.
184. Hackl, M., et al., *miR-17, miR-19b, miR-20a, and miR-106a are down-regulated in human aging.* Aging Cell, 2010. **9**(2): p. 291-6.
185. Bonauer, A. and S. Dimmeler, *The microRNA-17-92 cluster: still a miRacle?* Cell Cycle, 2009. **8**(23): p. 3866-73.
186. Sylvestre, Y., et al., *An E2F/miR-20a autoregulatory feedback loop.* J Biol Chem, 2007. **282**(4): p. 2135-43.
187. Yan, H.L., et al., *Repression of the miR-17-92 cluster by p53 has an important function in hypoxia-induced apoptosis.* EMBO J, 2009. **28**(18): p. 2719-32.
188. Guil, S. and J.F. Caceres, *The multifunctional RNA-binding protein hnRNP A1 is required for processing of miR-18a.* Nat Struct Mol Biol, 2007. **14**(7): p. 591-6.
189. Michlewski, G., et al., *Posttranscriptional regulation of miRNAs harboring conserved terminal loops.* Mol Cell, 2008. **32**(3): p. 383-93.
190. Korbler, T., et al., *A simple method for RNA isolation from formalin-fixed and paraffin-embedded lymphatic tissues.* Exp Mol Pathol, 2003. **74**(3): p. 336-40.
191. *Applied Biosystems web site*. Available from: https://products.appliedbiosystems.com/ab/en/US/adirect/ab?cmd=catNavigate2&catID=601803&tab=DetailInfo.
192. Komor, M., et al., *Transcriptional profiling of human hematopoiesis during in vitro lineage-specific differentiation.* Stem Cells, 2005. **23**(8): p. 1154-69.
193. *TargetScanHuman Release 5.1*. Available from: http://www.targetscan.org/.
194. Krutzfeldt, J., et al., *Silencing of microRNAs in vivo with 'antagomirs'.* Nature, 2005. **438**(7068): p. 685-9.
195. Schermuly, R.T., et al., *Reversal of experimental pulmonary hypertension by PDGF inhibition.* J Clin Invest, 2005. **115**(10): p. 2811-21.
196. Takakura, S., et al., *Oncogenic role of miR-17-92 cluster in anaplastic thyroid cancer cells.* Cancer Sci, 2008. **99**(6): p. 1147-54.
197. Stetler-Stevenson, W.G., *Matrix metalloproteinases in angiogenesis: a moving target for therapeutic intervention.* J Clin Invest, 1999. **103**(9): p. 1237-41.
198. Sekine-Aizawa, Y., et al., *Matrix metalloproteinase (MMP) system in brain: identification and characterization of brain-specific MMP highly expressed in cerebellum.* Eur J Neurosci, 2001. **13**(5): p. 935-48.
199. Hla, T. and T. Maciag, *An abundant transcript induced in differentiating human endothelial cells encodes a polypeptide with structural similarities to G-protein-coupled receptors.* J Biol Chem, 1990. **265**(16): p. 9308-13.

200. Liu, Y., et al., *Edg-1, the G protein-coupled receptor for sphingosine-1-phosphate, is essential for vascular maturation.* J Clin Invest, 2000. **106**(8): p. 951-61.
201. Spiegel, S. and S. Milstien, *Sphingosine-1-phosphate: an enigmatic signalling lipid.* Nat Rev Mol Cell Biol, 2003. **4**(5): p. 397-407.
202. Rodig, S.J., et al., *Disruption of the Jak1 gene demonstrates obligatory and nonredundant roles of the Jaks in cytokine-induced biologic responses.* Cell, 1998. **93**(3): p. 373-83.
203. Caruso, P., et al., *Dynamic changes in lung microRNA profiles during the development of pulmonary hypertension due to chronic hypoxia and monocrotaline.* Arterioscler Thromb Vasc Biol, 2010. **30**(4): p. 716-23.
204. Thum, T., et al., *MicroRNA-21 contributes to myocardial disease by stimulating MAP kinase signalling in fibroblasts.* Nature, 2008. **456**(7224): p. 980-4.
205. Morty, R.E., et al., *Dysregulated bone morphogenetic protein signaling in monocrotaline-induced pulmonary arterial hypertension.* Arterioscler Thromb Vasc Biol, 2007. **27**(5): p. 1072-8.
206. Valdimarsdottir, G., et al., *Stimulation of Id1 expression by bone morphogenetic protein is sufficient and necessary for bone morphogenetic protein-induced activation of endothelial cells.* Circulation, 2002. **106**(17): p. 2263-70.
207. Favre, C.J., et al., *Expression of genes involved in vascular development and angiogenesis in endothelial cells of adult lung.* Am J Physiol Heart Circ Physiol, 2003. **285**(5): p. H1917-38.
208. Inamoto, S., et al., *TGFBR2 mutations alter smooth muscle cell phenotype and predispose to thoracic aortic aneurysms and dissections.* Cardiovasc Res, 2010. **88**(3): p. 520-9.
209. Carmeliet, P., et al., *Branching morphogenesis and antiangiogenesis candidates: tip cells lead the way.* Nat Rev Clin Oncol, 2009. **6**(6): p. 315-26.
210. Hughes, C.C., *Endothelial-stromal interactions in angiogenesis.* Curr Opin Hematol, 2008. **15**(3): p. 204-9.
211. *BD web site*. Available from: http://www.bdbiosciences.com/eu/cellculture/ecm/features/matrigel.jsp#search=%28Matrigel%29.
212. Edgell, C.J., C.C. McDonald, and J.B. Graham, *Permanent cell line expressing human factor VIII-related antigen established by hybridization.* Proc Natl Acad Sci U S A, 1983. **80**(12): p. 3734-7.
213. Edgell, C.J., et al., *Endothelium specific Weibel-Palade bodies in a continuous human cell line, EA.hy926.* In Vitro Cell Dev Biol, 1990. **26**(12): p. 1167-72.
214. Matsubara, H., et al., *Apoptosis induction by antisense oligonucleotides against miR-17-5p and miR-20a in lung cancers overexpressing miR-17-92.* Oncogene, 2007. **26**(41): p. 6099-105.
215. Png, K.J., et al., *Regulation of Cancer Metastasis by Human MicroRNAs*, in *Keystone Symposium MicroRNAs in Human Diseases*2011: Fairmont Banff Springs.
216. Kuhnert, F. and C.J. Kuo, *miR-17-92 angiogenesis micromanagement.* Blood, 2010. **115**(23): p. 4631-3.
217. Lim, L.P., et al., *Microarray analysis shows that some microRNAs downregulate large numbers of target mRNAs.* Nature, 2005. **433**(7027): p. 769-73.
218. Guo, H., et al., *Mammalian microRNAs predominantly act to decrease target mRNA levels.* Nature, 2010. **466**(7308): p. 835-40.
219. Selbach, M., et al., *Widespread changes in protein synthesis induced by microRNAs.* Nature, 2008. **455**(7209): p. 58-63.
220. Baek, D., et al., *The impact of microRNAs on protein output.* Nature, 2008. **455**(7209): p. 64-71.
221. Hahn, C. and M.A. Schwartz, *Mechanotransduction in vascular physiology and atherogenesis.* Nat Rev Mol Cell Biol, 2009. **10**(1): p. 53-62.
222. Kim, K., et al., *Polycystin 1 is required for the structural integrity of blood vessels.* Proc Natl Acad Sci U S A, 2000. **97**(4): p. 1731-6.
223. Ecder, T. and R.W. Schrier, *Cardiovascular abnormalities in autosomal-dominant polycystic kidney disease.* Nat Rev Nephrol, 2009. **5**(4): p. 221-8.
224. AbouAlaiwi, W.A., et al., *Ciliary polycystin-2 is a mechanosensitive calcium channel involved in nitric oxide signaling cascades.* Circ Res, 2009. **104**(7): p. 860-9.
225. Besson, A., S.F. Dowdy, and J.M. Roberts, *CDK inhibitors: cell cycle regulators and beyond.* Dev Cell, 2008. **14**(2): p. 159-69.
226. Li, Z., et al., *Cyclin D1 functions in cell migration.* Cell Cycle, 2006. **5**(21): p. 2440-2.
227. Bruhl, T., et al., *p21Cip1 levels differentially regulate turnover of mature endothelial cells, endothelial progenitor cells, and in vivo neovascularization.* Circ Res, 2004. **94**(5): p. 686-92.
228. Guschin, D., et al., *A major role for the protein tyrosine kinase JAK1 in the JAK/STAT signal transduction pathway in response to interleukin-6.* EMBO J, 1995. **14**(7): p. 1421-9.

229. Shimoda, K., et al., *Jak1 plays an essential role for receptor phosphorylation and Stat activation in response to granulocyte colony-stimulating factor.* Blood, 1997. **90**(2): p. 597-604.
230. Hilfiker-Kleiner, D., et al., *Signal Transducer and Activator of Transcription 3 Is Required for Myocardial Capillary Growth, Control of Interstitial Matrix Deposition, and Heart Protection From Ischemic Injury.* Circ Res, 2004. **95**(2): p. 187-195.
231. Yamaoka, K., et al., *The Janus kinases (Jaks).* Genome Biol, 2004. **5**(12): p. 253.
232. Gerber, S.A. and J.S. Pober, *IFN-{alpha} Induces Transcription of Hypoxia-Inducible Factor-1{alpha} to Inhibit Proliferation of Human Endothelial Cells.* J Immunol, 2008. **181**(2): p. 1052-1062.
233. Dumler, I., et al., *Urokinase activates the Jak/Stat signal transduction pathway in human vascular endothelial cells.* Arterioscler Thromb Vasc Biol, 1999. **19**(2): p. 290-7.
234. Marsboom, G.R. and S.P. Janssens, *Models for pulmonary hypertension.* Drug Discovery Today: Disease Models, 2004. **1**(3): p. 289-296.
235. Sarkar, J., et al., *MicroRNA-21 plays a Role in Hypoxia-mediated Pulmonary Artery Smooth Muscle Cell Proliferation and Migration.* Am J Physiol Lung Cell Mol Physiol, 2010. **299**(6): p. L861-71.
236. Stenmark, K.R., et al., *Animal models of pulmonary arterial hypertension: the hope for etiological discovery and pharmacological cure.* Am J Physiol Lung Cell Mol Physiol, 2009. **297**(6): p. L1013-32.
237. Martin, J. and I.N.H. White. *Preparation of Rat Lung Cells for Flow Cytometry*. Springer Protocols 1992; Available from: http://www.springerprotocols.com/Abstract/doi/10.1385/0-89603-204-3:363#CR1.
238. Arribillaga, L., et al., *Therapeutic effect of a peptide inhibitor of TGF-beta on pulmonary fibrosis.* Cytokine, 2011. **53**(3): p. 327-33.
239. Chang, M.W., et al., *Adenovirus-mediated over-expression of the cyclin/cyclin-dependent kinase inhibitor, p21 inhibits vascular smooth muscle cell proliferation and neointima formation in the rat carotid artery model of balloon angioplasty.* J Clin Invest, 1995. **96**(5): p. 2260-8.
240. Tanner, F.C., et al., *Differential effects of the cyclin-dependent kinase inhibitors p27(Kip1), p21(Cip1), and p16(Ink4) on vascular smooth muscle cell proliferation.* Circulation, 2000. **101**(17): p. 2022-5.

Eidesstattliche Erklärung

Hiermit versichere ich, dass ich die vorliegende Dissertation selbständig und nur unter zu Hilfenahme der hier angegebenen Quellen und Hilfsmitteln verfasst habe.
Die Dissertation wurde bisher keiner anderen Fakultät vorgelegt. Ich erkläre, dass ich bisher kein Promotionsverfahren erfolglos beendet habe und dass keine Aberkennung eines bereits erworbenen Doktorgrades vorliegt.

Frankfurt, den 03. Mai 2011

Carmen Döbele

Lebenslauf

PERSÖNLICHE ANGABEN

Name	Carmen Döbele
Geburtsdatum & -ort	29.08.1982 in Waldshut
Anschrift	Westerbachstraße 38, 60489 Frankfurt am Main
Familienstand	ledig

BERUFLICHE TÄTIGKEITEN

04/2008 – jetzt	Wissenschaftliche Mitarbeiterin am Institut für Kardiovaskuläre Regeneration, Zentrum für Molekulare Medizin, der Goethe-Universität Frankfurt unter der Leitung von Frau Prof. Stefanie Dimmeler

BERUFSAUSBILDUNG

04/2008 - jetzt	Promotionsstudium an der Goethe-Universität in Frankfurt am Main; Anfertigung der Dissertation bei Frau Prof. Stefanie Dimmeler am Institut für Kardiovaskuläre Regeneration, Zentrum für Molekulare Medizin, Goethe-Universität Frankfurt am Main Thema: *Functional characterization of members of the microRNA-17-92 cluster in the vascular system* Gutachter: Herr Prof. Volker Dötsch (FB 14) Frau Prof. Stefanie Dimmeler
10/2002 – 12/2007	Studium Diplom-Biochemie an der Goethe-Universität in Frankfurt am Main; Anfertigung der Diplomarbeit bei Herrn Prof. Bernd Groner am Georg-Speyer-Haus, chemotherapeutisches Forschungsinstitut, Frankfurt am Main Thema: *Expression einer konstitutiv aktiven Stat5-Variante in Brustepithelzellen und ihr Einfluss auf das Zellwachstum* Gutachter: Herr Prof. Bernd Ludwig (FB 14) Herr Prof. Bernd Groner

SCHULBILDUNG

1999 - 2002	Abitur an der Justus-von-Liebig-Schule in Waldshut
1993 - 1999	Mittlere Reife an der Realschule Tiengen

PUBLIKATIONEN	Pullamsetti, S.#, **Doebele, C.**#, Fischer, A., Savai, R., Kojonazarov, B., Dahal, B.K., Ghofrani, H.A., Weissmann, N., Grimminger, F., Bonauer, A., Seeger, W., Zeiher, A.M. and Dimmeler, S.#, Schermuly, R.T.#. *Inhibition of microRNA-17 improves lung and heart function in experimental pulmonary hypertension*. # contributed equally. in preparation **Doebele, C.**, Bonauer, A., Fischer, A., Scholz, A., Reiss, Y., Urbich, C., Hofmann, W.K., Zeiher, A.M. and Dimmeler, S. (2010). *Members of the microRNA-17-92 cluster exhibit a cell-intrinsic antiangiogenic function in endothelial cells*. Blood 115, 4944-4950 Bonauer, A., Carmona, G., Iwasaki, M., Mione, M., Koyanagi, M., Fischer, A., Burchfield, J., Fox, H., **Doebele, C.**, Ohtani, K., et al. (2009). *MicroRNA-92a controls angiogenesis and functional recovery of ischemic tissues in mice*. Science 324, 1710-1713
KONGRESSBEITRÄGE	Vortrag "Role of the miR-17-92 cluster in endothelial cells and angiogenesis" beim internationalen Workshop *Emerging Roles of microRNAs in Development and Disease* vom 18. - 22.11.2008 an der International University of Andalucia in Baeza, Spanien Poster "*Role of the microRNA-17-92 cluster in endothelial cells and angiogenesis"* beim Keystone Symposium "The Biology of RNA Silencing" vom 25. – 30.04.2009 in Victoria, British Columbia (Kanada) Poster "*Role of the miR-17-92 cluster in endothelial cell function"* bei der 75. Jahrestagung der Gesellschaft für Kardiologie – Herz- und Kreislaufforschung e.V., 16. - 18.04.2009 in Mannheim Vortrag "*The microRNA-17-92 cluster exhibits a cell intrinsic antiangiogenic function in endothelial cells"* Scientific Sessions der American Heart Association 2009, 14. - 18.11.2009, Orlando, FL (USA) Poster "*The microRNA-17-92 cluster exhibits a cell intrinsic antiangiogenic function in endothelial cells"* 76. Jahrestagung der Gesellschaft für Kardiologie – Herz- und Kreislaufforschung e.V., 08. - 10.04.2010 in Mannheim Vortrag "*Blocking microRNA-17 by intravenous injection of Antagomirs improves pulmonary hemodynamics and right heart function in experimental pulmonary hypertension"* bei den Scientific Sessions der American Heart Association 2010, 13. - 17.11.2010, Chicago, IL (USA) Poster "*Blocking microRNA-17 by intravenous injection of Antagomirs improves pulmonary hemodynamics and right heart function in experimental pulmonary hypertension"* EMBL Symposium „The Non-Coding Genome" 2010, 13. - 16.10.2010 Poster "*Blocking microRNA-17 by intravenous injection of Antagomirs improves pulmonary hemodynamics and right heart function in experimental pulmonary hypertension*" Keystone Symposium "MicroRNAs and Human Disease" vom 11. - 16.02.2010 in Banff, Alberta (Kanada)

Danksagung

Nur durch die Unterstützung von Vorgesetzten, Arbeitskollegen, Kommilitonen, Freunden, Verwandten und meiner Familie ist diese Arbeit möglich gewesen. An dieser Stelle möchte ich mich ganz herzlich bei den Menschen bedanken, die mich in den vergangenen Jahren begleitet und zum Gelingen dieser Arbeit beigetragen haben.

Herzlichen Dank an …

… Frau Prof. Stefanie Dimmeler und Herr Prof. Zeiher, die es mir ermöglicht haben unter ausgezeichneten Arbeitsbedingungen interessante Forschungsprojekte zu bearbeiten und meine Dissertation anzufertigen. Vor allem bei Frau Prof. Dimmeler möchte ich mich für die stetige Unterstützung und exzellente Förderung besonders bedanken.

… Herrn Prof. Volker Dötsch, der sich sofort bereit erklärt hat meine Doktorarbeit fachbereichsintern zu begutachten und durch Vorlesungen, Seminare und die Organisation von Praktika einen wesentlichen Beitrag zur Gestaltung des Studiengangs Diplom-Biochemie geleistet hat.

… alle Professoren, Tutoren und Praktikumsbetreuer, die an der Vermittlung der Lerninhalte im Rahmen des Biochemie-Studiums beteiligt waren.

… Natalja Reinfeld, Andrea Knau, David Kaluza, Nicole Konecny, Angelika Bonauer, Henrik Fox, Eva Heinrich und Jasmin Weisel für das gute und in der Regel sehr positive Arbeitsklima. Es war mir ein Vergnügen mit euch unsere vier Laborwände und die Durchgänge samt Geräte geteilt zu haben.

… Eduard Hergenreider und Dr. Reinier Boon, die mich stets bereitwillig bei wissenschaftlichen und experimentellen Problemstellungen beraten haben.

… Natalja Reinfeld, die mir in den letzten sechs Monaten durch ihre tatkräftige Unterstützung einiges an Laborarbeit abgenommen und zuverlässig erledigt hat. Durch ihr ausgeglichenes Wesen hat sie zu einer angenehmen Arbeitsatmosphäre im Labor beigetragen und es war mir eine Freude mit ihr zusammen zu arbeiten.

... Ariane Fischer, Marion Muhly-Reinholz, Tino Röxe und Susanne Heydt für die technische Unterstützung bei Tierexperimenten und Immunhistochemie.

… Yosif Manavski und Niels Böckel, die es als einzige geschafft haben, mich aus der Reserve zu locken und sämtliche Emotionen aus mir rauszuholen.

… alle verbleibenden und nicht namentlich genannten Mitarbeitern der Kardiovaskulären Regeneration für ihre Hilfsbereitschaft und Offenheit.

… Dr. Ralph Schermuly und Dr. Soni Pullamsetti für ihr Einverständnis die funktionellen Daten der PAH-Tiermodelle in meine Dissertation aufzunehmen.

… Rike Müller-Werkmeister, die durch Ihre Unternehmungslust und ihr offenes Ohr zur „Entfrustung“ beigetragen hat.

… Michael Heerlein für seine Fahrdienste an Wochenenden sowie seine Geduld.

… Frau Dr. Katrin Lehmann-Barlen, die mich im Ramen des Mentoring-Programms des MentorinnenNetzwerks im letzten Jahr meiner Doktorarbeit begleitet hat und viel Zeit in unsere Mentoring-Kooperation investiert hat.

… Lioba Boll für ihre immerwährende Hilfsbereitschaft und die viele Zeit, die sie bereits für meine Belange geopfert hat.

… Uli Benz, der auch nicht vor dem Korrekturlesen fachfremder wissenschaftlicher Arbeiten zurück schreckt.

… Gerhard Boll für die Vermittlung von Textverarbeitungs- und EDV-Kenntnissen sowie die Hilfe bei Computerfragen jeglicher Art.

… meine Eltern und meine Geschwister für den familiären Zusammenhalt, die Unterstützung und die Liebe, die sie mir im Laufe meines bisherigen Lebens geschenkt haben und die Sicherheit immer auf ihre Hilfe zählen zu können. Meinen Eltern gilt ein ganz besonderer Dank, da sie in meine Bildung investiert und mir den Zugang zu so viel Wissen ermöglicht haben.